MICROCOPY RESOLUTION TEST CHART

NATIONAL BUREAU OF STANDARDS-1963-A

REPORT DOCUMENTATION PAGE		READ INSTRUCTIONS BEFORE COMPLETING FORM
1. REPORT NUMBER RADC-TR-82-269	2. GOVT ACCESSION NO. AD-A12 7993	3. RECIPIENT'S CATALOG NUMBER
4. TITLE (and Subtitle) MODEM SIGNATURE ANALYSIS		5. TYPE OF REPORT & PERIOD COVERED Final Technical Report Sep 80 - Nov 81
		6. PERFORMING ORG. REPORT NUMBER N/A
7. AUTHOR(s) Thomas V. Edwards Dr. Robert J. Dick Dr. James W. Modestino Curry M. Bartlett Michael B. Koligman		8. CONTRACT OR GRANT NUMBER(s) F30602-80-C-0264
9. PERFORMING ORGANIZATION NAME AND ADDRESS PAR Technology Corporation Seneca Plaza, Rt 5 New Hartford NY 13413		10. PROGRAM ELEMENT, PROJECT, TASK AREA & WORK UNIT NUMBERS 61102F 2305J806
11. CONTROLLING OFFICE NAME AND ADDRESS Rome Air Development Center (DCLF) Griffiss AFB NY 13441		12. REPORT DATE October 1982
		13. NUMBER OF PAGES 262
14. MONITORING AGENCY NAME & ADDRESS(if different from Controlling Office) Same		15. SECURITY CLASS. (of this report) UNCLASSIFIED
		15a. DECLASSIFICATION/DOWNGRADING SCHEDULE N/A

16. DISTRIBUTION STATEMENT (of this Report)

Approved for public release; distribution unlimited.

17. DISTRIBUTION STATEMENT (of the abstract entered in Block 20, if different from Report)

Same

18. SUPPLEMENTARY NOTES

RADC Project Engineer: John B. Evanowsky (DCLF)

19. KEY WORDS (Continue on reverse side if necessary and identify by block number)

Pattern Recognition
Automatic Technical Control
Telephone Channel Characterization

Channel Monitoring
Modem Signatures

20. ABSTRACT (Continue on reverse side if necessary and identify by block number)

The objective of this effort was to theoretically and experimentally investigate the use of modem signature analysis techniques for in-service channel-quality monitoring of voice bandwidth channels used for digital transmission. "Modem Signatures" is a term applied to any characteristic derived from the signal source by measurement or transformation (FFT, for example) for use by a generalized algorithm. Monitoring refers to the determination of the transmission channel condition and, ideally,

DD FORM 1473   EDITION OF 1 NOV 65 IS OBSOLETE
1 JAN 73

to the identification of the type and degree of impairments affecting the channel, to aid the operator in effectively managing available resources (channels) and maximizing up-time.

Throughout the course of this effort, algorithms effective in the monitoring of in-service voice frequency data lines were developed and demonstrated. A hierarchial approach to performance monitoring was presented and implemented in the form of a demonstration software system. Through demonstration, it was shown that reliable performance monitoring can be achieved for 1200 and 2400 bits/second modems. Not only could the type of impairment be recognized from among Gaussian noise, odd harmonic distortion and phase jitter, but the degree of the impairment was also indicated. Some success was also shown for the higher speed modems although the accuracy decreased.

Accession For	
NTIS GRA&I	☒
DTIC TAB	☐
Unannounced	☐
Justification	
By	
Distribution/	
Availability Codes	
Dist	Avail and/or Special
A	

TABLE OF CONTENTS

LIST OF TABLES

LIST OF FIGURES

1. INTRODUCTION

The U.S. Air Force has sponsored several programs in pursuit of the Automatic Technical Control (ATEC) of telecommunications networks. Systems have been developed which perform extensive "out-of-service" channel analysis and which have a limited capability for "in-service" monitoring. "Out-of-service" refers to channels not in use at the time of testing. "In-service" refers to non-intrusive probing of a channel while it is transferring information. When a channel has degraded to such a degree that it will no longer transfer data with sufficient accuracy to maintain effective communications, it has "failed." When a channel fails, it is necessary to re-route the data through a back-up channel and subject the failed channel to out-of-service testing. The development of in-service channel monitoring techniques is desirable since it would minimize the number of reserve channels required and would provide advanced warning of channel failures before acceptable service is disrupted. The implementation of such an in-service monitoring capability would probably provide more reliable service, while reducing overall system maintenance costs, by scheduling down time on failing channels for testing during off-peak hours.

The objective of this effort was to theoretically and experimentally investigate the use of modem signature analysis techniques for in-service channel-quality monitoring of voice bandwidth channels used for digital transmission. "Modem signatures" is the term applied to any characteristic derived from the signal source by measurement or transformation (FFT, for example) for use by a generalized algorithm. Monitoring refers to the determination of the transmission channel condition and, ideally, to the identification of the type and degree of impairments affecting the channel, to aid the operator in effectively managing available resources (channels) and maximizing up-time.

2. BACKGROUND

Recent developments in microprocessor and VLSI technology have reduced modem and computer costs and have resulted in an increased utilization of telecommunications channels for data communication purposes. In response to the increasing demand for enhanced in-service monitoring capabilities, the Air Force Communications Service (AFCS), in 1977, performed an in-house investigation which showed that a "large variety" of in-service data modem samples could be distinguished from one another. After the installation of the Wire-Line simulator at the Digital Communications Experimental Facility (DICEF), RADC, it became possible to simulate degraded channel conditions in a controlled fashion. With this capability, a four-modem database was generated. The modems were each processed through the wire-line simulator where varying degrees of impairments were added. The modems of the original database are listed in Table 2-1. Each modem sample cut was approximately 1 1/2 seconds long and digitized at 12800 samples per second. The type and degree of impairments collected are shown in Table 2-2.

The features used in the experiment were functionally equivalent to calculating the autocorrelation of the signal after it had been quantized to 1 bit. This is shown graphically in Figure 2-1. Generally, the lowest lags of the autocorrelation provided the best discrimination between modems.

It was shown that the four-modem database could be separated with complete reliability in the presence of noise, harmonic distortion, and phase jitter. No attempt, however, was made to characterize the channel condition. The problem of identifying signal features and classification algorithms to perform channel degradation detection and classification were the goals of the Modem Signature Analysis (MSA) effort. The remainder of this report discusses the results of this program.

MODEM	MODULATION	BITS/SEC	BAUD	BITS/SYMBOL	CARRIER (Hz)
CODEX LSI-9600	QAM	9600	2400	3	1706
HUGHES HC-276 (MD-823)	DPSK	2400	1200	2	1800
PARADYNE LSI-96	PAM[1]	9600	4800	2	2853
LENKURT 26-C	FSK	1200	1200	1	1200,2400

[1] transmitted as vestigial sideband

Table 2-1 Original Four Modem Database

MODEM	HARMONIC DISTORTION	GAUSSIAN NOISE	PHASE JITTER @ 10hz	PHASE JITTER @ 60hz	PHASE JITTER @ 120hz
CODEX LSI-9600	-30dB to -8dB	-30dB to -15dB	5°P/P to 40°P/P	5°P/P to 40°P/P	5°P/P to 40°P/P
HUGHES HC-276	-30dB to -4dB	-30dB to -6dB	10°P/P to 80°P/P	10°P/P to 80°P/P	10°P/P to 80°P/P
PARADYNE LSI-96	-30dB to -4DB	-30dB to -6dB	5°P/P to 80°P/P	5°P/P to 80°P/P	5°P/P to 80°P/P
LENKURT 26-C	-30dB to -4dB	-30dB to -6dB	5°P/P to 80°P/P	5°P/P to 80°P/P	5°P/P to 80°P/P

Table 2-2 Range and Type of Impairments Collected In The Original Four Modem Data Base
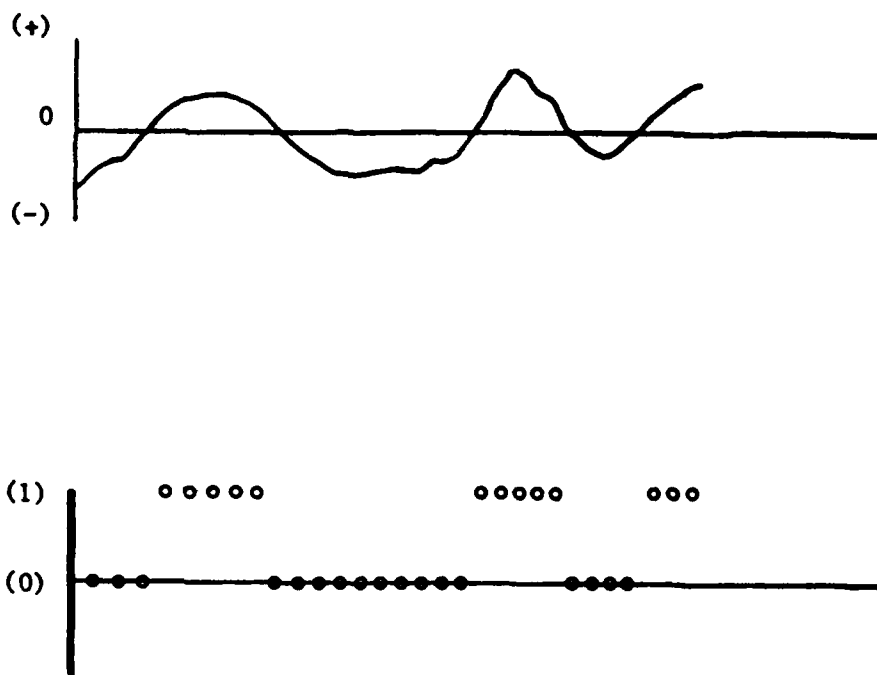
Figure 2-1: Illustration of the Effects of Quantizing a Signal to 1 Bit

3. DATABASE OVERVIEW

Under the present effort, it was agreed to expand the original four-modem database. As more modems were added to the database it became more difficult to classify a modem type. Further, the problem of deducing the channel quality had more cases of "normal" operating parameters to consider. It was, however, decided that the original four modems did not provide a sufficient basis for an investigation of this scope.

The seven additional modems collected under this effort, together with the original four, are listed in Table 3-1. All of the later collections were at a sampling rate of 17.2 KHz in contrast to the earlier collection which used 12.8 KHz. All the signals of the first collection included cuts impaired with varying amounts of Gaussian noise, harmonic distortion, or phase jitter at 10, 60 and 120 Hz. In addition, each signal included some cuts impaired with a combination of Gaussian noise and phase jitter at 60 Hz.

Under this effort, there was concern that the wireline simulator's capability to inject harmonic distortion was not functioning correctly. Because of this, no cases of harmonic distortion were collected under this effort. All signals were, however, collected while impaired with Gaussian noise and/or phase jitter. The range of impairments collected for each modem of the complete database is shown in Table 3-2.

The complete database contained a total of 311 modem samples. Each modem type was supplied on a raw formatted tape accompanied by a log sheet describing the 30 or so cuts on that particular tape. The cross-referencing between the logsheets and data tapes soon became unmanageable as the database grew larger. It was decided to eliminate the need for the log sheet referencing by encoding the modem type and collection parameters into the name of the file which stored each cut of data.

Modem	Modulation	Bits/Sec.	Baud	Bits/Symbol	Carrier (hz)	Sample Rate	Generic Code
Lenkurt 26-C	FSK	1200	1200	1	1200,2400	12.8 Kc	L11F
MD-674	FSK	1200	1200	1	1200,2400	17.2 Kc	X11F
Hughes HC-276(MD-823)	DPSK	2400	1200	2	1800	12.8 Kc	H12D
Weco 207A2	DPSK	2400	1200	2	1800	17.2 Kc	W12D
CODEX LSI-48 Mode B	DPSK	2400	1200	2	1800	17.2 Kc	B12D
CODEX LSI-48 Mode A	DPSK	4800	1600	3	1800	17.2 Kc	A32D
CODEX LSI-48 Mode C	QAM	4800	1600	3	1706	17.2 Kc	D32Q
CODEX LSI-9600	QAM	9600	2400	4	1706	12.8 Kc	C43Q
Paradyne LSI-96	PAM*	9600	4800	2	2853	12.8 Kc	P45P
Paradyne MP-9600	QAM	9600	2400	4	1700	17.2 Kc	M43Q
Harris 5238	QAM	16000	2667	6	1800	17.2 Kc	H54Q

* Transmitted as vestigial sideband.

Table 3-1 The Modems and Operating
Parameters Of The Complete Data Base

MODEM	GAUSSIAN NOISE	PHASE JITTER @ 10 hz	PHASE JITTER @ 60 hz	PHASE JITTER @ 120 hz	PHASE JITTER @ 180 hz
MD-674	-30dB to -14dB	80°P/P	5°P/P to 80°P/P	20°P/P to 80°P/P	30°P/P to 80°P/P
WECO 207A 2	-30dB to -12dB	---	10°P/P to 120°P/P	---	---
CODEX LSI-48 Mode B	-30dB to -11dB	---	10°P/P to 64°P/P	---	---
CODEX LSI-48 Mode A	-30dB to -12dB	---	10°P/P to 30°P/P	---	---
CODEX LSI-48 Mode C	-30dB to -11dB	---	10°P/P to 30°P/P	---	---
PARADYNE MP-96	-30dB to -14dB	---	5°P/P to 50°P/P	---	---
HARRIS 5238	-36dB to -14dB	---	5°P/P to 60°P/P	---	---

Table 3-2 Range and Type of Impairments Collected Under This Effort By RADC

Software development was performed on a VAX 11/780 and on a PDP 11/45. The target processor was a PDP 11/40. Both operating systems (VAX VMS and PDP-11 RSX11M) support FILES-11 disk file structure. FILES-11 allows each file to be named by a nine-character name and a three-character extension.

The filename encoding scheme employed is shown in Table 3-3. The first four characters include the generic code information, including the number of bits/second, the baud rate, and modulation type. The first character is an arbitrary, unique symbol assigned to represent each individual modem type. Table 3-1 includes the generic code label for each modem.

Several benefits are immediately evident from this scheme. For example, if all modems with a baud rate of 2400 are desired, it is simply necessary to scan all the file names for those with a "3" in the third position. Furthermore, reviewing the success of a processing run is simplified because all available groundtruth is encoded into the filename of the data sample.

In addition to the generic and ID information encoded into the filename, the impairments present on the channel are also encoded. The fifth character describes the nature of the impairment. As shown in Table 3-3, codes "0" and "1" refer to the raw modem signal which has not been passed through the 4A line, and to the modem signal which has been passed through the 4A line with no impairments added, respectively. The two-character field "F1" identifies the amount of Gaussian noise or harmonic distortion added to the sample in dB's. Field "F2" indicates the amount of phase jitter in degrees peak-to-peak. This allows the encoding of combined noise and phase jitter information in the filename. Note that whenever phase jitter occurs in combination with Gaussian noise, the frequency of the phase jitter component is always 60 Hz. This case corresponds to an "I" code of "4". The other frequencies of phase jitter each are identified by a separate "I" code of "6" through "9"; field "F2" shows the degrees peak-to-peak.

Table 3-3

MODEM ID DATA BASE FILENAME CONVENTION

T   #   #   M I F1 F2 ".WAV"

TYPE		BITS/SEC.	BAUD	MODULATION
P - PARADYNE 9600		1-1200	1-1200	F-FSK
		2-2400	2-1600	D-PSK/DPSK
L - LENKURT 26C		3-4800	3-2400	Q-QAM
		4-9600	4-2667	P-PAM
H - HUGHES 276		5-16000	5-4800	

TYPE	(I) IMPAIRMENT	(F1) FIELD 1	(F2) FIELD 2
C - CODEX LSI 9600			
	0 - NO 4A	00	00
M - PARADYNE MP	1 - 4A CLEAN	00	00
	2 - HARMONIC DIST.	+dB	00
A - CODEX LSI 48 MODE A	3 - GAUSSIAN NOISE	+dB	00
	4 - NOISE & PHASE JITTER	+dB	P/P°
B - CODEX LSI 48 MODE B	5 - CALIBRATION SIGNAL	00	00
	6 - JITTER @ 10 hz	00	P/P°
D - CODEX LSI 48 MODE C	7 - JITTER @ 60 hz	00	P/P°
	8 - JITTER @ 120 hz	00	P/P°
W - WECO	9 - JITTER @ 180 hz	00	P/P°
R - HARRIS			
X - MD-674			

Table 3-3

Code "5", described as calibration signals in Table 3-3, includes a variety of test signals. These are typically test tones or Gaussian noise passed through the simulated 4A channel.

3.1 DATA COLLECTION

All of the data collection was performed at the RADC/DICEF, Griffiss Air Force Base by RADC personnel. The original data collection setup is shown in Figure 3-1. The random sequence generator provides a repetitive random stream into the modem under test. The modem output is fed to the wireline simulator. The signal is digitized in the simulator and the channel characteristics and programmed impairments are added. The resultant signal is D/A converted and then leaves the simulator. After anti-aliasing filtering the signal is re-digitized at 12.8 KHz for data collection and recorded on 7-track magtape by the DICEF 9303 processor. For the purpose of this investigation, the data was converted by RADC personnel to 9-track magtape and supplied to PAR Technology Corporation.

The original database for the MSA effort contained 4 modem types:

● CDX LSI-9600 – QAM

● Hughes HC-276 – DPSK

● Paradyne LSI-96 – PAM (Vestigual Side Band)

● Lenkurt 26-C – FSK

The second series of data collections were performed on the setup shown in Figure 3.2 Note the 51.6 KHz sample rate into the AP120B. Data was resampled by three to reduce the sampling rate to 17.2 KHz before being passed to the PDP 11/40 processor and saved to magtape.

3-6
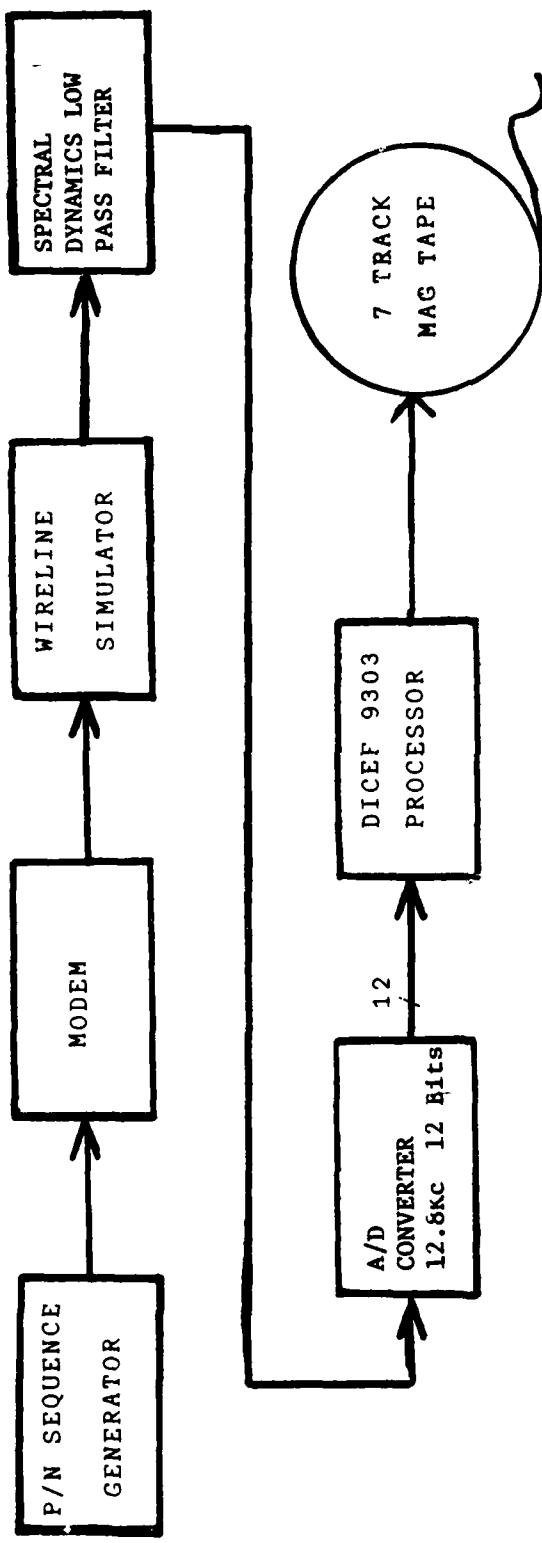
Figure 3-1: Original Modem Signature Collections System

3-7
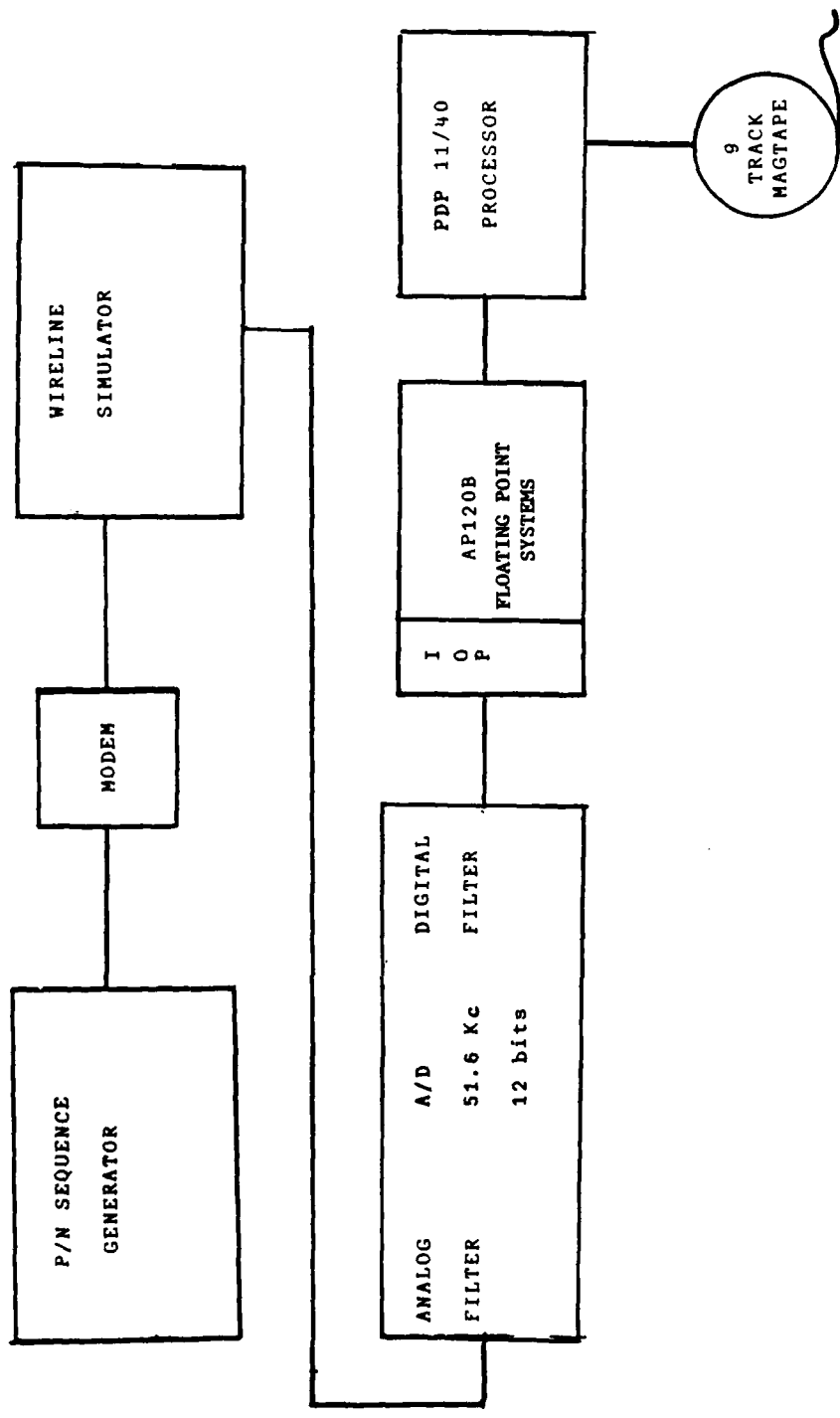
Figure 3-2   Second MSA Data Collection System

From the two collections a total of 11 modems were sampled. Four sampled at 12.8 KHz and seven sampled at 17.2 KHz. In order that features extracted from the modem signals be comparable, it is required that all of the samples have the same sampling rate. Therefore, it was determined that the sample rate of the database be unified. Further, in order that minimum error be introduced into the signals, it was decided that the 17.2 KHz sampling rate would be resampled down to approximate the lower sampling rate, 12.8 KHz.

A method known in engineering as Sampling Rate Decimation, was applied to the 17.2 KHz sampled selected Modem types in the MSA database to alleviate this sampling rate discrepancy. The implementation of this sampling reduction algorithm is fairly straight forward and is described elsewhere[1]. A summary of the method is given here.

The two sampling rates contained in the MSA database were 12.8 KHz and 17.2 KHz. Since 12.8 KHz is approximately three-quarters of 17.2 KHz, the sampling rate reduction technique to be applied is straightforward. The approach accomplishes the reduction of the sampling rate from 17.2 KHz to 12.9 KHz within 0.8% of the desired sampling rate 12.8 KHz. The procedure is indicated below:

1. Initial Data is obtained at a sampling rate of 17.2 KHz.

2. Pad each sample in the Raw Input Data File with 2 zeros

3. Apply a Low pass filter with a 6 KHz cutoff and a gain of 3.0

4. Resample by a factor of 4

___

1 Proceeding of the IEEE, Vol. 69, No. 3, March 1981 "Interpolation and
  Decimation of Digital Signals -- A Tutorial Review." by Ronald E.
  Crochiere, Lawrence R. Rabiner.

After execution of step (2), the data stream will have an effective sampling rate of 51.6 KHz. The 6 KHz low-pass, linear-phase FIR filter will interpolate the padded zeros and act as an anti-aliasing filter.

Since the effective sampling rate is currently 51.6 KHz, resampling of the data by a factor of 4 yields a sampling rate of 12.9 KHz, which is within 0.8% of our desired sampling rate, 12.8 KHz. Following the conversion of all modem types originally collected at a sampling rate of 17.2 KHz to the 12.9 KHz sample rate, extensive tests were performed to insure the validity of the resampled data. Figure 3-3 shows a time plot containing the first 1024 samples of the PARADYNE MP-96 modem with AGN added.

This illustration was plotted from the original modem database which was generated at a 17.2 KHz sampling rate. Figure 3-4 illustrates a power spectral density plot of the same data. Figure 3-5 shows the same data after resampling (sampling rate = 12.9 KHz). The difference between the plot shown in Figure 3-5 and the plot shown in Figure 3-3 indicates the error introduced by the reduction of the sample rate. By visual inspection, it is clear that the plots are identical. Inspection of the Power Spectral Densities of the same modem data at different sampling rates, Figures 3-4 and 3-6, we concluded that the carrier frequencies and bandwidths of both signals are equal, thus showing the success of the sampling rate reduction.

The sampling reduction technique was applied to each file in the MSA database which has been generated using a sampling rate of 17.2 KHz. The resulting database currently exists with a sampling rate of 12.9 KHz.

Figure 3-7 illustrates the frequency response of the 6 KHz low-pass filter used in the resampling technique. Figure 3-8 lists the coefficients which make up the 6 KHz filter.

1024 Point Plotted Sampling Rate = 17.2kHz
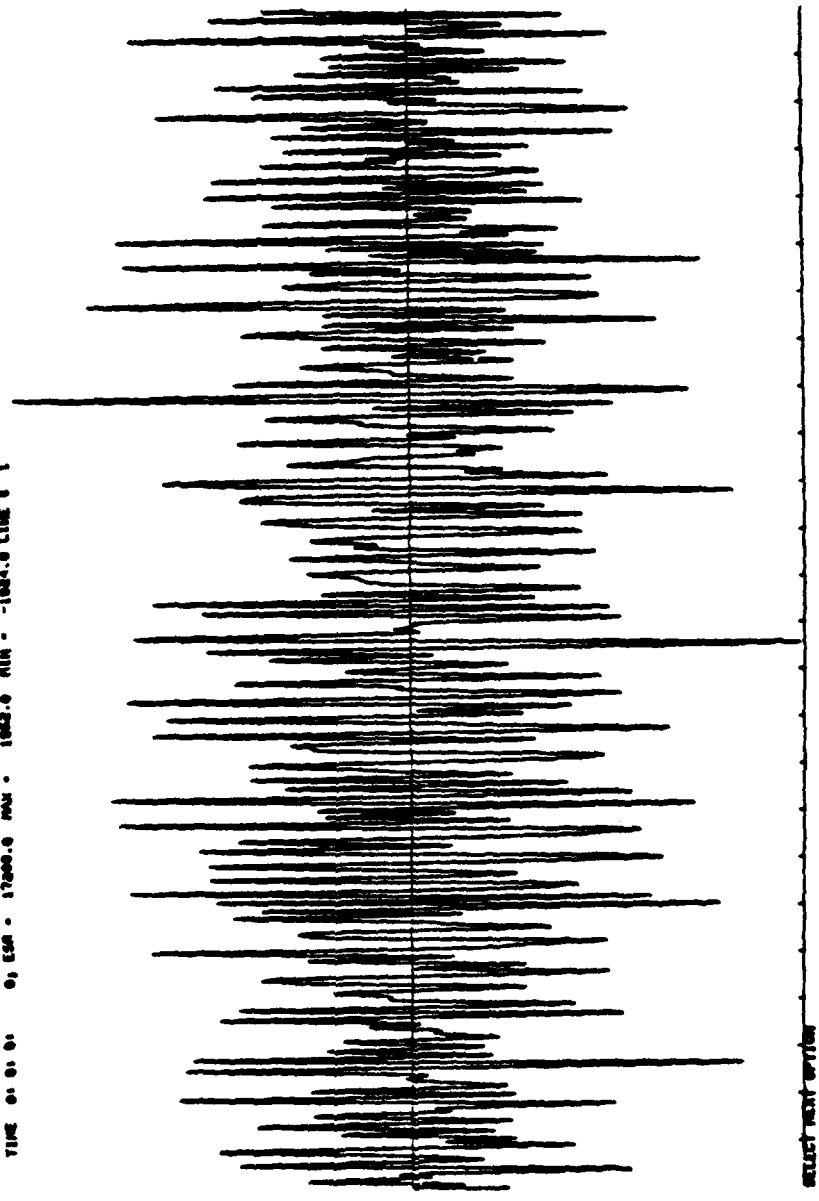
Figure 3-3: Time Plot Paradyne MP-96 AGN 20 dB S/N
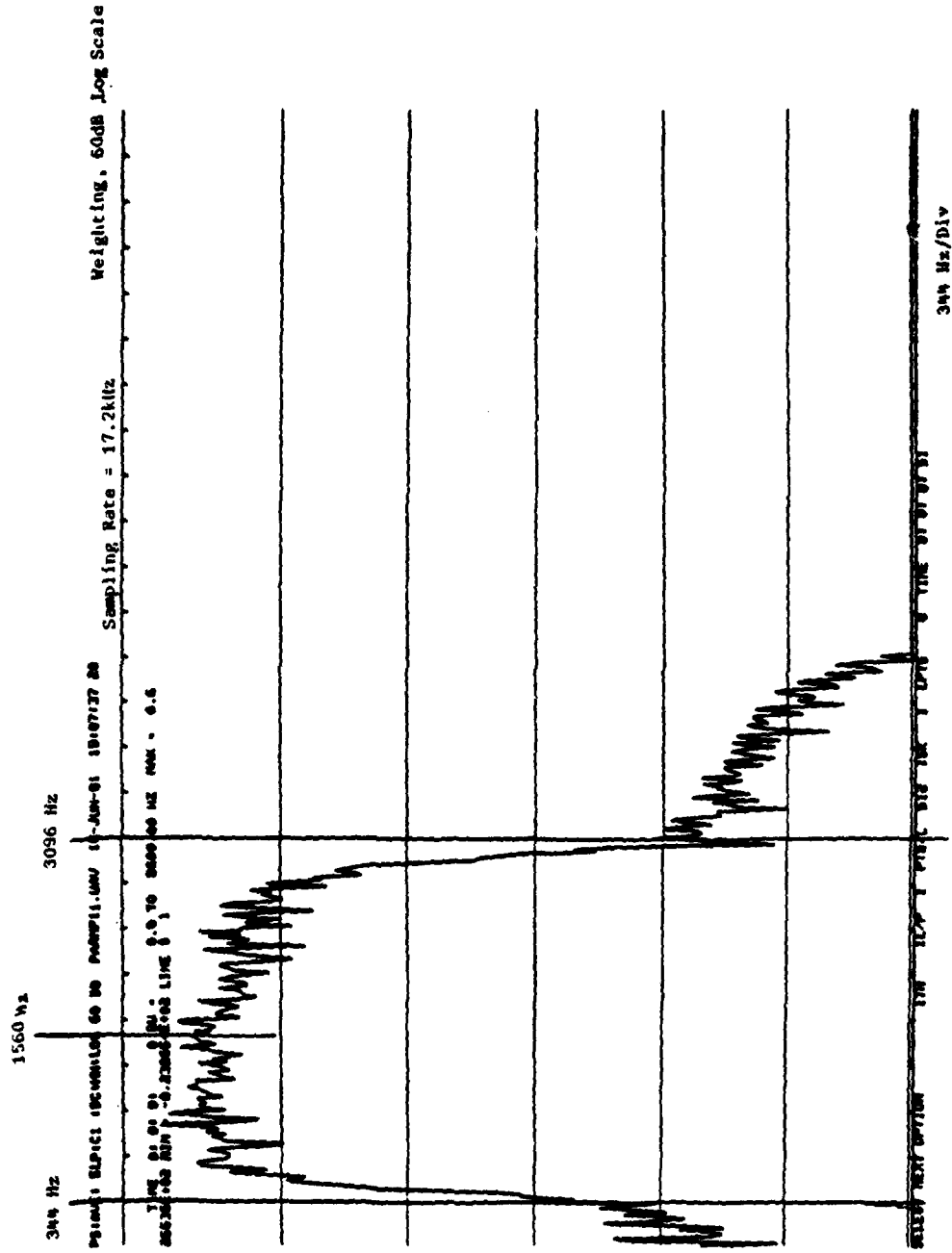
Figure 3-4: Power Spectral Density, Paradyne MP-96, AGN 20 dB S/N 5 Line Avg., DC Removed, Hanning

3-12
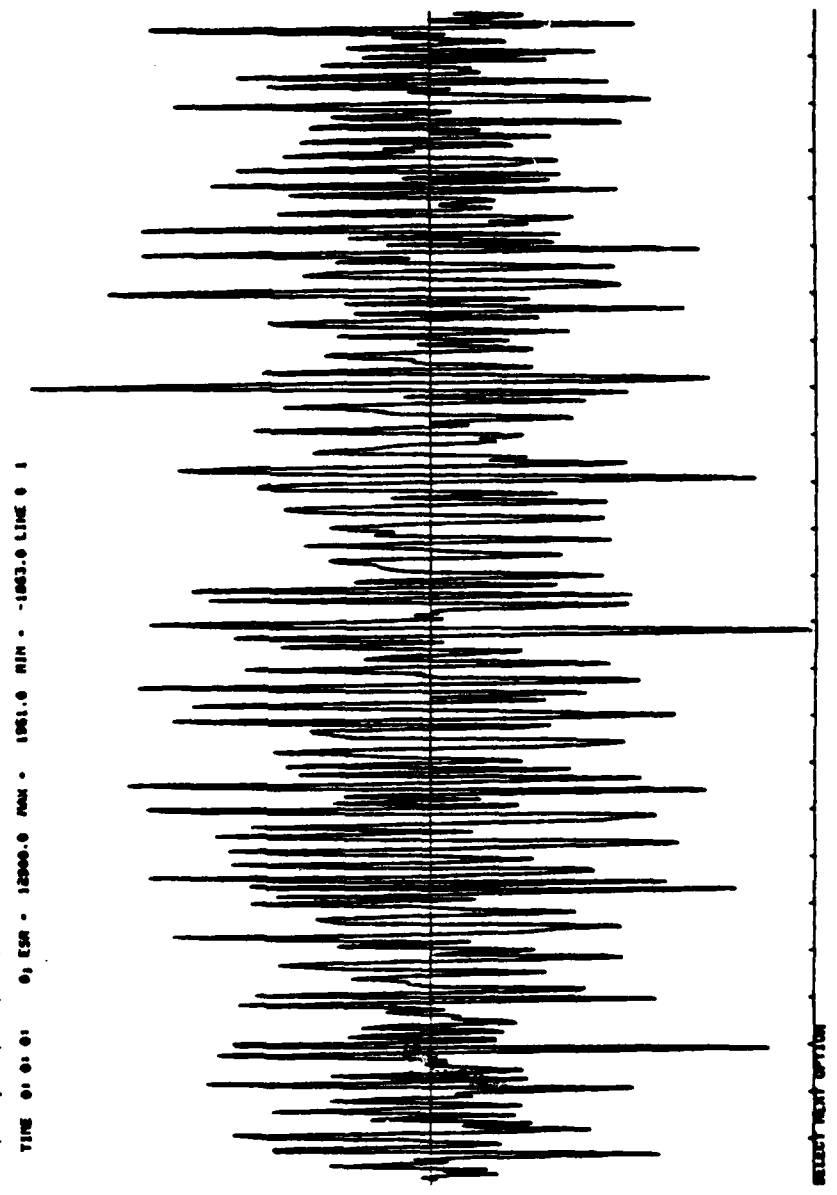
Figure 3-5: Time Plots, Paradyne MP-96, AGN 20 dB S/N
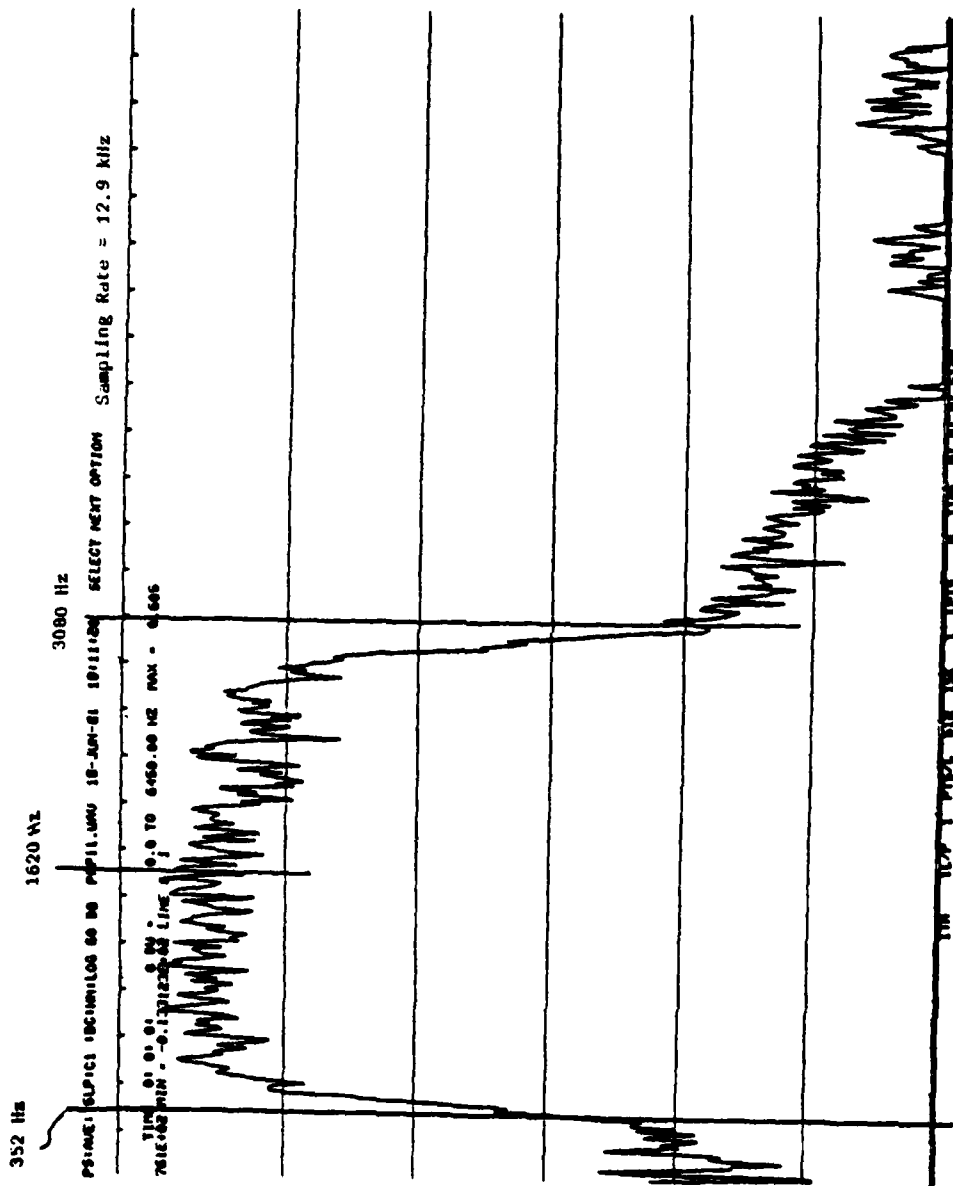
Figure 3-6: Power Spectral Density, Paradyne MP-96, AGN 20 dB S/N 5 Line Avg., DC Removed, Hanning Weighting, 60 dB; bg Scale

FIR FILTER: LP6K.FIR

QUANTIZATION IN BITS: 22   GAIN IN DB: 9.54   NUMBER OF TAPS: 64

18-JUN-81
18:54:18

FREQUENCY
RESPONSE
LOGARITHMIC

PHASE
RESPONSE

STEP
RESPONSE

IMPULSE
RESPONSE

	BAND1	BAND2
LOWER BAND EDGE	0.00000	0.12010
UPPER BAND EDGE	0.07360	0.50000
DESIRED VALUE	3.00000	0.00000
WEIGHTING	1.00000	1.00000
DEVIATION	0.00644767	0.01526628
DEVIATION IN DB	-43.81194	-36.325?
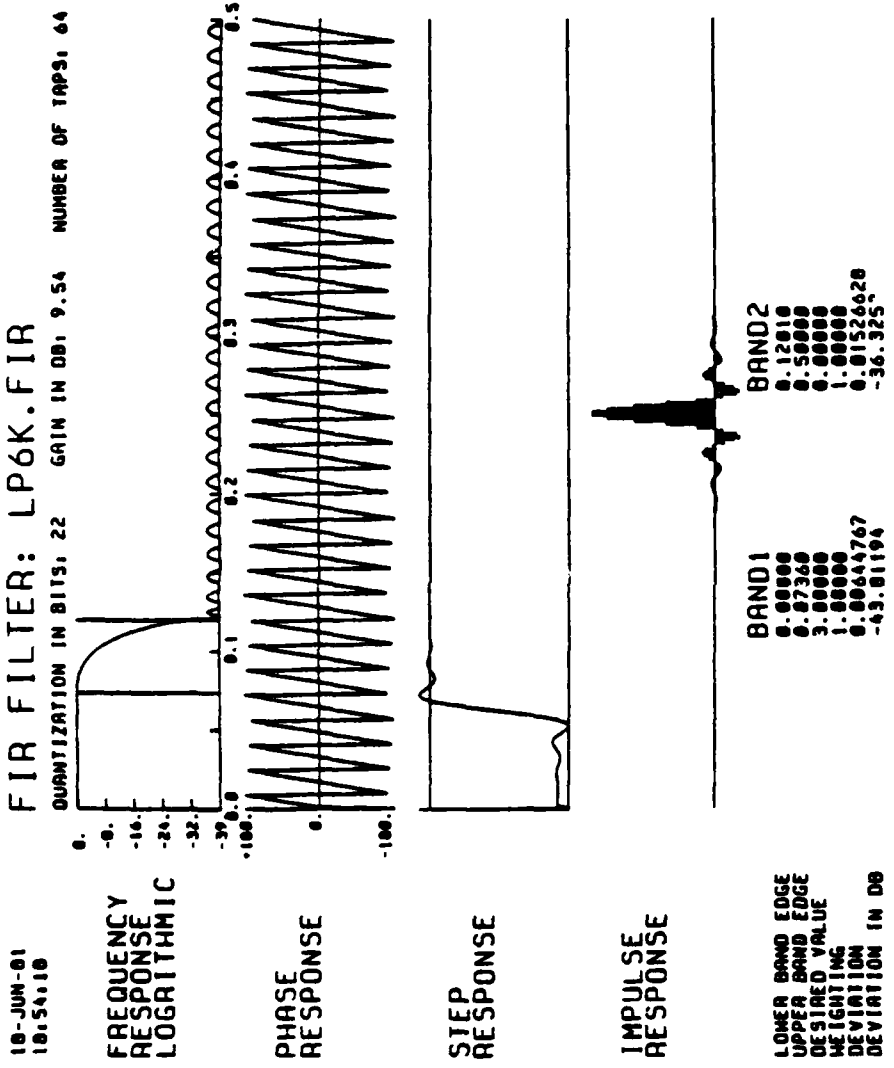
Figure 3-7:   Frequency Response for 6kHz Lowpass Filter Used in Sample Reduction
Algorithm Implementation Filter Length = 64 Taps

Figure 3-8: Top Weights of the Lowpass Filter Used for Resampling

3.2 THE WIRELINE SIMULATOR

The wireline simulator was used to produce all of the channel impairments which were compiled into the MSA database. Since the MSA database will be studied to suggest possible algorithms and will also serve as a test data set for any algorithms developed, how the simulator performs the corruption of the channel will be described. The description will focus on the theory of operation rather than the implementation details and will emphasize the particular parameters used during this program rather than the myriad of options. For further information the reader is referred to at least three detailed technical manuals available in the DICEF on this subject.

The wireline simulator was originally installed at DICEF in 1970. In 1976 the simulator was upgraded with the addition of a special purpose programmable signal processor and a new control minicomputer. The description can be conveniently separated into the original simulator and the upgrade. A block diagram of the original is shown in Figure 3.9. It comprises a programmable digital filter, a frequency offset unit, an impulse noise generator, and interfaces with a general purpose digital computer and with input and output analog signals.

The digital filter is based on a direct convolutional algorithm employing a special high-speed arithmetic unit with a 400 nanosecond multiply/add time. The frequency offset unit performs a digital single-sideband modulation including jitter of the offset frequency. The impulse generator produces rectangular pulses, noise bursts and damped sinusoids each with variable parameters. Automatic amplitude scaling A/D and D/A converters provide an input/output dynamic range well in excess of the basic converter accuracy.

A block diagram of the upgraded wireline simulator is shown in Figure 3-10. In this figure the original simulator is represented by the large block in the left center. It is noted that the upgrade was added in a serial fashion to the original. That is, before digital-to-analog conversion at the

Paper Tape
Data Input

TTY

Control
Unit
(PDP-8)

Data
Input

Floating
Point
A/D Converter

Digital
Filter

Frequency
Shift
Unit

Impulse
Noise
Generator

Ext
Noise
Input

Floating
Point
D/A Converter

Line
Amp

Data
Output

8-5330
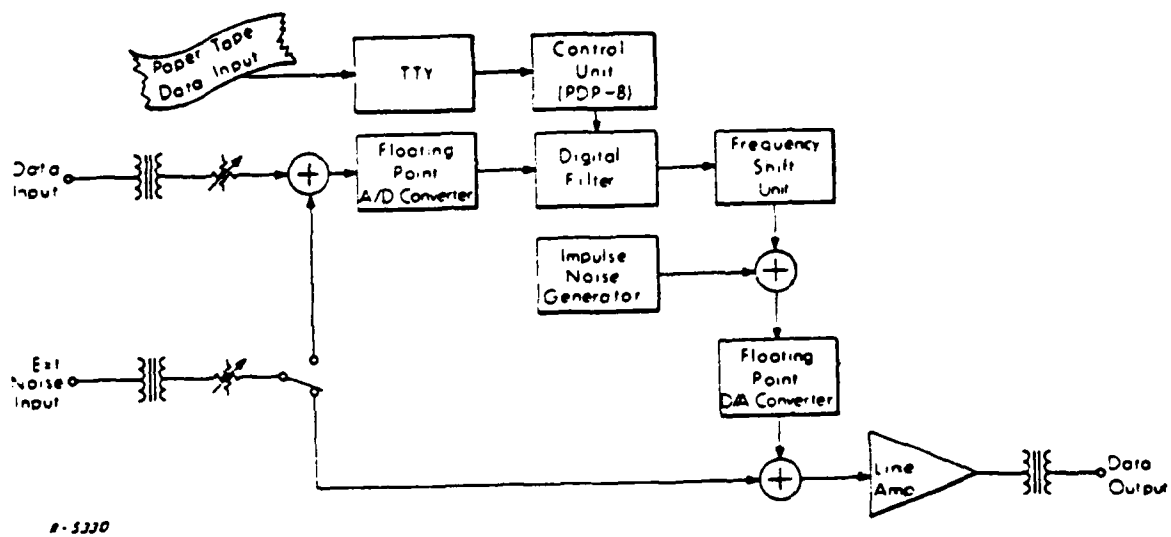
Figure 3-9: Original Wireline Simulator
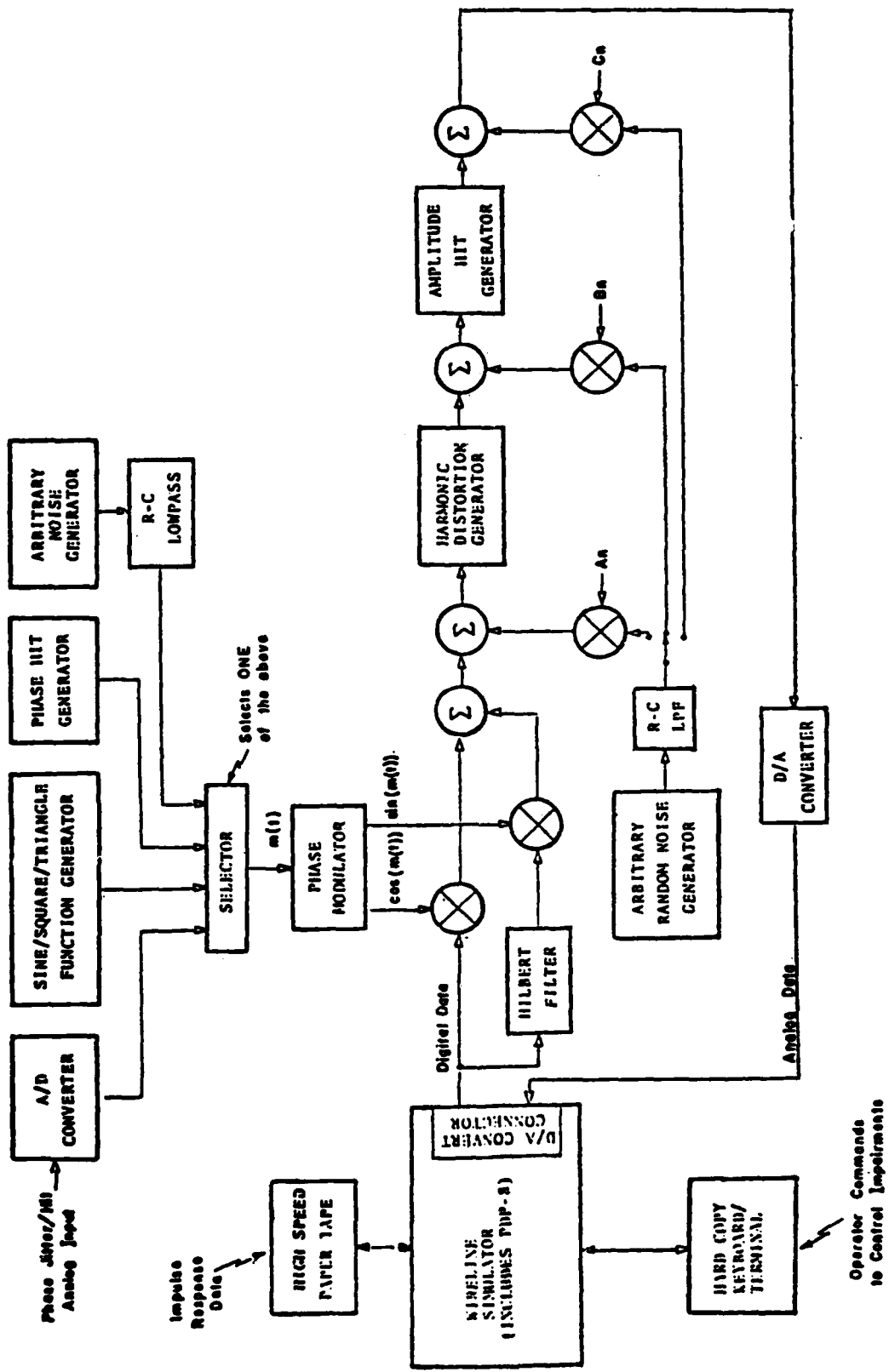
Figure 3-10: Upgraded Wireline Simulator

3-19

output port of the original, the sampled signal was interrupted and sent to the upgrade for the addition of more parameters.

The first parameter of interest is additive Gaussian noise. An external General Radio Type 1390-A Random Noise Generator was applied to the noise input shown in Figure 3-9. This source was applied before the input A/D converter and as a result was weighted by the remainder of the simulation.

The next major component applicable to this program is the programmable digital filter used to simulate the attenuation and delay distortion characteristics of the wireline channel. The impulse response is represented by 256 samples. Thus, each output sample is generated by 256 multiply/add operations in the convolutional filter. The filter performs a multiply/add operation in 400 nanoseconds. This results in a sampled rate of $1/(400 \times 10^{-9} \times 256) = 9765.50$ samples/ sec. The filter employed a typical convolution algorithm where the nth sample of the output function $g(n)$, is given by

$$g(n) = \sum_{k=0}^{N} h(k) f(n - k) \qquad (1)$$

where $h(k)$ is the sampled impulse response of the filter and $f(k)$ is the input function. Implementation of Eq. (1) requires two circulating memories, one which stores $h(k)$ and one which stores $f(n - k)$, and a multiplication/addition unit which generates $g(n)$. Note that as n advances, a particular sample of $f(k - n)$ slides relative to $h(k)$. This is achieved in practice by making the memory which stores $f(n - k)$ one word longer than the memory which stores $h(k)$. Then, when the $h(k)$ memory completes a full cycle and a new value of $g(n)$ has been generated, the $f(n - k)$ memory lacks one word of completing a full cycle. Thus the data in the $f(n -k)$ memory is shifted back by one position relative to the data in the $h(k)$ memory every cycle. The vacant position at the beginning of the $f(n - k)$ memory is filled by the new input sample.

Figure 3-11 shows a block diagram of the programmable digital filter used in the simulator. The h(k) memory contains 256 samples of the filter impulse response and the f(n - k) memory contains 257 samples of the input function. The particular impulse response required for the filter is loaded into the h(k) memory from paper tape, through a paper tape reader and control unit.

Voice channel communications often go through carrier systems which employ single sideband modulation techniques. Usually, the transmitter and receiver carriers are not exactly locked. In particular, one carrier will drift in frequency and phase relative to the other one, producing a variable spectrum shift in the data signal. The frequency shift unit is intended to simulate this effect. It is capable of introducing a frequency offset in the spectrum of the data signal. The frequency offset can be modulated by either a square or sinusoidal modulation waveform where the frequency and deviation of the modulation can be controlled. This unit was used to impart phase jitter to the MSA database.

The frequency shift unit, as implemented, performs a single sideband modulation directly at audio frequency. The mathematical block diagram of the unit is shown in Figure 3-12 and a functional diagram is shown in Figure 3-13. The mathematics of the signal processing are outlined below.

The input to the unit, $f(t)$, is to be shifted in frequency by ω_m. Since the duration of $f(t)$ is always finite, it can be represented over its entire duration by a Fourier series

$$f(t) = \sum_n \left[a_n \cos n\omega_0 t + b_n \sin n\omega_0 t \right] \tag{2}$$

The signal $f(t)$ is first passed through a 90° phase shift device and the resulting quadrature signal is $f_q(t)$, where

$$f_q(t) = \sum_n \left[b_n \cos n\omega_0 t - a_n \sin n\omega_0 t \right] \tag{3}$$

3-21
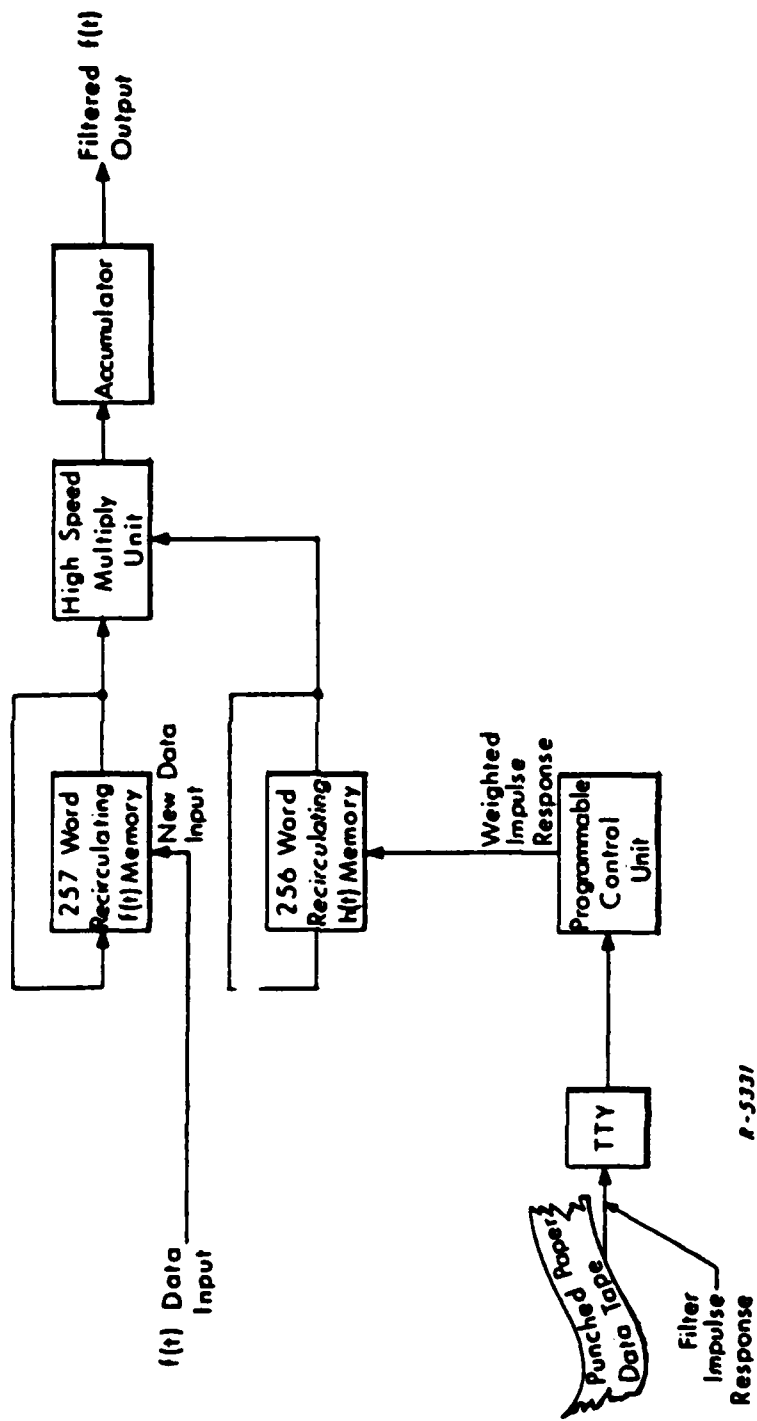
Figure 3-11: Digital Filter Block Diagram

$f(t) = \sum_n [b_n \cos n\omega_0 t - a_n \sin n\omega_0 t]$

$x(t)$

$f_s(t)$

$90°$

$\sin \omega_m t$

Frequency Shift Reference Oscillator

$90°$

$\cos \omega_m t$

$y(t)$

$f(t) = \sum_n [a_n \cos n\omega_0 t + b_n \sin n\omega_0 t]$
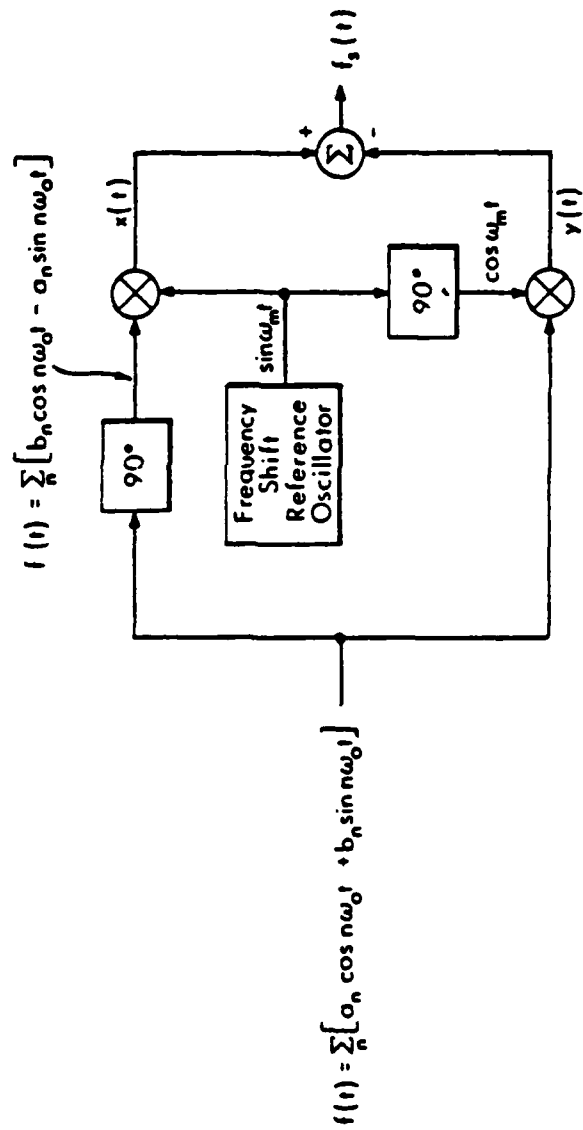
Figure 3-12: Frequency Shift Unit
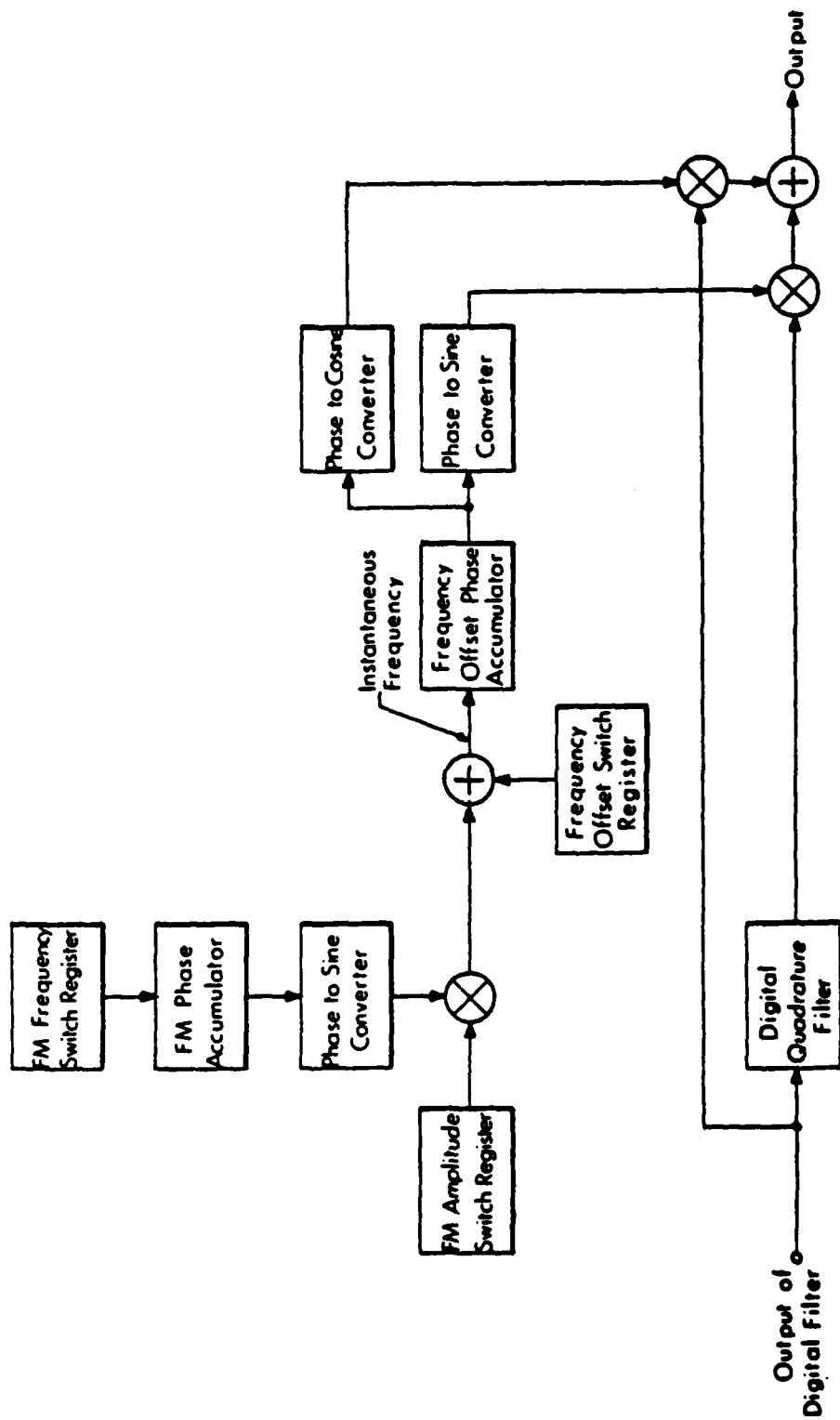
Figure 3-13: Digital Frequency Shift Unit

3-24

Finally, the single sideband modulation is performed as the difference of two products:

$$f_s(t) = f_q(t) \sin\omega_0 t - f(t)\cos\omega_0 t$$

$$= \sum_n \left[b_n \left\{ \cos n\omega_0 t \, \sin\omega_m t + \sin n\omega_0 t \, \cos\omega_m t \right\} \right.$$

$$\left. + a_n \left\{ \cos n\omega_0 t \, \cos\omega_m t - \sin n\omega_0 t \, \sin\omega_m t \right] \right.$$

$$= \sum_n \left[a_n \cos(n\omega_0 - \omega_m)t + b_n \sin(n\omega_0 - \omega_m)t \right]$$

Thus, $f_s(t)$ is the same signal as $f(t)$ with the spectrum shifted by an increment ω_m.

The next impairment function to be considered is the harmonic distortion generator. This device presented a unique design problem since for high distortion levels it is possible to produce spectral widening with its associated aliasing. The inputs to the distortion generation elements are band limited so that the distorted output signal will not contain significant aliasing. This is accomplished as shown in Figure 3-14. All low-pass filters are compensated for zero delay and zero delay distortion.

The input signal which is sampled at 9765.63 Hz, is first band limited to 2500 Hz and then squared. The output of the squarer will contain second harmonic components which have a maximum frequency at 5000 Hz. Thus, no inband aliasing is produced. That output will in turn be band limited to 2500 Hz and again squared to produce components with 4th harmonic components. The
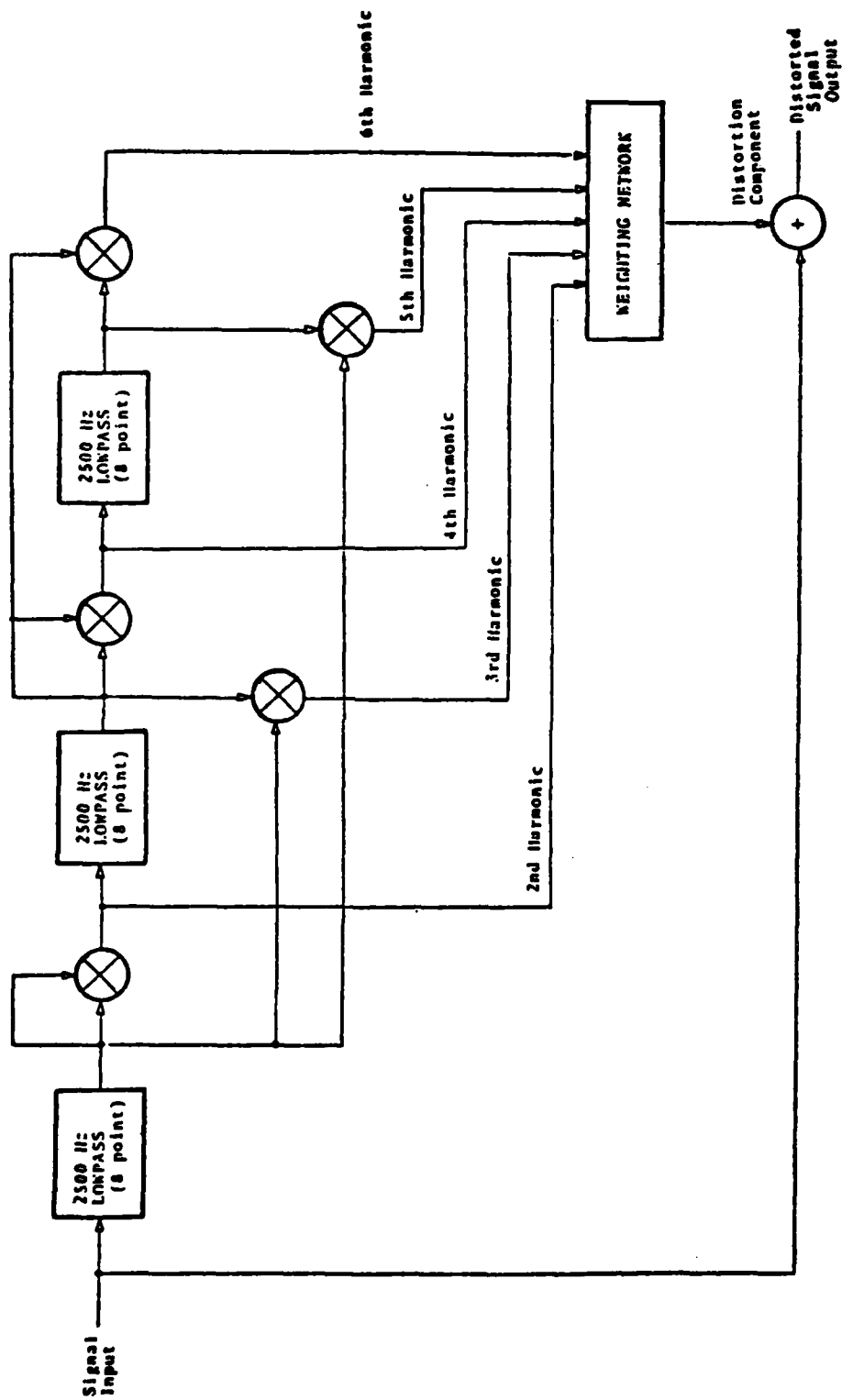
Figure 3-14: Distortion Generator

3-26

second and the filtered 4th harmonic components are multiplied to produce 6th harmonic components. The odd harmonic components are generated by mixing even harmonic components with the fundamental. Examination of the figure will reveal that no signal component used will have a spectrum wider than half the sampling rate. This will avoid all aliasing problems. It should be noted that none of these components is pure, but the appropriate harmonic energy is present and by combination of the components, it is possible to generate arbitrary harmonic distortion. This capability is provided by the weighting network which implements the coefficients of a Taylor series expansion of the distortion characteristic to produce the desired harmonic energy. The operator enters harmonic amplitude and the PDP-8 computes the coefficients. When the harmonic distortion signal has been generated, the result is then added to the original, undistorted, signal.

The harmonic distortion process is performed by combining the terms in a Taylor series expansion.

$$\text{Distortion Component} = a_o + a_1 S(t) + a_2 S^2(t) + a_3 S^3(t) + a_4 S^4(t) + a_5 S^5(t) + a_6 S^6(t)$$

where $S(t)$ is the input signal to the distortion generator. The 6th order term in the expansion also contains 4th and 2nd harmonic energy in addition to the 6th harmonic energy. The PDP-8 OPCOM program is designed to operate on operator inputs specifying harmonic levels to create the set of coefficients for the Taylor series which cancel undesired harmonics. Note, this procedure can function only when signal level is known and $S(t)$ is a sine wave. It is possible to generate pure 6th harmonic by requesting the OPCOM program to generate only a 6th harmonic component. The 3rd harmonic was utilized for the MSA data collection.

4. A HIERARCHICAL APPROACH TO PERFORMANCE MONITORING OF VOICE FREQUENCY CHANNELS

It is desired to develop simple and reliable techniques for performance monitoring of voice frequency communications channels. The problem is considerably simplified if the performance monitoring unit can observe modem outputs. In particular, a number of existing techniques are available in this case for predicting bit error probability, which is often the single important measure of channel quality. Unfortunately, in the present application it cannot be assumed that the modem outputs are available. This severely complicates the problem and requires a careful hierarchical approach if the design objectives are to be achieved. In this section, such an approach is outlined.

The decision hierarchy is illustrated in Figure 4-1. On the basis of observations taken on the voice frequency (VF) line, and without knowledge of the modem type, a preliminary and obviously gross assessment must be made concerning whether or not the channel has suffered a catastrophic failure. This might be the result of total loss of signal, or even the SNR ratio falling to an unacceptably low value. Here in the first step (Phase 1) of the hierarchy, some tests dealing with estimates of the channel SNR, or possibly tests using spectral analysis techniques may be considered.

Assuming that there is no indication of gross channel failure, the next phase (2) is the task of specifically identifying the modem type in service on the VF communication channel. This level of identification is necessary in order to be able to predict what is the "normal" channel activity for this modulation type. The classifier need not be completely effective. The classifier may fail to identify the correct modulation format with a sufficient degree of certainty. In this case the classifier may be directed to repeat the classification attempt on successive channel samples a fixed number of times. If a confident decision has not been achieved in this period, it can be declared that a degradation in the modem signal structure
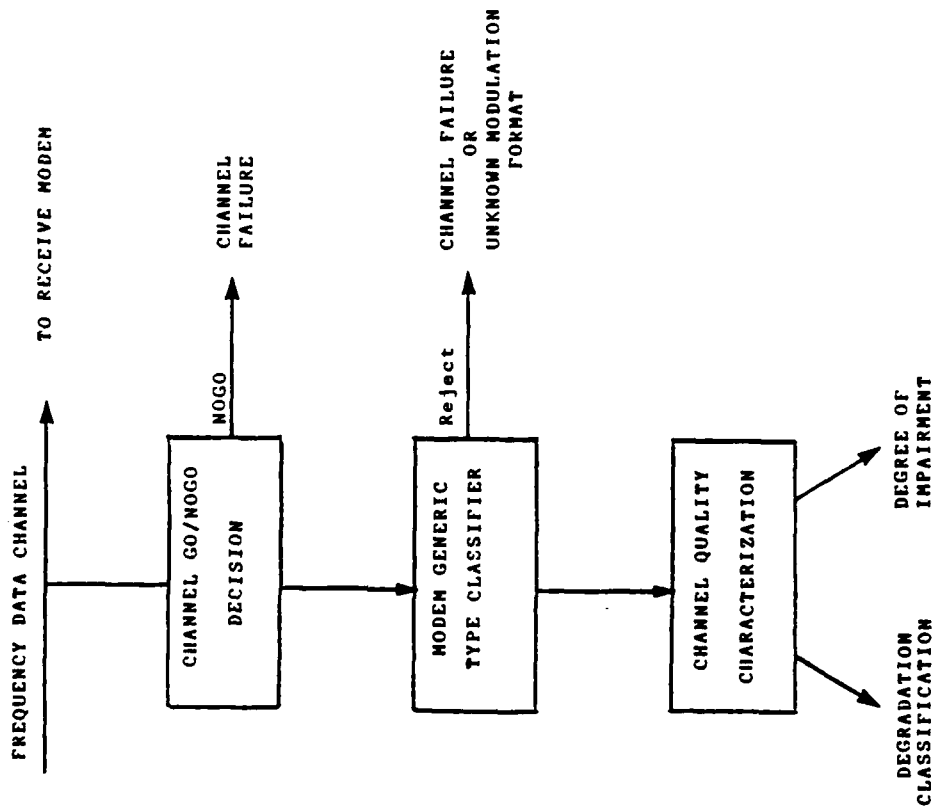
Figure 4-1: Hierarchical Approach to Performance Monitoring on Voice Frequency Channel

has occurred, rendering the signal unrecognizable, or that the actual modem type is not a member of the established set which the classifier is prepared to recognize.

Assuming the confident classification of the modulation format in Phase 2, it is then required to provide some quantitative evaluation of the amount and type of degradation affecting the channel. Phase 3 of the hierarchy is the quantitative evaluation of degradation and is by far the most difficult of the hierarchical tasks to be performed. It may require replication of typical modem receive functions such as bit synchronization, phase tracking, data demodulation, and in some cases adaptive equalization. It should be noted that the actual implementation of the modem receive functions may differ from that of any specific modem types. That is, if a correct identification of the modulation format has been made in Phase 2, then it is possible in principle to construct (in software) a generic modem which is functionally equivalent to the actual modem on the VF line under test. While in principle this replication of modem receive functions is possible, it is potentially complex in terms of implementation. Nevertheless, we proceeded under the assumption that any implementation can be achieved, so that the direction of the investigation would not be biased toward the readily realizable solution.

5. ALGORITHM INVESTIGATION

Throughout the course of this effort, a variety of algorithms were investigated for all phases of the hierarchical approach described in Section 4. It is frequent that algorithms overlap the boundaries between hierarchical tasks, being able to contribute to more than one phase of the problem. For this reason, the algorithms investigated will be presented here without strict observance in identifying the precise hierarchy. Rather, the choice of algorithms to be demonstrated, and the structure of the demonstration system will be the subject of Section 6.

5.1 MODEM SPECTRAL PROFILE ANALYSIS

The goal of the spectral analysis investigation was to evaluate the use of signal power spectra for use as a feature space from which decisions concerning the channel traffic type and/or channel quality could more readily be performed. One member of each modem group was selected. The spectral estimates of these signals are shown in Figures 5-1 through 5-11. Each plot represents the average of ten 1024-point power spectra. Hanning weighting has been applied and the plot is clipped off 40 dB down from the spectrum maximum. The horizontal divisions each mark 10dB. The frequency range is from 0 to 6400 Hz, or 256 Hz per vertical tic mark. Any DC component has been removed.

The first two spectra illustrate the FSK modulation type. The familiar carrier frequencies are easily detectable. The three DPSK, 1200 baud modems are shown in Figures 5-3 through 5-5. The lower edge of the pass band region for each sample contains spurious channel data, such as noise. The roll-off of the lower-edge for the three modems is not identical, which is required if any feature measurements are to be made in this region for the purposes of generic type identification. A potentially valuable feature is shown in the PAM, 4800 baud signal spectrum (PARADYNE LSI-96) shown in Figure 5-10. Here the 2853 Hz carrier is apparent above the other pass band components.
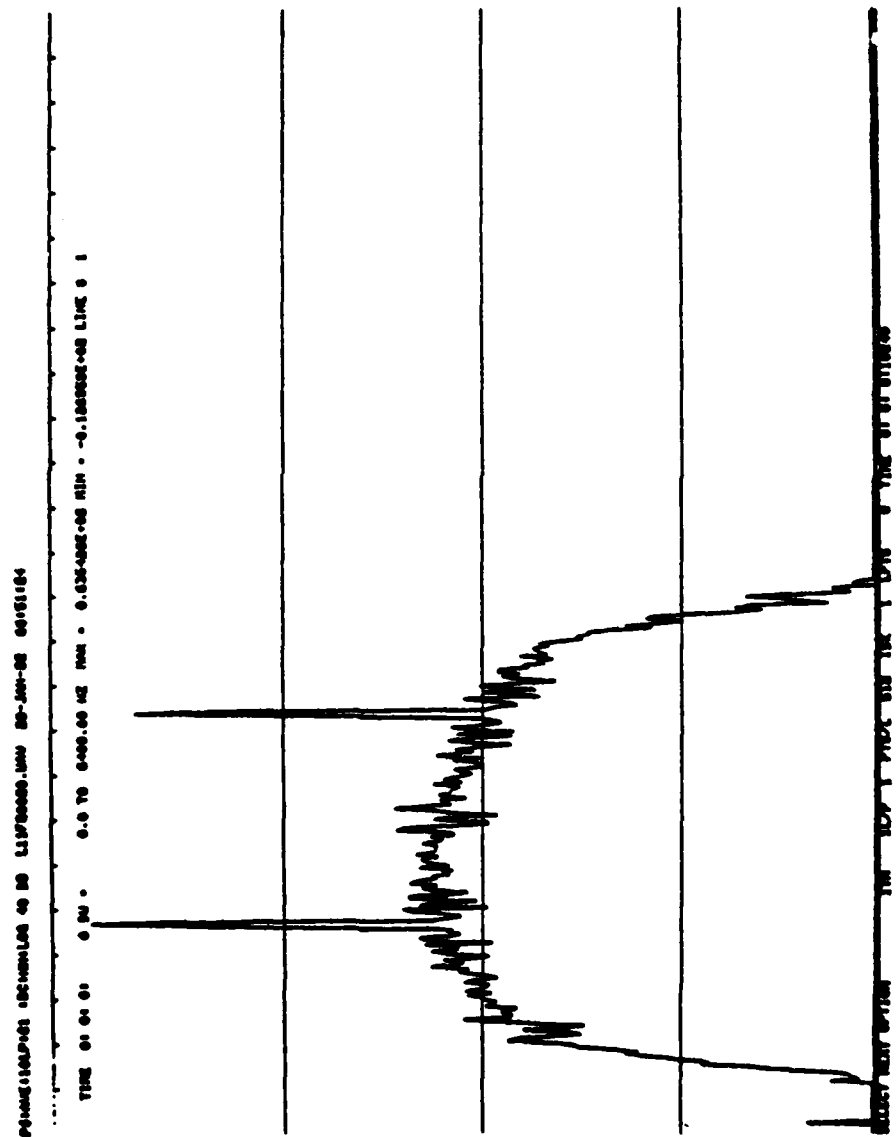
Figure 5-1: LENKURT 26-C Signal Spectrum Average of 10 Lines, Hanning Weighted on a 40 dB Log Scale
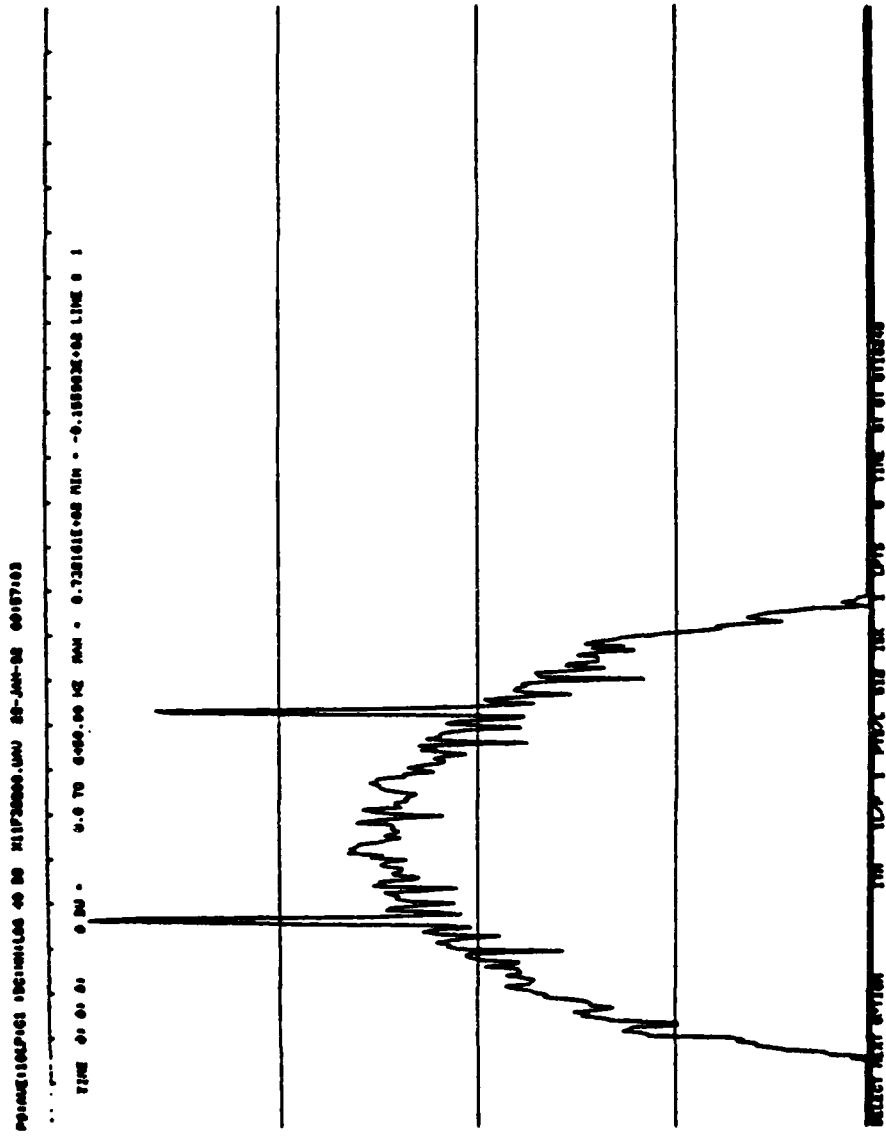
Figure 5-2: MD-674 Signal Spectrum Average of 10 Lines, Hanning Weighted on a 40 dB Log Scale
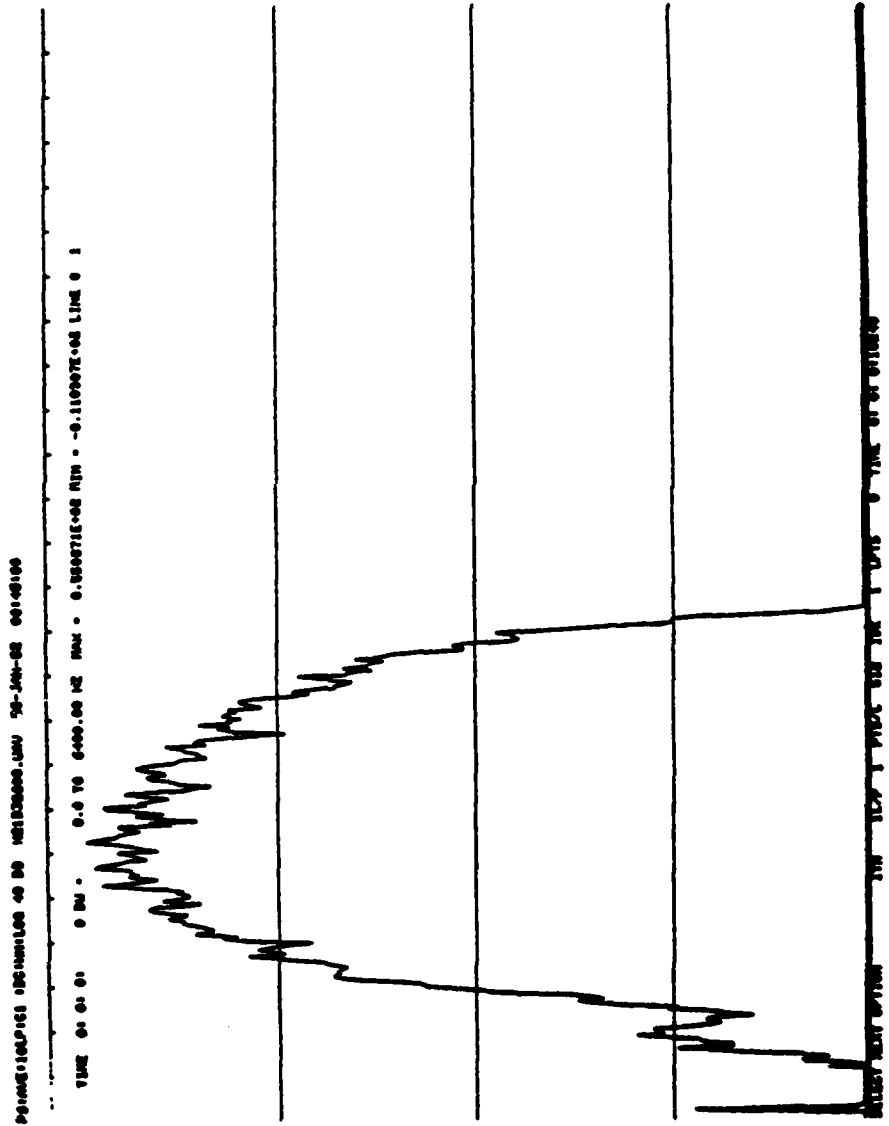
Figure 5-3: HUGHES HC-276 Signal Spectrum Average of 10 Lines, Hanning Weighted on a 40 dB Log Scale
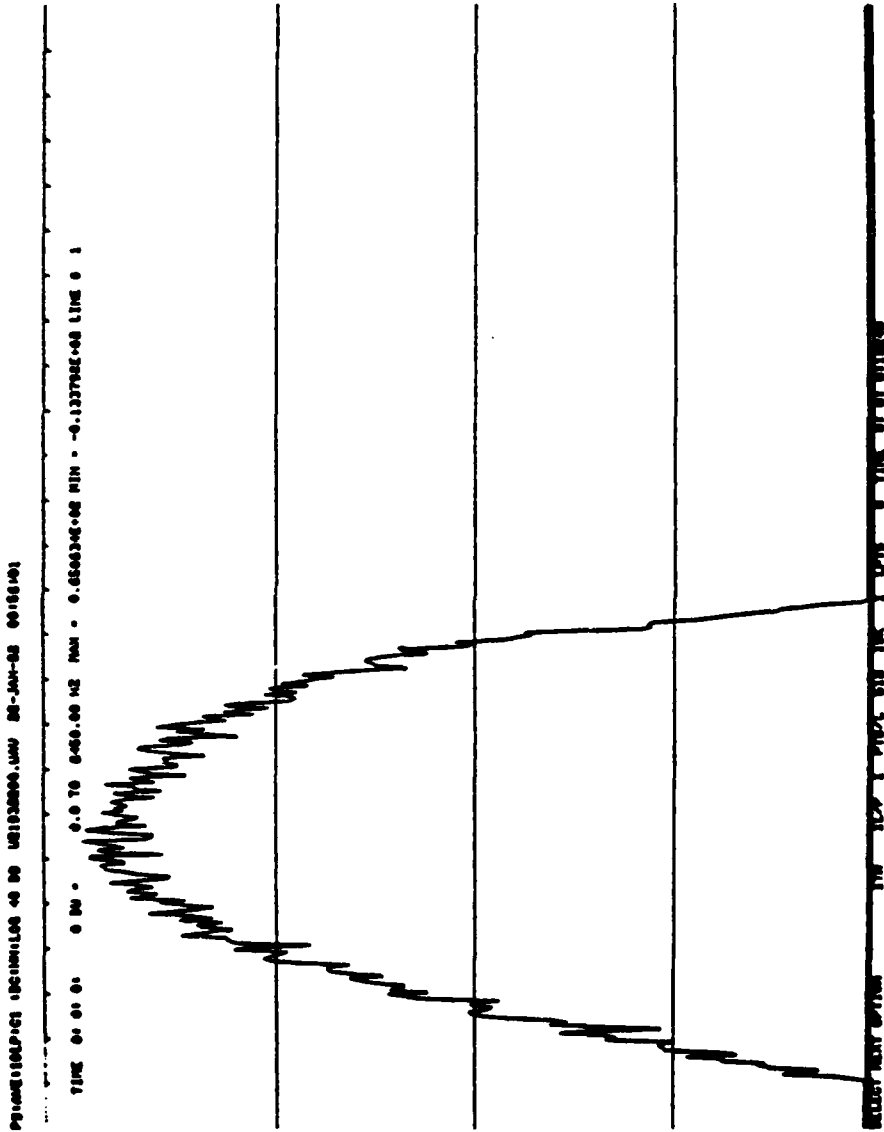
Figure 5-4: MECO 207A2 Signal Spectrum Average of 10 Lines, Hanning Weighted on a 40 dB Log Scale
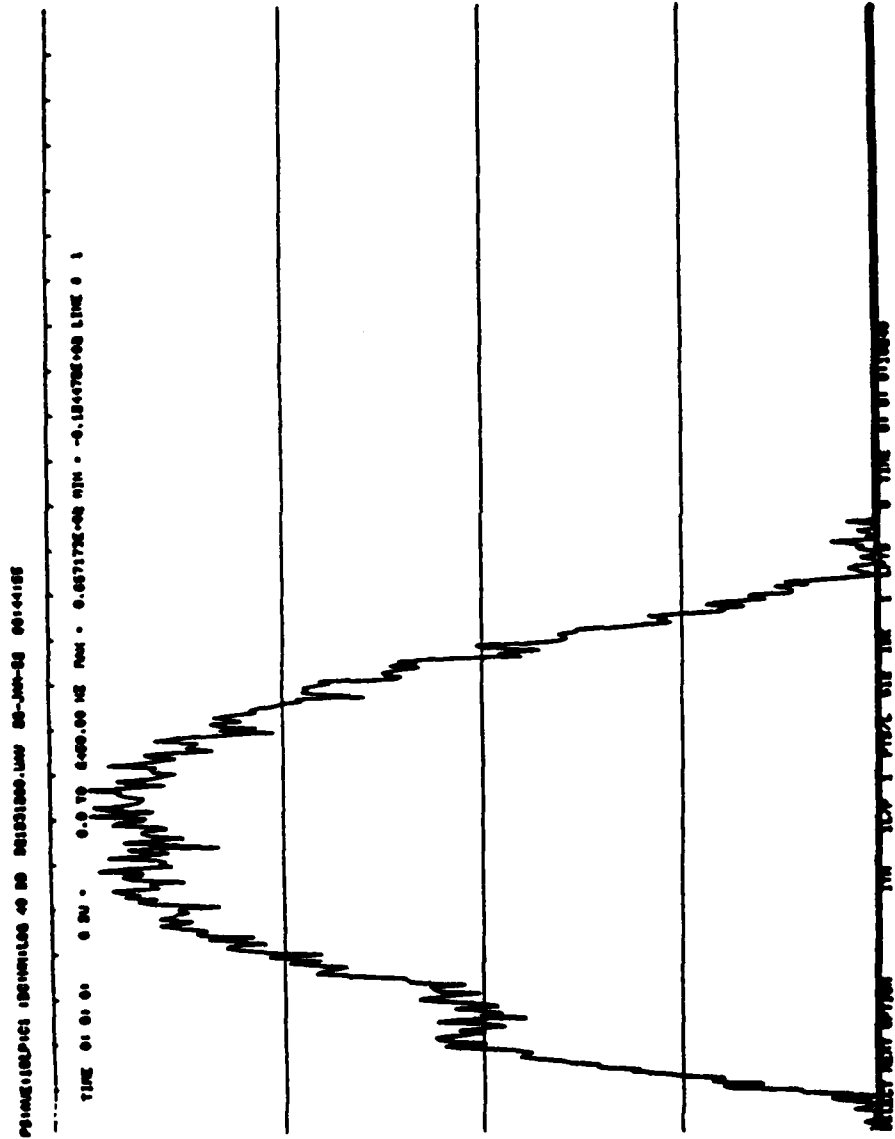
Figure 5-5: CODEX LSI-48 Mode B Signal Spectrum Average of 10 Lines, Hanning Weighted on a 40 dB Log Scale

Figure 5-6: CODEX LSI-48 Mode A Signal Spectrum Average of 10 Lines, Hanning Weighted on a 40 dB Log Scale
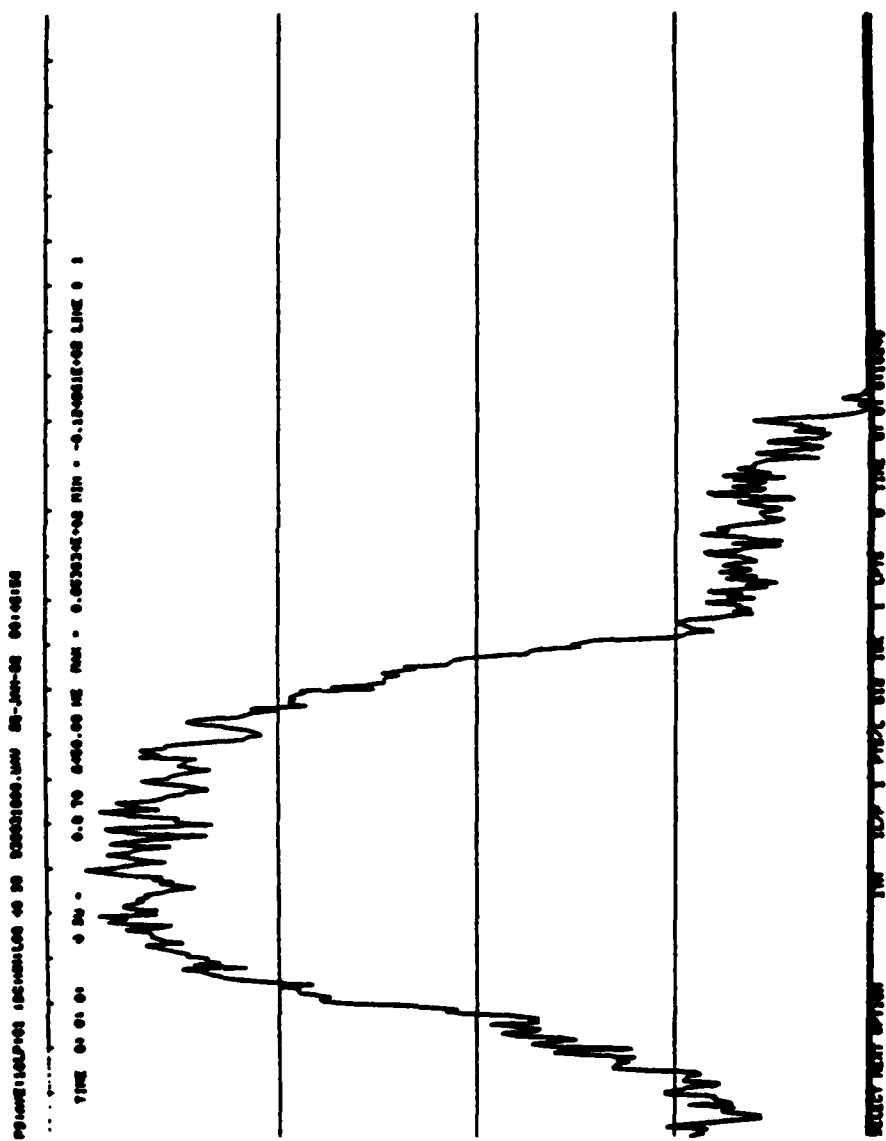
Figure 5-7: CODEX LSI-48 Mode C Signal Spectrum Average of 10 Lines,
Hanning Weighted on a 40 dB Log Scale
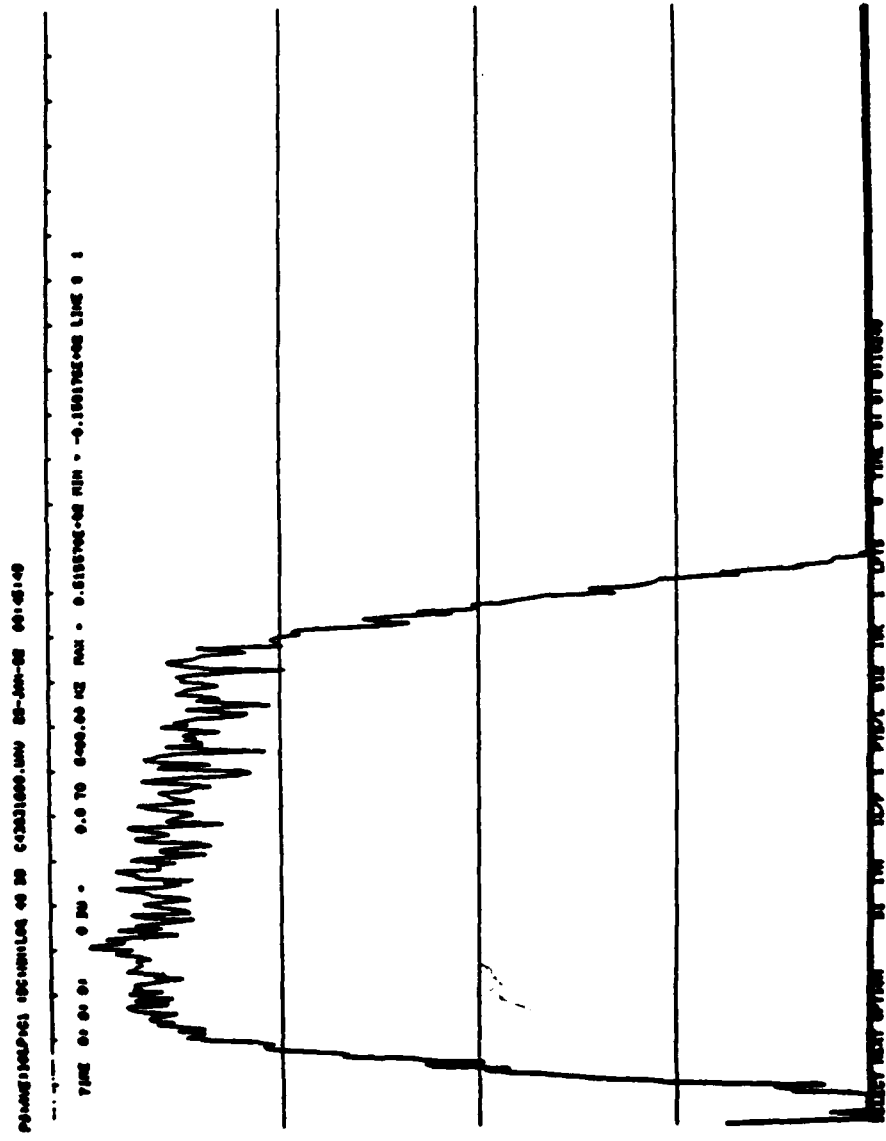
Figure 5-8: CODEX LSI-96 Signal Spectrum Average of 10 Lines, Hanning
Weighted on a 40 dB Log Scale
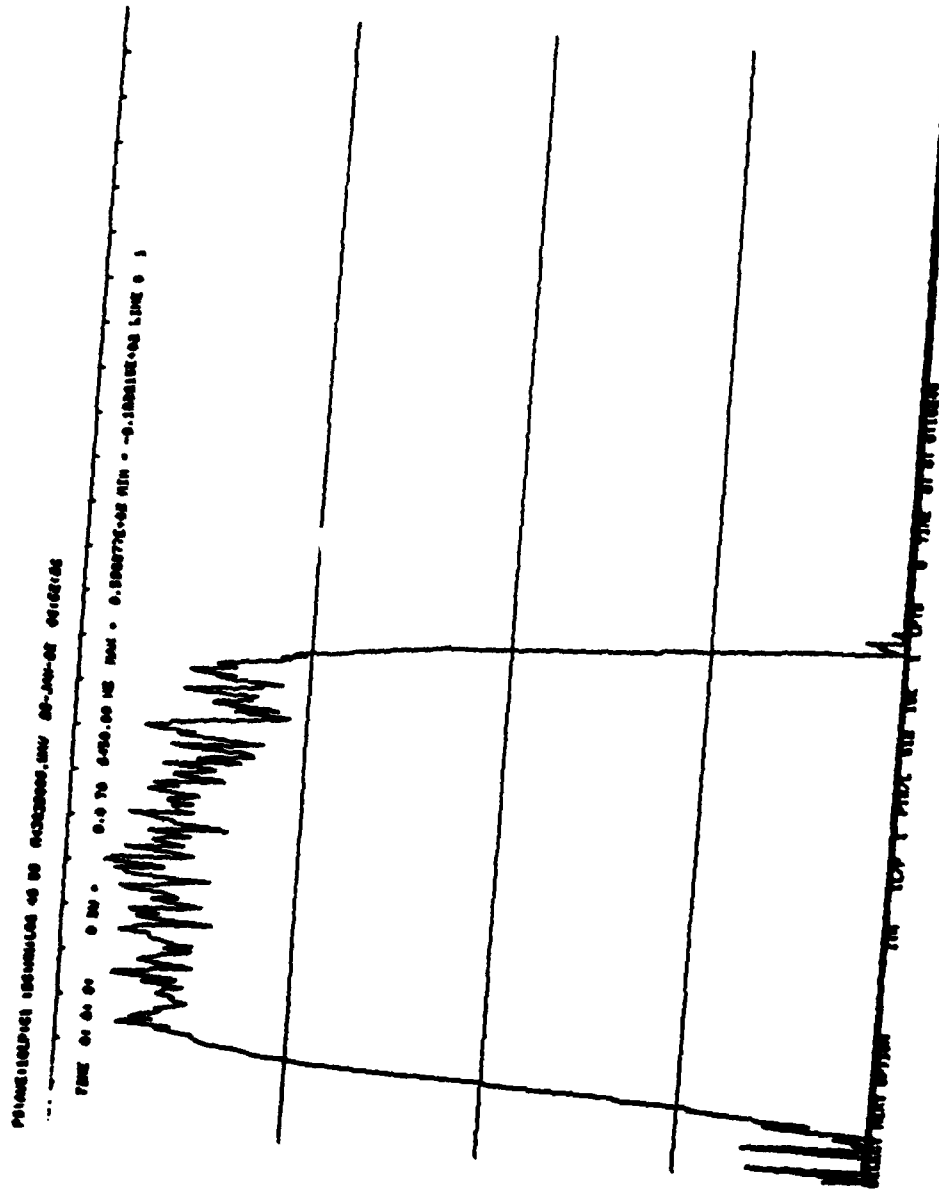
Figure 5-9: PARADYNE MP-96 Signal Spectrum Average of 10 Lines, Hanning Weighted on a 40 dB Log Scale
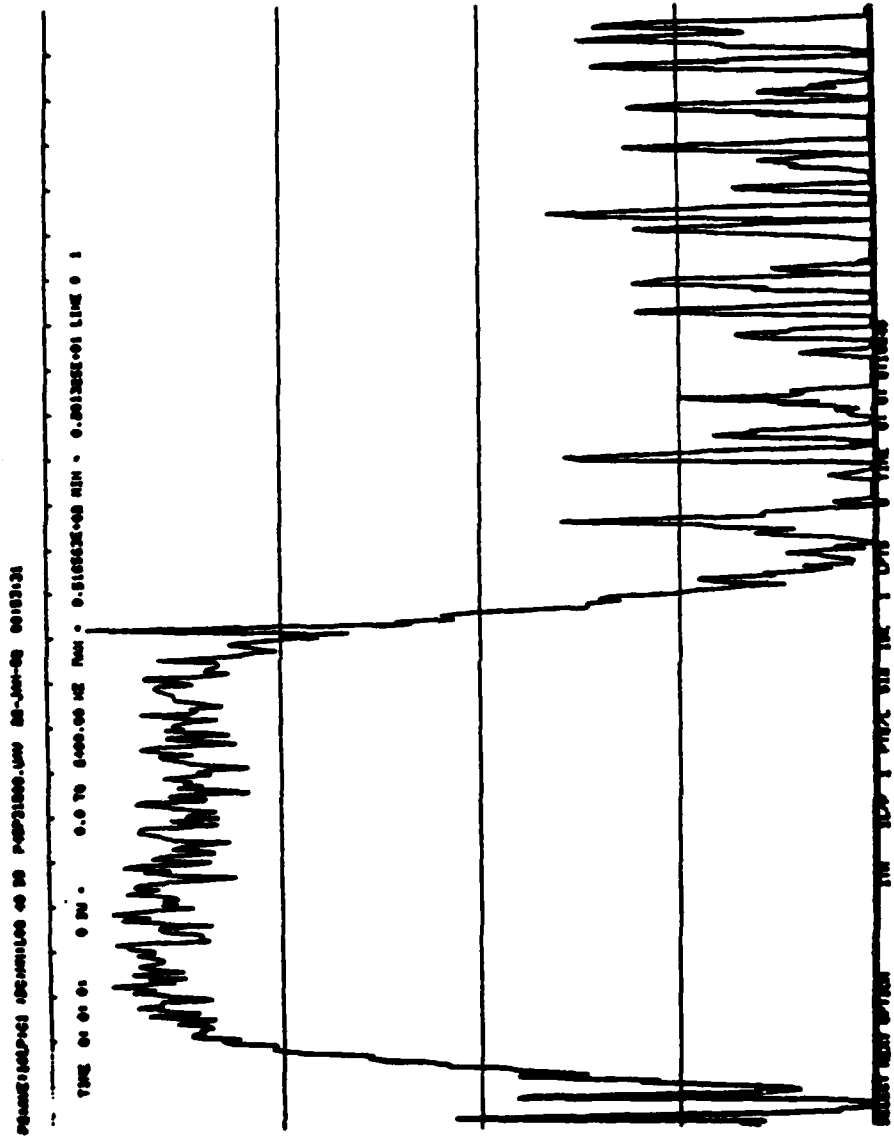
Figure 5-10: PARADYNE LSI-96 Signal Spectrum Average of 10.Lines, Hanning Weighted on a 40 dB Log Scale
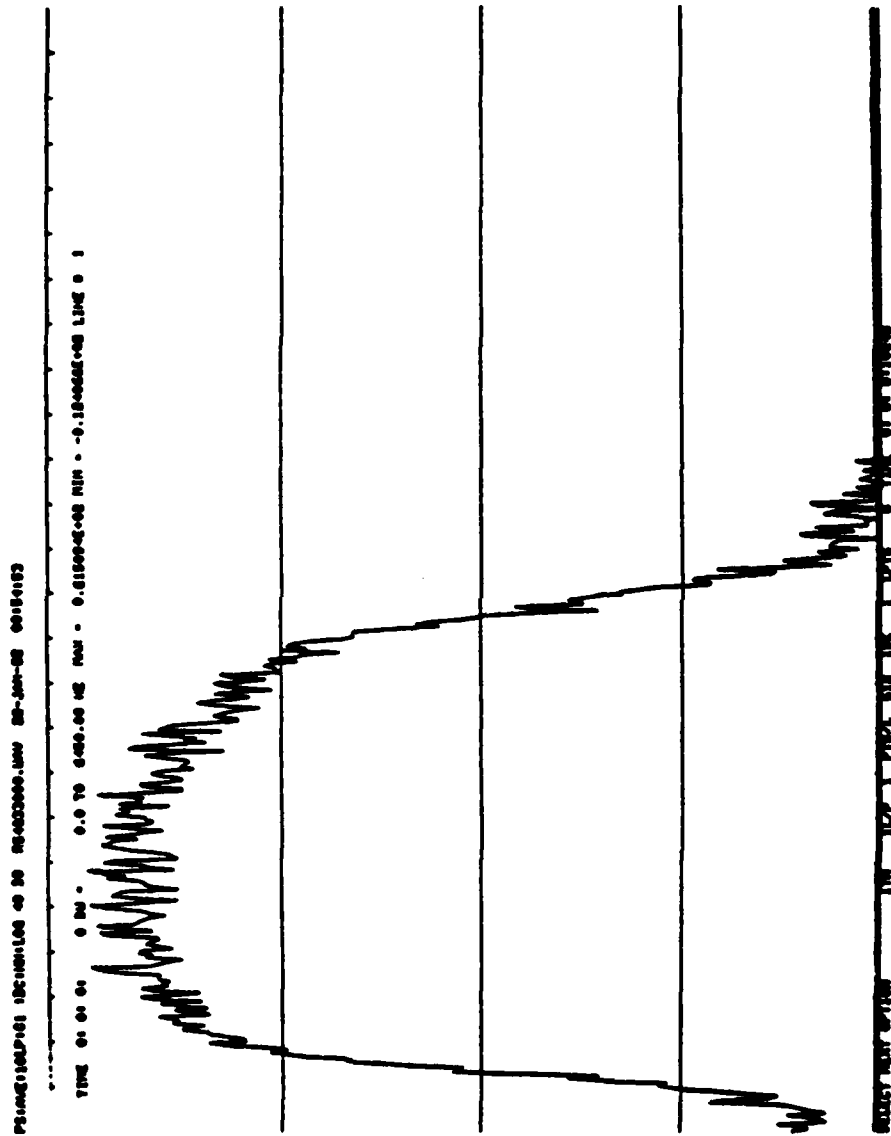
Figure 5-11: HARRIS 5238 Signal Spectrum Average of 10 Lines, Hanning Weighted on a 40 dB Log Scale

Another technique used to reveal signal properties was to apply full-wave rectification prior to the spectrum computation. This process was shown to be very effective in enhancing the spectral component at the baud rate. Figures 5-12 through 5-15 show the power spectral average for the FSK 1200 baud, DPSK 1200 baud, DPSK 1600 baud and QAM 1600 baud signals, respectively. No baud component enhancement occurred for the higher speed modems.

5.2 AUTO-CORRELATION ANALYSIS

As a prerequisite to the determination of the type and degree of impairments affecting the channel under study, an identification of the channel traffic to a level of generic type must be performed. Without such information, it is not known what signal parameters represent a "normal" low-error operating mode.

Previous attempts at classification of the modems used an equivalent to the autocorrelation function generated from a 1-bit quantized version of the modem signal. Based on the previous success of these features, the autocorrelation function was used as the feature space in which the generic modem type separation would be investigated. The classification problem has become greatly complicated since the work performed on the original four modem database. The 11 modems studied represent seven unique generic signaling strategies. The goal of this investigation is to design a practical classifier for the seven generic classes to determine the modulation type, baud rate, and carrier location information required in the forthcoming channel impairment characterization.

The training set for the classifier corresponded to the first 30 lags of the autocorrelation function given by

$$C_{(m)} = \sum_{q=\phi}^{M-m-1} A(m+q) * A(q)$$
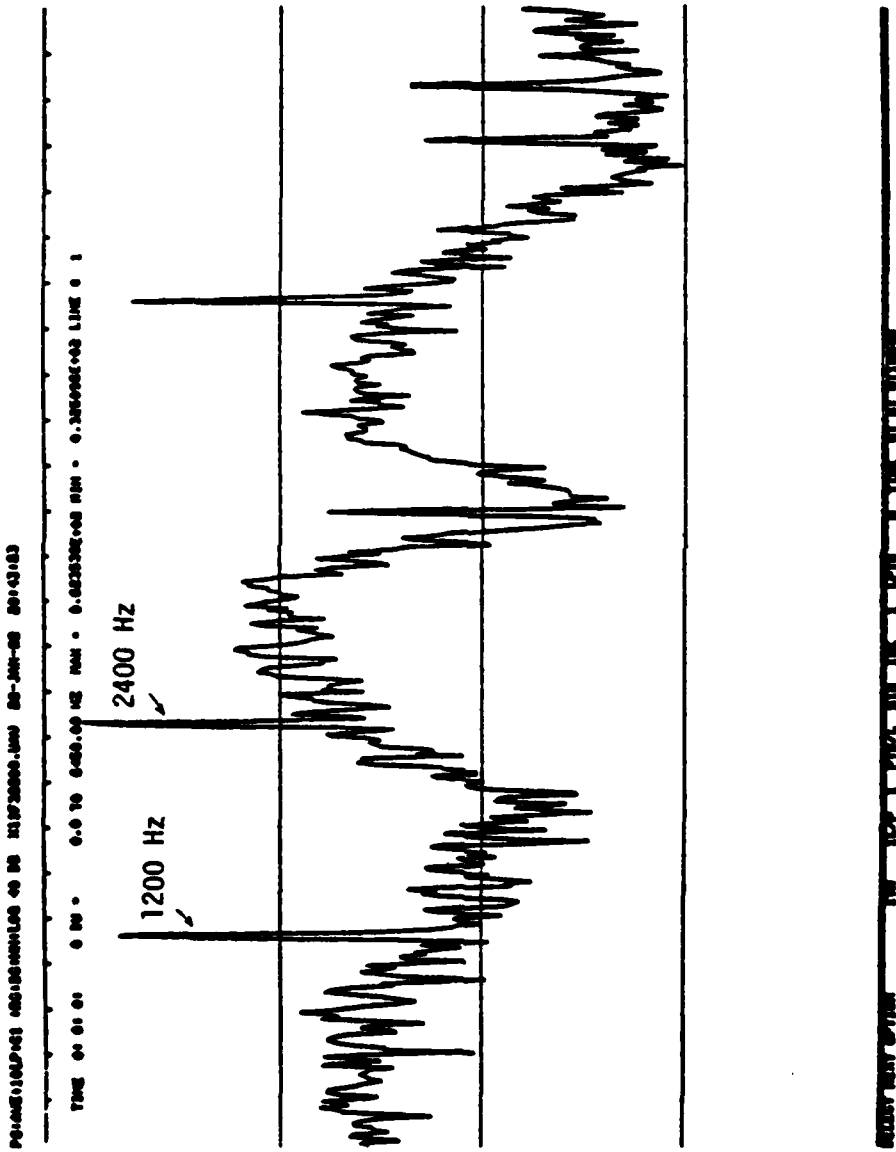
Figure 5-12   FSK 1200 Baud Modem Spectral Average of Rectified Signals on a
40 dB Log Scale
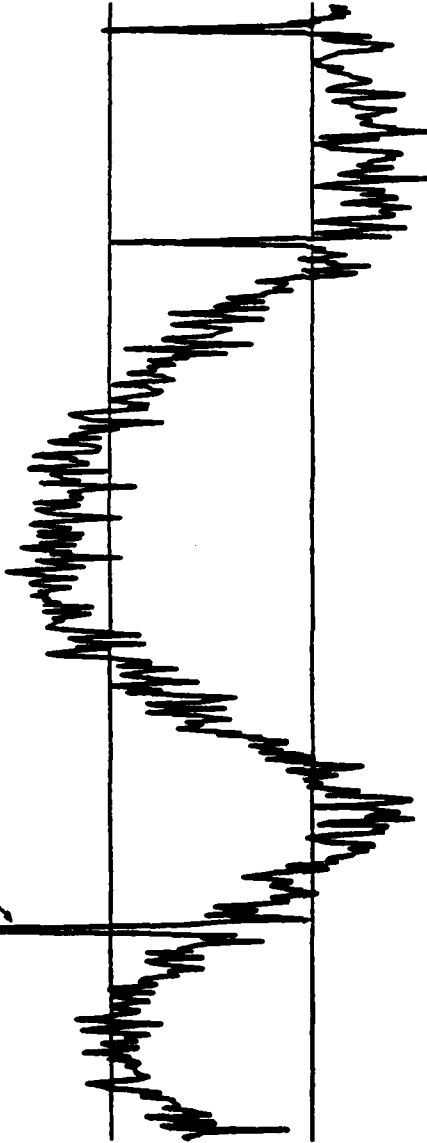
Figure 5-13   DPSK 1200 Baud Modem Spectral Average of Rectified Signal on a 40 dB Log Scale
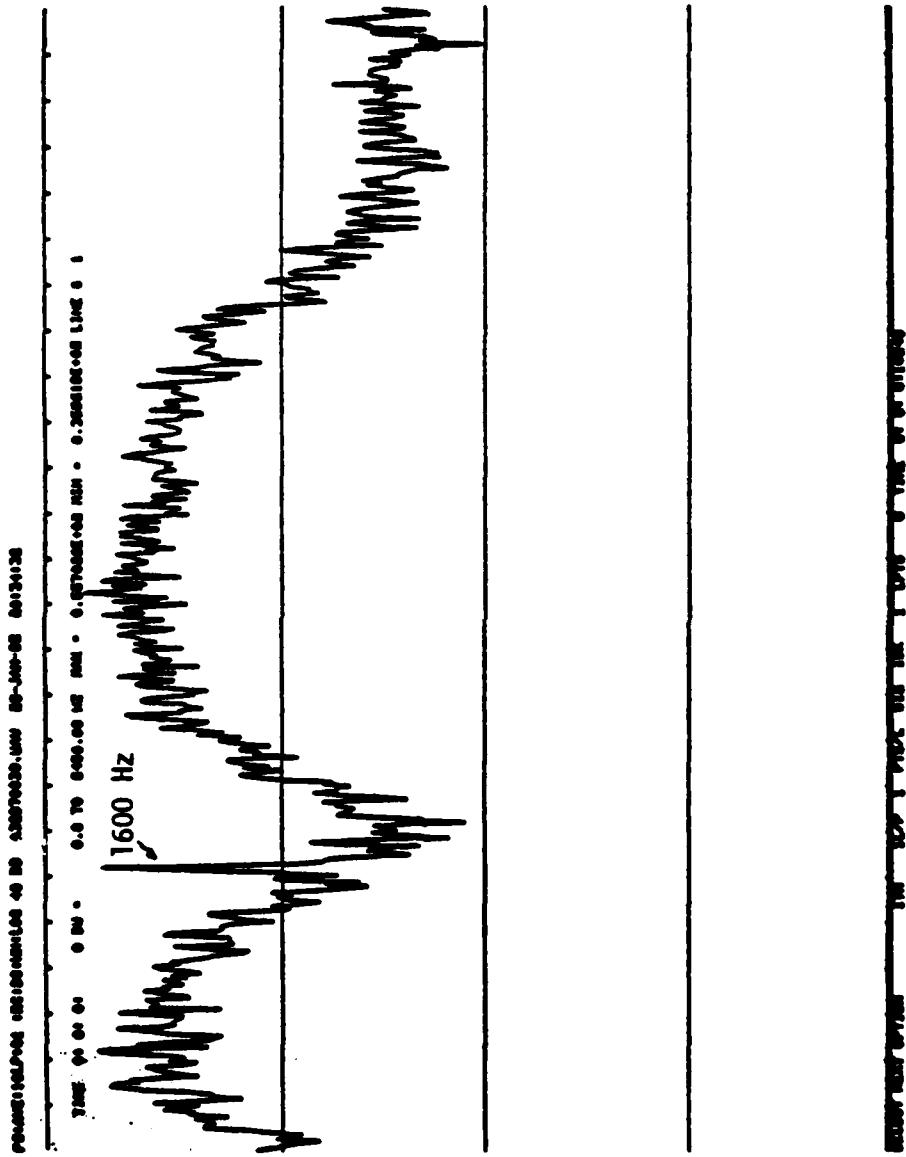
Figure 5-14   DPSK 1600 Baud Modem Spectral Average of Rectified Signal on a 40 dB Log Scale
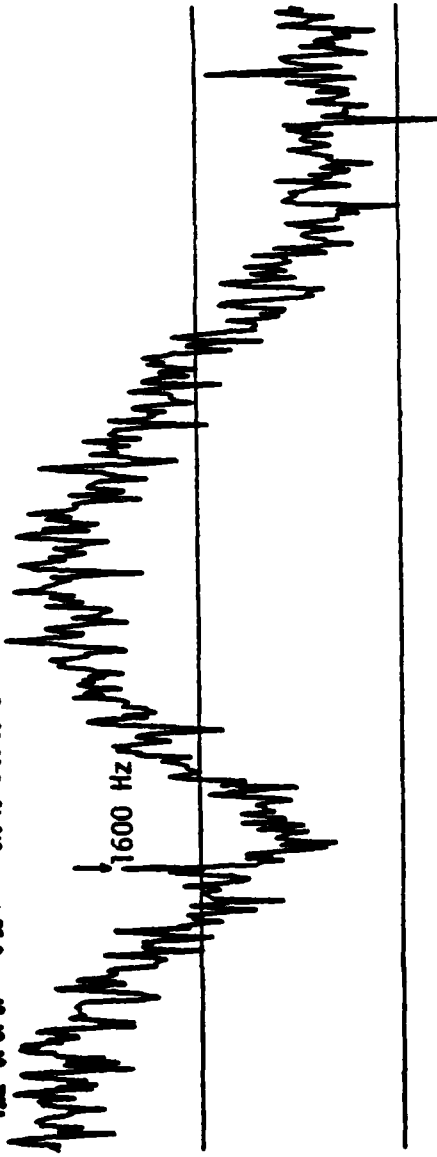
Figure 5-15 QAM 1600 Baud Modem Spectral Average of Rectified Signal on a 40 dB Log Scale

where:

        m is the desired lag

        M is the number of data points in the correlation window

        A is the input modem signal waveform

Clearly, lag ($\emptyset$) corresponds to the input signal squared, or the total power for the zero-mean input signal. In order to minimize the effects of collection gain variations, lag ($\emptyset$) was always used to normalize the feature vector (of the first 30 lags).

After much preliminary investigation, it was decided to narrow the scope of the investigation to two autocorrelation window lengths, 3,000 samples and 8,000 samples. Both the un-quantized signal and the 1-bit quantized signal were considered; where the 1-bit quantization is defined as:

IF A (i) > $\emptyset$, then A (i) = 1; else A (i) = $\emptyset$

It was concluded that both the 1-bit quantized signal waveform autocorrelation and the full 12-bit quantized version showed merit. These four cases will be explored in the remainder of this section.

Figures 5-16 through 5-26 show a plot of the autocorrelation function of each modem for the case of an 8,000 sample correlation window of 1-bit quantized signal data. Also contained in these figures is the signal spectrum estimate obtained from performing an FFT on the autocorrelation function. During this investigation, only the autocorrelation functions were used as features. The signal spectrum is provided for inspection purposes only.
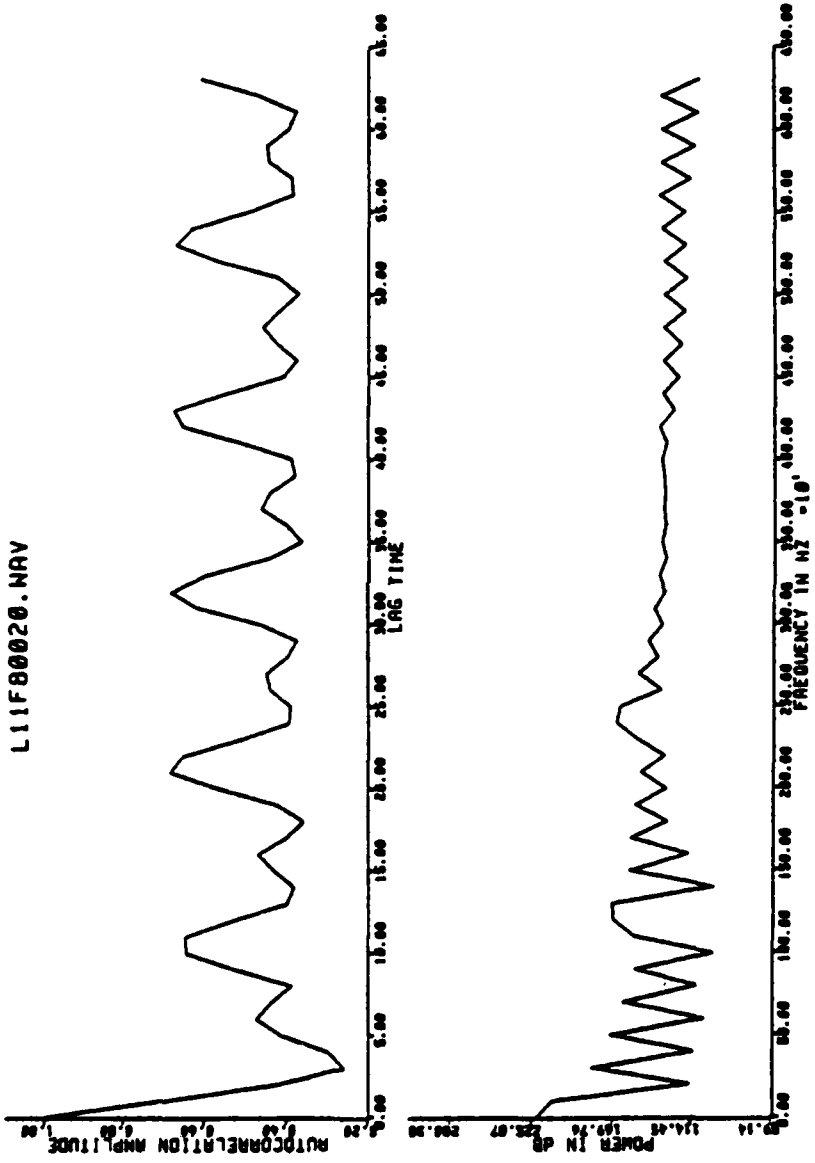
Figure 5-16: First 64 Lags of the Auto-Correlation Function for the LENKURT 26-C Modem

X11F32200.WAV
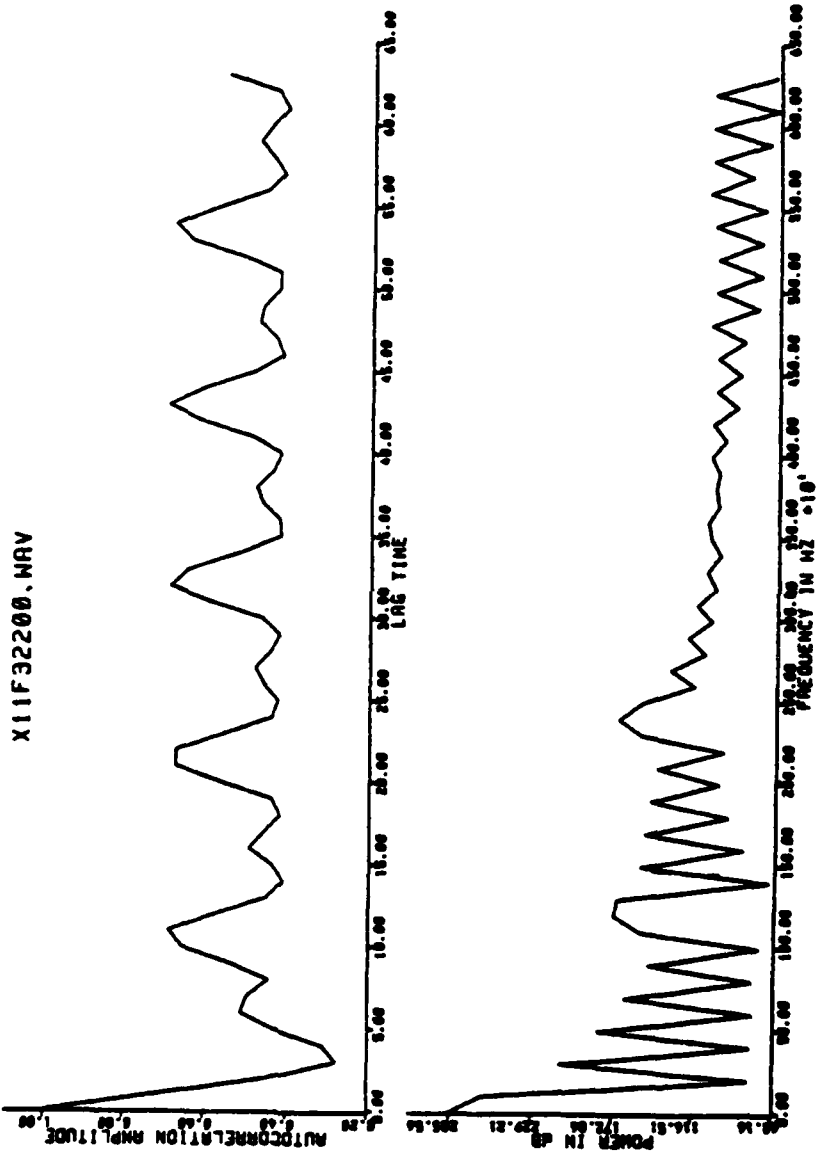
Figure 5-17: First 64 Lags of the Auto-Correlation Function for the MD-674 Modem
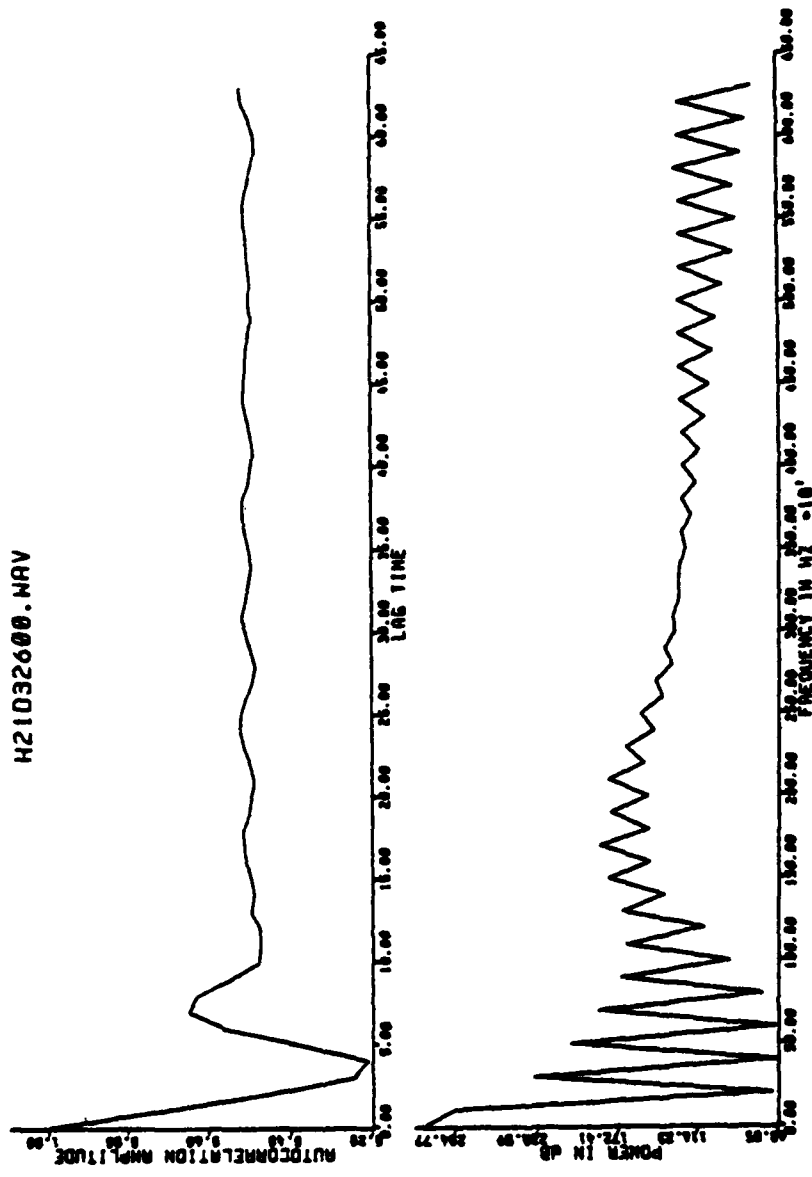
Figure 5-18: First 64 Lags of the Auto-Correlation Function for the HUGHES
HC-276 Modem
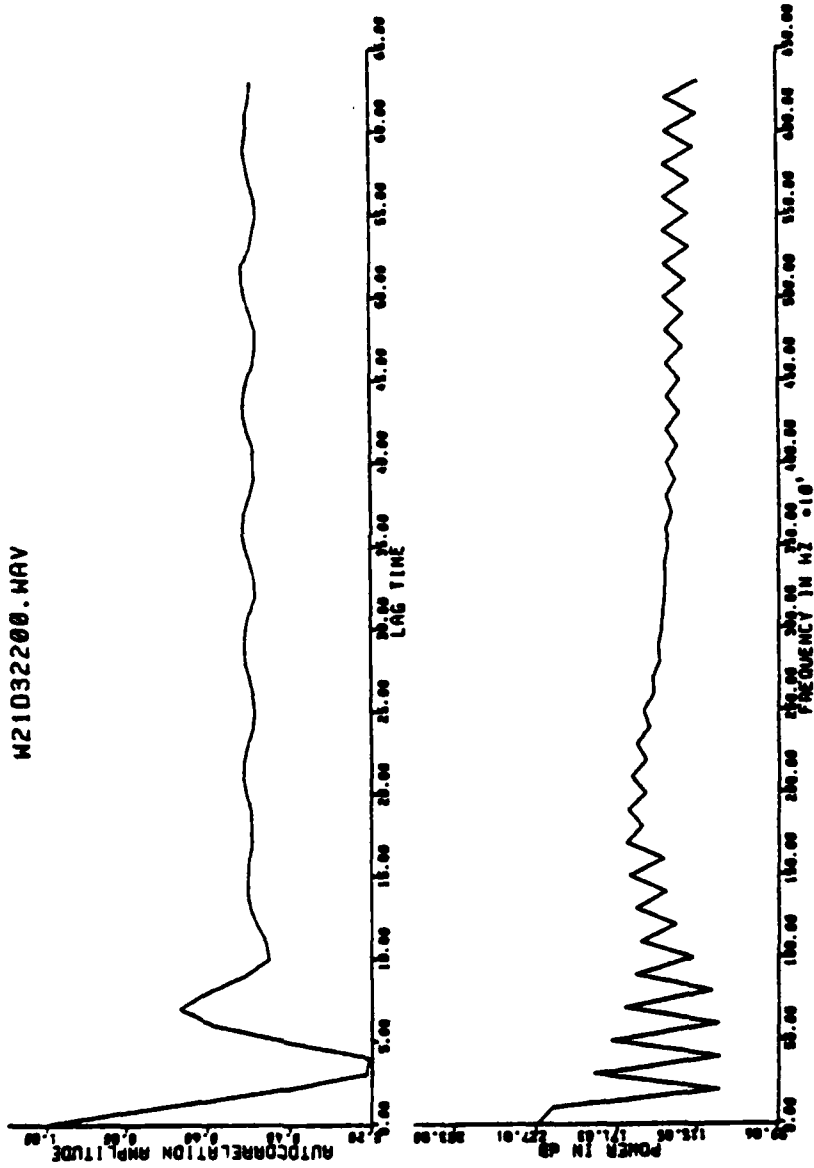
Figure 5-19: First 64 Lags of the Auto-Correlation Function for the WECO 207A2 Modem
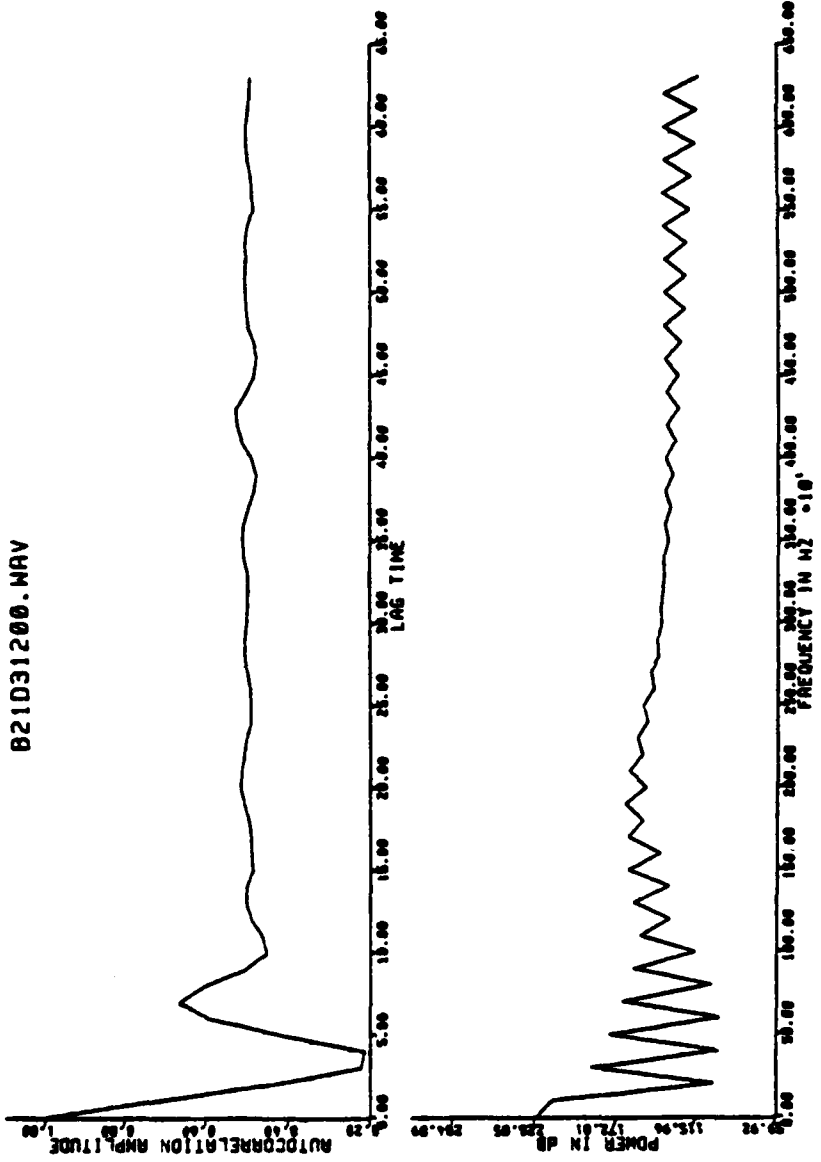
Figure 5-20: First 64 Lags of the Auto-Correlation Function for the CODEX
LSI-48 Mode B Modem

A32D70030.NAV
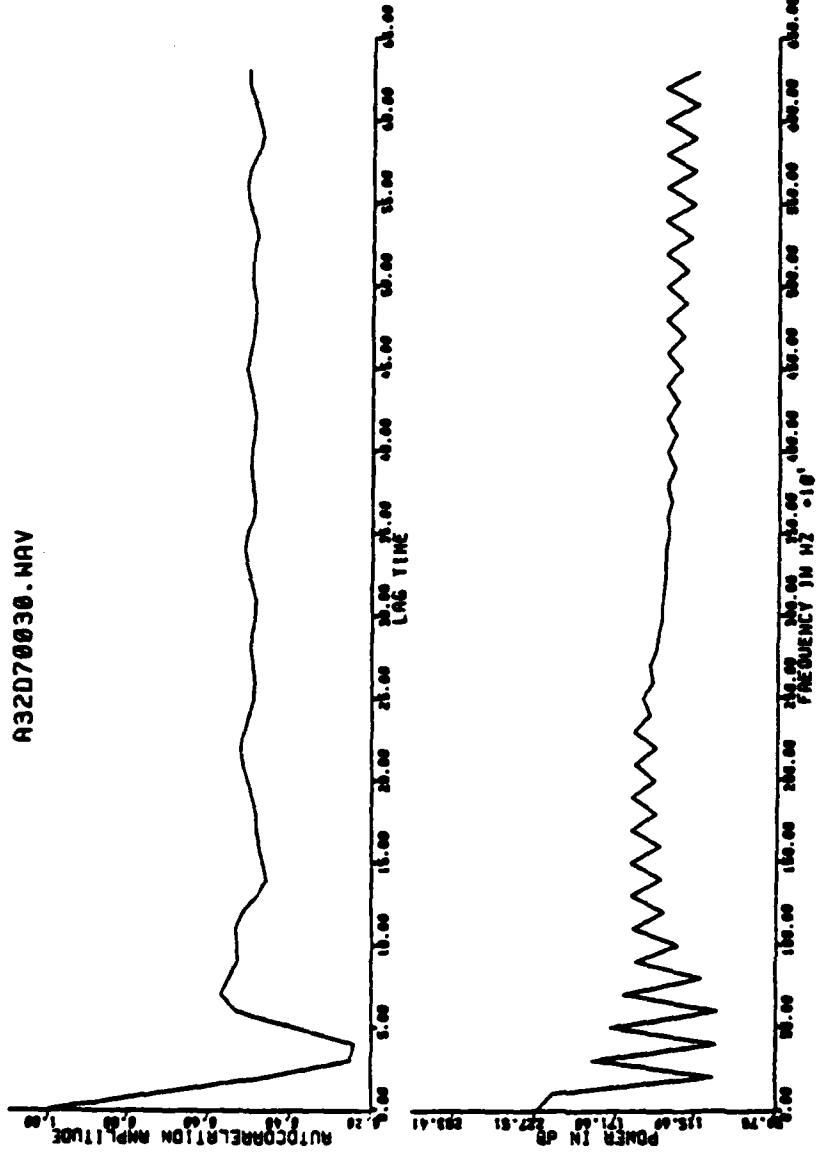
Figure 5-21: First 64 Lags of the Auto-Correlation Function for the CODEX
LSI-48 Mode A Modem
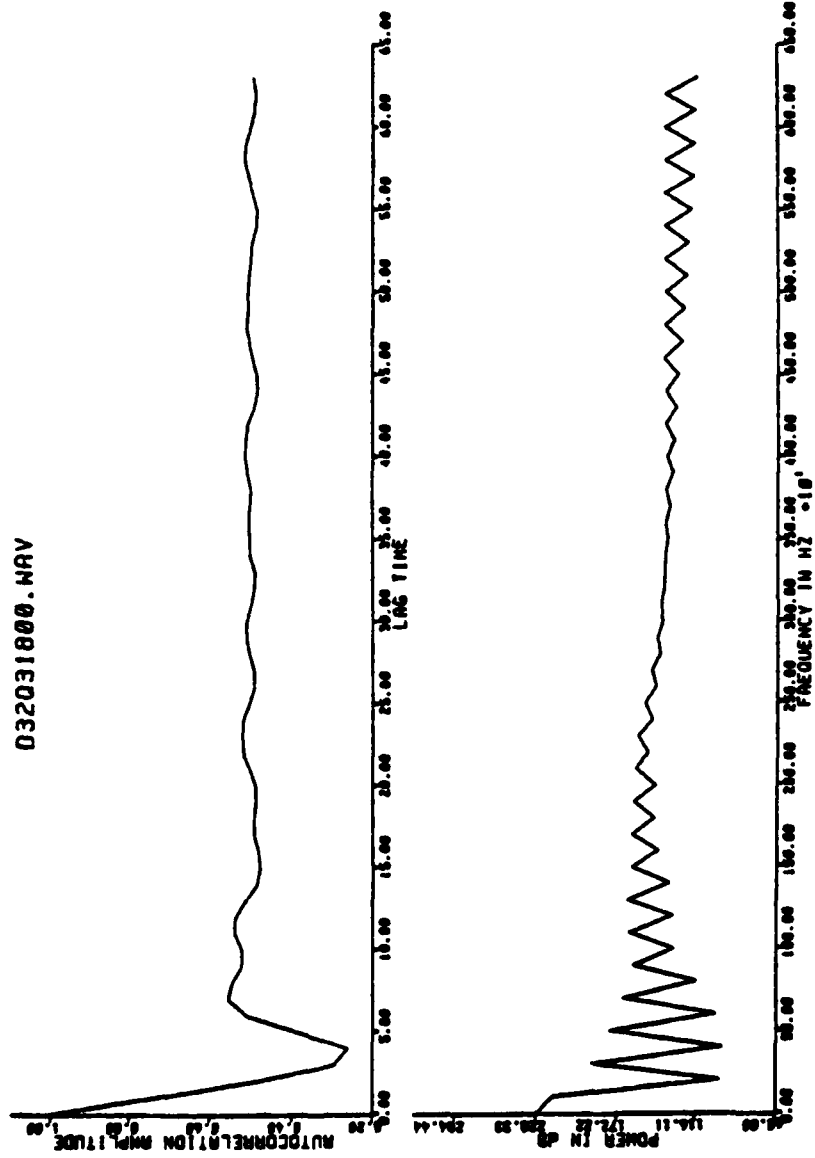
Figure 5-22: First 64 Lags of the Auto-Correlation Function for the CODEX LSI-48 Mode C Modem

C42031600.WAV
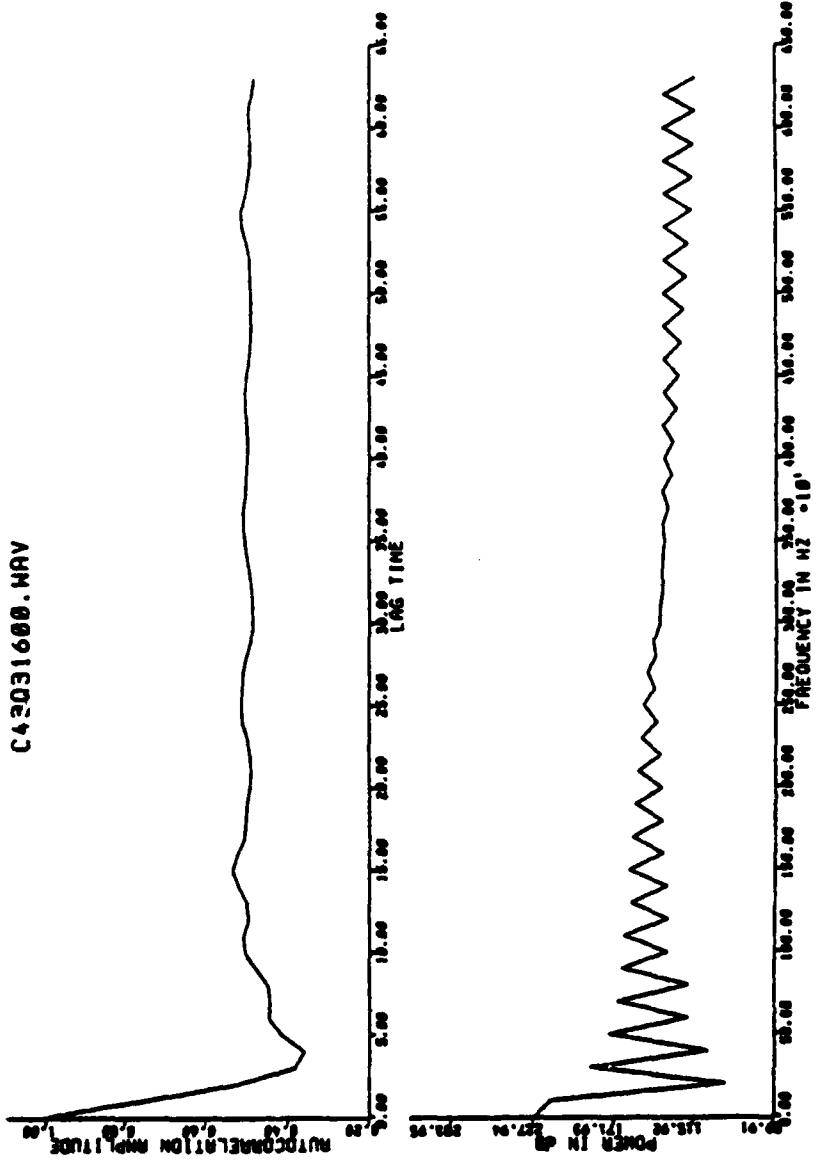
Figure 5-23: First 64 Lags of the Auto-Correlation Function for the CODEX
LSI-96 Modem

P4SP31800.WAV
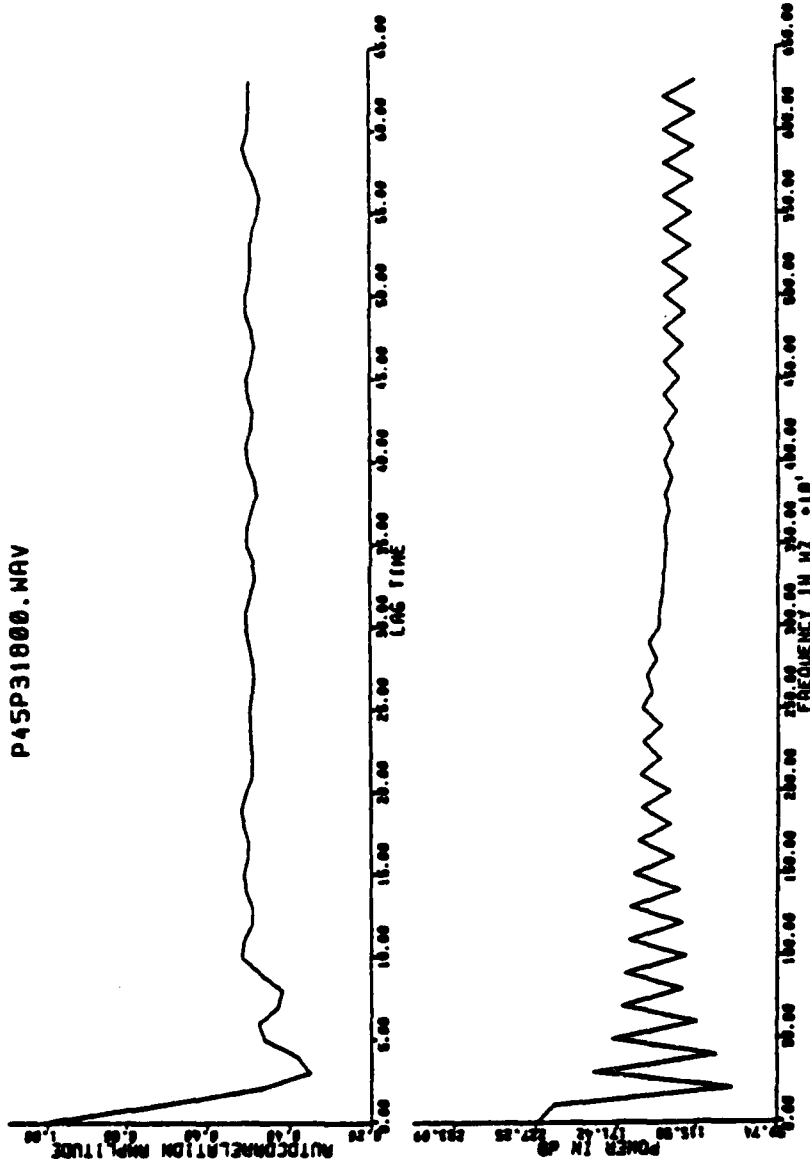
Figure 5-24: First 64 Lags of the Auto-Correlation Function for the
PARADYNE LSI-96 Modem
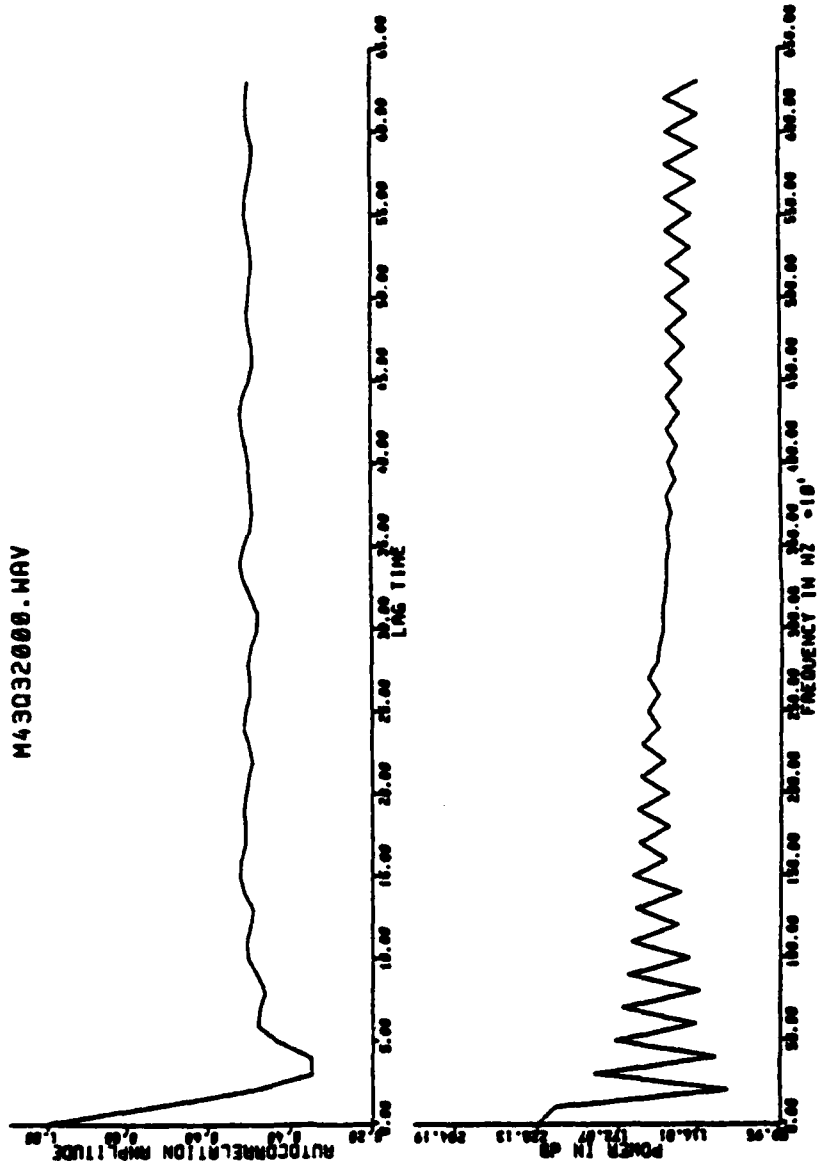
Figure 5-25: First 64 Lags of the Auto-Correlation Function for the PARADYNE MP-96 Modem
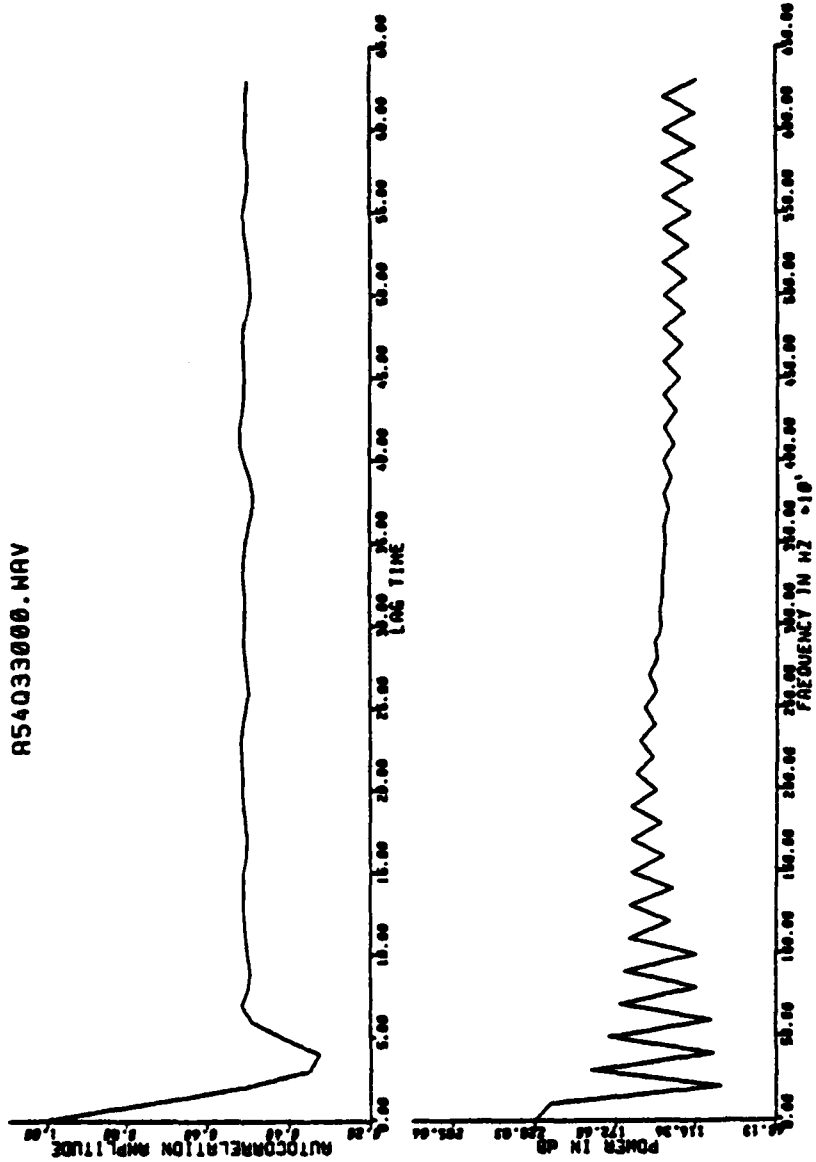
Figure 5-26: First 64 Lags of the Auto-Correlation Function for the HARRIS 5238 Modem

5.2.1 OLPARS Investigation Of A Practical Generic Classifier

The pattern recognition problem of the MODEM Signature Analysis effort is composed of feature extraction, that is, the definition of measurements, and of pattern classification. The objective in selecting features for the MSA data base is to provide a set of measurements which yield information to aid in discriminating among the various modem generic types, even in the presence of severe channel distortions. The features used for discriminating among different modem types in the OLPARS analysis are the lag amplitudes of the autocorrelation function of the raw time waveforms and the 1-bit quantized waveforms of the MSA data base. The analysis of the MSA data base was aided by use of the OLPARS system which helped perform both the pattern analysis and pattern classification for the MSA effort.

After computation of the feature vectors from the autocorrelation functions, we were ready to begin a pattern recognition and classification analysis on the data. The OLPARS system uses a structured vector filing system for data handling. A tree structure was created from the MSA data base which included 7 classes, each class being a particular modem generic type. Figure 5-27 illustrates the 7-class tree structure. Each class such as C1200PSK and C1600PSK represent the modems with modulation strategies of PSK at 1200 and 1600 baud, respectively. Following each class name is the assigned class symbol and the total number of vectors for each sub-class are printed.

The modem naming convention seen throughout the OLPARS analysis is that presented in Table 3-3. The right-most column of names in Figure 5-27 is the list of vector file names. Each of these names represents one modem type for all cases of particular impairment. For example, the first vector file name of the right-most column of Figure 5-27 is "L11F2". Table 3-3 decodes this as "LENKURT 26-C, 1200 bits per second, 1200 baud, FSK, harmonic distortion added". This file contains all cases of harmonic distortion for the LENKURT 26-6 modem. Vector file name "L11F3" decodes as "LENKURT 26-C, 1200 bits per second, 1200 baud, FSK, Gaussian noise added", and contains all cases of

VECTOR COUNT

Label		
L11F2	40.	10
L11F3	35.	10
L11F6	75.	10
X11F3	27.	10
X11F6	42.	10
B21D3	24.	10
B21D6	12.	10
H21D2	16.	10
H21D3	14.	10
H21D6	24.	10
U21D3	24.	10
U21D6	21.	10
A32D3	21.	10
A32D6	9.	8
D32O3	21.	10
D32O6	9.	8
C43O2	24.	10
C43O3	32.	10
C43O6	32.	10
M43O3	9.	8
M43O6	7.	6
R54O3	36.	10
R54O6	21.	10
P45P2	16.	10
P45P3	14.	10
P45P6	32.	10

L11F
X11F
B21D
H21D
U21D
A32D
D32O
C43O
M43O
R54O
P45P

PLOT SYMBOL

C1200FSK F
C1200PSK D
C1600PSK d
C1600QAM Q
C2400QAM q
C2667QAM A
C4800PAM P

BAUDMOD

> : <CR> TO CONTINUE EOJ:

5-31

Figure 5-27: Data Tree Structure Illustration for the Generic Modem Type Separability Investigation

additive Gaussian noise for the LENKURT 26-C modem. "L11F6" contains all cases of added phase jitter for the LENKURT 26-C modem. Note that for the OLPARS analysis, all cases of added phase jitter for a particular modem, regardless of the frequency, were combined into a single vector file and labeled by the impairment code "6". (Table 3-3 identifies impairment code "6" as 10 Hz phase jitter). Next vectors files L11F2, L11F3 and L11F6 which contain cases of harmonic distortion, Gaussian noise and phase jitter, respectively, are combined into "L11F" (on Figure 5-27). "L11F" decodes as "LENKURT 26-6 1200 bits per second, 1200 baud, FSK" and contains all cases of all impairments for the LENKURT 26-C modem. Similarly, "X11F" contains all cases of all available impairments for "MD-674, 1200 bits per second, 1200 baud, FSK". "L11F" and "X11F" are combined into "C1200FSK" which is all cases

of 1200 baud FSK for all impairments. This class has been assigned the plot symbol "F". In a similar fashion, Table 3-3 can be used to decode any of the generic name information of Figure 5-27 and the remainder of the OLPARS analysis.

With the class structure defined, the next step is to perform a structure analysis on the data. Structure analysis is performed as a prelude to classifier design in order to verify that the specified tree structure (of 7 classes) is actually present in the data as defined by the extracted features. The second reason for structure analysis is to detect the presence of multi-modality in the data. Since classifier design is usually dependent on the class statistics, multi-modality can cause gross classifier errors depending on the particular modality. OLPARS supports a variety of options to aid the user in this investigation. A subset of that investigation will be discussed here.

After the means and covariance matrices are computed for each class, the two eigenvectors corresponding to the two largest eigenvalues of the convarience matrix are used as a projection basis into a two-dimensional space. This 2-D subspace has the property of being the optimal subspace in a least-squares sense (best fit to the current data). This projection (shown in

Figure 5-28) is displayed as an indication of the class clustering and separation between different classes in the modem data base.

It is apparent from the projection that the separation between the seven classes is quite good based on the features used. The features which were used in the eigenvector projection shown in Figure 5-28 are lags 1,2,3,4, and 6 from the computed autocorrelation function of the modem data. An 8K sample window size was applied coupled with a 1-bit quantization of the data in order to compute the autocorrelation function.

The features being used in the current analysis of the modem data, in OLPARS, were selected from a total of 30 possible lags of the autocorrelation functions computed on the MSA data base. An in-depth analysis was performed on all of the features. This was accomplished by using the discriminant measure analysis frame in OLPARS. The 6 features used were chosen for their ability to discriminate between the different modem classes.

Figure 5-29 illustrates the discriminant analysis output from OLPARS. The analysis is broken down into 3 categories: rank by logic file, rank by class-alone and rank by class-pair. The ranking of the features is based on the Fisher direction of all possible class pairs in N-space. The class-alone ranking is derived by summing all Fisher direction components involving the class chosen. The rankings of all features are listed in order from the largest summed Fisher direction magnitude to the smallest. The class-pair ranking is computed in the same manner, but by considering only the Fisher directional component for the specified class pair. Finally, the logic file ranking is derived from the sum of all possible class pairs listed from the largest Fisher direction magnitude to the smallest.

From Figure 5-29 it is seen that the best features for discriminating among modems are 1,4,2,6,and 3, respectively. The best features for discriminating class C or the CODEX 9600 modem from all other classes are 1,4, 2,3, and 6, while features 4,1,3,2, and 5 are the best choices for
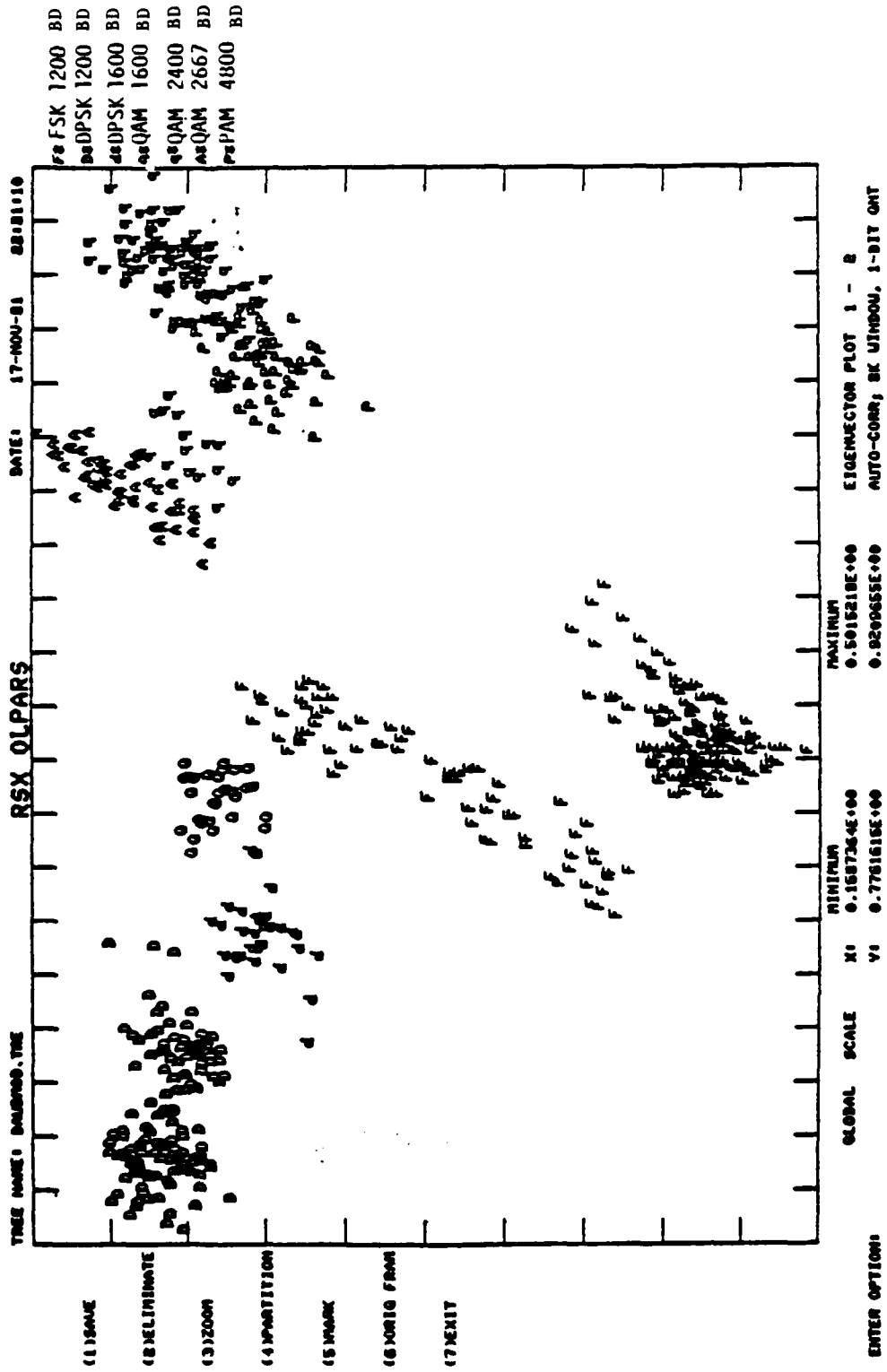
Figure 5-28: Scatter Plot of the Eigenvector Projection for the 5 Best Lags Computed from the 8K Point Auto-Correlation from the 1-Bit Quantized Data

Figure 5-29: Discriminative Measure Analysis Features (1, 2, 3, 4, 5, 6, 7, 8) 1-Bit Quantization 3K Window Size

discriminating the CODEX LSI-9600 from the PARADYNE LSI-9600, based on the Fisher directions. While investigating the discriminant analysis for best features, other classes and class-pairs were chosen as projection planes in the analysis. Features 1,2,3,4, and 6 were always ranked as the most discriminate for the classes.

Figure 5-30 illustrates the Fisher pairwise logic evaluation for modem generic type separation using features 1,2,3,4, and 6. Shown in Figure 5-30 is a confusion matrix for classifying each class correctly. Choosing class A (HARRIS 5238 modem) as an illustration, it is shown that five QAM 2667 baud feature vectors were incorrectly classified as QAM 2400 baud. None of the QAM 2667 baud data was rejected thus giving a correct classification of 91.23 percent and an incorrect classification of 8.77 percent. An overall performance is also given for discriminating between all classes for the logic evaluation.

The Fisher logic evaluation shows that 98.8 percent of combined design and test set data was classified correctly and 1.20 percent was misclassified. An extensive analysis was performed on the logic evaluation of the MSA data base. Figures 5-31 and 5-32 show the Eigenvector projection and Fisher logic result for the same features (lags 1,2,3,4, and 6) but using a 3K sample window for the autocorrelation estimation. Note the increased class overlaps and slight decrease in overall percentage correct. Analyzing different combinations of window sizes and quantization of the data, it was determined that quantizing the data to 1-bit resolution and using an 8K window size resulted in best discrimination and modem separation for features 1,2,3,4, and 6. Using a 1-bit quantization apparently removes the amplitude of the data as a feature while keeping the zero crossing information intact. The resulting data is easier to separate due to more discrimination in the computed lags extracted from the autocorrelation function.

Figure 5-30: Fisher Logic Evaluation Based on Lags 1, 2, 3, 4, 6 of the 1-Bit Quantized Signal Auto-Correlation Using an 8K Sample Window
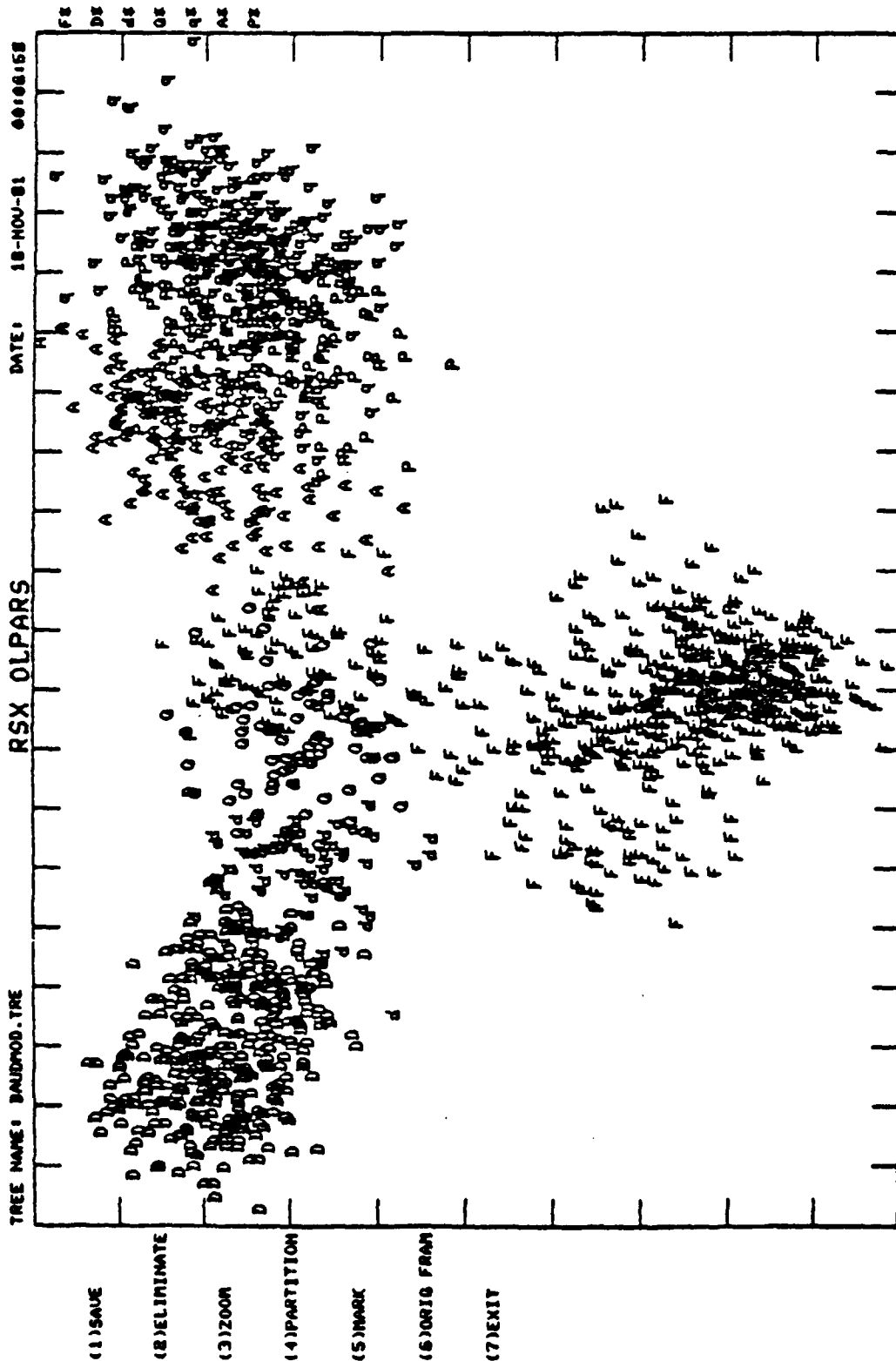
Figure 5-31: Scatter Plot of the Eigenvector Projection for the 5 Best Lags Computed from the 3K Point Auto-Correlation from the 1-Bit Quantized Data

Figure 5-32: Fisher Logic Evaluation Based on Lags 1, 2, 3, 4, 6 of the 1-Bit Quantized Signal Auto-Correlation Using a 3K Sample Window

A similar investigation to the above generic typing study was performed on the data which was structured by baud rate (1200, 1600, 2400, 2667, and 4800) and then structured by modulation type (QAM, PSK, PAM and FSK). The respective tree displays are shown in Figures 5-33 and 5-34.

The results of the three investigations are summarized in Table 5-1. The design set corresponds to ten randomly selected vectors of each lowest subclass, for example, all LENKURT 26-C modems with noise added. The test set includes all of the isolated impairment cases together with the cases of combined noise and phase jitter added.

5.3 LATTICE FILTERING

Lattice filtering is an adaptive linear prediction algorithm. An adaptive lattice filter attempts to set prediction coefficients in such a way that the difference between a sampled time signal's new value and the linear prediction based on its N previous values is minimized. The lattice filter chooses the coefficients in a time-symmetric fashion, so that it predicts equally well the sample N+1 units in the past, given the most recent N samples.

Another interpretation of the lattice filter is that it models a signal's power spectrum. It does this by placing zeros in the z plane (the sampled data equivalent of the frequency domain) so that if the zeros were replaced by poles, they would represent a good model of the signal's power spectrum. The lattice filter's zeros then tend to cancel the peaks in the signal's power spectrum. For this reason the adaptive lattice filter is a spectrum whitener.

Figure 5-35 gives a schematic diagram of a lattice filter. The signals along the upper line of the lattice are known as the forward residuals, because each represents the difference between the actual input signal and a linear prediction of it. Similarly the signals along the lower line of the lattice are backward residuals with each representing the difference between a
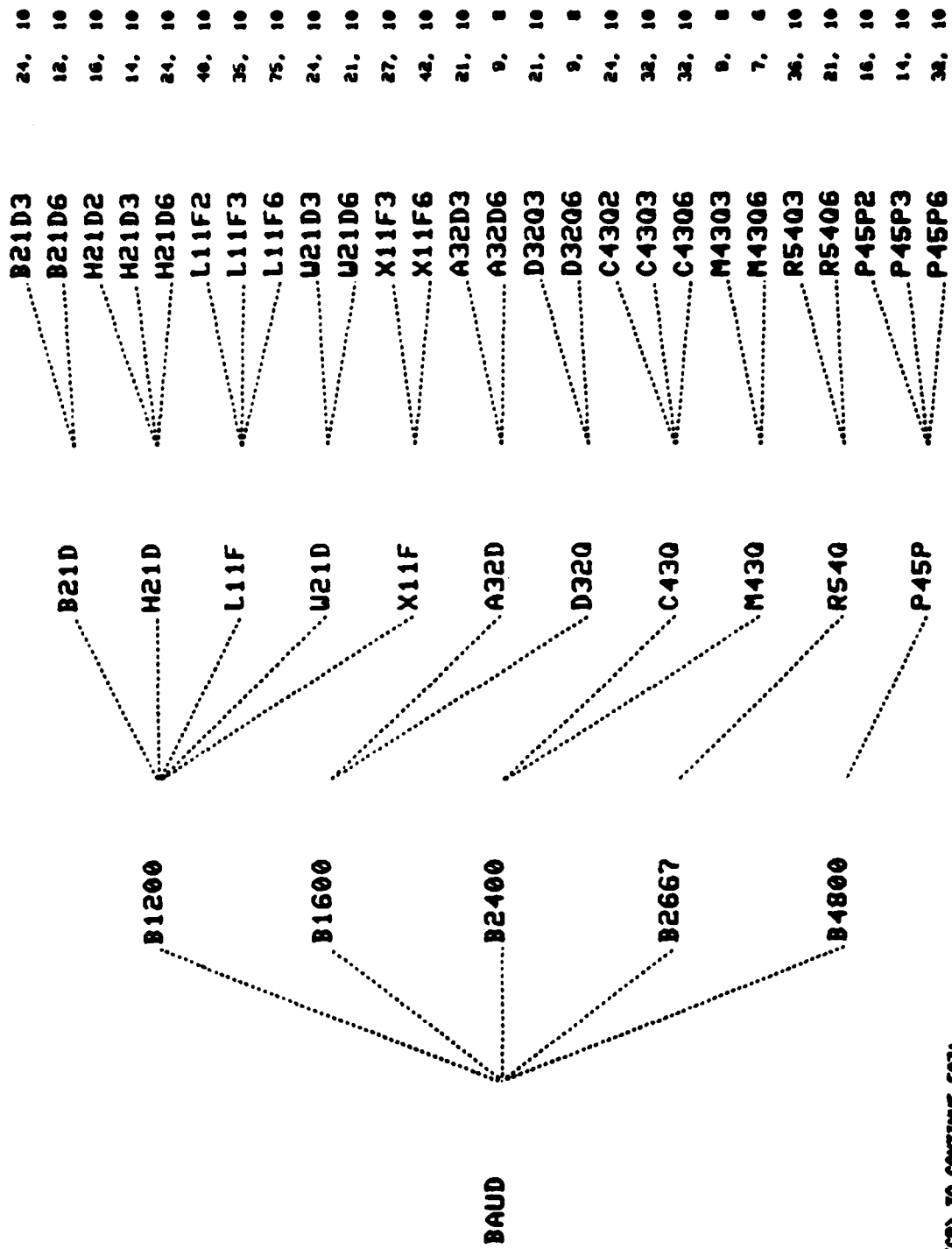
Figure 5-33: Data Tree Illustration for the Baud Rate Separability Investigation

BAUD

B1200
B1600
B2400
B2667
B4800

B21D
H21D
L11F
U21D
X11F
A32D
D32Q
C43Q
M43Q
R54Q
P45P

Node		
B21D3	24,	10
B21D6	12,	10
H21D2	16,	10
H21D3	14,	10
H21D6	24,	10
L11F2	40,	10
L11F3	35,	10
L11F6	75,	10
U21D3	24,	10
U21D6	21,	10
X11F3	27,	10
X11F6	42,	10
A32D3	21,	10
A32D6	9,	8
D32Q3	21,	10
D32Q6	9,	8
C43Q2	24,	10
C43Q3	32,	10
C43Q6	32,	10
M43Q3	9,	8
M43Q6	7,	6
R54Q3	36,	10
R54Q6	21,	10
P45P2	16,	10
P45P3	14,	10
P45P6	38,	10

L11F2   40, 10
L11F3   35, 10
L11F6   75, 10
X11F3   27, 10
X11F6   42, 10
P45P2   16, 10
P45P3   14, 10
P45P6   32, 10
A32D3   21, 10
A32D6   9, 8
B21D3   24, 10
B21D6   12, 10
H21D2   16, 10
H21D3   14, 10
H21D6   24, 10
U21D3   24, 10
U21D6   21, 10
C43Q2   24, 10
C43Q3   32, 10
C43Q6   32, 10
D32Q3   21, 10
D32Q6   9, 8
M43Q3   9, 8
M43Q6   7, 6
R54Q3   36, 10
R54Q6   21, 10

L11F

X11F

P45P

A32D

B21D

H21D

U21D

C43Q

D32Q

M43Q

R54Q

MFSK

MPAM

MPSK

MQAM

MODTYP

*30   (G)D TO CONTINUE CODE

Figure 5-34: Data Tree Illustration for the Modulation Type Separability Investigation

Bits Res	Window Size	Features Used	Data Tree	Fisher All	Fisher Design	Fisher Test	Mahalanobis		
							All	Design	Test
1	8K	1,2,3,4,6	MODTYP	98,55	99.6	97.96	99.57	100.	99.32
1	8K	1,2,3,4,6	BAUD	97.32	97.53	97.2	97.11	97.2	97.05
1	8K	1,2,3,4,6	BAUDMOD	-----	-----	97.28	-----	----	98.64
1	3K	1,2,3,4,6	MODTYP	97.73	98.84	97.56	98.36	98.85	98.29
1	3K	1,2,3,4,6	BAUD	95.3	95.6	95.25	94.62	----	-----
1	3K	1,2,3,4,6	BAUDMOD	95.9	93.8	95.74	-----	----	96.34
12	3K	1,2,3,4,6	MODTYP	72.13	67.20	72.88	-----	----	-----

Table 5-1 OLPARS Classifier Design Summary
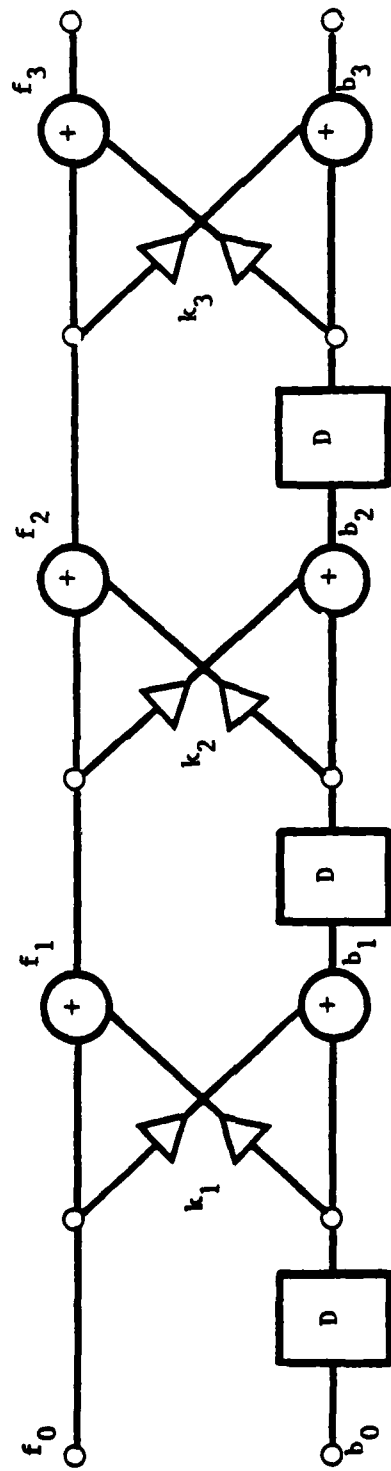
Figure 5-25 An Adaptive Lattice Filter Block Diagram

delayed version of the input signal and an estimate of it based only on the recent past.

In the figure each box marked D is a unit delay. Each triangle represents an amplifier. The two amplifiers for a given stage have the same gain. Circles containing pulses are summers. Given the ith forward residual $f_i(t)$ and the ith backward residual $b_i(t)$ the gain k_{i+1} is computed according to

$$k_{i+1} = \frac{-2\sum_t f_i(t) \, b_i(t-1)}{\sum_t f_i^2(t) + \sum_t b_i^2(t-1)}$$

Then, given k_{i+1}, the next forward and backward residuals are computed according to

$$f_{i+1}(t) = f_i(t) + k_{i+1} b_i(t-1)$$
$$b_{i+1}(t) = k_{i+1} f_i(t) + b_i(t-1).$$

In its capacity as a spectrum whitener, the adaptive lattice filter is useful for the present effort in that it can help identify the type of modem, based only on the observation of a noisy signal coming from it. Whitening the spectrum of a signal has two distinct effects. It reduces pulse trains into impulse trains, narrowing and sharpening the pulses. It also decorrelates noise, so that the total result is approximately white noise with short, sharp pulses mixed in.

The whitening of a PSK signal then tends to produce a series of pulses occurring at the baud rate. Each pulse represents the transition of the carrier signal from one phase to another. Some pulses will be positive, representing one polarity of phase transition, while others will be negative representing the opposite polarity. Then, rectifying the lattice forward residual output (for PSK input) will result in a pulse train of positive

pulses with varying amplitude, with the repetition rate of the pulses matching the baud rate.

The whitening of an FSK signal tends to a similar result. In an FSK signal, a tone frequency is turned on and off while a tone at a second frequency is turned off and on. This is done so that one or the other tone, but not both, is on at all times. The adaptive lattice filter will tend to respond (in its forward residual) with impulses at the points where the tones are turned on and off and will tend to block out the tones elsewhere. Again, rectifying will result in a series of pulses at the baud rate.

Theoretical study indicates that two stages of lattice filter suffice for PSK, and four stages suffice for (two tone) FSK. A sinusoidal signal has two poles in the z plane, while a signal composed of two sinusoids has four poles. A lattice filter has one zero per stage, so it can fit a PSK signal with two stages and an FSK signal with four.

Experiments were performed applying lattice filtering to the modem signals in the data base. Zero, two and four stages of lattice filtering were applied, usually followed by rectification and then power spectra were taken. Table 5-2 gives the results. Line height refers to how high in dB a line (spike) in the power spectrum stood out above its neighbors. All but two of the 11 modems tested could be distinguished by generic type, including all the lower speed modems. While the initial tests were run on low noise and distortion signals, later tests which were run on noisy and distorted signals confirmed the results.

Figure 5-36 through 5-43 illustrate the power spectra that resulted from the processing. For example, Figure 5-36 illustrates the result of four stages of lattice filter followed by rectification and then taking a power spectrum, applied to the CODEX LSI-96 modem signal. The spectrum is plotted on a logarithmic scale with 10dB per division. A spike or line is clearly visible at 2400 Hz, extending about 5dB above its surroundings. In some of

2/3
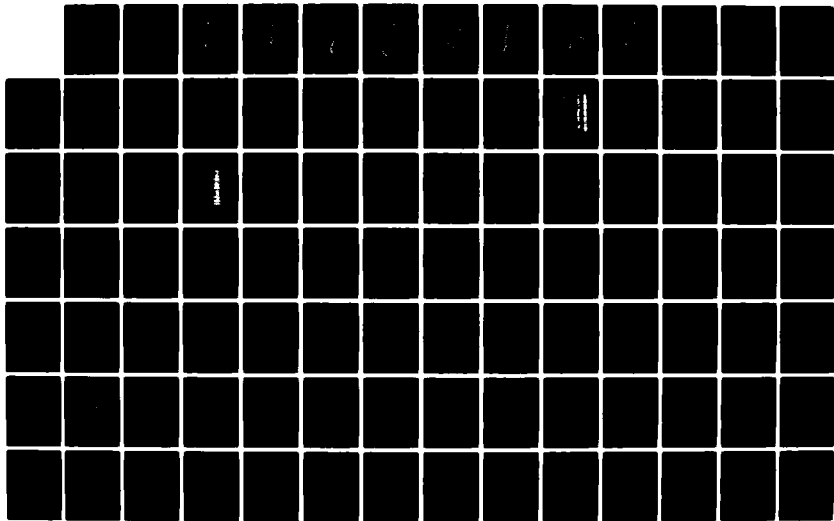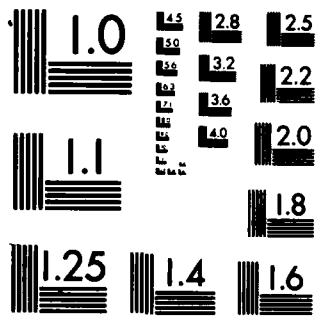
MICROCOPY RESOLUTION TEST CHART

NATIONAL BUREAU OF STANDARDS-1963-A

MODEM	(HERTZ) CARRIER	(HERTZ) BAUD RATE	(HERTZ) BIT RATE	BEST PROCESSING	(POWER SPECTRUM) FEATURES	LINE HEIGHT (dB)	FIGURE
CODEX LSI-96	1706	2400	9600	S4 RCT	2400 Hz Line	5	5-36
HARRIS 5238	1800	2667	16000	-----	---------	--	
HUGHES HC 276	1800	1200	2400	S2 RCT	1200 Hz Line	12	5-37
LENKURT 26-C	1200, 2400	1200	1200	RAW	1200, 2400 lines	10	5-38
CODEX LSI-48	1800	1600	4800	S2 RCT	1600 Hz Line	7	5-39
CODEX LSI-48	1800	1200	2400	S2 RCT	1200 Hz Line	12	5-40
CODEX LSI-48	1706	1600	4800	S4 RCT	1600 Hz Line	7	5-41
PARADYNE MP-96	1700	2400	9600	-----	---------	--	
PARADYNE LSI-96	2853	4800	9600	S4	2853 Hz Line	9	5-42
NECO 207A2	1800	1200	2400	S2 RCT	1200 Hz Line	12	5-43

S2 or S4 means 2 or 4 stages of lattice filter
RCT means rectify after lattice filtering
RAW means no lattice filtering or rectifying

Table 5-2 Results of Lattice Filter Experiments
On The Non-Impaired Signals.

2400 Hz

2391 Hz

CAR 1706
BAUD 2400
BPS 9600
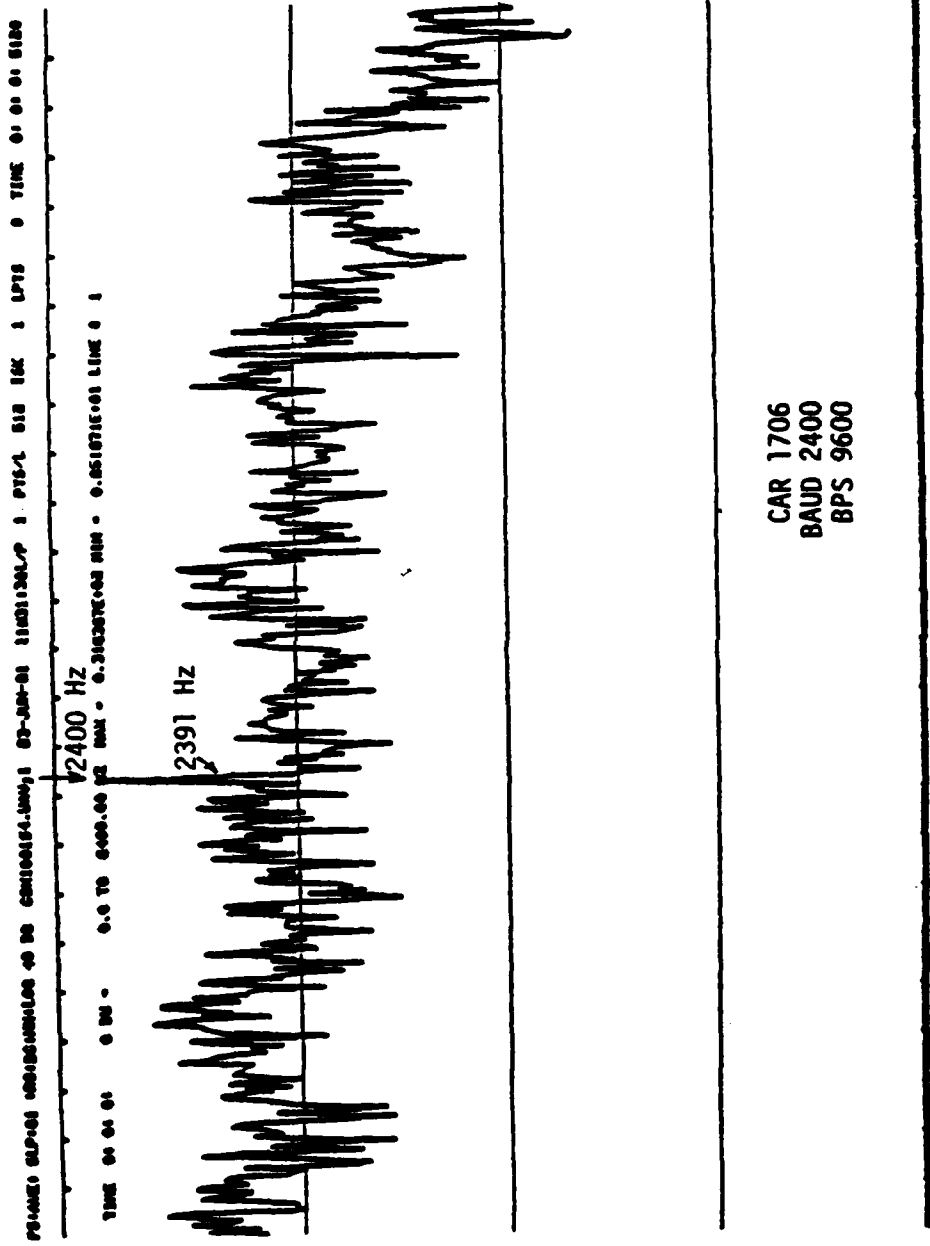
Figure 5-36 Codex LSI-96, Power Spectrum of the Rectified Residual from Four-Stages
of Lattice Filtering on a 40dB Log Scale
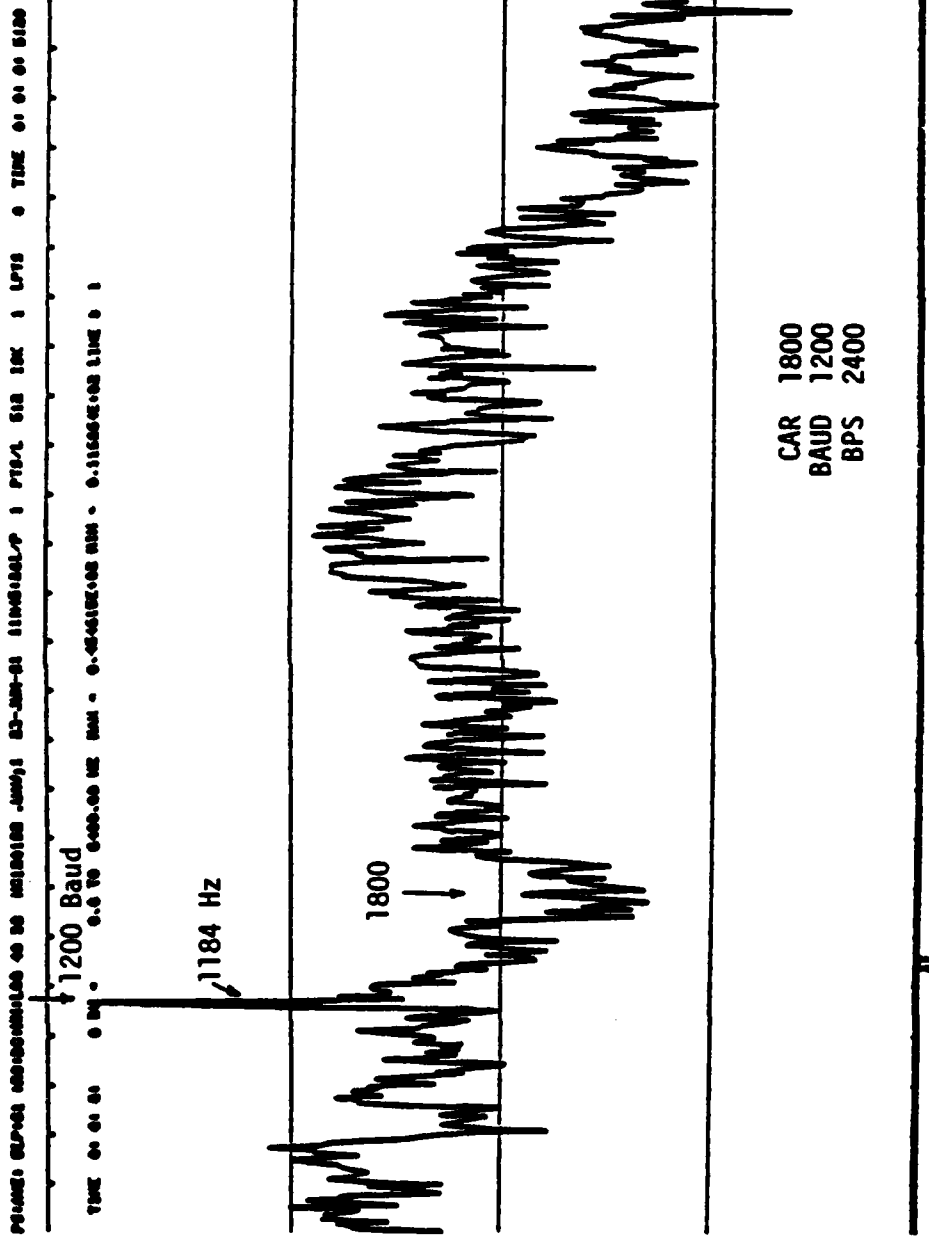
Figure 5-37   Hughes HC-276, Power Spectrum of the Rectified Residual from Two-Stages of Lattice Filtering on a 40 dB Log Scale
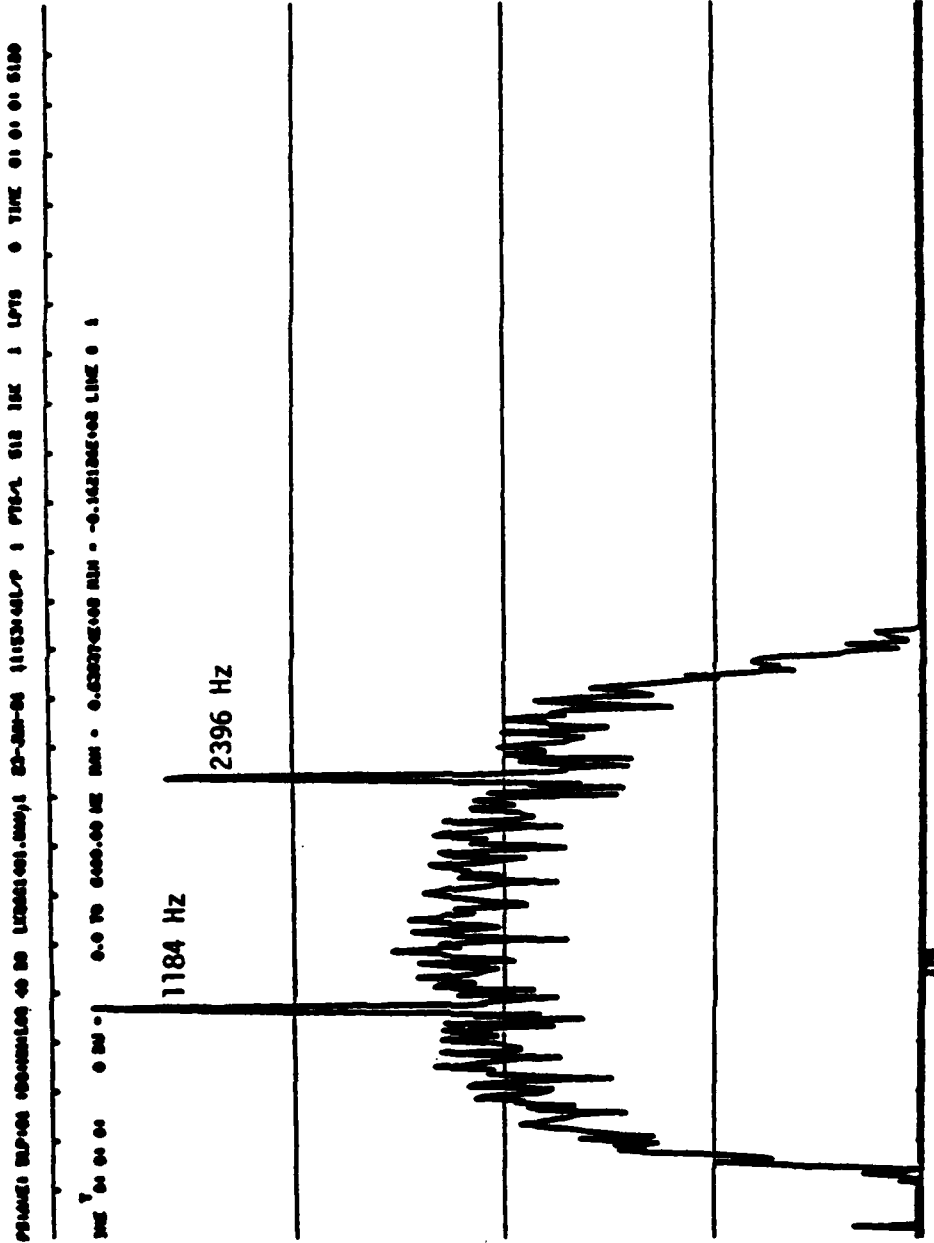
Figure 5-38   Lenkurt 26-C, Power Spectrum of the Raw Signal on a 40 dB Log Scale
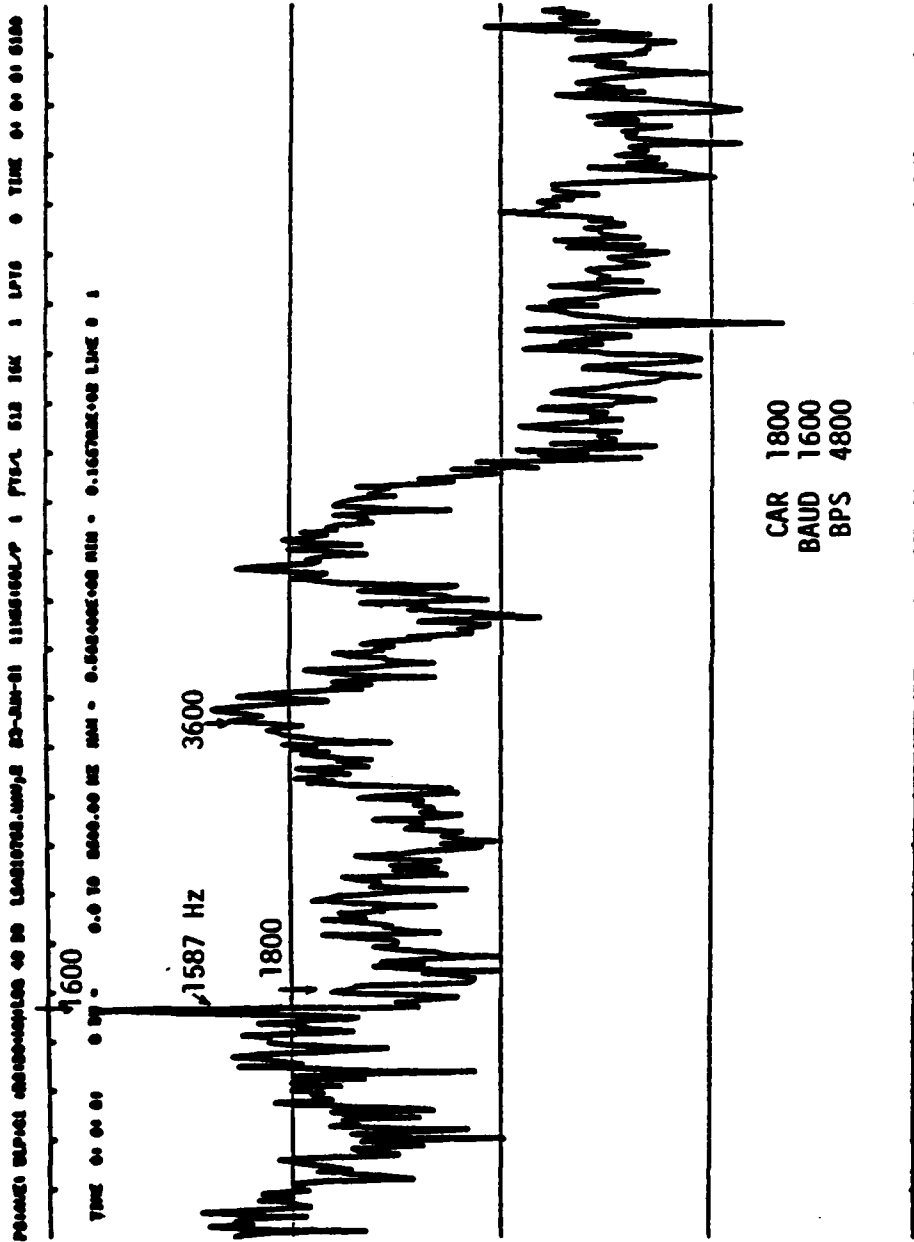
Figure 5-39 Codex LSI Mode A, Power Spectrum of the Rectified Residual from Two-Stages of Lattice Filtering on a 40 dB Log Scale
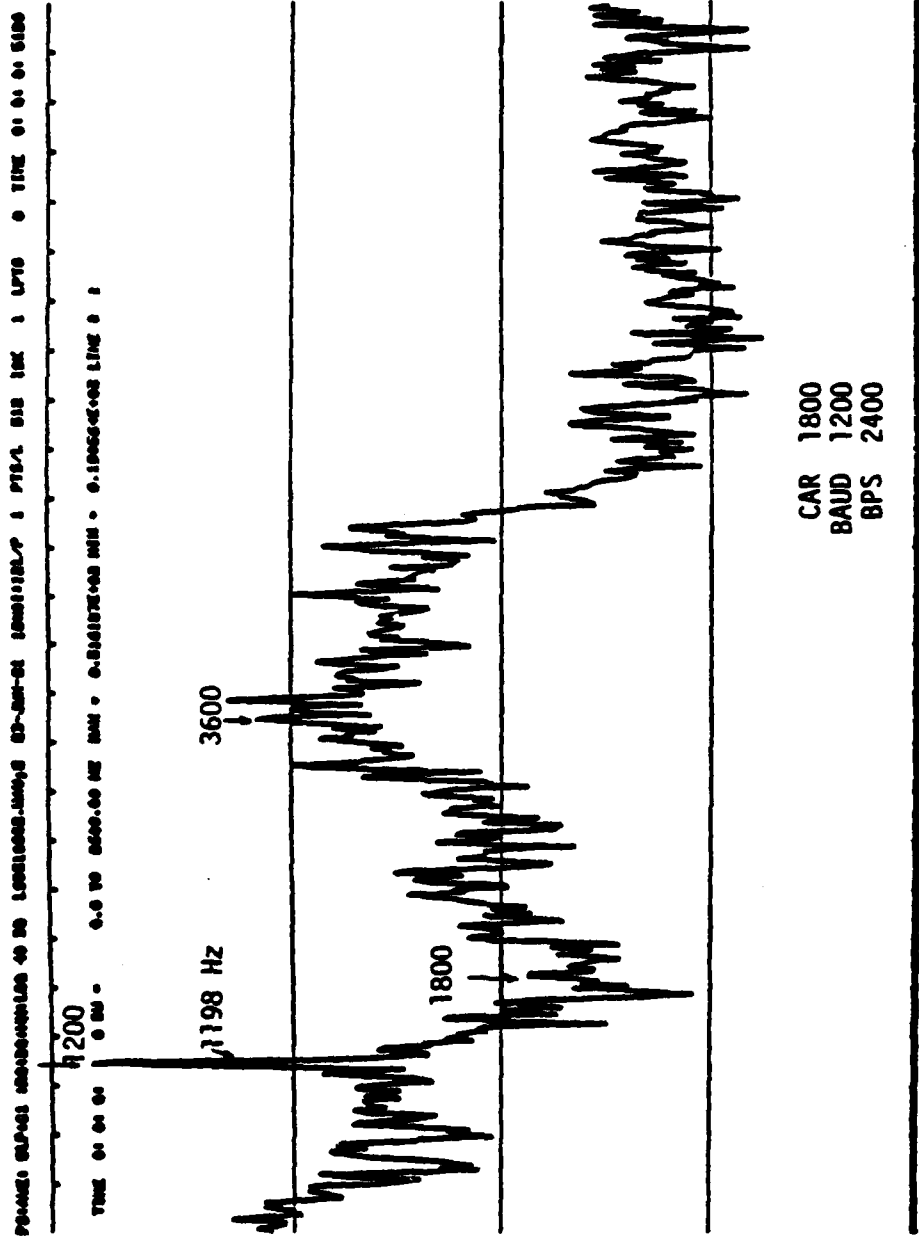
Figure 5-40 Codex LSI Mode B, Power Spectrum of the Rectified Residual from Two-Stages of Lattice Filtering on a 40 dB Log Scale

CAR 1800
BAUD 1200
BPS 2400
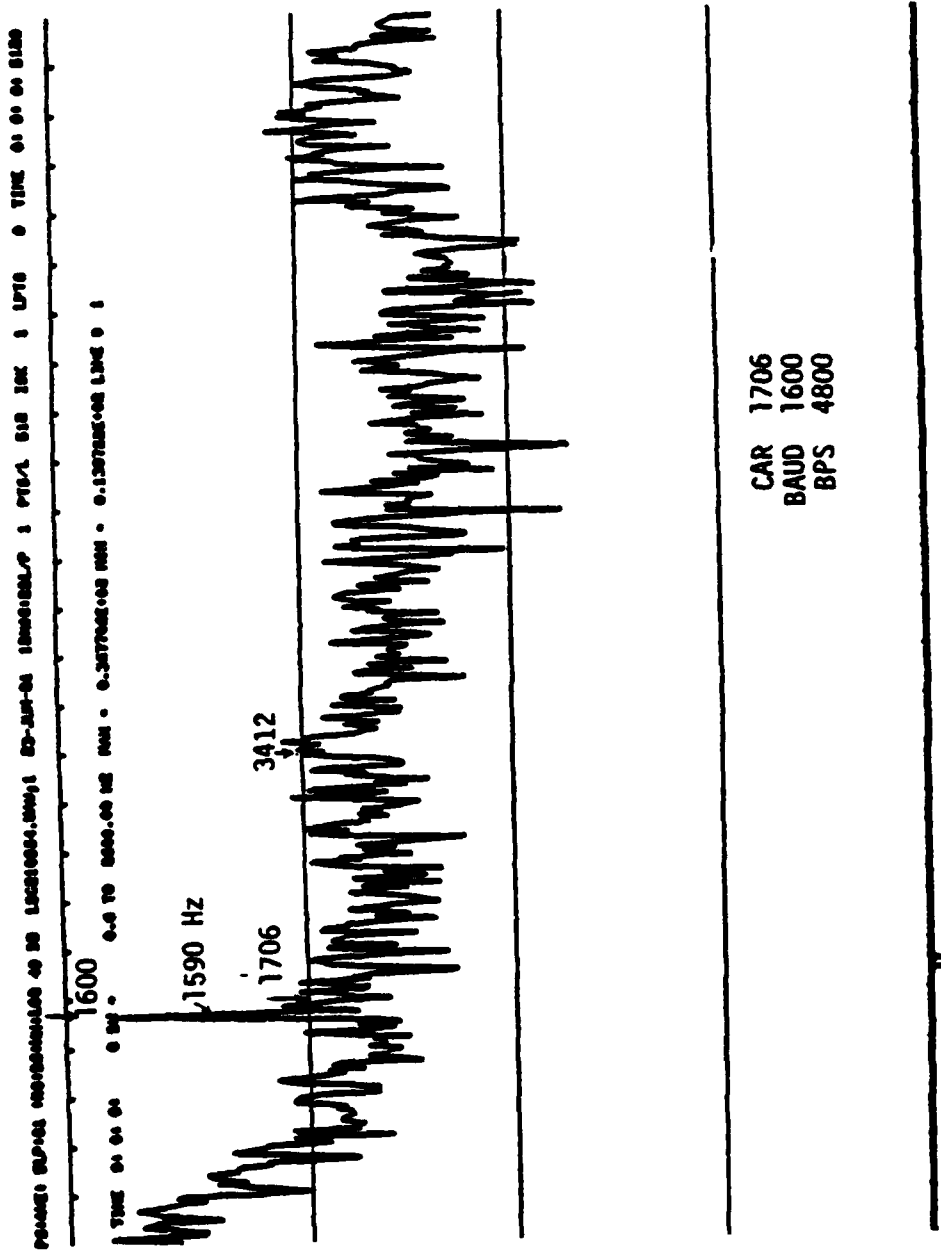
Figure 5-41   Codex LSI Mode C, Power Spectrum of the Rectified Residual from Four-Stages of Lattice Filtering on a 40 dB Log Scale

CAR 1706
BAUD 1600
BPS 4800

Figure 5-42 Paradyne LSI-96 Power Spectrum of the Residual from Four-Stages of Lattice Filtering on a 40 dB Log Scale

CAR 1800
BAUD 1200
BPS 2400
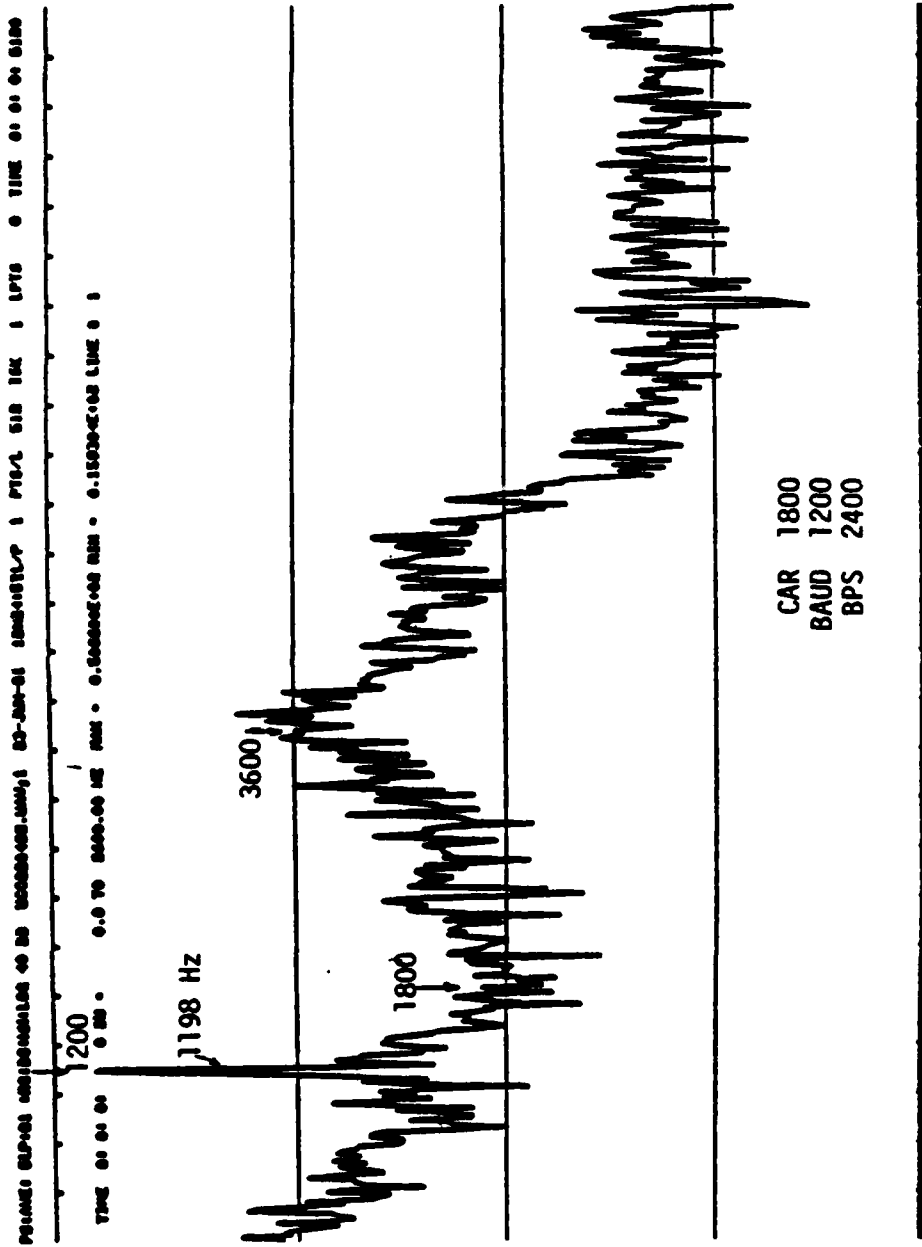
Figure 5-43 WECO-207A2, Power Spectrum of the Rectified Residual from Two-Stages of Lattice Filtering on a 40 dB Log Scale

the plots the lines in the spectrum do not fall exactly at their nominal frequencies, but in all cases they are within 16 Hz of their nominal frequencies.

Lattice filtering was found to be useful in identifying modems or modem generic type. As a result, it is useful in a go/no-go decision process to determine if a received signal is degraded or not through the identification of spectral components at the known baud and/or carrier associated locations. Lattice filtering and the required spectral estimation are both computationally complex and potentially non-realizable in a real-time system.

5.4 EYE PATTERN ANALYSIS

The hardware eye-monitor has long been a standard industry tool in the assessment of the quality of analog data communications links. In this section, we consider the aspects of a software implementation of an eye-monitor and its application to channel quality monitoring of digitized signals. The form of eye-monitor investigated was the I/Q monitoring technique.

The received VF line signal is assumed to be of the form

$$r(t) = \sqrt{2} \quad \mathrm{Re}\{ \tilde{r}(t) \, e^{j \, 2\pi f_c t}\},$$

where f_c is the carrier frequency and

$$\tilde{r}(t) = r_c(t) - j \, r_s(t)$$

is the complex envelope represented in terms of the I/Q components $r_c(t)$ and $r_s(t)$, respectively. The I and Q components are plotted against each other as shown in Figure 5-44 (a). Bit synchronization with the input data stream must be achieved and used to sample the I/Q components at the mid-baud interval point. This is the point where a decision as to the symbol sent would
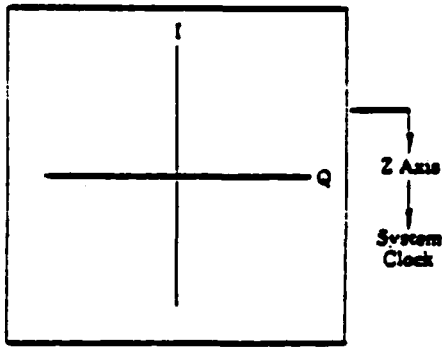
(a) Oscilloscope setup for eye pattern monitoring: the I channel provides vertical drive. The Q channel horizontal drive, and the system data clock Z-axis drive.
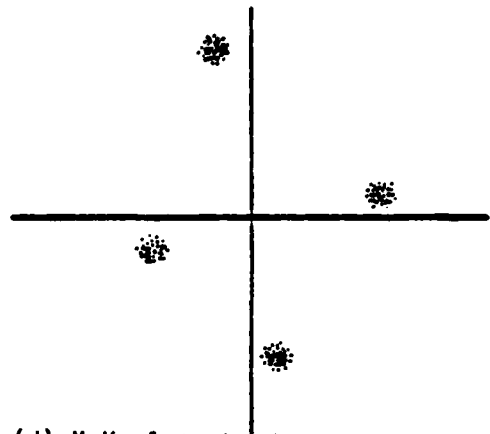
(d) X-Y plot showing skewing from phase shifts.
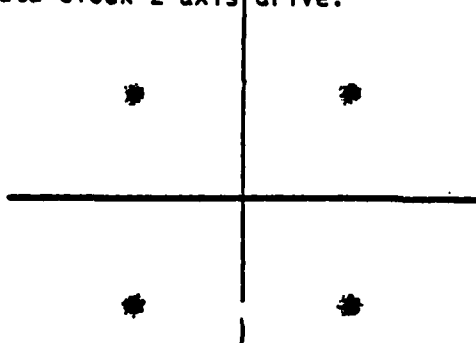
(b) X-Y plot of good data from I and Q channels.
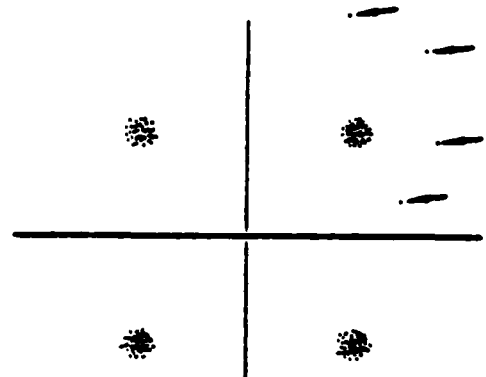
(e) X-Y plot showing scattered points due to transient noise and phase hits.
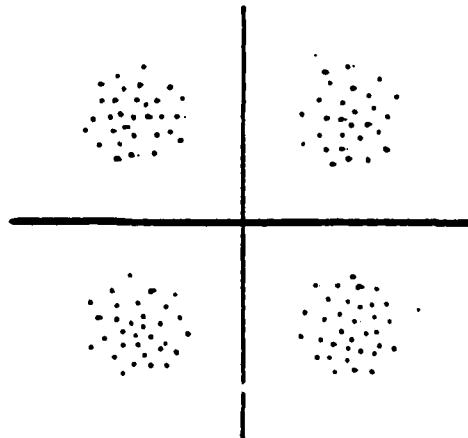
(c) Plot showing effect of noisy data.

Figure 5-44: Sample I/Q Plots for Common Channel Conditions

5-57

actually be made in the receiver portion of the modem. The I/Q plot for a good data channel is shown in 5-44 (b). The effect of adding noise to the channel is shown in Figure 5-44 (c). Note that as the clusters disperse, the likelihood of a sample crossing the boundary into an adjacent region and causing a symbol decision error increases. As phase jitter is introduced into the system, skewing of the plot occurs as illustrated in Figure 5-44 (d). The effects of transient noise and phase hits is shown in Figure 5-44 (e). In order to maintain stability in the I/Q plot, it is necessary to implement some form of carrier phase tracking to prevent random phase walk or mistuning from rotating the I/Q plot.

For the purposes of this investigation, several assumptions were made to expedite the determination of the effectiveness of this approach to performance monitoring. First, in lieu of carrier phase synchronization, it was assumed that the carrier was constant in frequency over a short period of approximately 60 ms. With this assumption, we can eliminate the requirement for carrier phase tracking if we know the precise short term carrier frequency. This was determined using the Interactive Digital Receiver Simulator (IDRS). The signal was demodulated for the phase waveform. The complex heterodyne frequency was adjusted to show a phase waveform drift of zero over the time window being monitored.

The problem of achieving bit synchronization for establishing a mid-baud interval strobe was accomplished in the following manner. The signal segment was demodulated for the FM component and displayed to the user. Using the cross-hair input of the graphic terminal (Tektronix 4014), the user marked the mid-baud point on the FM waveform. Since the baud rate was known, the software could sync a strobe to the user-specified point. It was assumed that the baud clock of the modem was stable over the 60 ms window being considered.

Figure 5-45 shows the I/Q plot for the CODEX LSI-48 Mode B modem (DPSK, 1200 baud). As the signal is passed through the 4A line simulator, the I/Q plot degrades as shown in Figure 5-46. The non-linear phase response of the

Figure 5-45 shows the I/Q plot for the CODEX LSI-48 Mode B modem (DPSK, 1200 baud). As the signal is passed through the 4A line simulator, the I/Q plot degrades as shown in Figure 5-46. The non-linear phase response of the channel characteristic is the primary cause for the distortion. The other DPSK 1200 baud signals are comparable.

Figure 5-47 shows the I/Q plot for the CODEX LSI-48 Mode A (DPSK, 1600 baud) for the no 4A line case. Figure 5-48 shows the CODEX LSI-48 Mode C (QAM, 1600 baud) also for the no 4A case. For both of these modems, the distortion introduced by applying the 4A characteristic was sufficient to distort the I/Q plot beyond recognition. Further, none of the higher speed modem signals could be processed to present a stable I/Q plot using this technique.

Several conclusions result. The requirement for some form of equalization of the signal as the baud rate increases is indicated. The severity of the group-delay characteristic is sufficient to distort the phase plot. Further, the stability of the I/Q plot relies on carrier synchronization. For longer term monitoring, carrier phase tracking appears to be required. Also over a longer sample duration, bit synchronization is required as a strobe indicating when to sample the I/Q components.

The next section of this report proposes an alternative method of extracting the information available in the I/Q plot.

5.5 ORBITAL VELOCITY

One possibility for signal analysis is to make use of features extracted from the polar coordinate representations of the in-phase/quadrature (I/Q) components of the received VF line signal. For want of a better name, we will refer to this polar plot as a phase trajectory. In the present subsection, we describe an approach to performance monitoring or evaluation which exploits a feature derived from the phase trajectory.

SHIFT FREQ. 1799.50 NUMBER OF POINTS 824.
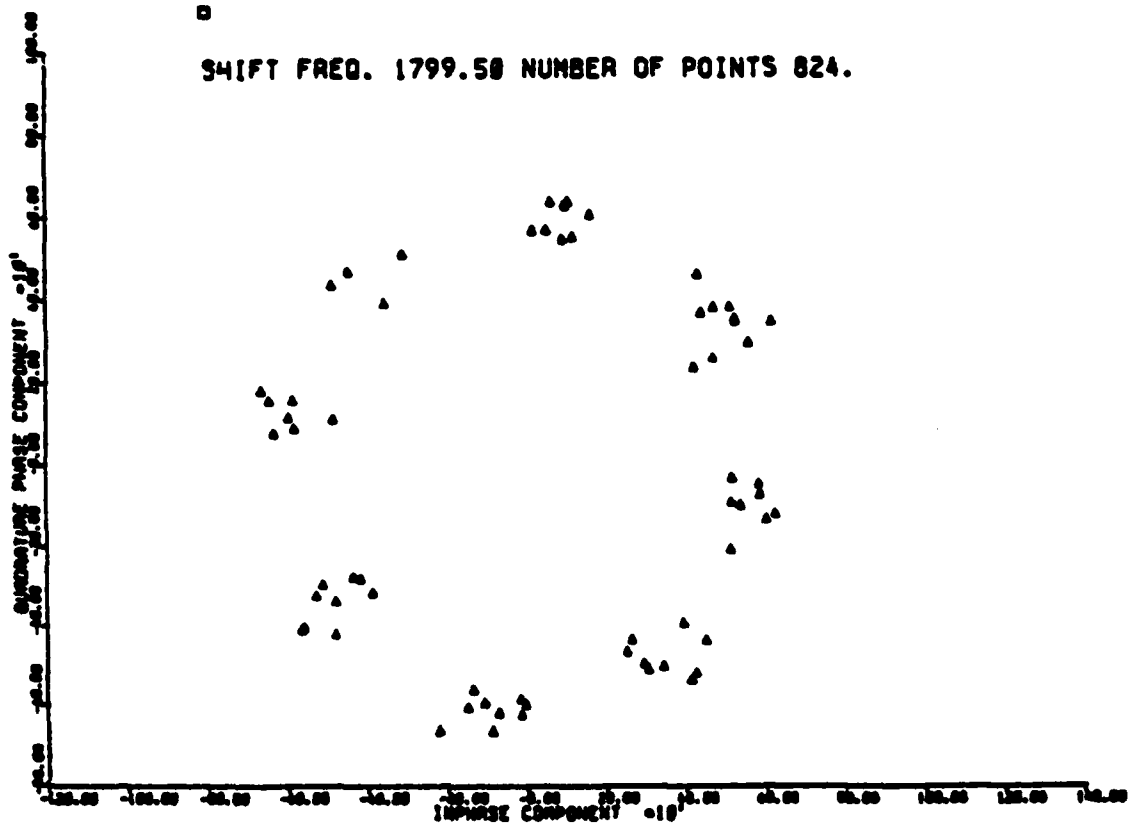
Figure 5-45:   I/Q Plot of the CODEX LSI-48 Mode B Modem Signal Without
the 4A Line Simulator

PAR TECHNOLOGY CORPORATION
CODEXLSI48 MODE B THRU 4A LINE

SHIFT FREQ. 1800.00 NUMBER OF POINTS 824.
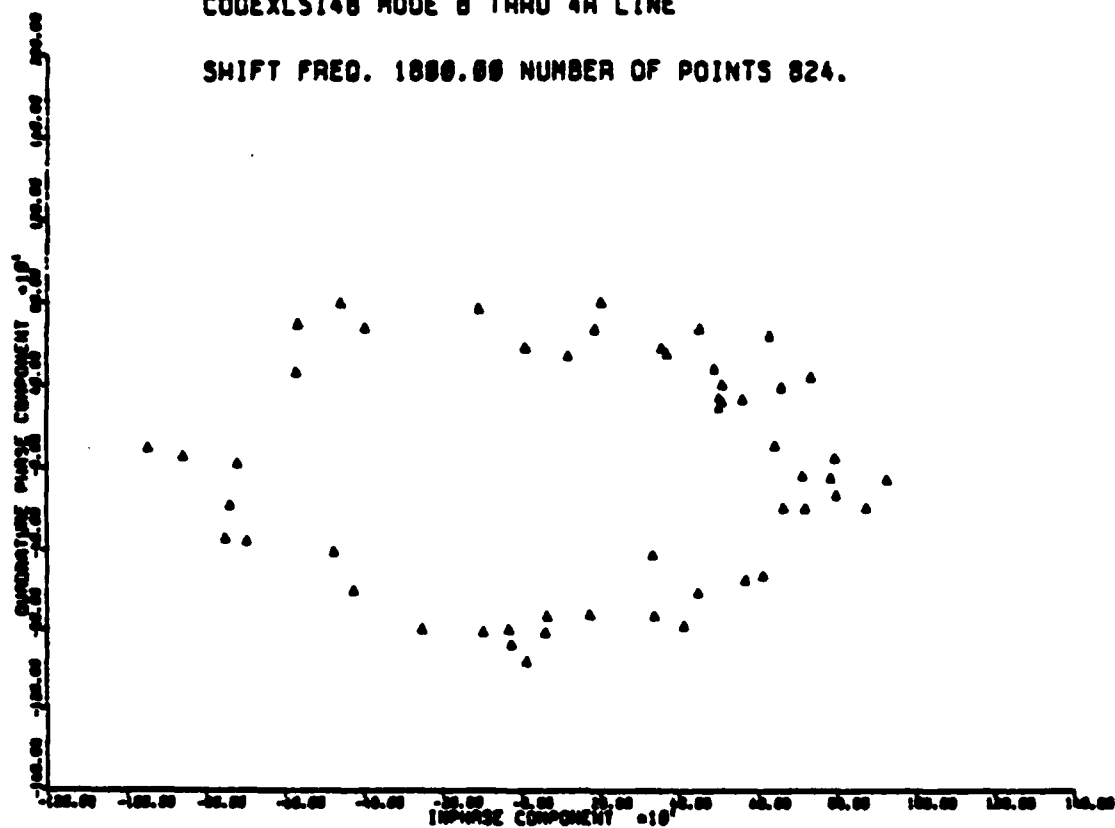
Figure 5-46: I/Q Plot of the CODEX LSI-48 Mode B Modem Signal Through
the 4A Line Simulator

PAR TECHNOLOGY CORPORATION
CODEXLSI48 MODE A NO 4A

SHIFT FREQ. 1800.88 NUMBER OF POINTS 824.
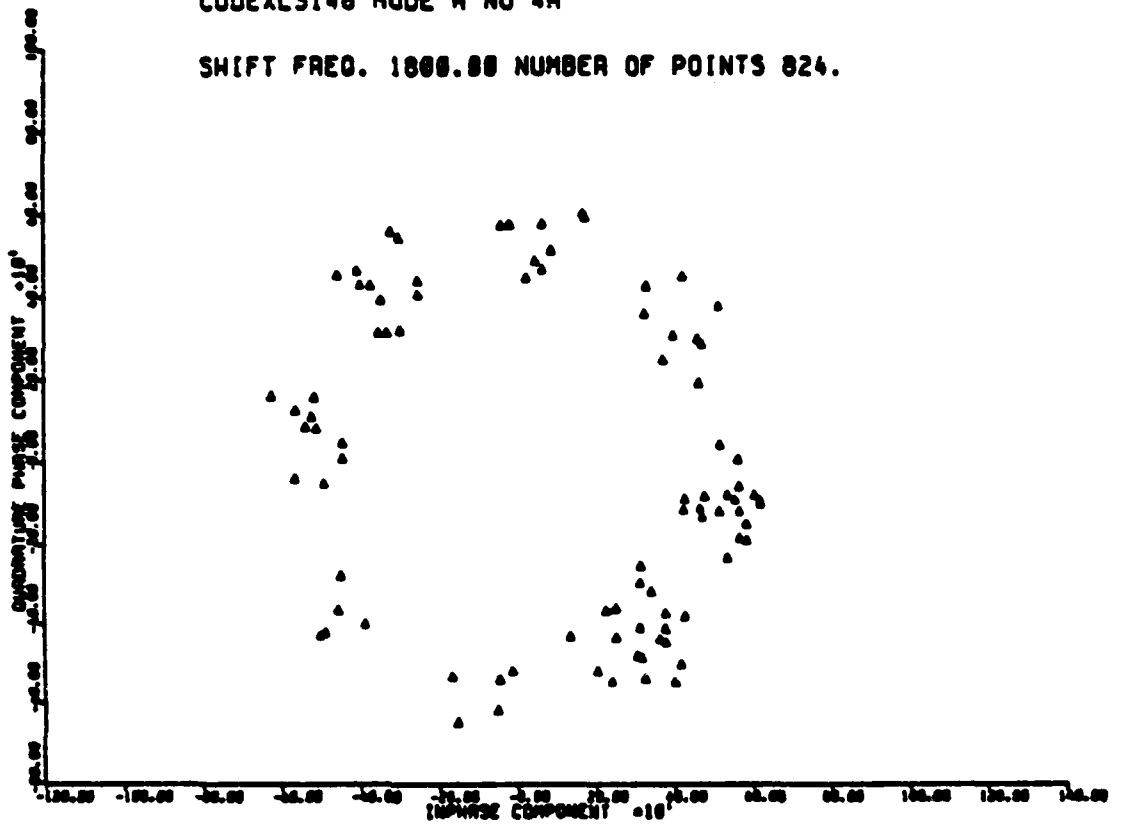
Figure 5-47:   I/Q Plot of the CODEX LSI-48 Mode A Modem Signal Without
the 4A Line Simulator

PAR TECHNOLOGY CORPORATION
CODEX LSI48 MODE C NO 4A

SHIFT FREQ. 1786.88 NUMBER OF POINTS 824.
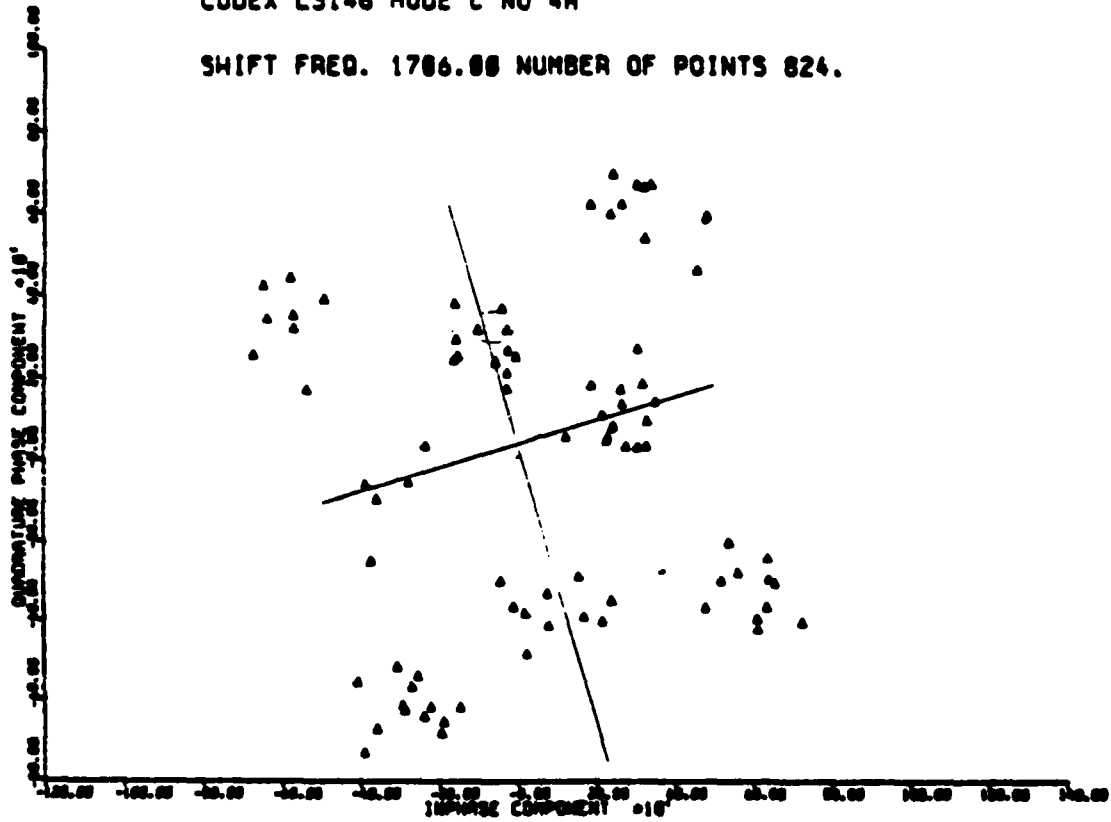
Figure 5-48: I/Q Plot of the CODEX LSI-48 Mode C Modem Signal Without
the 4A Line Simulator

5-63

The received VF line signal is assumed to be of the form

$$r(t) = \sqrt{2} \; Re \left\{ \tilde{r}(t) e^{j2\pi f_c t} \right\} \qquad (1)$$

where f_c is the carrier frequency and $\tilde{r}(t) = r_c(t) - jr_s(t)$ is the complex envelope represented in terms of the I/Q components $r_c(t)$ and $r_s(t)$, respectively. The phase trajectory is then an appropriately normalized version of $r_s(t)$ plotted against $r_c(t)$. It is important that this plot be appropriately normalized to avoid coloration by an unimportant scale factor. Specifically, we consider plotting the quantity $\tilde{r}'(t) = \tilde{r}(t)/\sigma$, where

$$\sigma^2 \overset{\Delta}{=} E\{|\tilde{r}(t)|^2\} = E\{r_c^2(t)\} + E\{r_s^2(t)\} \; , \qquad (2)$$

is the mean-square value of the complex envelope $\tilde{r}(t)$. σ^2 is also the mean-square value of the real process $r(t)$. The quantity σ^2 can be estimated from the received line signal as the corresponding sample mean-square value computed over some finite data window.

There are several features that can be extracted from the phase trajectory that should prove useful in performance monitoring. In Figure 5-49 we illustrate a typical phase trajectory associated with the normalized complex envelope $\tilde{r}'(t)$. Here the point $\tilde{r}'(t)$ on the trajectory is parameterized in terms of its polar coordinates:

$$a(t) = |\tilde{r}'(t)| \; , \qquad (3)$$

$$\theta(t) = \arg \tilde{r}'(t) \qquad (4)$$
$$= -\tan^{-1} \frac{r_s'(t)}{r_c'(t)}$$

The negative sign here follows from the fact that, to be consistent with previous work, we have used the representation $\tilde{r}'(t) = r_c'(t) - jr_s'(t)$.
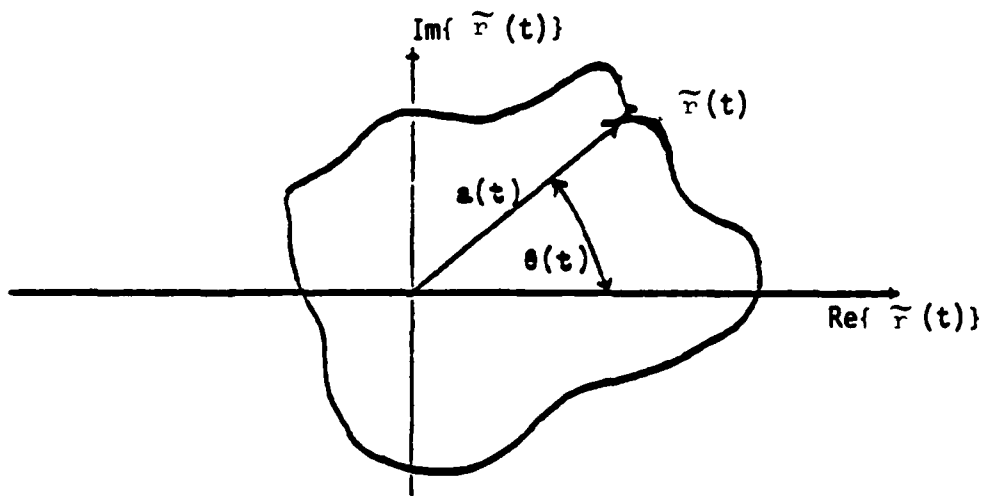
Figure 5-49: Typical Phase Trajectory Associated with
Normalized Complex Envelope

In Figure 5-49 we have illustrated only one circuit of the complex plane, whereas the phase trajectory associated with a particular observation interval will exhibit many such circuits, which will differ from each other for different transmitted data sequences and/or channel conditions. The phase trajectory appears to be useful since it avoids all problems of phase synchronization and/or timing recovery.

One of the features readily extracted from the phase trajectory which one might consider useful in performance evaluation is the instantaneous orbital velocity of the point represented by r'(t) as it traverses the trajectory. We define the orbital velocity as

$$\dot{s}(t) = \frac{ds(t)}{dt} \triangleq |\dot{\vec{r}}'(t)|$$
$$= \sqrt{\dot{a}^2(t) + a^2(t)\dot{\theta}^2(t)} \qquad (\cdot)$$

Here, $\dot{a}(t)$ is merely the time derivative of the instantaneous AM waveform while

$$\dot{\theta}(t) = w(t)$$

is the instantaneous FM waveform. Both of these quantities are easily extracted from the normalized complex envelope r'(t). It was hypothesized that second-order statistics extracted from s(t) would prove useful in performance evaluation. This would include lagged products obtained from autocorrelation functions and/or spectral properties obtained from the power spectral density function. Note that if the phase trajectory is along an arc of constant radius, then s(t) is merely proportional to the magnitude of the instantaneous radial frequency. The use of orbital velocity in this sense is to recognize that motion is not generally along an arc of constant radius but along a highly variable and sometimes erratic path. This might be due to filter transient effects, intersymbol interference, channel noise, etc.

It should be noted that in making use of orbital velocity we have assumed implicitly that any residual frequency offsets have been removed. This requires some form of frequency acquisition and tracking scheme which should not be too difficult to implement.

The parameter $\dot{s}(t)$ was calculated for several modems of the database using equation (5). Spectral analysis of the orbital velocity showed essentially those characteristics seen in the FM power spectrum.

5.6 AM/FM ANALYSIS

We have seen that carrier phase instability results in drift in the modem signal's phase related waveforms and I/Q plots. As an alternative, the FM and AM signal components were thought potentially useful features in the analysis of line quality due to the immunity to mistuning and carrier drift. The mistuned receiver creates a drift in the demodulated phase waveform. The FM component, however, being the derivative of the phase waveform, shows the mistuning as a DC offset of the FM signal component. The AM of course is determined by the signal envelope and is not effected severely by mistuning.

The problem of carrier drift can be quite severe. The specifications for most modems require carrier accuracy nominally to be ± 3 Hz. It is not uncommon to find a ± 5 Hz range in practice.

The synchronous demodulation investigation was performed using the Interactive Digital Receiver Simulator (IDRS).[4] The result of the demodulation of the WECO 207A2 modem which has not passed through the 4A simulator is shown in Figures 5-50 through 5-56. A frequency shift of 1800 Hz was used with a Chebyshev 1200 Hz 2-pole low-pass complex filter. No smoothing filter was applied. Figure 5-54, showing the AM power spectrum average with Hanning weighting, clearly shows the 1200 Hz baud rate component and harmonics. The power spectrum average of the rectified FM signal shown in Figure 5-56 also displays the baud rate.

Figure 5-50: WECO 207A2 Time Wavefrom Segment
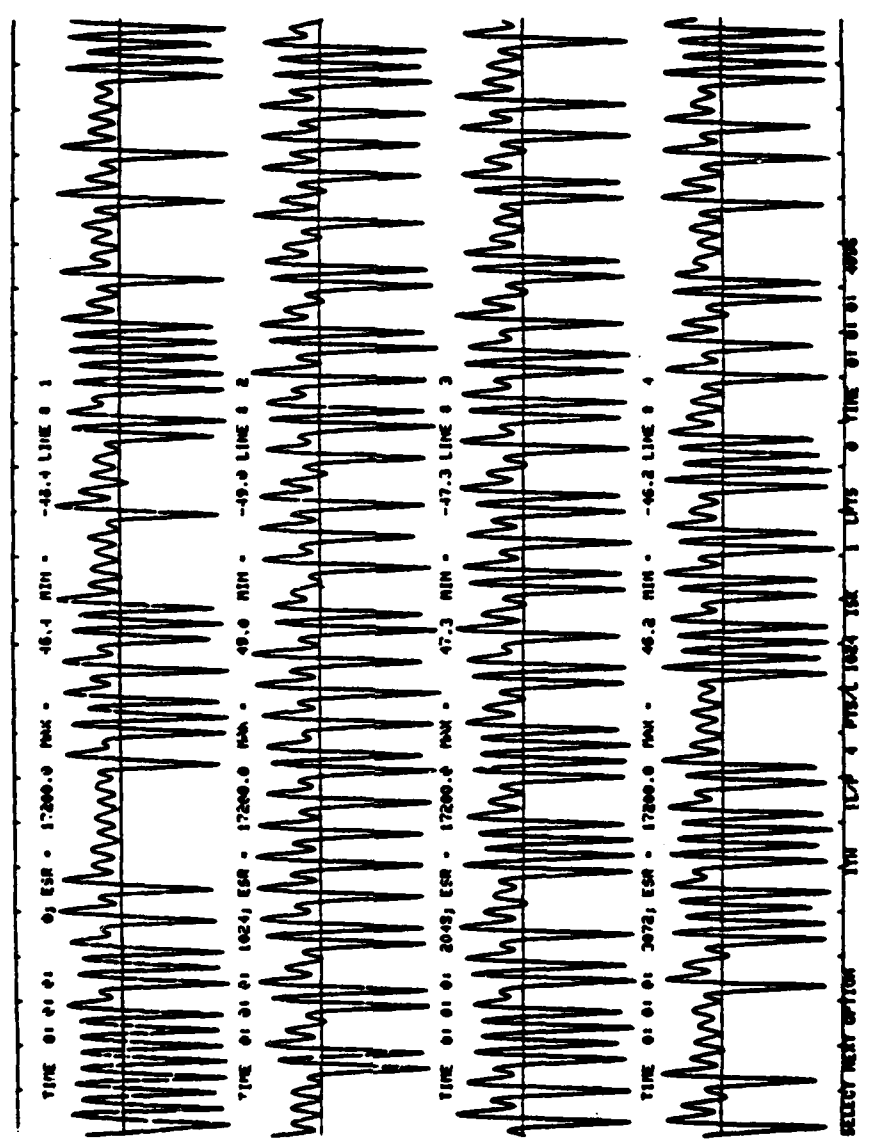
Figure 5-51: WECO 207A2 Demodulated AM Component Waveform
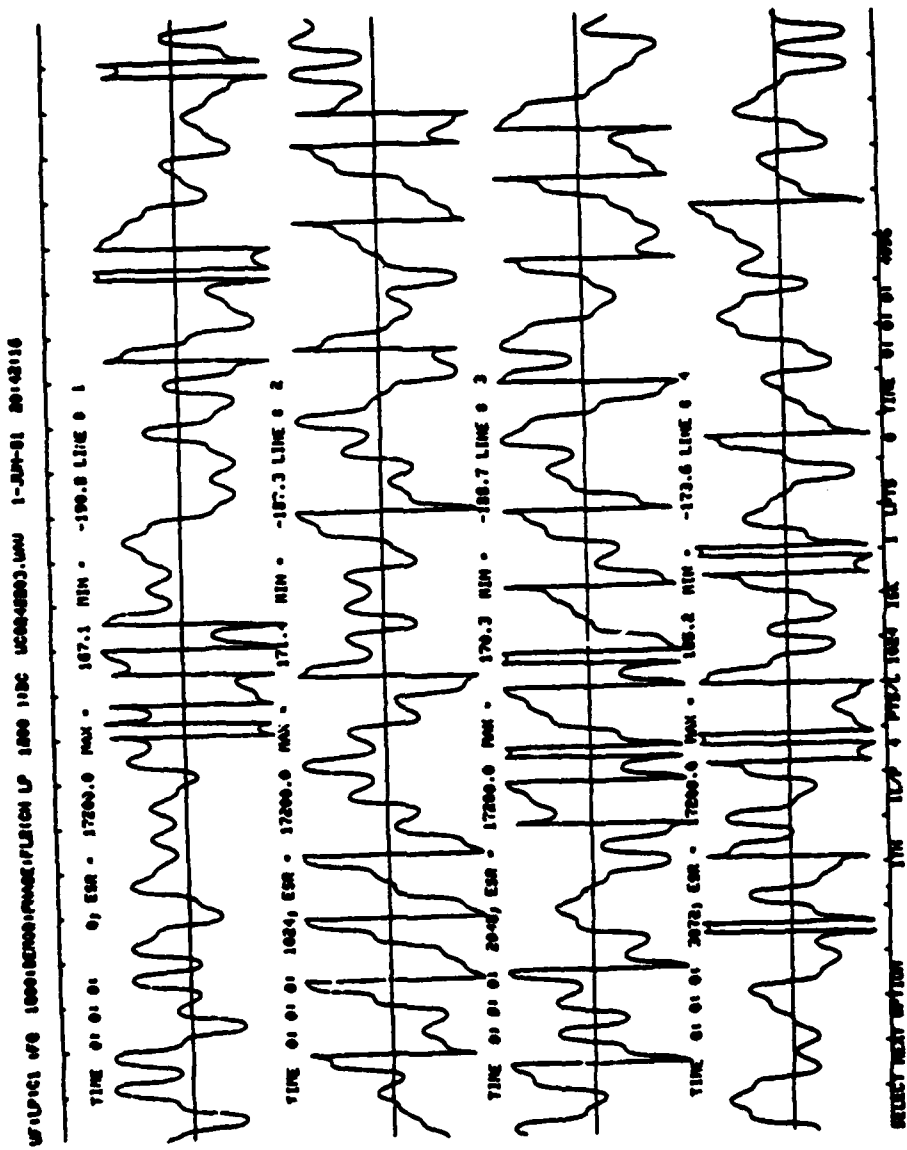
Figure 5-52: WECO 207A2 Demodulated Phase Waveform

5-70
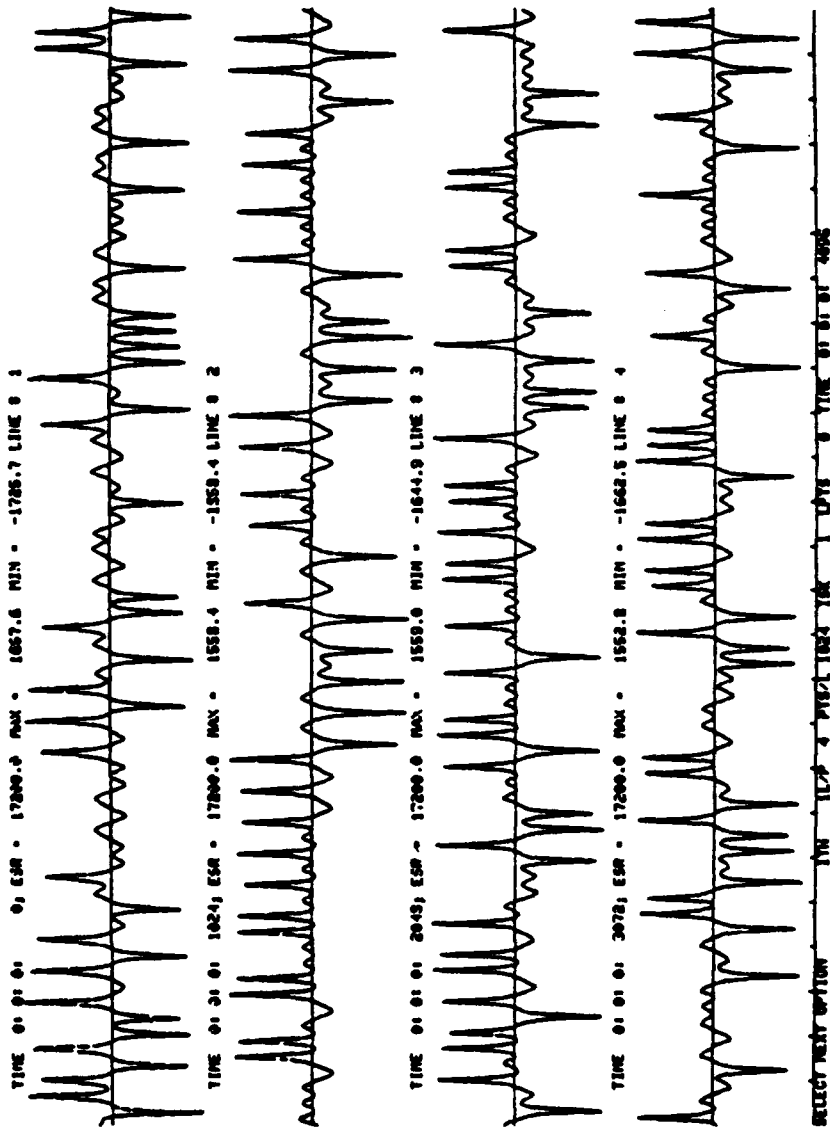
Figure 5-53: WECO 207A2 Demodulated FM Component Waveform
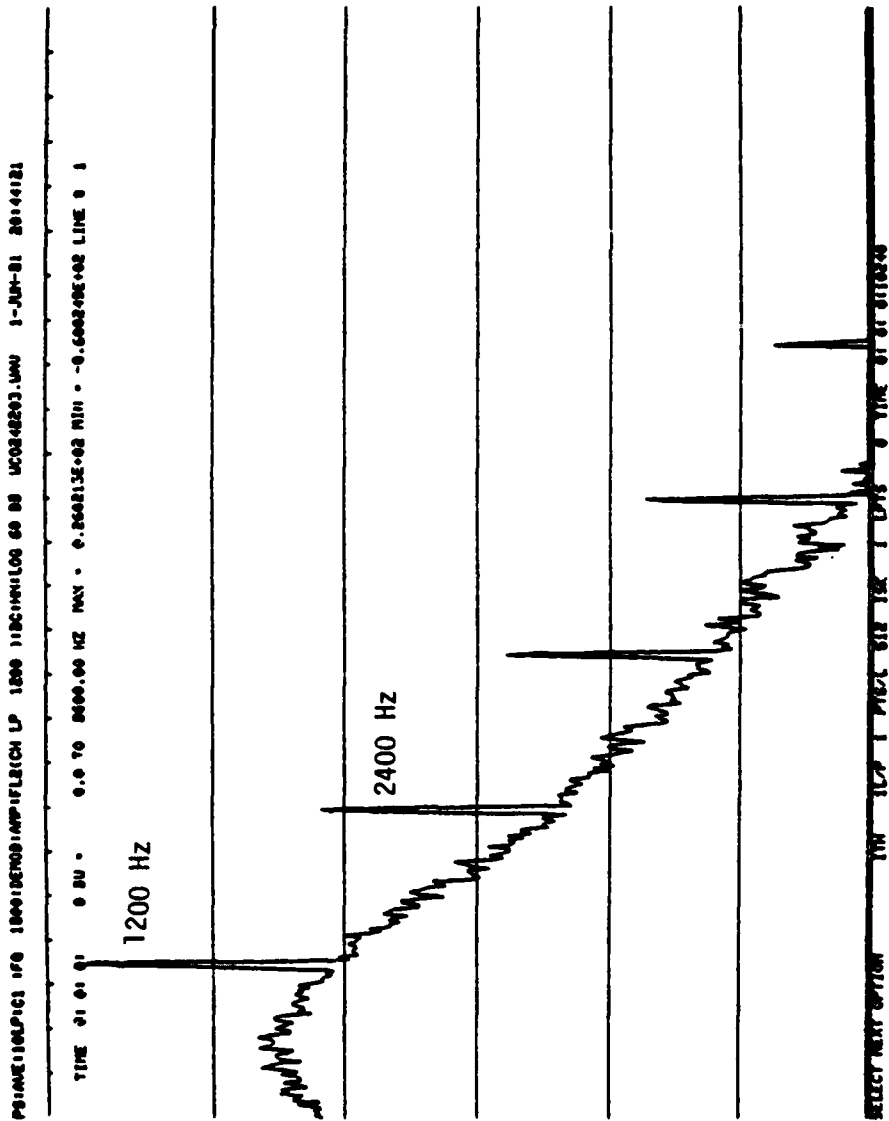
Figure 5-54: Power Average 10 Lines WECO 207A2 AM Component Waveform with 60 dB Log Scale Cutoff
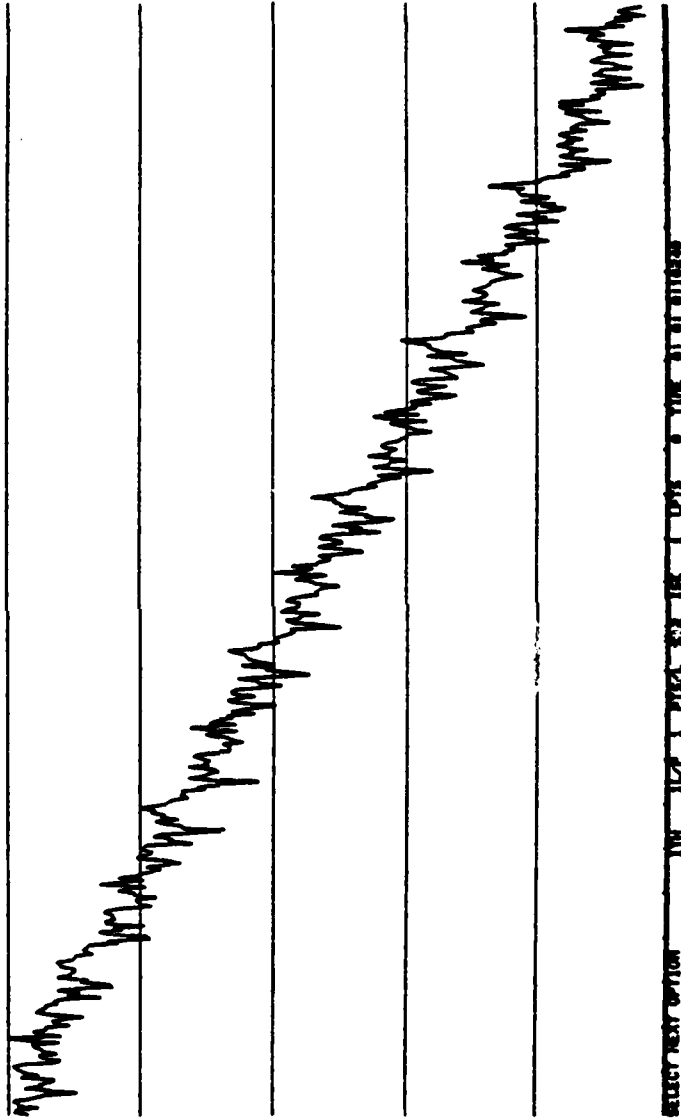
Figure 5-55: Power Average of 10 Li·es of WECO 207A2 FM Component Waveform with 60 dB Log Scale Cutoff

5-73
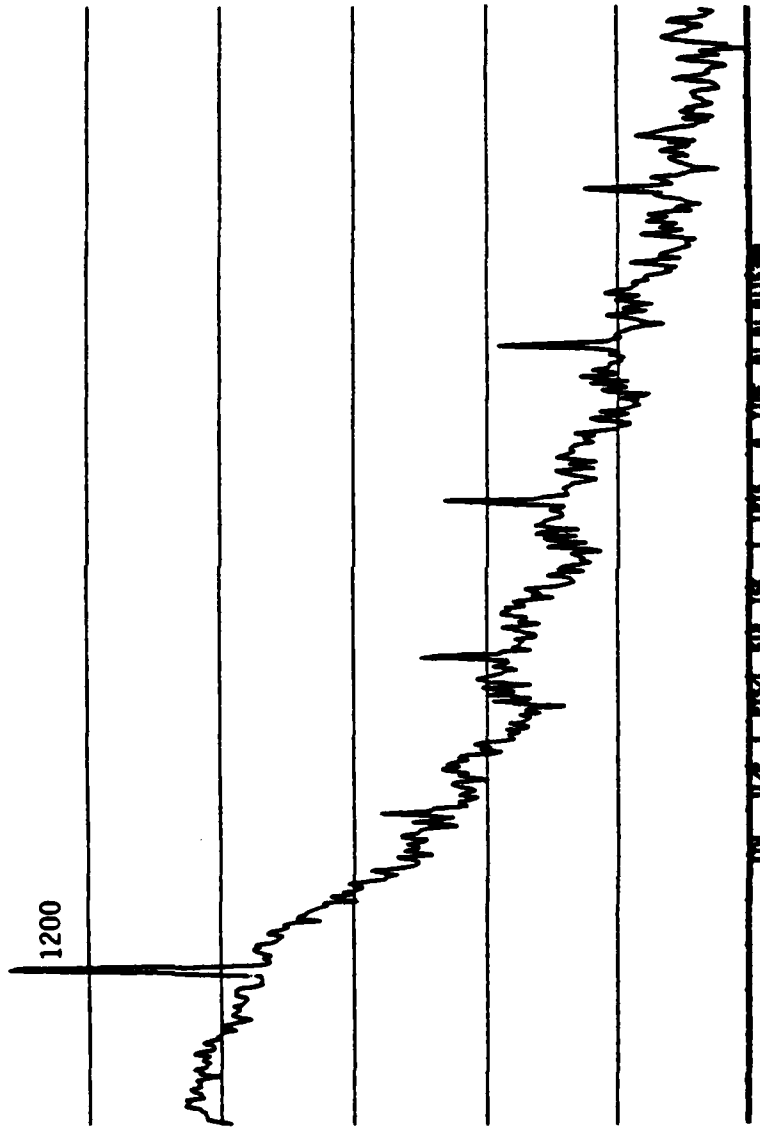
Figure 5-56: Power Average of 10 Lines of Rectified WECO 207A2 FM Component
Waveform with 60 dB Log Scale Cutoff

It was desired to investigate the effects of the degrading channel on the demodulated AM and FM components. Using the spectral average of the AM and the rectified FM power average as features, the baud rate components were monitored while impairments were added. In the case of the DPSK 1200 baud modems, no significant variation in the AM and FM spectrums were observed.

With the higher baud rate modems it becomes difficult to perform demodulation without the benefit of line equalization. No unique spectral components were observed for the HARRIS 5238 or PARADYNE MP-96 modems. The CODEX LSI-96 AM shows a 2400 Hz (baud rate) component which varies as a function of noise added. The two 1600-baud modems (CODEX LSI-48 Modes A and C) both showed the baud rate components and varied only slightly with impairments added.

The demodulation analysis of the FSK modems, however, provided some valuable insight. Although no stable relationship between the channel impairments and the AM and FM spectral behavior was observed, an interesting case was discovered. Figures 5-57 through 5-60 show the time waveform, demodulated phase waveform, FM waveform and FM power spectra, respectively, for the LENKURT 26-C modem with phase jitter added at 10 Hz, 80°P/P. Observe that the phase waveform (Figure 5-58) shows a single cycle of phase shift over a period of 1024 samples (10 Hz). The amplitude of the shift is estimated at roughly 90° P/P from the vertical axis. The FM waveform and FM spectrum show no such contents, however, because the 10 Hz modulation is masked by the intentional data transitions of the signal. In the next section we shall examine a technique to extract this unintentional phase jitter modulation.

In summary, the spectral analysis of the AM and FM derived without carrier phase tracking or equalization are affected by channel impairments, but not to a degree which is readily exploitable or exceptionally stable.

LK26C1406 JITTER 10HZ 80DEG. DMX-500 SMO-1000 MIX-1003.5
RAW WAVEFORM
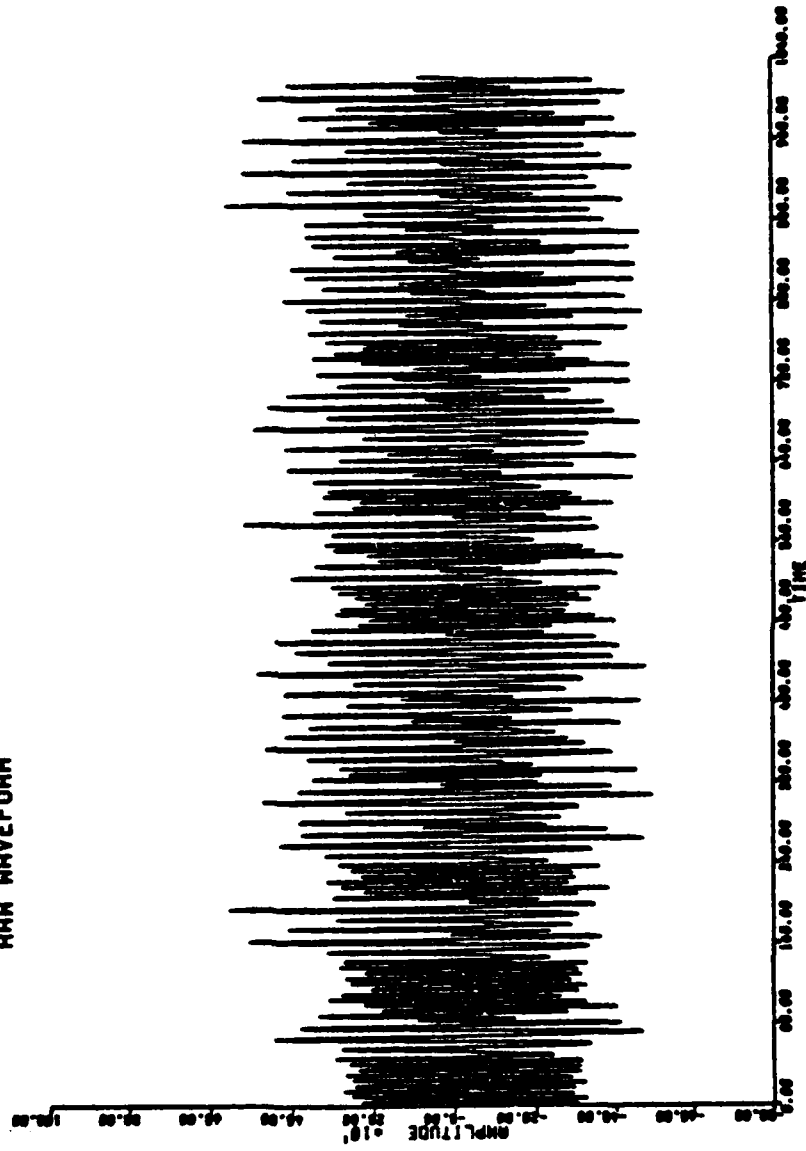
Figure 5-57: LENKURT 26-C Time Waveform Segment
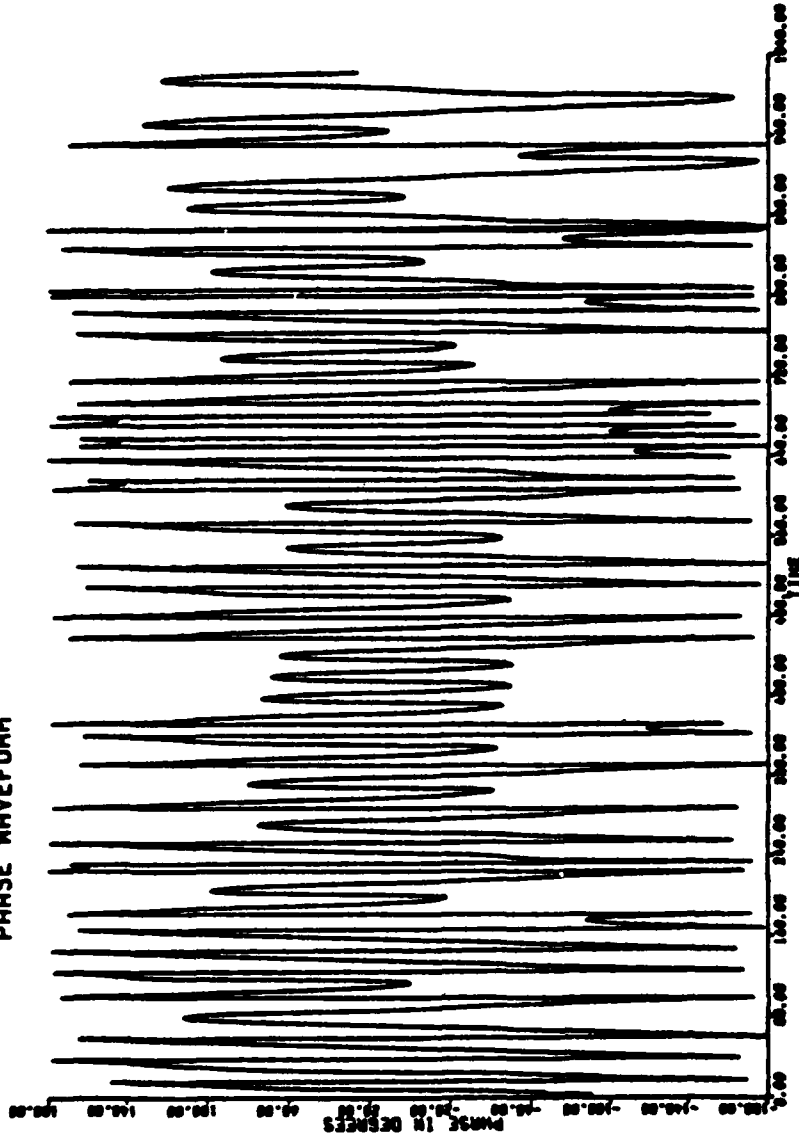
Figure 5-58: LENKURT 26-C Demodulated Phase Waveform for 10 Hz Phase Jitter at 80° P/P

90°
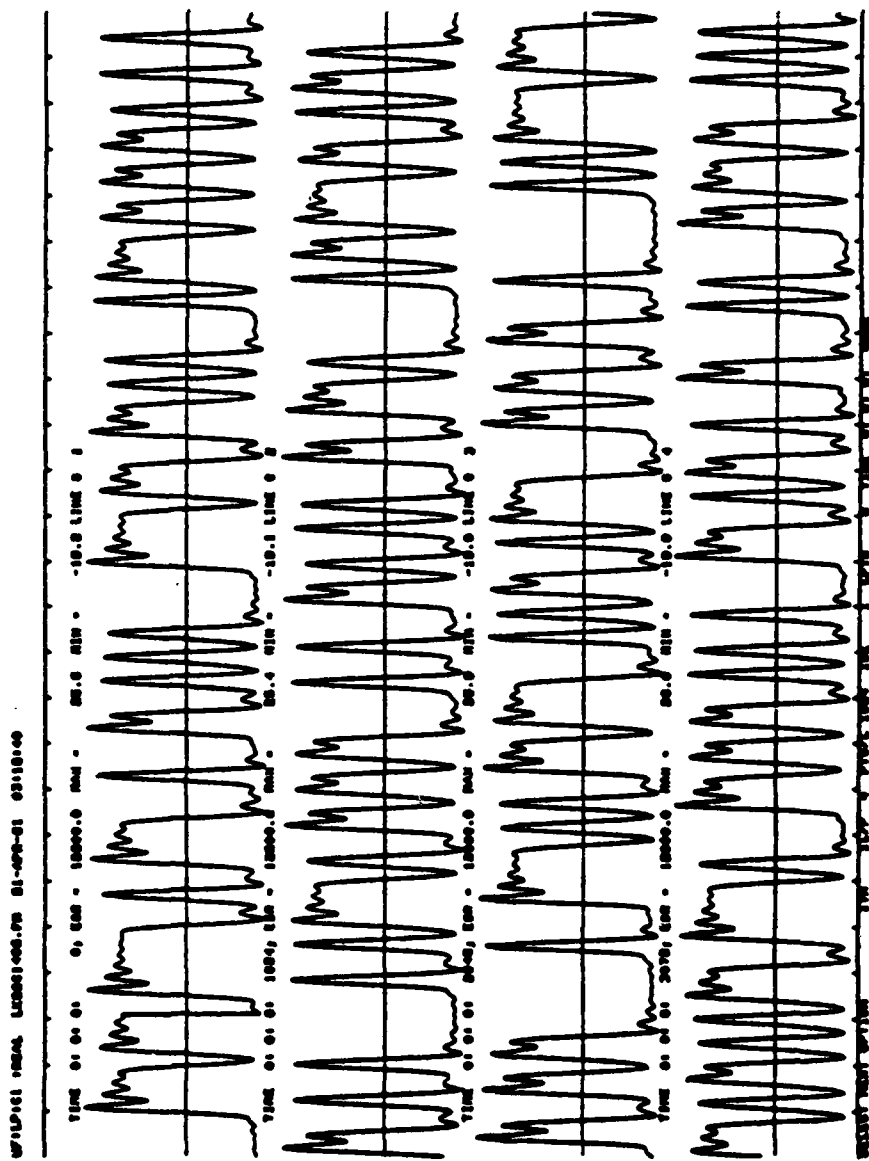
Figure 5-59: LENKURT 26-C FM Waveform for 10 Hz Phase Jitter at 80° P/P
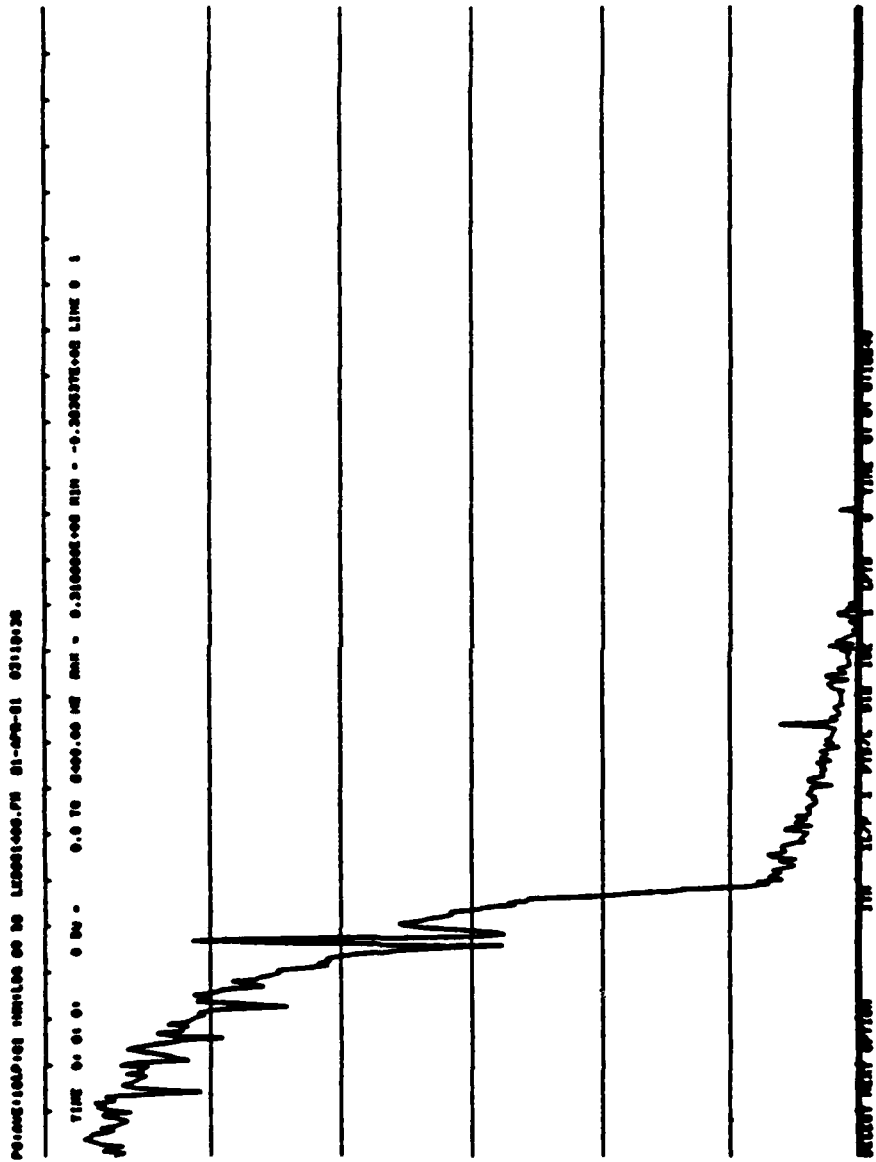
Figure 5-60: Power Spectrum Average of LENKURT 26-C FM for the Case of 10 Hz Phase Jitter at 80° P/P

5.7 RESIDUAL FM ANALYSIS

In the previous section we observed how the phase jitter impairment is seen in the phase waveform. Since the FM is the derivative of the phase, the derivative of the sinusoidal variation seen in the phase waveform must be present in the FM also as a sinusoidal component. The FM recall is largely insensitive to carrier drift and mistuning, making a much more attractive basis for feature extraction than the phase waveform.

Figure 5-61 shows the histogram of the demodulated FM component of the unimpaired LENKURT 26-C modem. Since most time is spent at the extremes in the FM signal, we expect the "U" shaped profile. The means of the histogram extremes, μ_1 and μ_2, are marked. The thresholds T_1 and T_2 are defined as $\mu_1/2$ and $\mu_2/2$, respectively.

Based on the histogram information, it is possible to effectively remove the intentional data transition. Monitoring the FM signal amplitude, we can detect whenever threshold T_1 is crossed and subtract out the expected value of the data transitions, μ_1. Similarly, a FM transition crossing T_2 is detected by thresholding the signal at T_2 and subtracting out the expected value of that transition, μ_2. This is shown in Figure 5-62.

Figure 5-63 shows the effect of removing the intentional data transitions on the LENKURT 26-C sample which has phase jitter at 60 Hz, 80°P/P. Low-pass filtering this residue leaves much of the undistorted, unintentional modulation seen as five periods/1024 sample line as illustrated in Figure 5-64. The signal is resampled by 4 and a high resolution power spectrum generated (Figure 5-65). The 60 Hz jitter component is enhanced by 13dB above the noise floor. Figure 5-66 shows the spectrum of the LENKURT 26-C sample for the unimpaired case which has undergone the same signal processing steps. Note the total absence of 60 Hz spectral components.
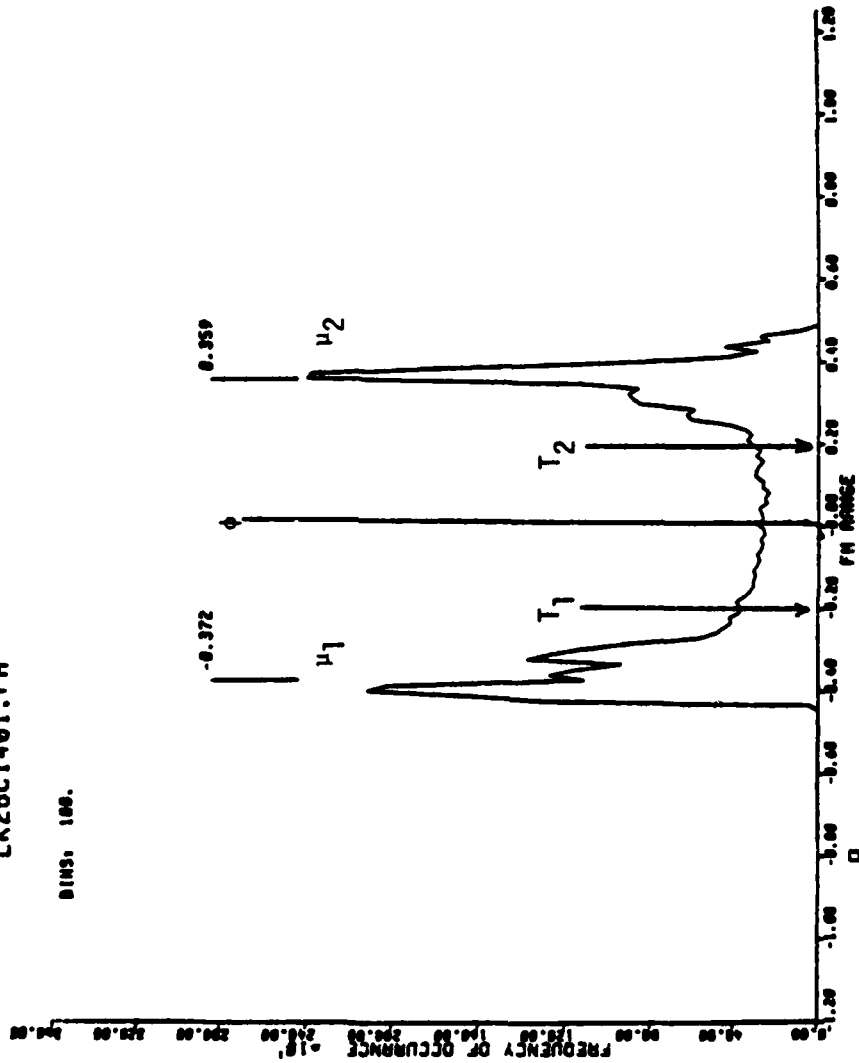
Figure 5-61: FM Histogram for LENKURT Modem Showing Transition Detection Thresholds (T_1, T_2) and Expected Final Data Bit Values (μ_1, μ_2)
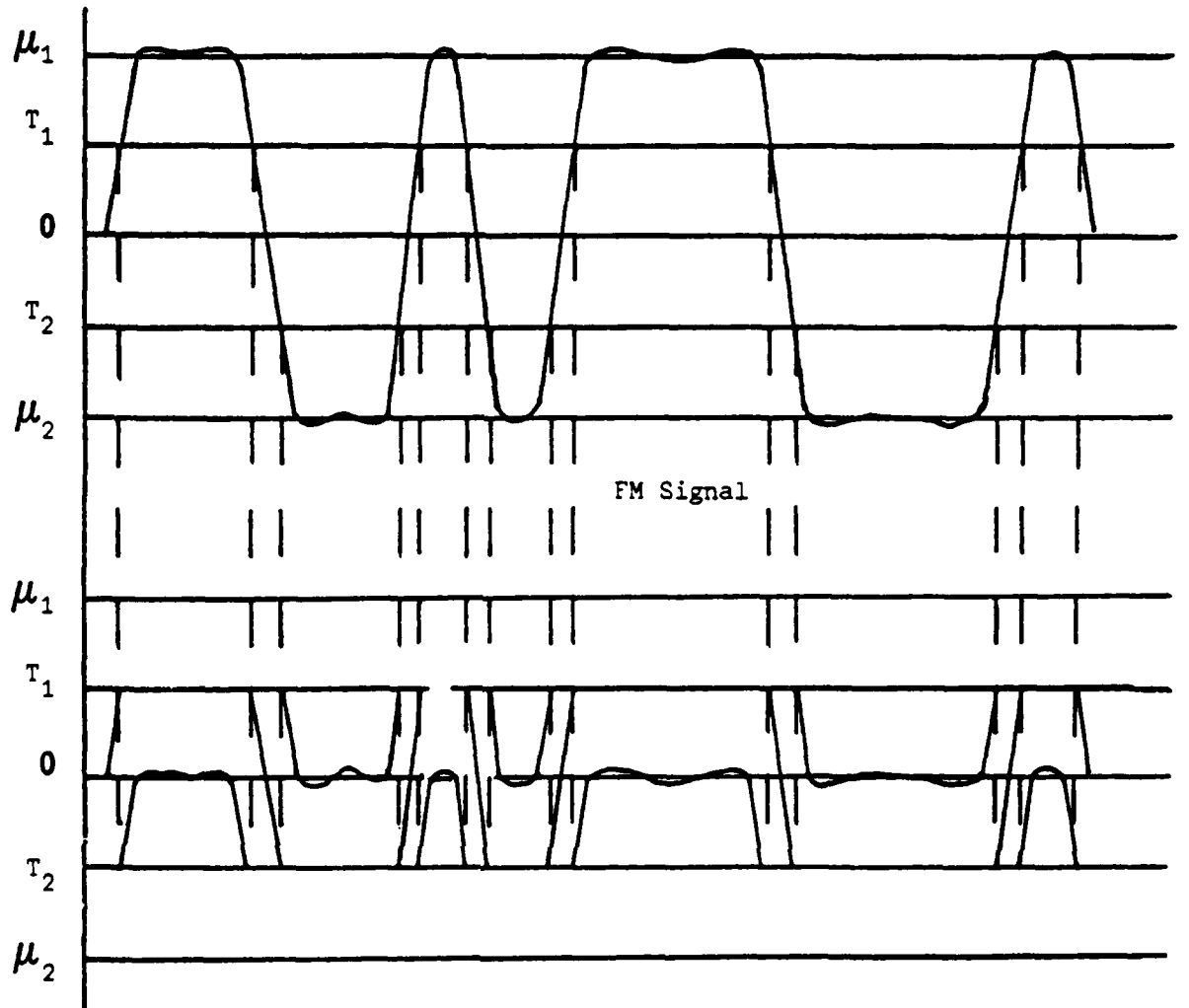
FM Signal

Resultant FM Signal

Figure 5-62   Illustration Of Data Transition
Removal Via Thresholding By T_m
And Subtracting Out The
Anticipated value, $_m$
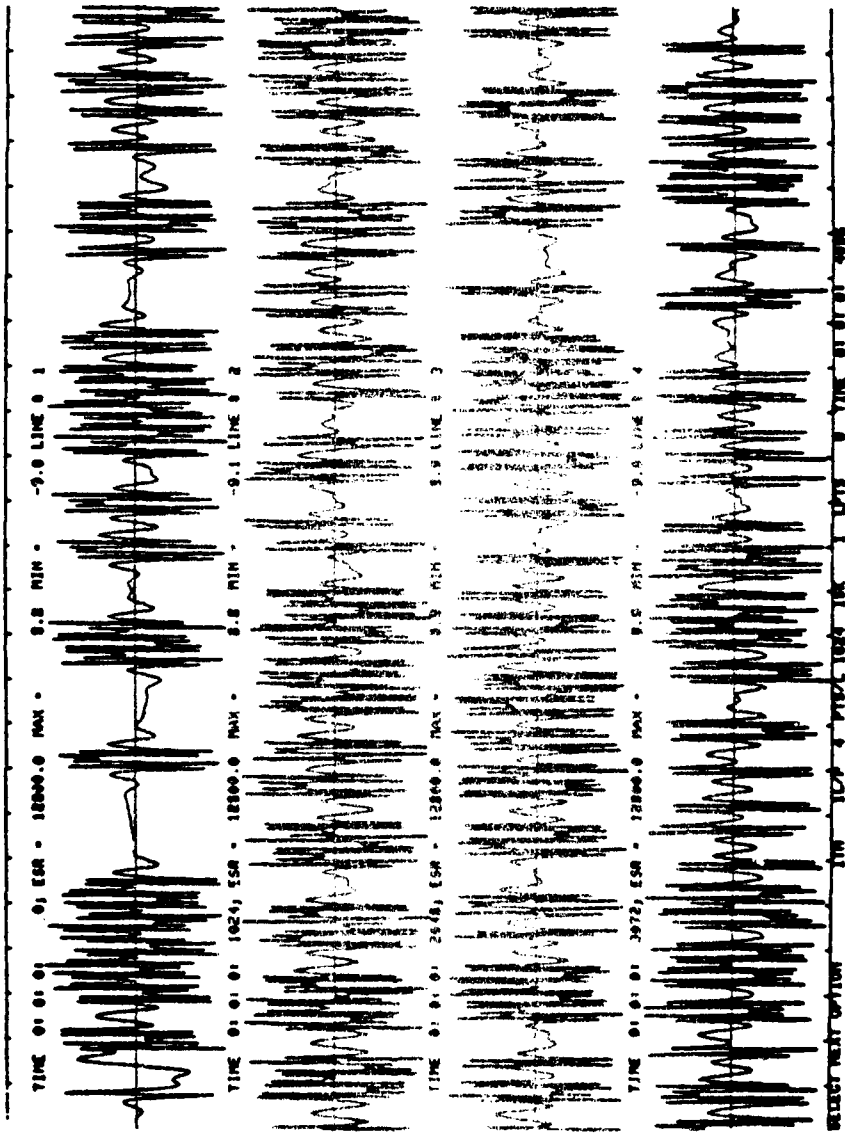
Figure 5-63: Residual FM After Removing Data Transition
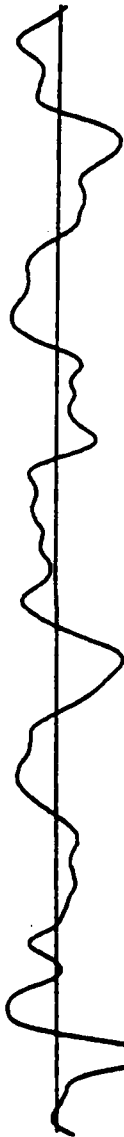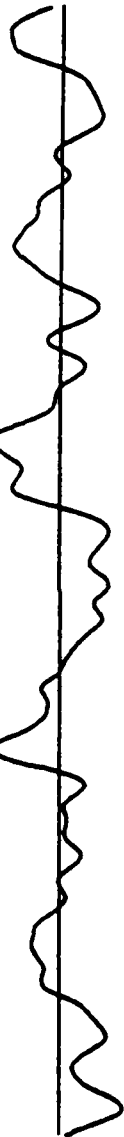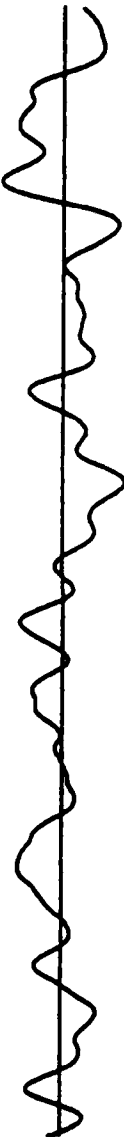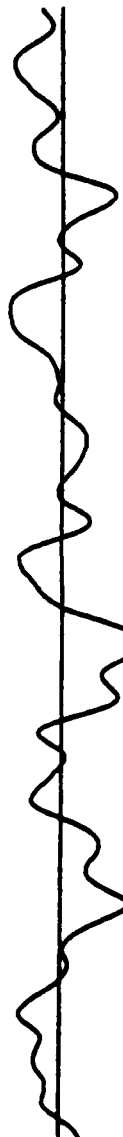
Figure 5-64: Low Pass Filtered FM Residual Waveform
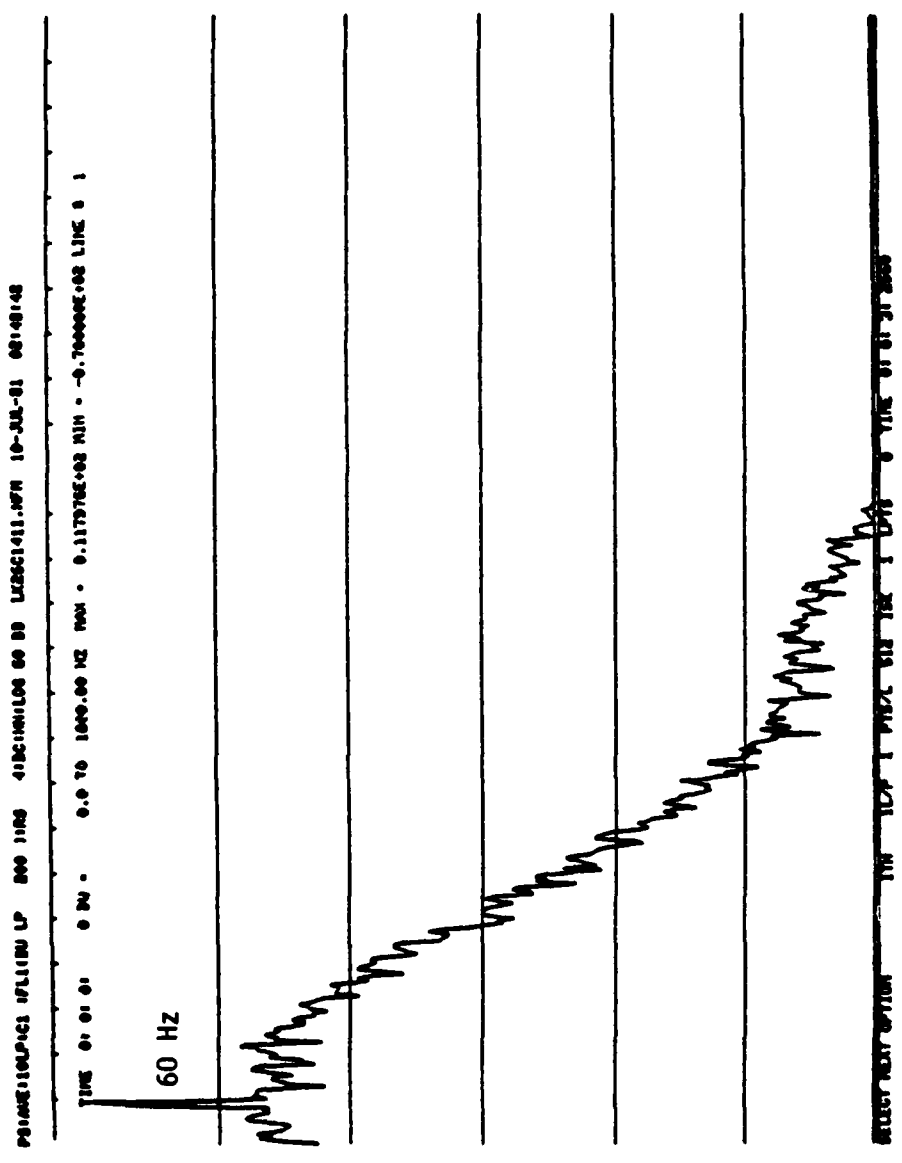
Figure 5-65: High Resolution Power Overage of FM Residual Showing Enhancement
of 13 dB of the 60 Hz Jitter Component

5-85
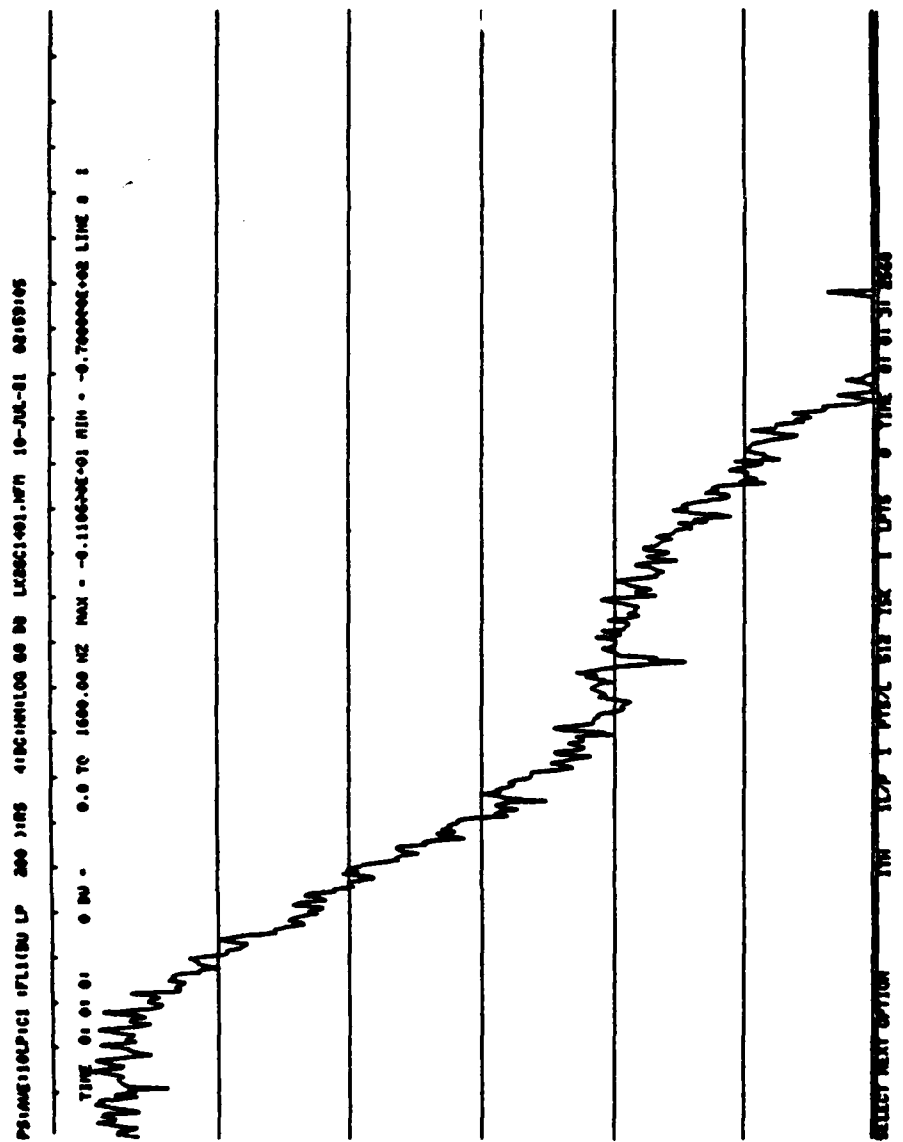
Figure 5-66: High Resolution Power Average of FM Residual Showing a Case Where No Jitter is Present

5-86

This technique was applied to all modem types. It was effective in enhancing the jitter component in almost all cases. The results for the higher speed modems (4800, 9600 and 1600) usually produced a measurable spectral component for cases of 50–60° P/P and above. Sample FM histograms used for the determination of the detection thresholds for the DPSK 1200-baud and DPSK 1600-baud are shown in Figures 5-67 and 5-68. For the DPSK 1200-baud modems, the detection threshold was approximately 30° P/P. For the FSK modems, phase jitter at 10° P/P could generally be seen.

A shortcoming of the algorithm, however, is its lack of sensitivity in the detection of the 10 Hz phase jitter except at the most severe cases of 60°–80° P/P.

5.8 ADAPTIVE CHANNEL MODELING

In adaptive channel modeling, a mathematical model having a number of adjustable parameters is formulated to represent the physical transmission facility. The free parameters are then adjusted by adaptive algorithms to provide a close fit to the observed signal. Then the values of the adapted free parameters describe the channel. The parameters are adapted using decision feedback. That is, the received signal is demodulated, the data sequence is estimated, and the result is fed back to reduce data-dependent effects and to better reveal channel effects.

Appendices A and B present studies of the adaptive modeling concept. Appendix A derives a linear filtering model of the channel, while Appendix B derives and describes a nonlinear model. The linear filtering model is basically an adaptive equalizer combined with a demodulator and remodulator. The demodulator determines the data sequence, and the remodulator determines what a noise-free undistorted version of the signal would look like. Then the adaptive equalizer estimates what linear filtering would best make the original signal resemble the received signal. The linear filtering is modeled with a tapped delay line. Once the linear filtering is determined, then the
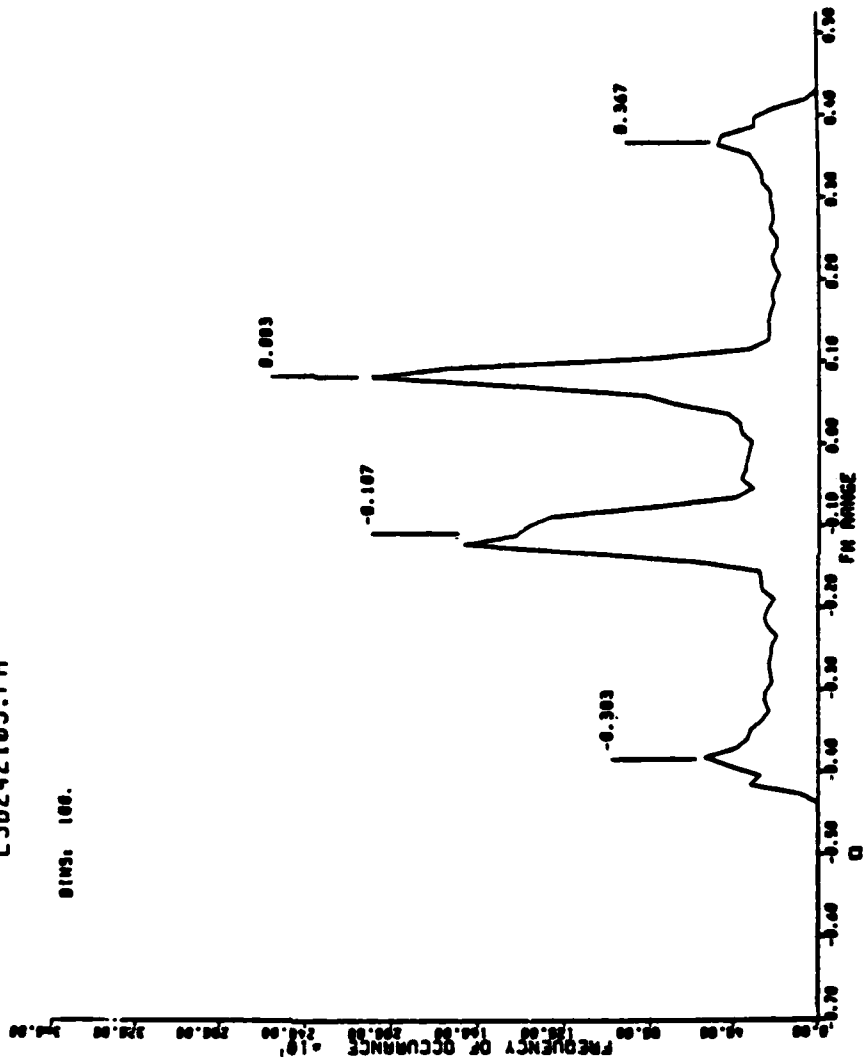
Figure 5-67: FM Histogram for the DPSK 1200 Baud Modems

LSA482104.FM

BINS: 100.
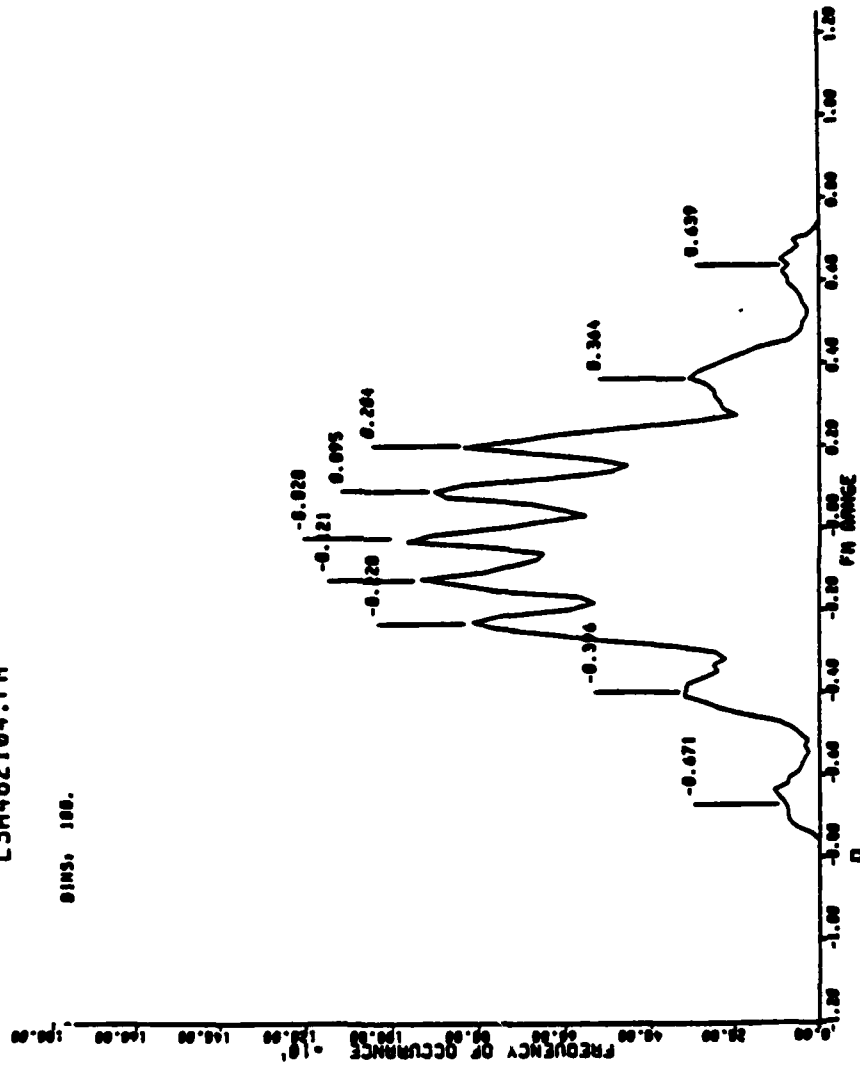
Figure 5-68: FM Histogram for the DPSK 1600 Baud Modem

difference between the filtered original signal and the received signal is considered additive noise.

The adaptive equalizer can be replaced with a non-linear adaptive device. A method for doing this is derived in Appendix B. The method is based on the Volterra series method of handling nonlinearities. The resulting adaptive nonlinear device is shown in Figure 3 of Appendix B. It consists of two tapped delay lines. One is used to model linear filtering effects of the channel, as before. The other has its output squared and is used to model quadratic nonlinearities.

The adaptive channel models, while theoretically interesting, turn out to be highly complex compared to the requirements of the present application. Each requires a model of both the modulator and demodulator sections of each modem, in addition to adaptive linear or nonlinear devices. One possible method of implementation might then be to use a bank of one each of all the modems whose signals might be received. An alternative would be to model all the modems using software. Due to complexity constraints, the adaptive channel models were not implemented in the present effort.

5.9 CHANNEL SIGNAL TO NOISE ESTIMATION

The ability to estimate the signal to noise ratio (SNR) of the VF line would potentially be valuable in the Phase 1 go/no-go decision as well as in the Phase 3 impairment characterization. Certainly a VF line which exhibited an exceptionally poor SNR has degraded beyond being able to supply acceptable service.

Two approaches to estimating the channel SNR were considered: spectral analysis and statistical analysis. The spectral approach traditionally operates on a sufficient average of spectral estimations of the VF line. A region of the spectral average is identified as being within the passband of the observed process but not as being used by the system for data

transmission. An estimate of this idle passband region power is formed by averaging the spectral components in the region. A similar estimate is performed in another region which is also known to be in the passband of the system but which also is known to be active with signal transmission. Since the latter estimation contains both signal and noise, the estimate of the noise power is subtracted out before forming the SNR as

$$SNR = \frac{Ps - Pn}{Pn}$$

where Ps and Pn represent the signal power and noise power estimates, respectively.

Examination of the typical signal spectrum from Section 5.1 shows that all of the VF line bandwidth is utilized by the signaling strategy. There is typically no idle band in the VF data communications system.

This suggests the requirement for statistical estimation of the channel SNR. If the modem input is assumed to be a random sequence $(R(t))$ then over some sufficiently long interval Δt we expect the modem transmitter output $(S(t))$ to exhibit the same output amplitude profile.

As noise $(N(t))$ is added, the composite output signal $C(t)$ is formed as illustrated in Figure 5-69. We now define the peak to average ratio of the composite signal over the N sample window T_j as

$$PA_j = \frac{C_p}{\mu_c}$$

where μ_c is defined as the mean of the full wave rectified signal;

$$\mu_c = \frac{1}{N} \sum_{i=1}^{N} |C(i)|$$

and C_p the peak value of $C(t)$ over the N sample window.
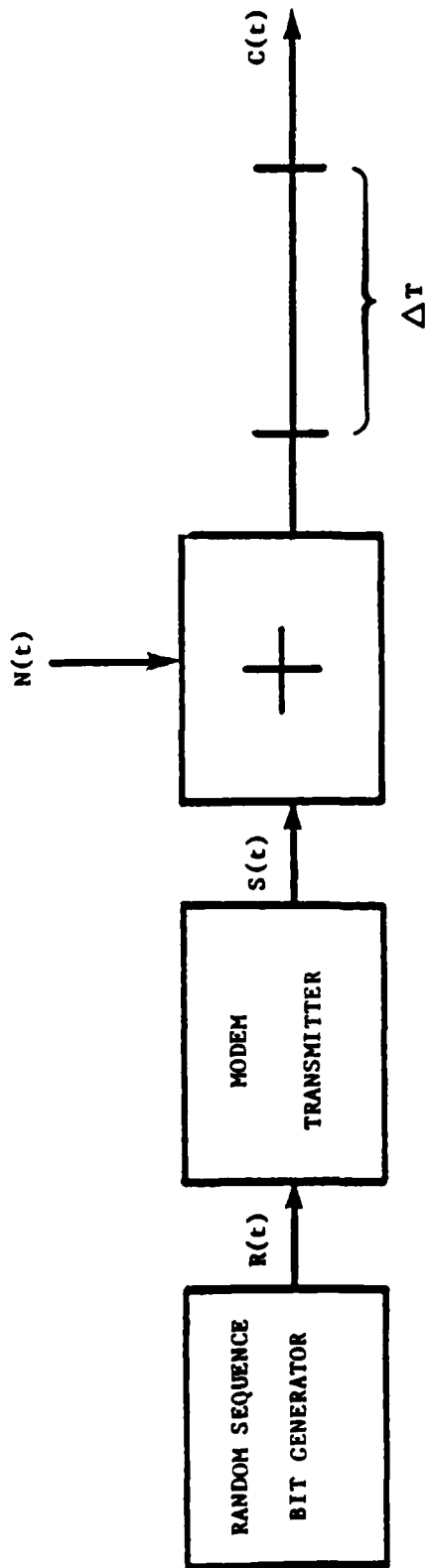
Figure 5-69 Model Of Additive Noise In a VF Communication Channel

The average peak to average ratio over all N sample windows of the signal sample is

$$\mu_{PA} = \frac{1}{N} \sum_{j=1}^{L} PA_j$$

over the L available N sample windows. The variance of the rectified peak to average ratio, μ_{PA}, is given as

$$\sigma_{PA} = \frac{1}{N} \sum_{j=1}^{L} (\mu_{PA} - PA_j)^2$$

As Gaussian noise is added to the system, the expected value of the rectified signal, μ_c, is unchanged. The peak value of C(t) over the observation window is increased by the peak amplitude of N(t). The increase in PA_j is therefore a direct function of the amount of noise added to the channel. The average value of the peak to average ratio μ_{PA} is expected to be a stable measure of the noise present on the channel. This is illustrated in Figure 5-70.

If the N sample observation window is not of infinite duration, then μ_{PA} will vary in proportion to the probability of experiencing a maximum value of N(t) over the observation window. In the absence of noise, however, μ_{PA} is quite stable. Therefore we expect that the variance of μ_{PA}, σ_{PA}, will also vary in proportion to the amount of noise present on the line.

Let us now consider how impairments other than additive Gaussian noise will affect the parameters μ_{PA} and σ_{PA}. Referring to the wireline simulator functional diagram in Figure 5-71, it is observed that phase jitter can be considered to be low frequency FM of the entire signal spectrum. The parameter phase jitter frequency controls the oscillator frequency. The gain in degrees peak to peak of phase jitter controls the amount of FM at the specified frequency. FM modulating the signal directly alters the signal zero crossing information. The signal amplitude is affected only by a small amount of residual AM which accompanies the intentional FM modulation.

WAVEFORM SEGMENT

SEGMENT 1   SEGMENT L

RECTIFIED SEGMENT (MAGNITUDE)

PEAK _____   PEAK _____

AVE   AVE

SEGMENT 1   SEGMENT L
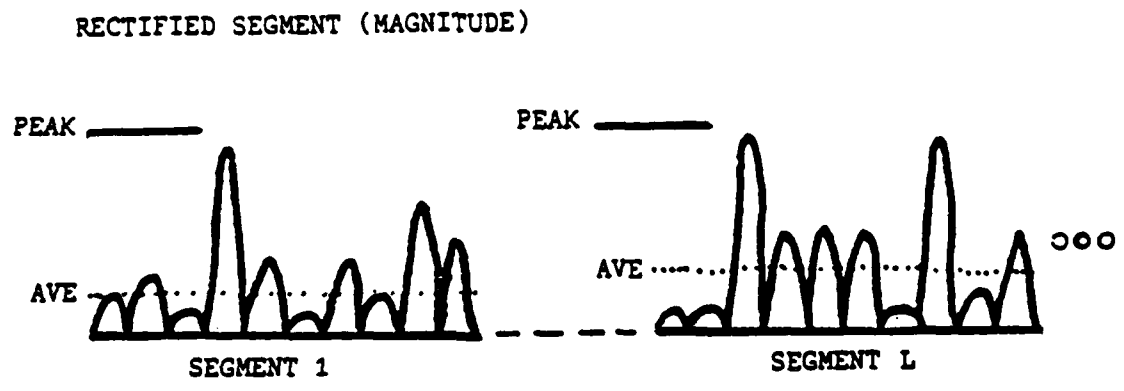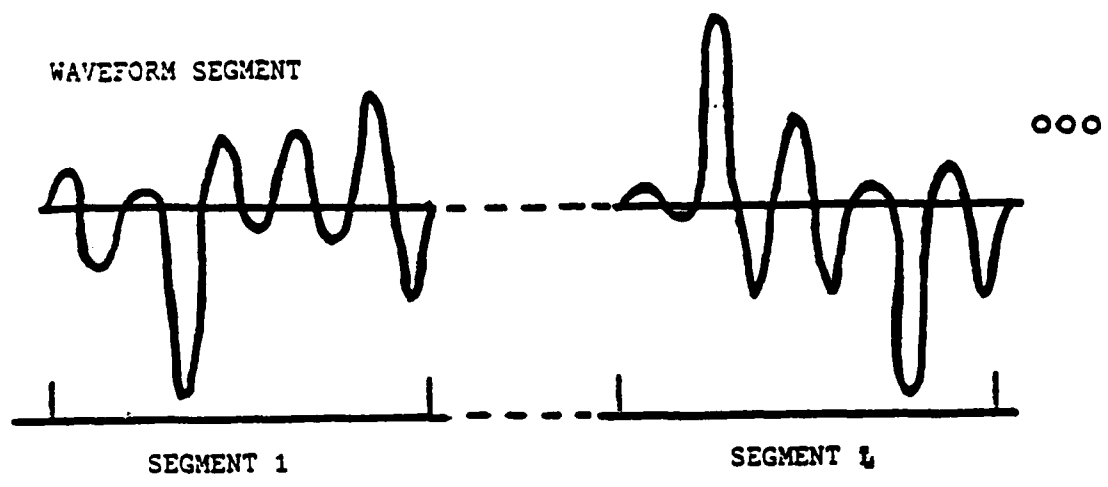
Figure 5-70 Illustrations Of The Calculation Of
Peak To Average Signal Value
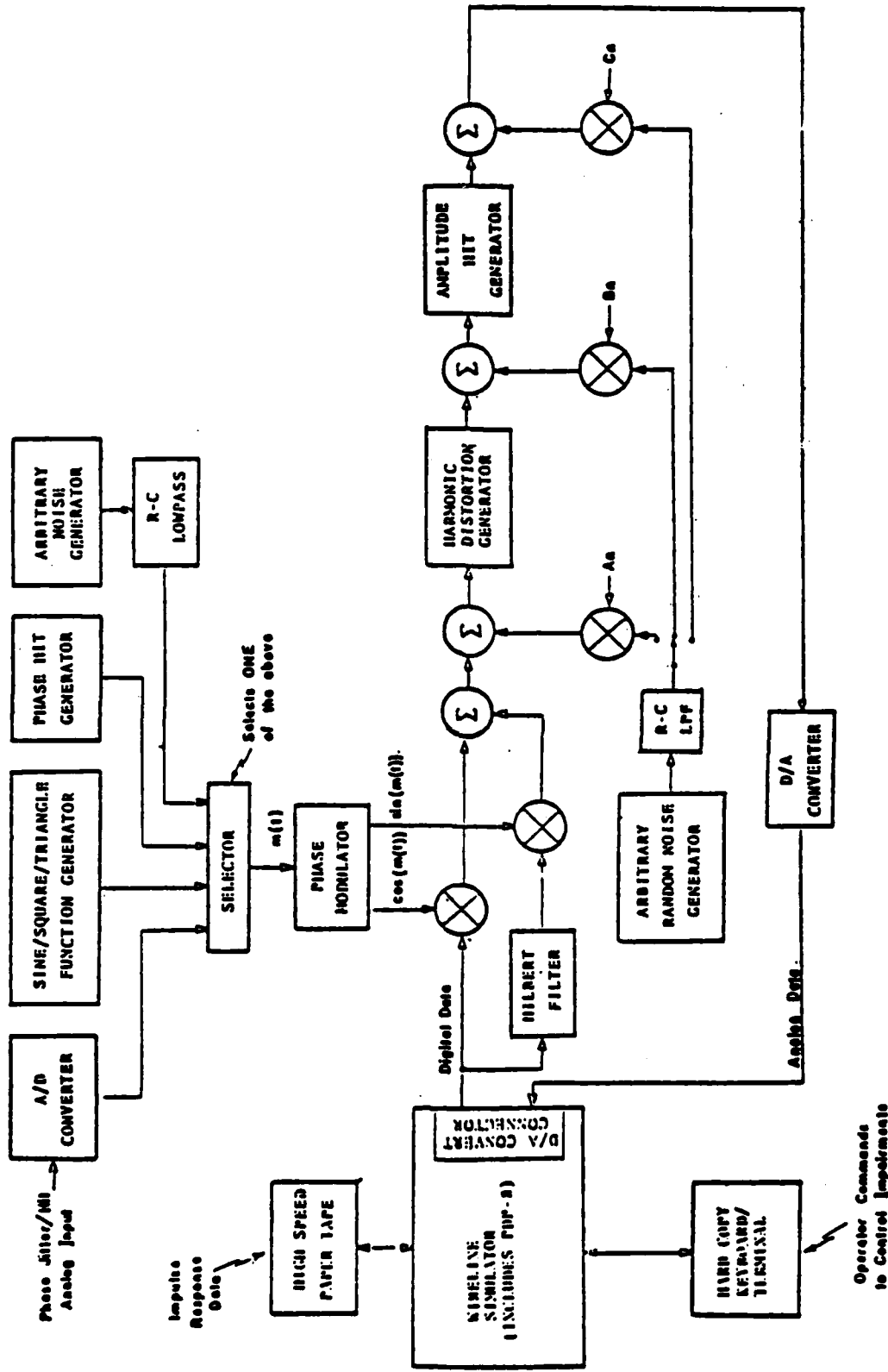
Figure 5-71   Upgraded Wireline Simulator

The parameters μ_{PA} and σ_{PA} are dependent only upon the signal amplitude information. Variations in the zero crossing information of the signal should not affect the measurements. Therefore, the signal parameters μ_{PA} and σ_{PA} are largely immune to the presence of phase jitter on the channel.

The effect of harmonic distortion on μ_{PA} and σ_{PA} is not as clear. Referring again to the functional block diagram of the wireline simulator shown in Figure 5-71, we observe how the harmonic distortion is achieved. The signal S(t) is passed through a series of nonlinear devices which raise the input signal to the power of 2,3,4,5, etc., each added with a specified gain to the input signal. The resultant composite signal C(t) is of the form

$$C(t) = S(t) + aS^2(t) + a_2S^3(t) + a_3S^4(t) + a_4S^{5}(t)\ldots$$

where a_n are the desired gains for the power series components.

For the MSA database collection, odd harmonic distortion was specified, the effect of which is typical of the application of a soft-limiting device. The composite output signal C(t) is of the form:

$$C(t) = S(t) + a_2S^3(t) + a_4S^5(t)$$

Each of the terms, $a_iS^N(t)$ can be shown to contain the component S(Nwt).

The odd harmonic distortion which occurs during soft limiting of the signal through typical telephone exchanges is illustrated in Figure 5-72.

Viewing this distortion as a series of the form

$$C(t) = S(w_ot) + a_2S(3w_ot) + a_4S(5w_ot),$$

the resultant waveform is being squared off due to the addition of the higher in-phase odd harmonics. The more severe the odd harmonic distortion, the more

CLIP LEVEL →
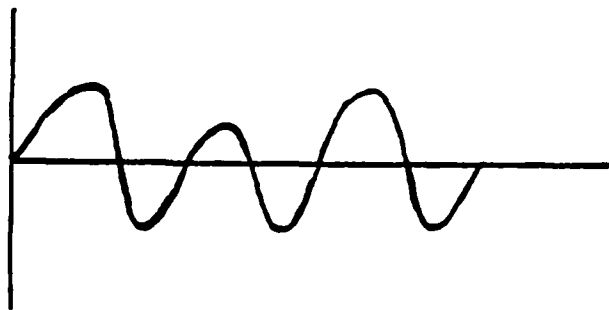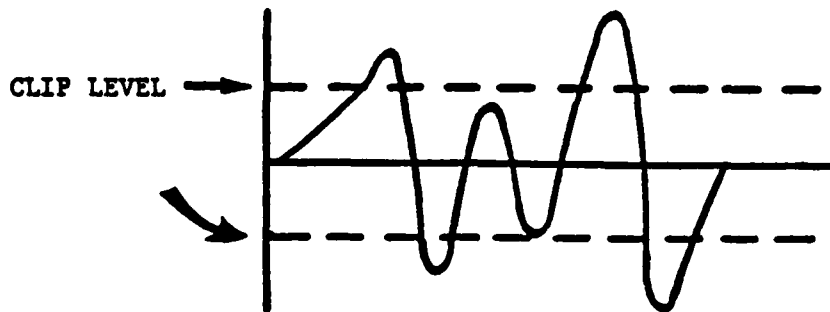
Figure 5-72   Effects Of Soft-Limiting On
An Active Line Signal

constricted the resultant waveform and the lower the peak to average ratio, μ_{PA} as well as the variance σ_{PA}.

From the above discussion, we expect that the effects of adding noise, phase jitter and odd harmonic distortion to the signal will affect the parameters μ_{PA} and σ_{PA} as follows:

PARAMETERS	GAUSSIAN NOISE	PHASE JITTER	ODD HARMONIC DISTORTION
μ_{PA}	increase	no change	decrease
σ_{PA}	increase	no change	decrease

An extensive experimental investigation of the MSA database has shown this to be the case.

Software was developed which would calculate, for each waveform file of a specified list, the parameters μ_{PA} and σ_{PA} for a specified window length. A list of waveform filenames corresponding to all samples of a single modem was generated for each of the 11 modems. Recalling the file naming convention described in Section 2, the list of all LENKURT 26-C modem cuts, for example, is simply all files beginning with the character "L". The modem waveform list included all impaired cuts for that modem as well as any "clean" cuts available. The list of modem sample cuts was processed to produce two output files, one containing the estimated values of μ_{PA} for each cut, and the second containing the σ_{PA} estimations. A separate program accepted these files, ordered the data points by degree of impairment, and produced an output plot for each parameter.

Figure 5-73 and Figure 5-74 show these plots for the HUGHES HC-276 2400 bit/ second DPSK modem using a window length of 256 samples. The left axis corresponds to the degree of impairment, either Gaussian noise or harmonic distortion added. Harmonic distortion is represented on the plot by the symbol "$\square$". For the HC-276, harmonic distortion was added over a range from -30dB to a worst case of -4dB in 8 steps. Gaussian noise in isolation added to the signal is represented by the symbol "$\triangle$", and is present from -30dB to -6dB in 7 steps. The symbol "∇" denotes cuts which have a combination of Gaussian noise and phase jitter added. Since we expect that the phase jitter

will not affect the parameters under investigation, the cuts containing both impairments are plotted only by the Gaussian noise content. Recall that any time phase jitter occurs in combination with Gaussian noise, the frequency of the phase jitter is 60 Hz.

The right hand axis corresponds to the isolated phase jitter cases of all frequencies. The range for the HC-276 is from 10°P/P to 80°P/P. All frequencies of phase jitter are denoted by the same symbol, "O".

Two other symbols may be present. First, the symbol "$*$" which indicates a cut passed through the wireline simulator 4A characteristic but with no impairments added. Secondly, the symbol "+" which is a direct modem sample by-passing the simulator.

Examining Figures 5-73 and 5-74 we observe the "root" of the function on the plot base-line corresponding to additive Gaussian noise (AGN) at -30dB and harmonic distortion (HD) at -30dB. We are considering a channel with -30dB of HD or AGN to be completely acceptable. Note that as HD increases on the line (the symbol $\square$), the parameters μ_{PA} and σ_{PA} decrease in a regular fashion. Similarly, as AGN on the line increases, the parameters σ_{PA} and μ_{PA} increase regularly regardless of the frequency or amount of phase jitter (PJ) combined with the noise.

Figure 5-73: Peak to Average Ratio of the Rectified Signal
Waveform for the Highes HC-276 Modem

HC276.M3
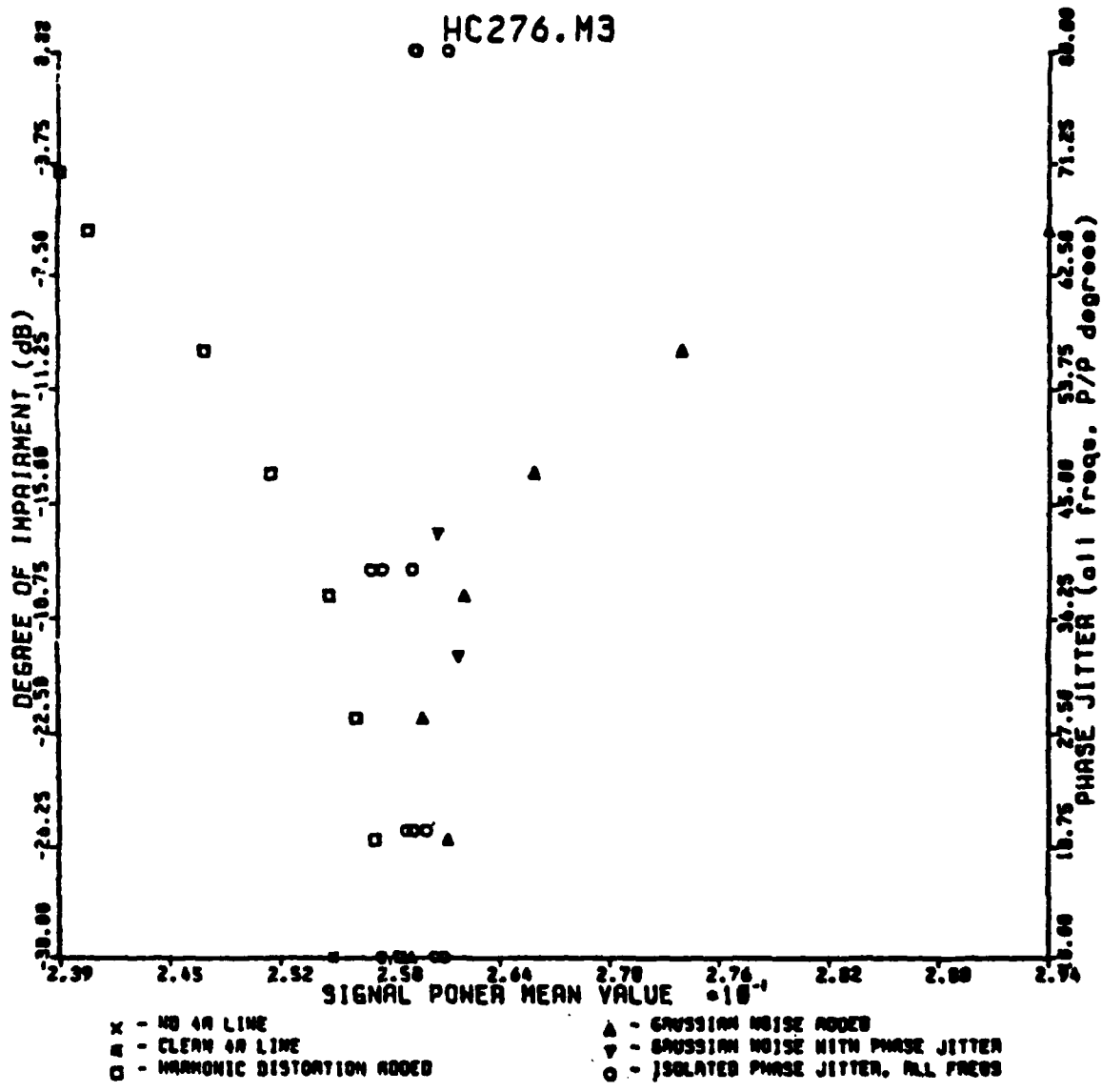
Figure 5-74: Peak to Average Ratio Variance of the Rectified
Signal Waveform for the Hughes 276 Modem

5-101

Figure 5-75 and 5-76 show the μ_{PA} and σ_{PA} plots for the WECO 207A2 2400 baud, DPSK modem. No HD was collected for the WECO modem; however, the profile of the plot is as anticipated. The increased AGN raises the σ_{PA} and μ_{PA} parameters. The PJ cuts are within a small range corresponding to "good data".

The CODEX LSI-48 mode B 2400 baud DPSK modem is shown in Figures 5-77 and 5-78. Again, no HD was collected. The PJ and AGN points exhibit the same characteristic profile. The three modems, HC-276, WECO 207A2, and CODEX LSI-48 Mode B shown in Figures 5-73 through 5-78 are the same generic modem type; DPSK 2400 bits/ second, 1200 baud with a 1800 Hz carrier. We would hope that the characteristic μ_{PA} and σ_{PA} functions would occupy the same range for each modem. Figure 5-79 and 5-80 show the three modems on the same plot for a 256 point sample window. The characteristic profile of each modem is slightly offset from the rest. Varying the length of the window used in the calculation from 128 samples to 1024 samples did not improve the result. It was decided that some subtle variation in the modem signaling format or the collection process caused the disagreement. Software was developed to normalize the input signal by first removing any bias inadvertently added in the collection process, and second by normalizing the total power to unity in an attempt to remove any discrepancies in collection gain. Some improvement was shown. The best attempt at removing the offset between the functions is the plot of the normalized signals shown in Figures 5-79 and 5-80.

Figures 5-81 and 5-82 show the μ_{PA} and σ_{PA} plots for the LENKURT 26-C modem respectively. Figures 5-83 and 5-84 show the μ_{PA} and σ_{PA} for the MD-674 modem. Both modems belong to the same generic group: FSK modulation with carriers at 1200 Hz and 2400 Hz and with a baud rate of 1200. The LENKURT 26-C plots show cases of harmonic distortion which were not collected for the MD-674 modem.
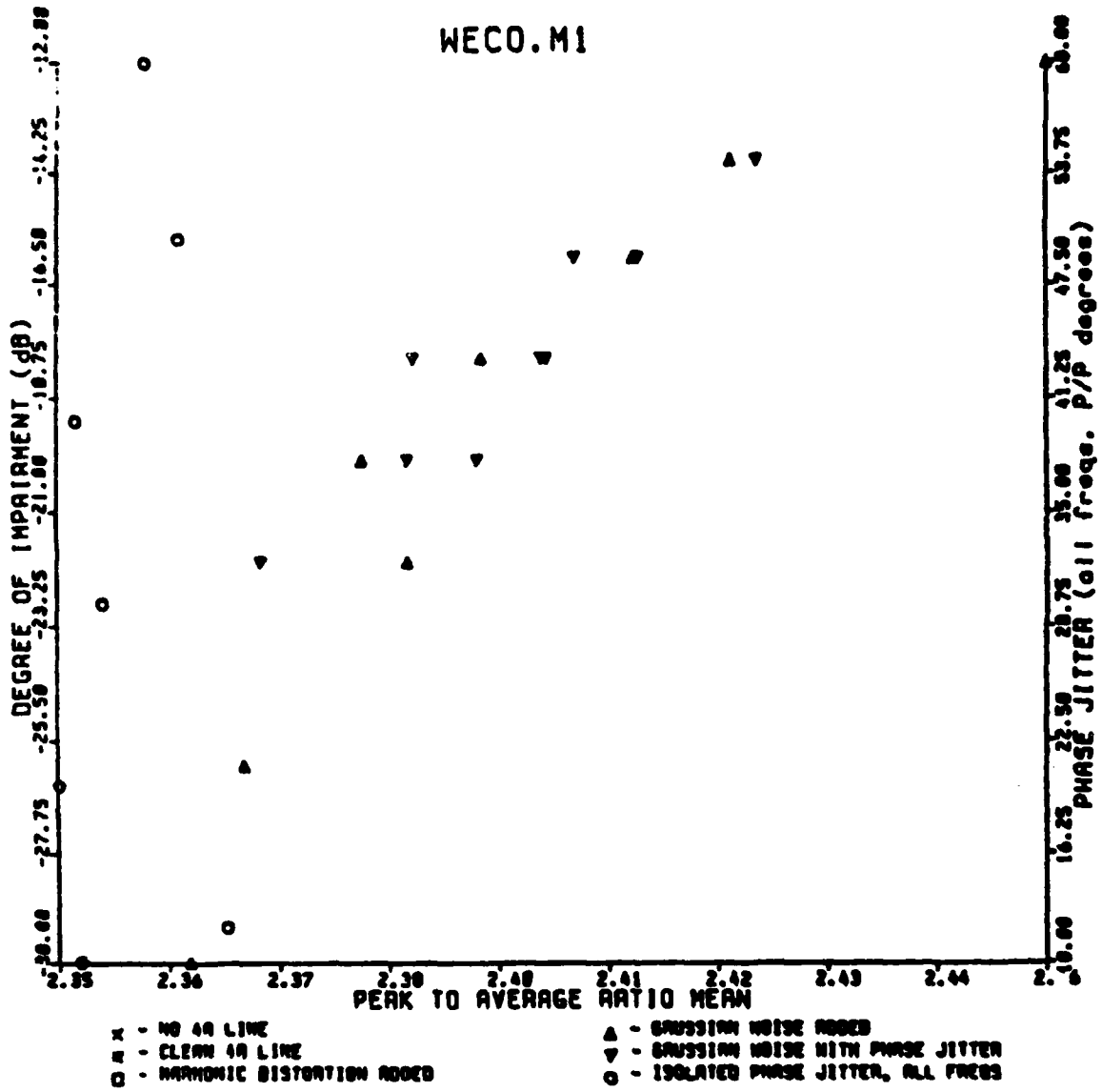
Figure 5-75: Peak to Average Ratio Variance of the Rectified
Signal Waveform for the WECO 207A2
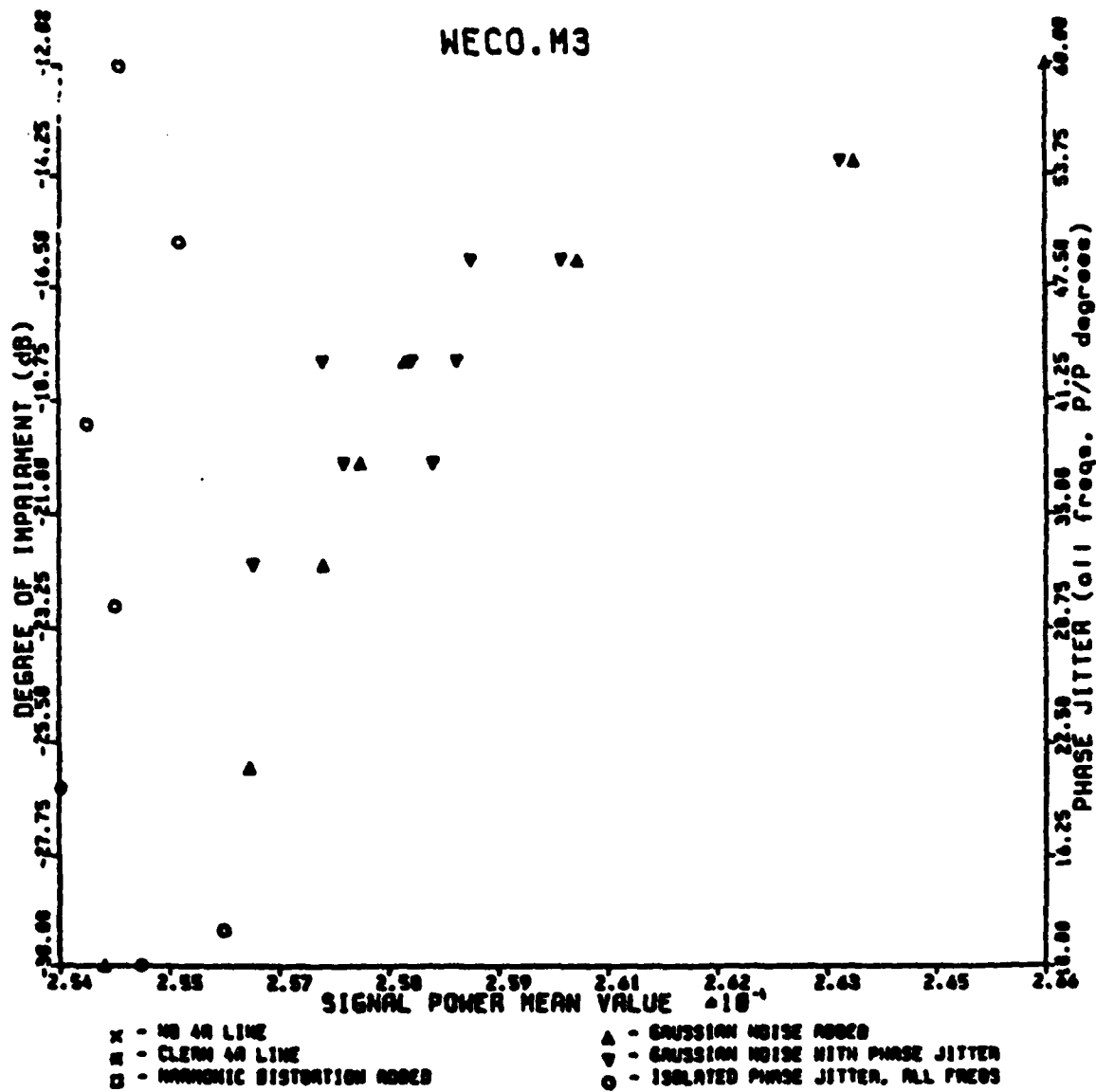
Figure 5-76: Peak to Average Ratio Variance of the Rectified
Signal Waveform for the WECO 207A2 Modem
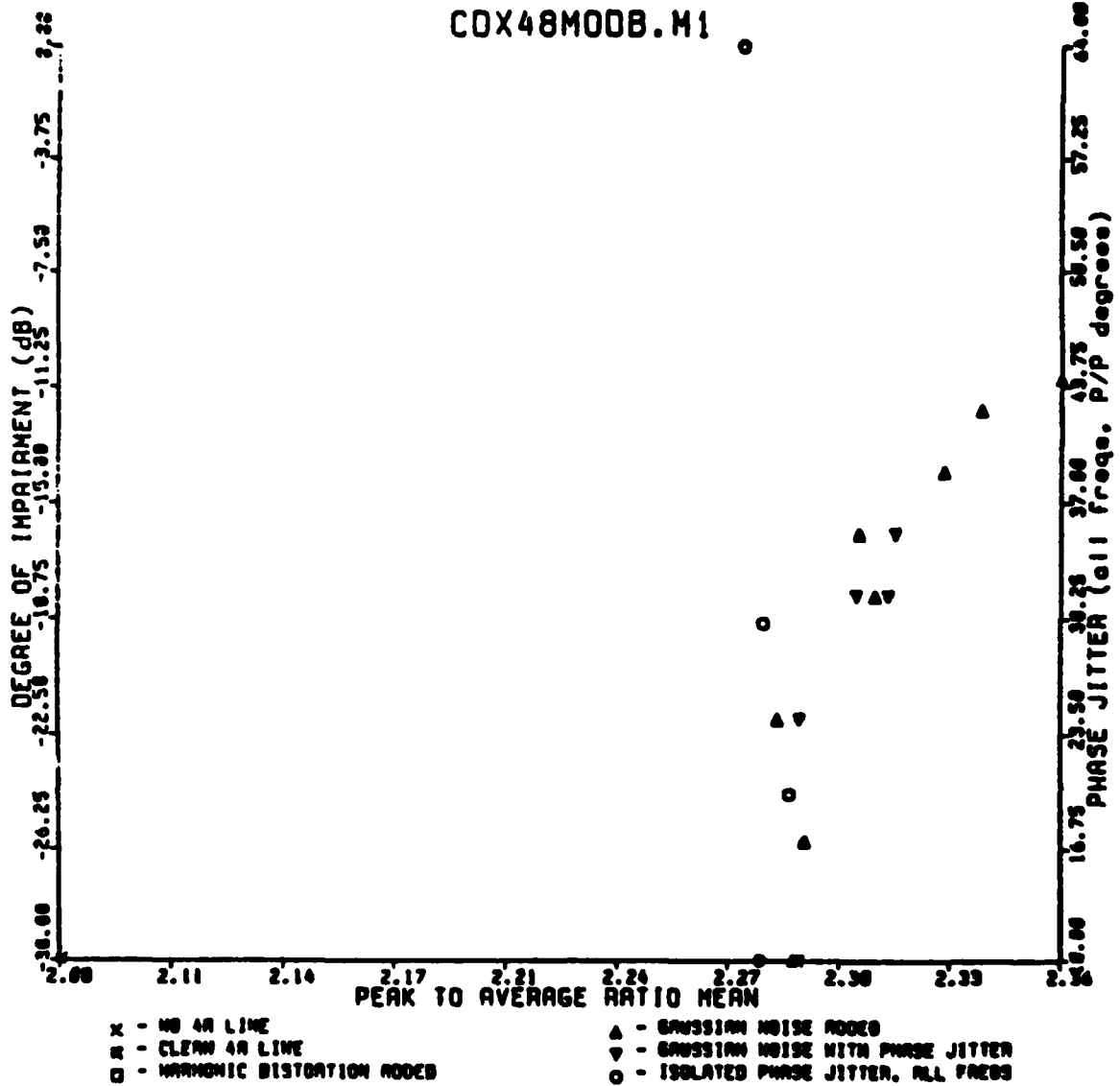
Figure 5-77: Peak to Average Ratio of the Rectified Signal
Waveform for the CODEX LSI-48 Mode B Modem

COX48MODB.M3
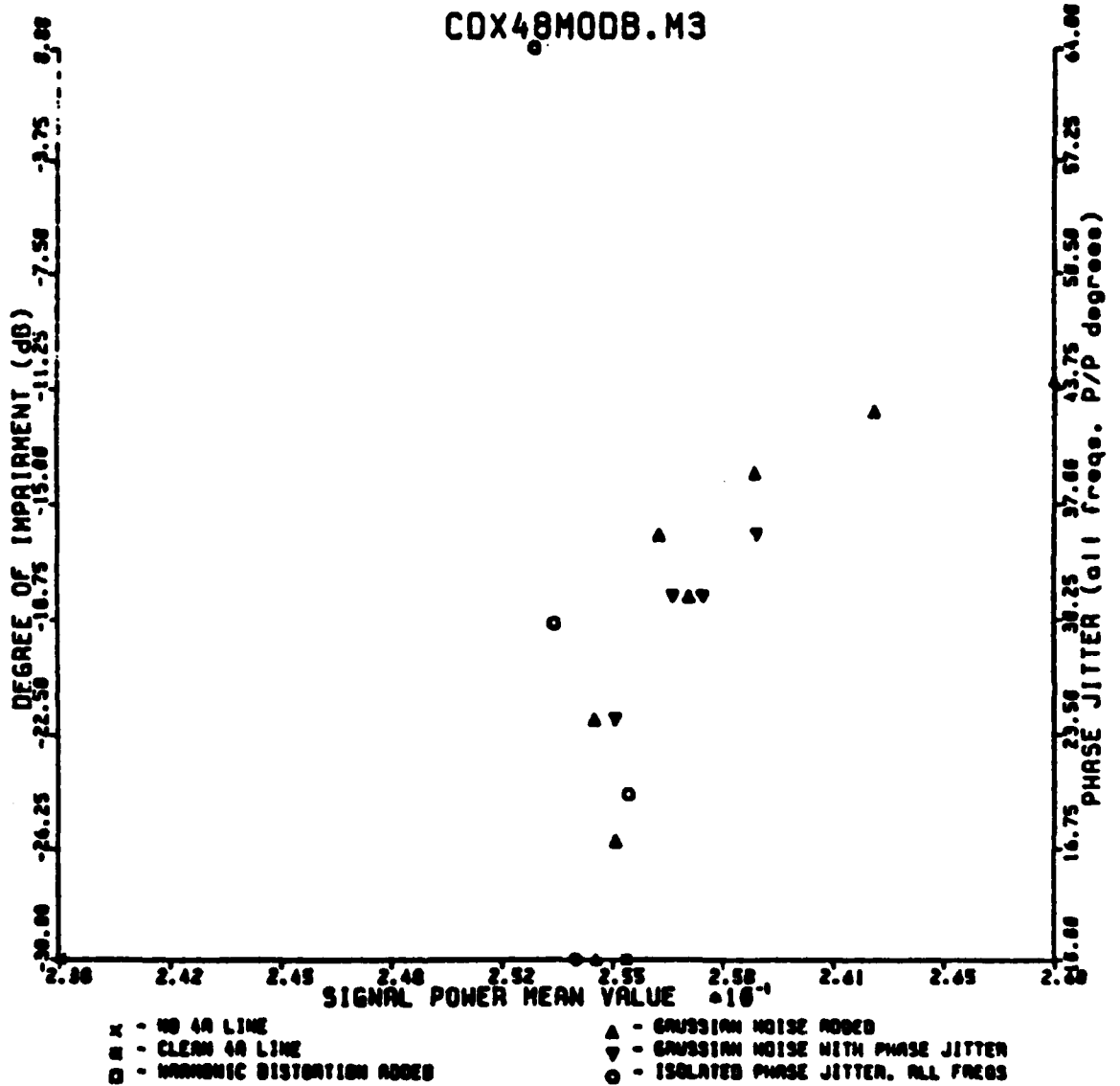
Figure 5-78: Peak to Average Ratio Variance of the Rectified
Signal Waveform for the CODEX LSI-48 Mode B Modem
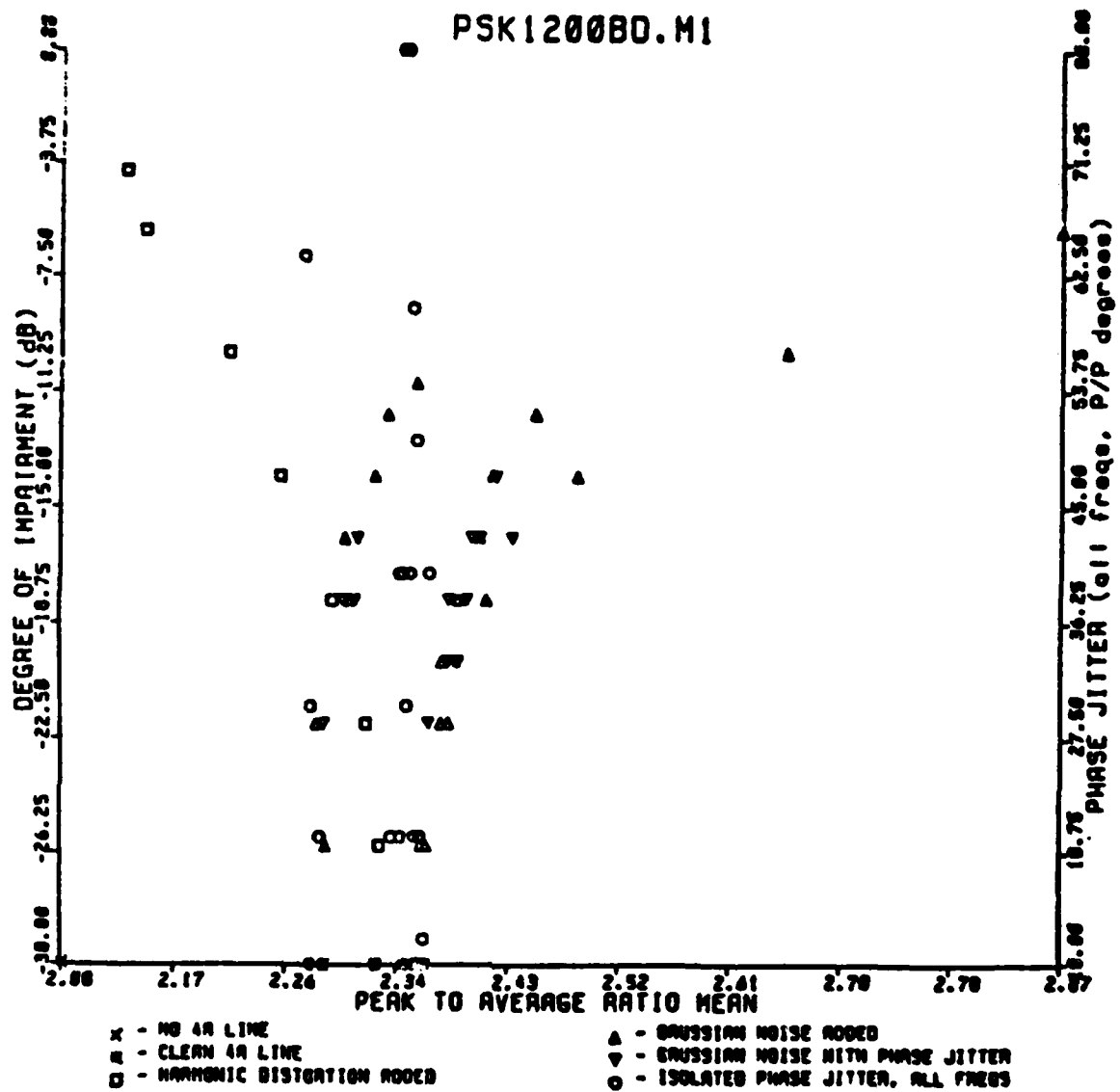
Figure 5-79: Peak to Average Ratio of the Rectified Signal
Waveform for the HUGHES HC-276, WECO 207A2 and
CODEX LSI-48 Mode B
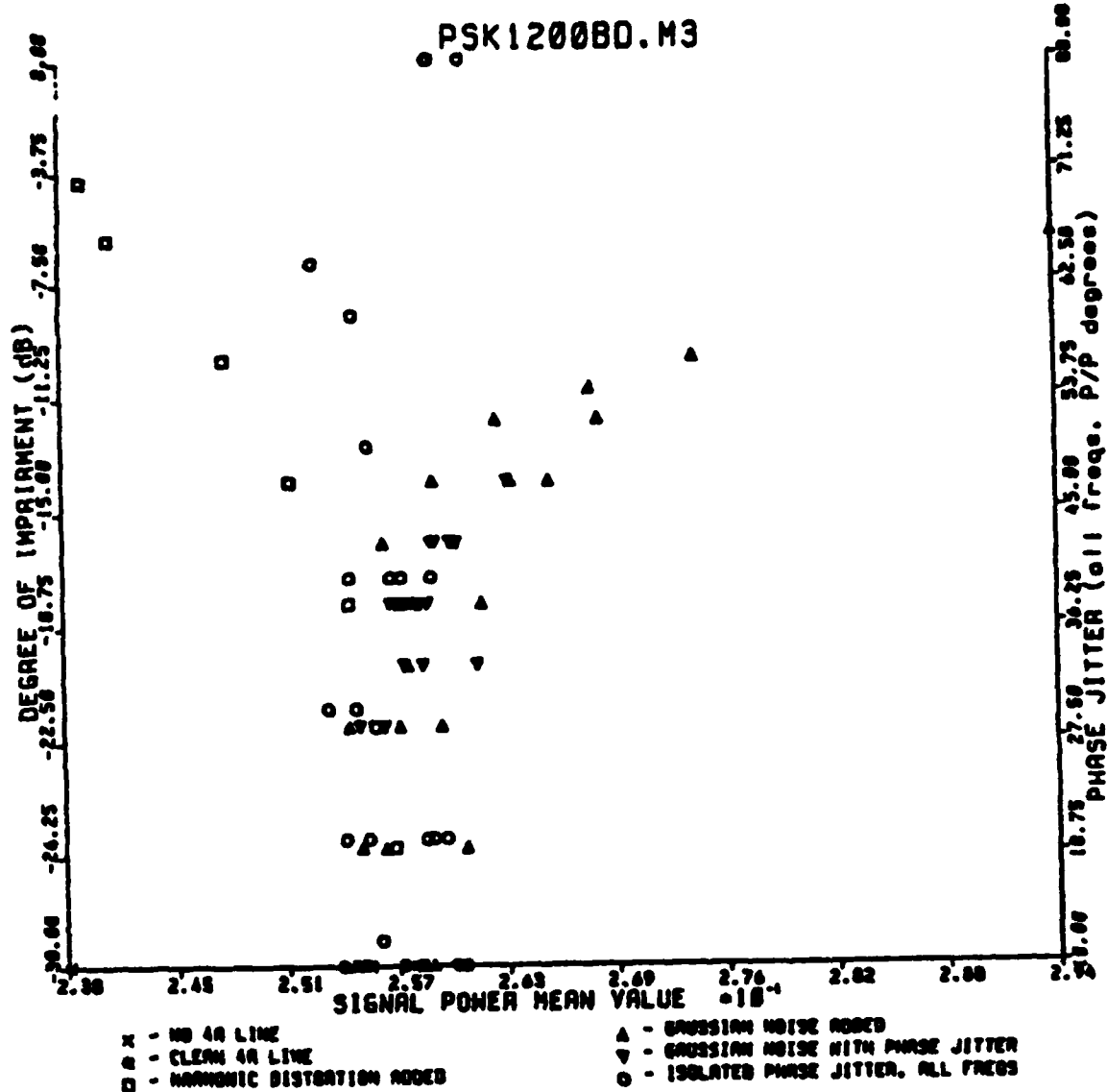
Figure 5-80: Peak to Average Ratio Variance of the Rectified
Signal Waveform for the Hughes HC-276, WECO 207A2
and CODEX LSI-48 Mode B Modems

LK26C.M1
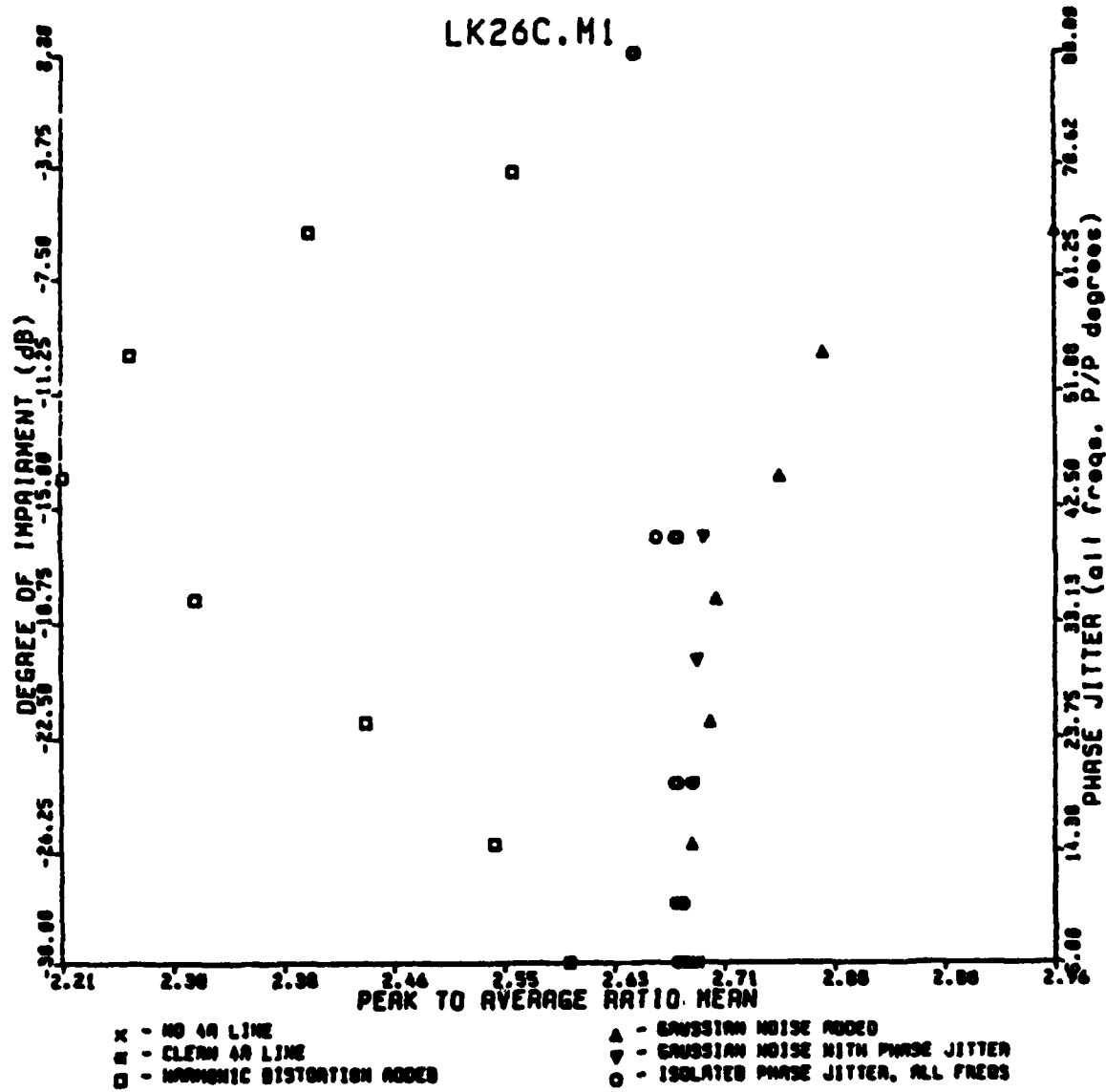
Figure 5-81: Peak to Average Ratio of the Rectified Signal
Waveform for the LENKURT 26C Modem
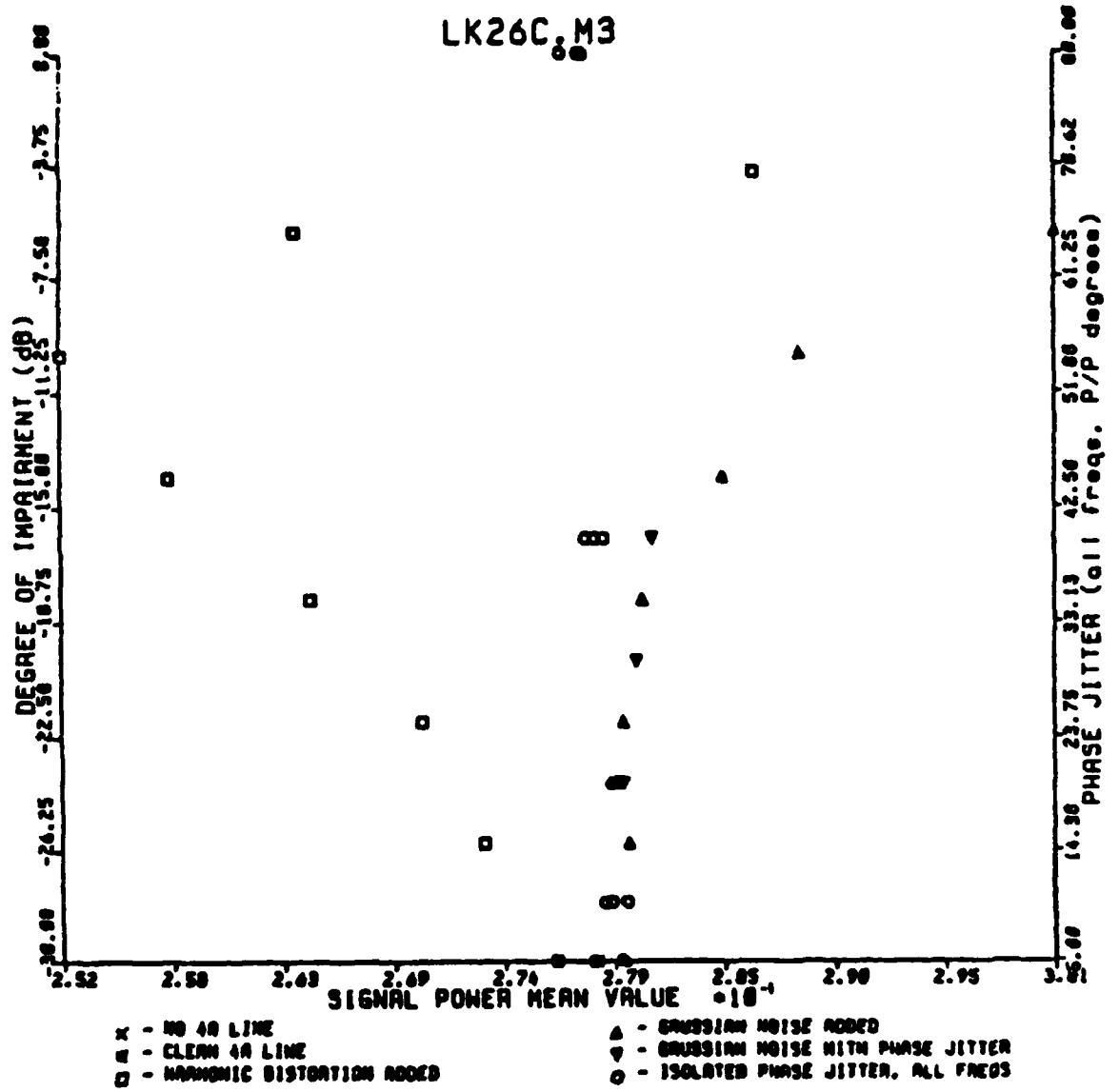
Figure 5-82: Peak to Average Ratio Variance of the Rectified
Signal Waveform for the LENKURT 26C Modem
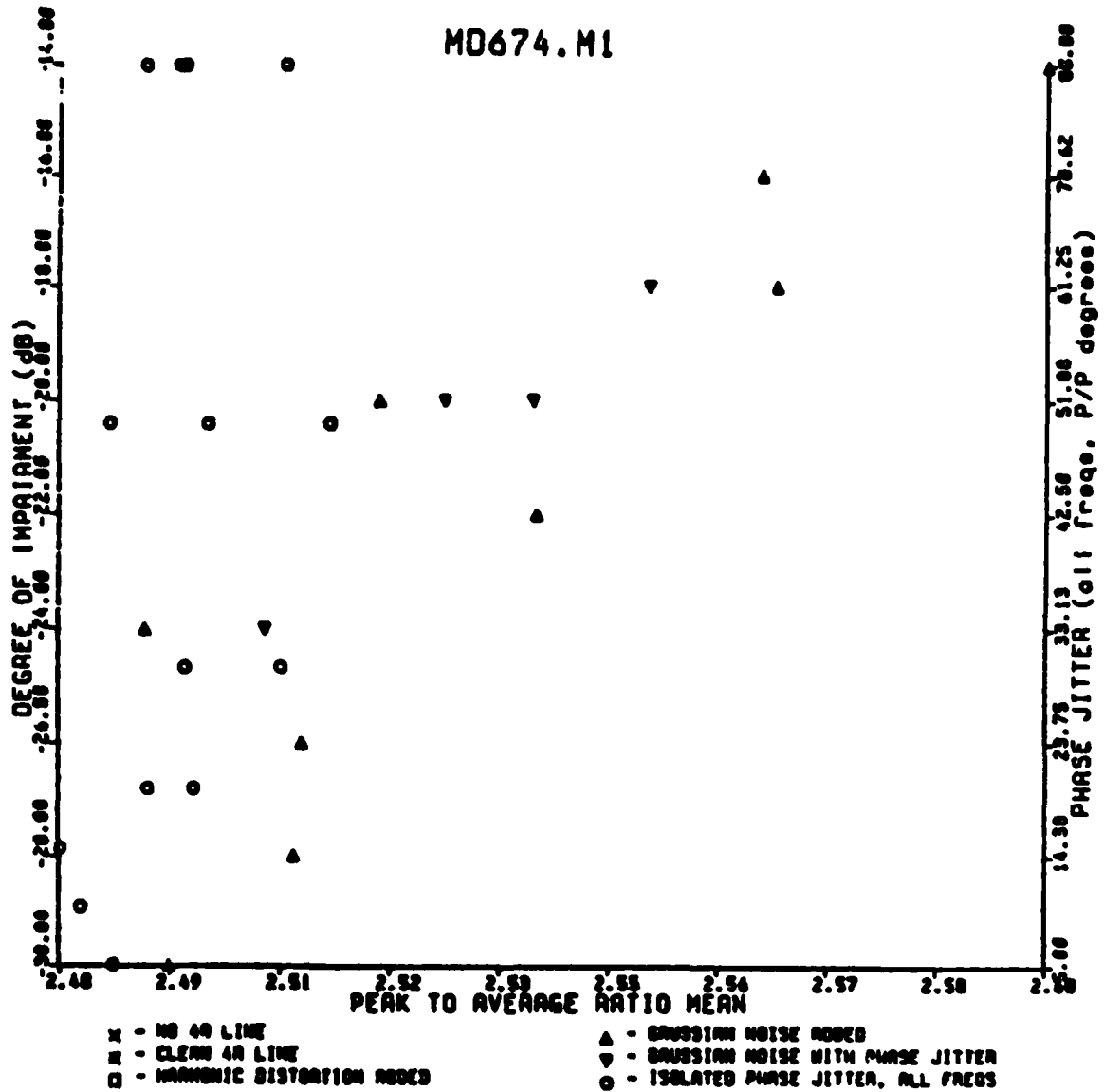
Figure 5-83: Peak to Average Ratio of the Rectified Signal
Waveform for the MD-674 Modem
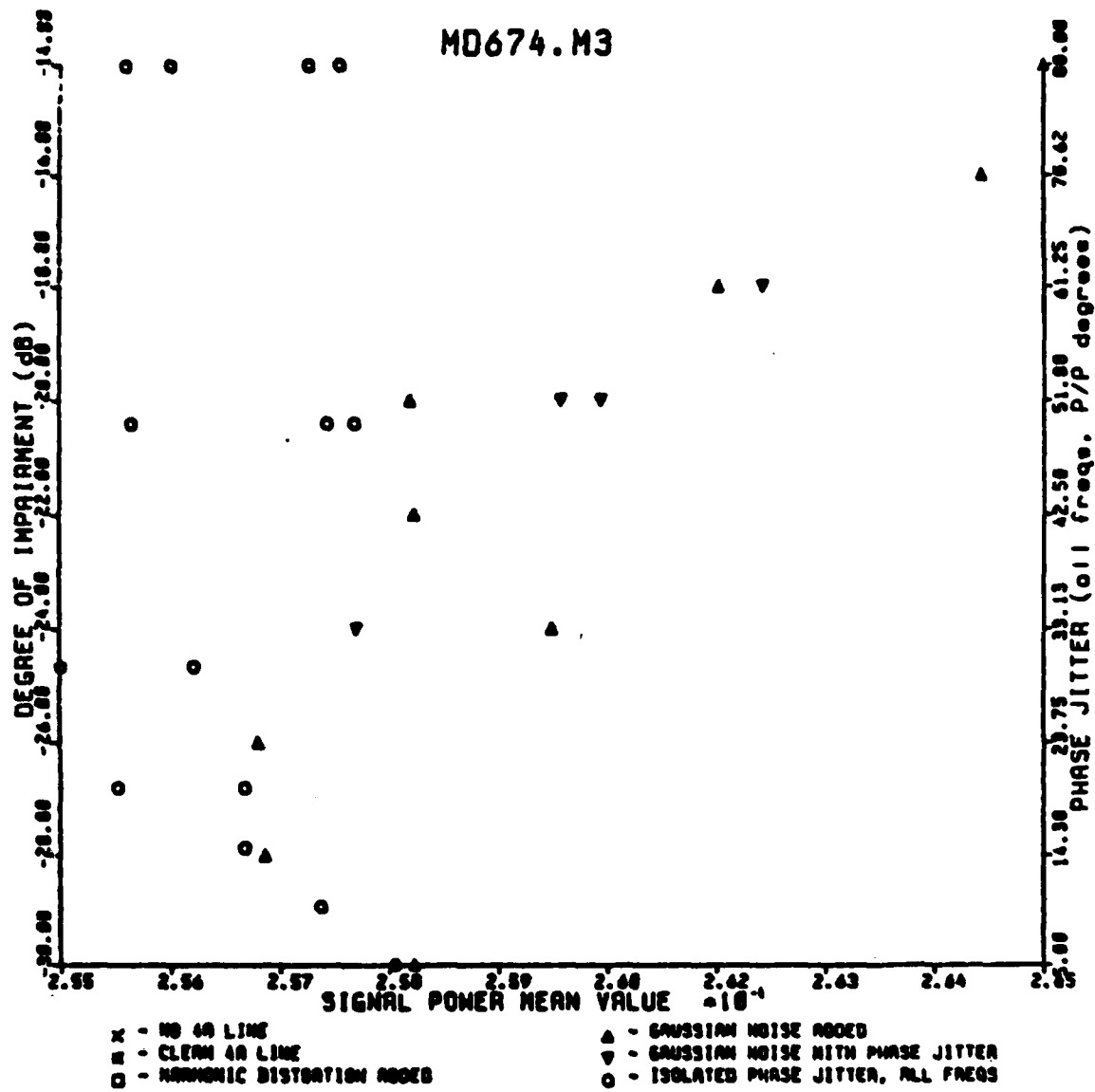
Figure 5-84: Peak to Average Ratio Variance of the Rectified Signal Waveform for the MD-674 Modem

The cases of severe harmonic distortion for the LENKURT 26-C modem are interesting. Both the μ_{PA} and σ_{PA} functions reverse direction for cases of severe harmonic distortion. The overall characteristics of both modems, however, are as expected.

Figures 5-85 and 5-86 show the two FSK modem parameters, shown previously combined on the same plots. Note the excessive offset between the "roots" of the functions. There are several possible explanations for this. First, the duration of the sample MD-674 waveform is approximately 1.9 seconds, as opposed to 3.5 seconds for the LENKURT 26-C modem. All of the waveform is used in the calculation of the statistics so the longer wave will produce more stable measurements. Secondly, the MD-674 signal has been re-sampled down to 12.9 K Hz from 17.2 K Hz. Although care was taken in the resampling process to prevent coloration of the data, the possibility exists. Finally, the histogram of the time domain LENKURT 26-C signal, shown in Figure 5-87, shows an anomaly in the symmetry of the signal. The specific cause for the offsets of the roots of the functions of Figures 5-85 and 5-86 has not been determined.

In actuality, all of the original four modems suffered a bias level of approximately 20 units. Further, those modems had a dynamic range corresponding to only 6 or 7 bits out of the 12 available from the A/D converter. In the later collection of 7 modems both of these problems were corrected.

The peak to average related statistics for the CODEX LSI-48 Mode A modem (4800 bits/sec, DPSK, 1600 baud) are shown in Figures 5-88 and 5-89. Although the characteristic plots are not as well defined, they are evident.

The same statistics for the CODEX LSI-48 Mode C modem (4800 bits/sec, QAM, 1600 baud) are shown in Figures 5-90 and 5-91. The measurements μ_{PA} and σ_{PA} are unstable for this modem.
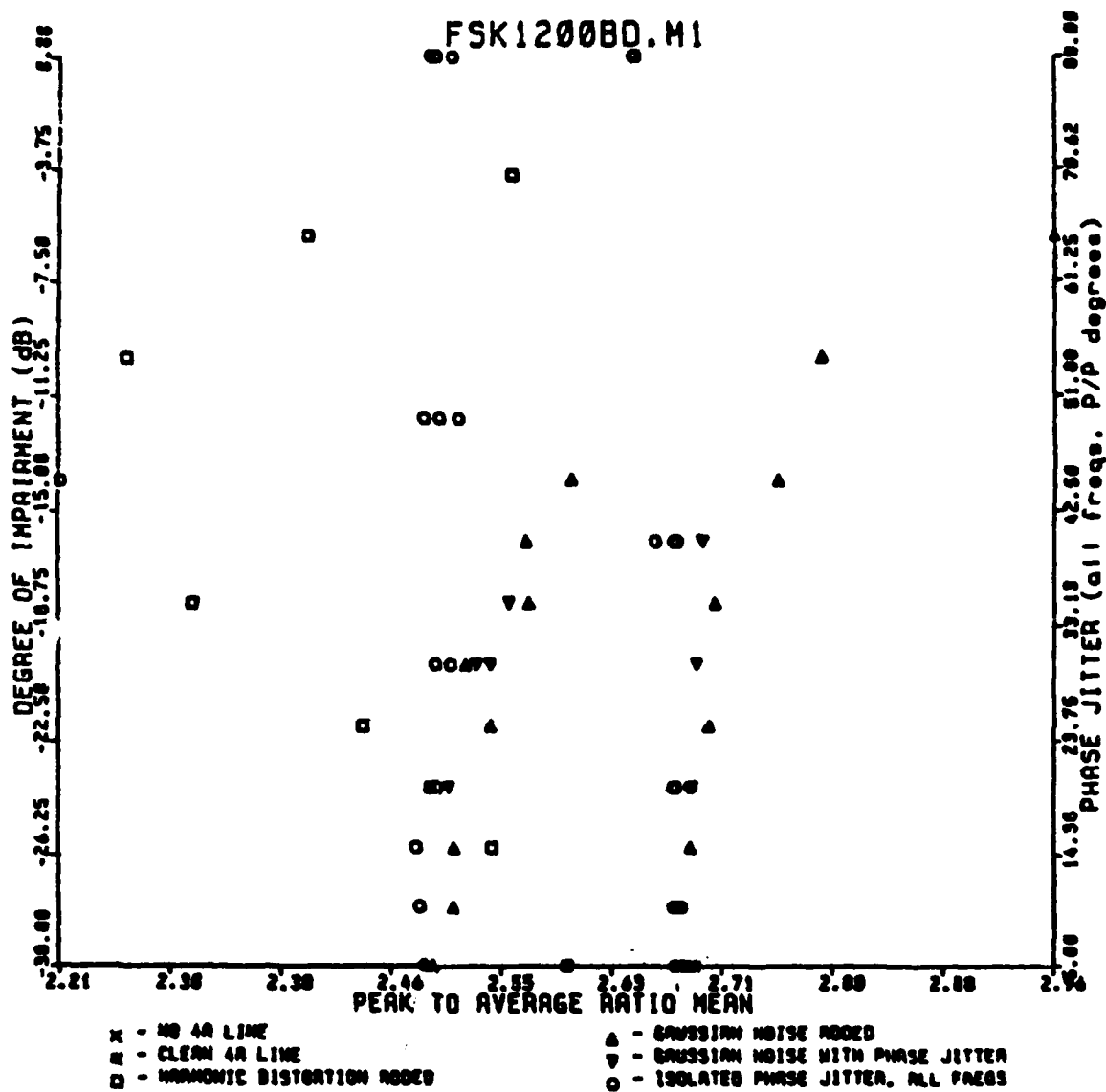
Figure 5-85: Peak to Average Ratio of the Rectified Signal
Waveform for the LENKURT 26C and MD-674 Modems
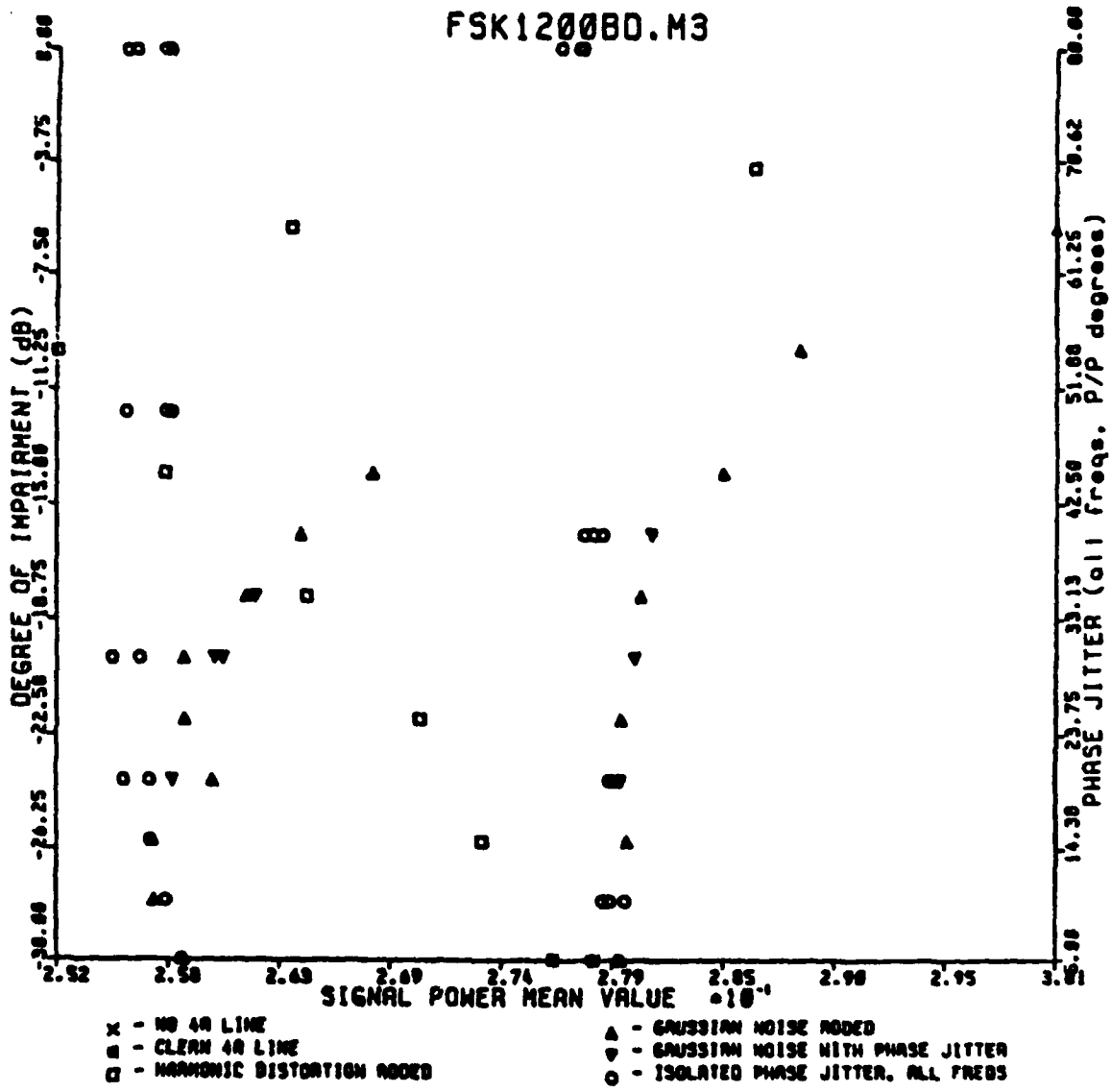
Figure 5-86: Peak to Average Ratio Variance of the Rectified
Signal Waveform for the LENKURT 26C and MD-674 Modems
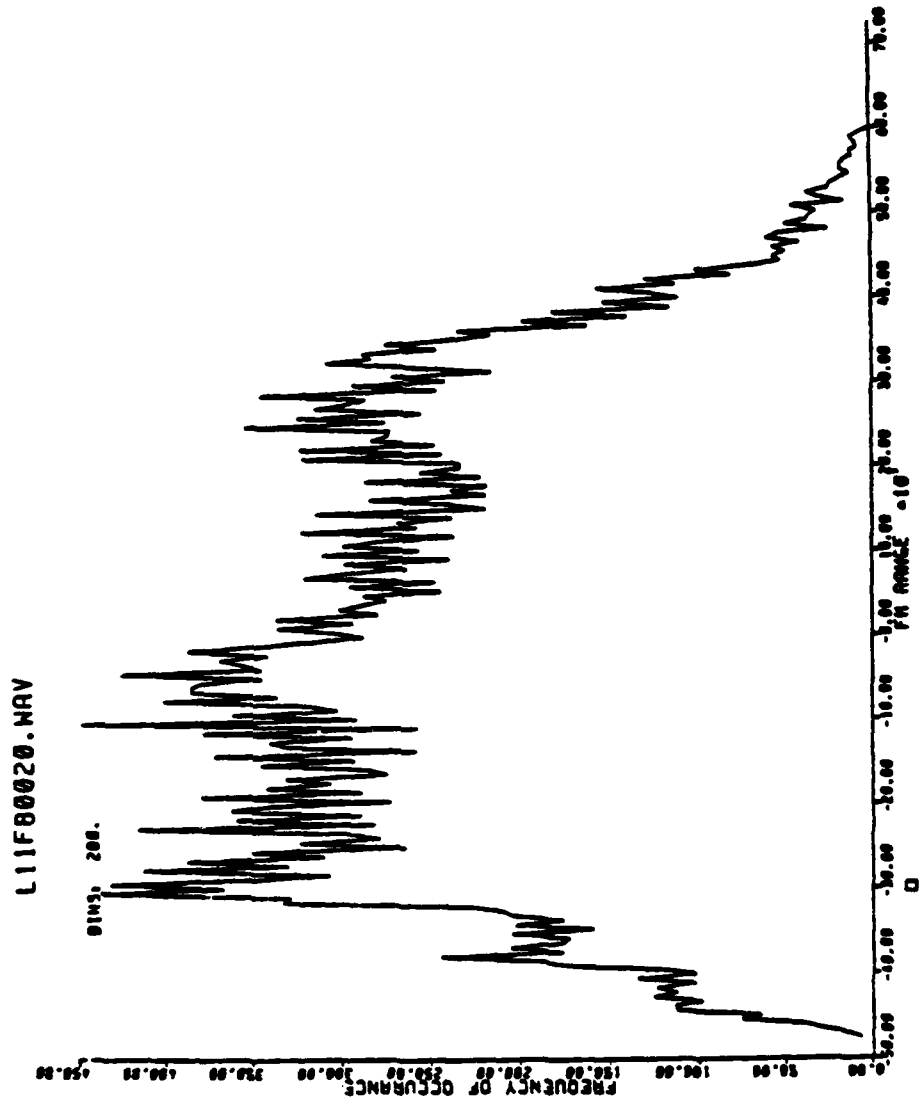
Figure 5-87: Histogram of the LENKURT 26-C Modem Time Waveform
Showing Asymmetry

CDX48MODA.M1
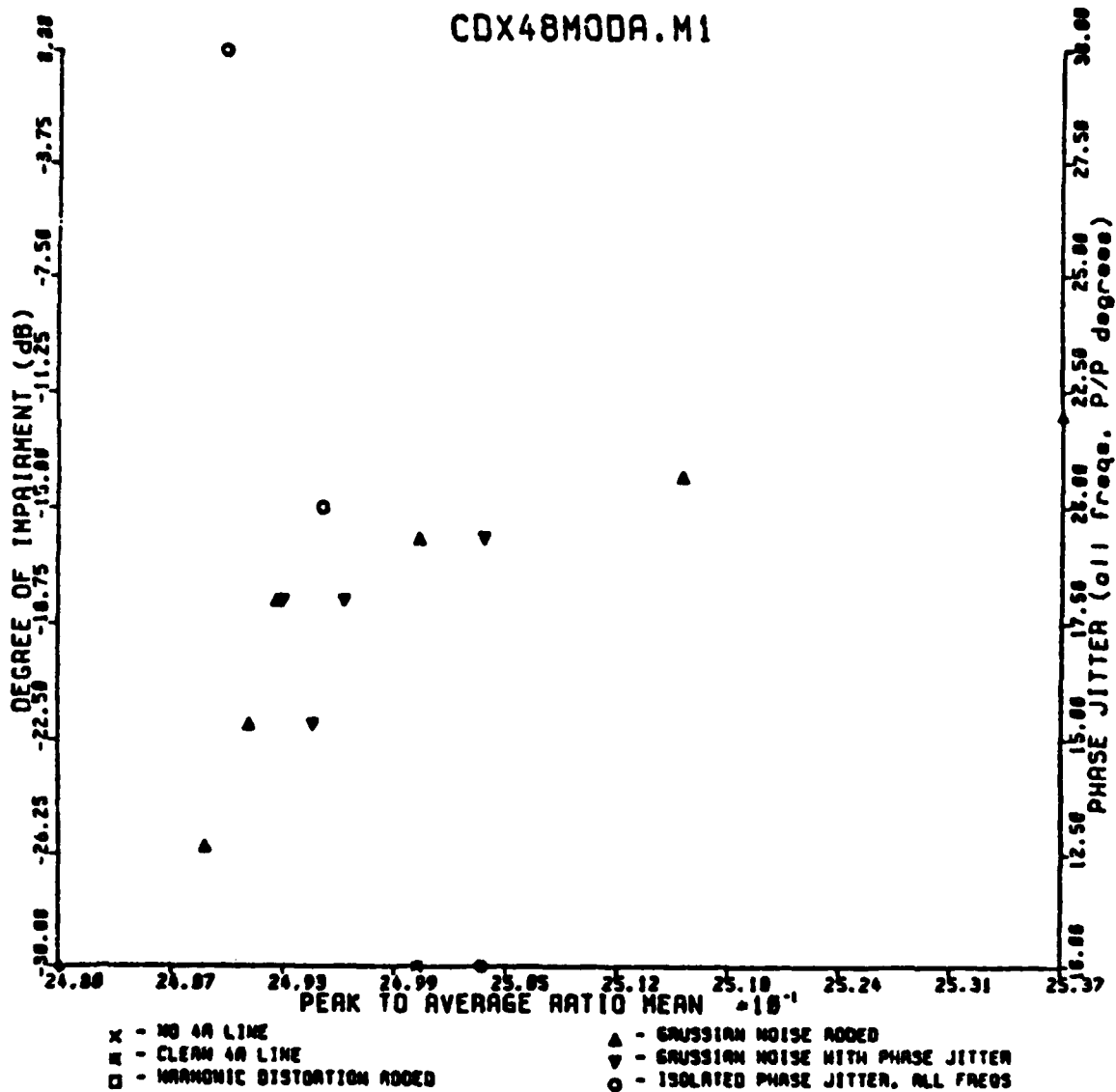
Figure 5-88: Peak to Average Ratio of the Rectified Signal
Waveform for the CODEX LSI-48 Mode A Modem

CDX48MODA.M3
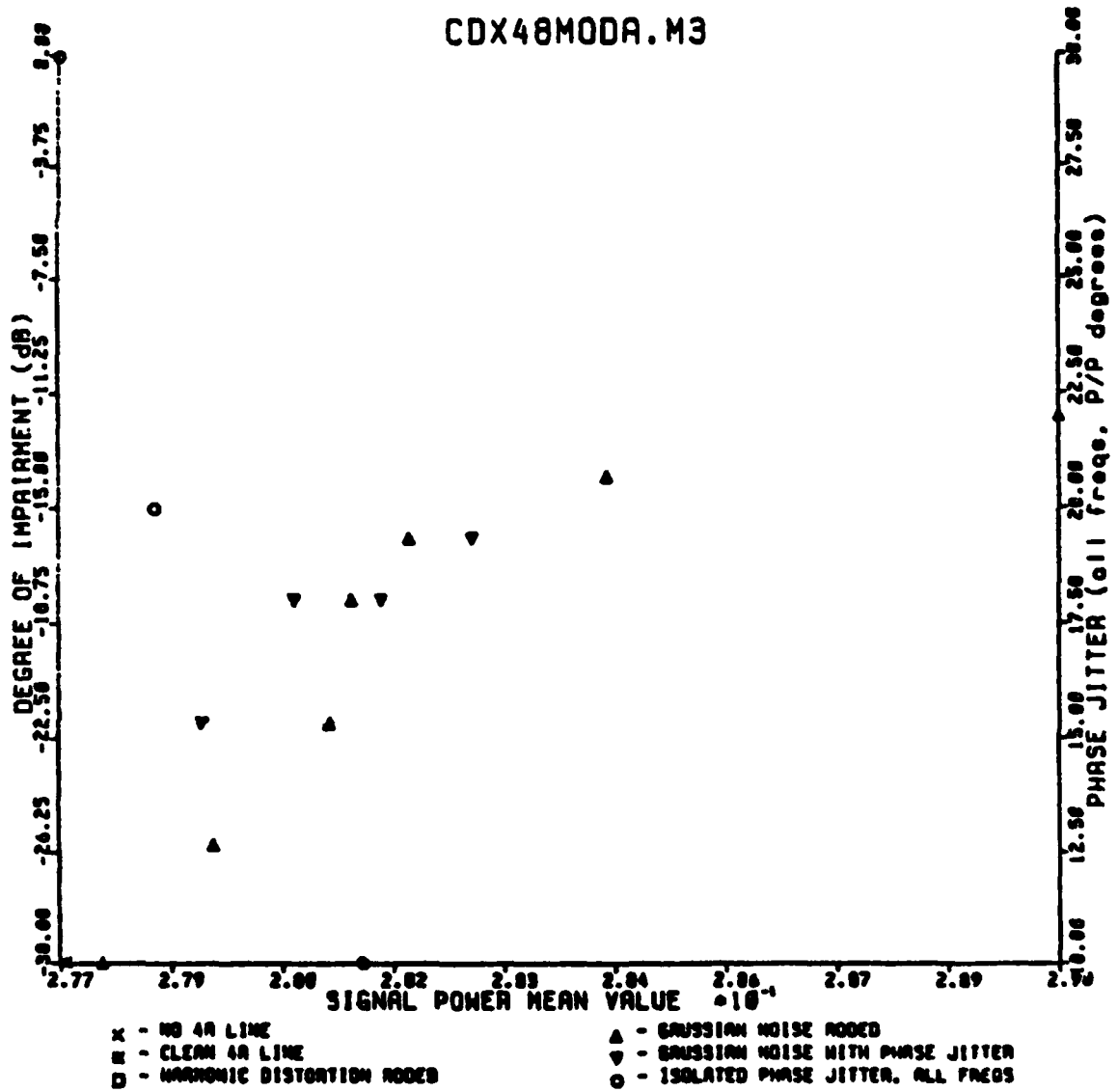
Figure 5-89: Peak to Average Ratio Variance of the Rectified
Signal Waveform for the CODEX LSI-48 Mode A Modem
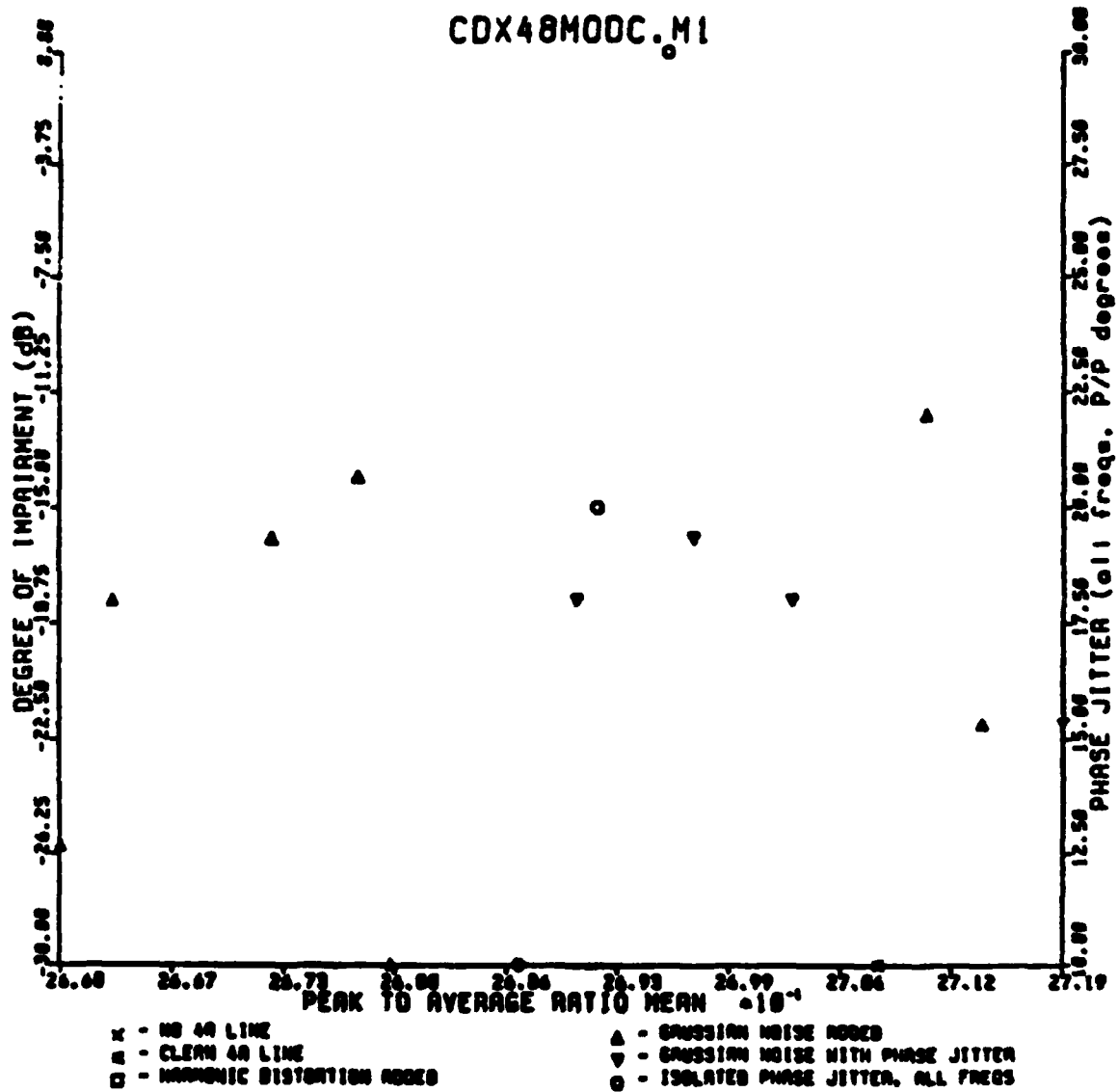
Figure 5-90: Peak to Average Ratio of the Rectified Signal
Waveform for the CODEX LSI-48 Mode C Modem
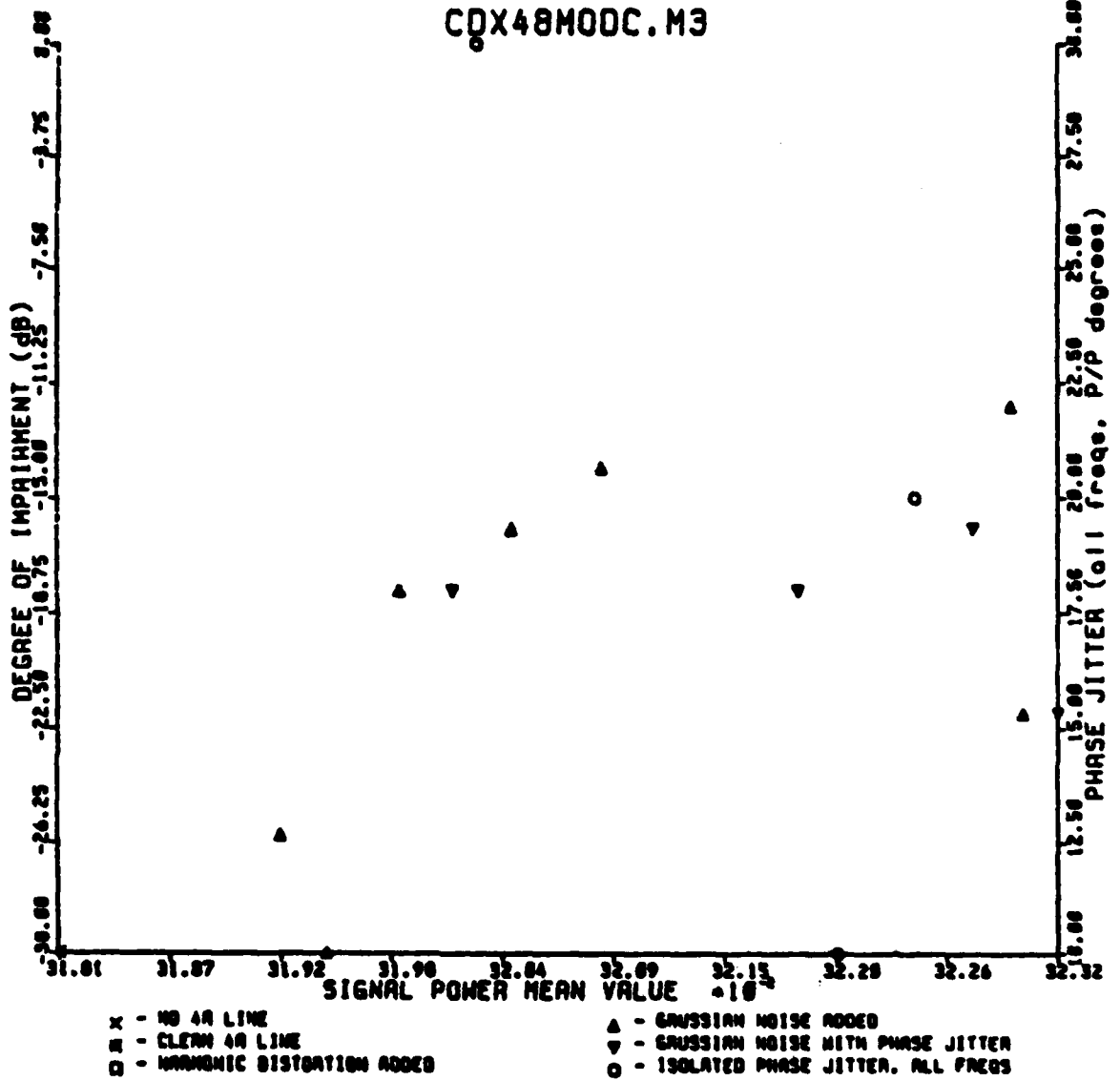
Figure 5-91: Peak to Average Ratio Variance of the Rectified
Signal Waveform for the CODEX LSI-48 Mode C Modem

Figures 5-92 and 5-93 show the plots for the CODEX LSI-96 modem (9600 bits/second QAM, 2400 baud). Note that even at 9600 bits/second harmonic distortion is readily detectable, the phase jitter region is bounded, and the average of the noise samples tends to the upper right.

The PARADYNE LSI-9600 modem (9600 bits/second PAM, 4800 baud) is shown in Figures 5-94 and 5-95. Harmonic distortion for this modem is detectable at 18 dB and greater. Also, the phase jitter samples are well behaved while the noise samples branch off in the 16dB and greater region.

The plots illustrating the PARADYNE MP-96 (9600 bits/second, QAM, 2400 baud) and HARRIS 5238 (16000 bits/second, QAM, 2667 baud) modems are shown in Figures 5-96 through 5-99. For these two modems, as with the CODEX LSI-48 Mode C, the measurements are largely ineffective.

The findings of this investigation appear to provide valuable insight into the estimation of channel quality. The two features identified are, first, the peak to average ratio of the rectified signal waveform, and second, the variance of that measurement over the duration of the signal waveform sample. The effectiveness of these measurements in a demonstration system shall be discussed in the next section.
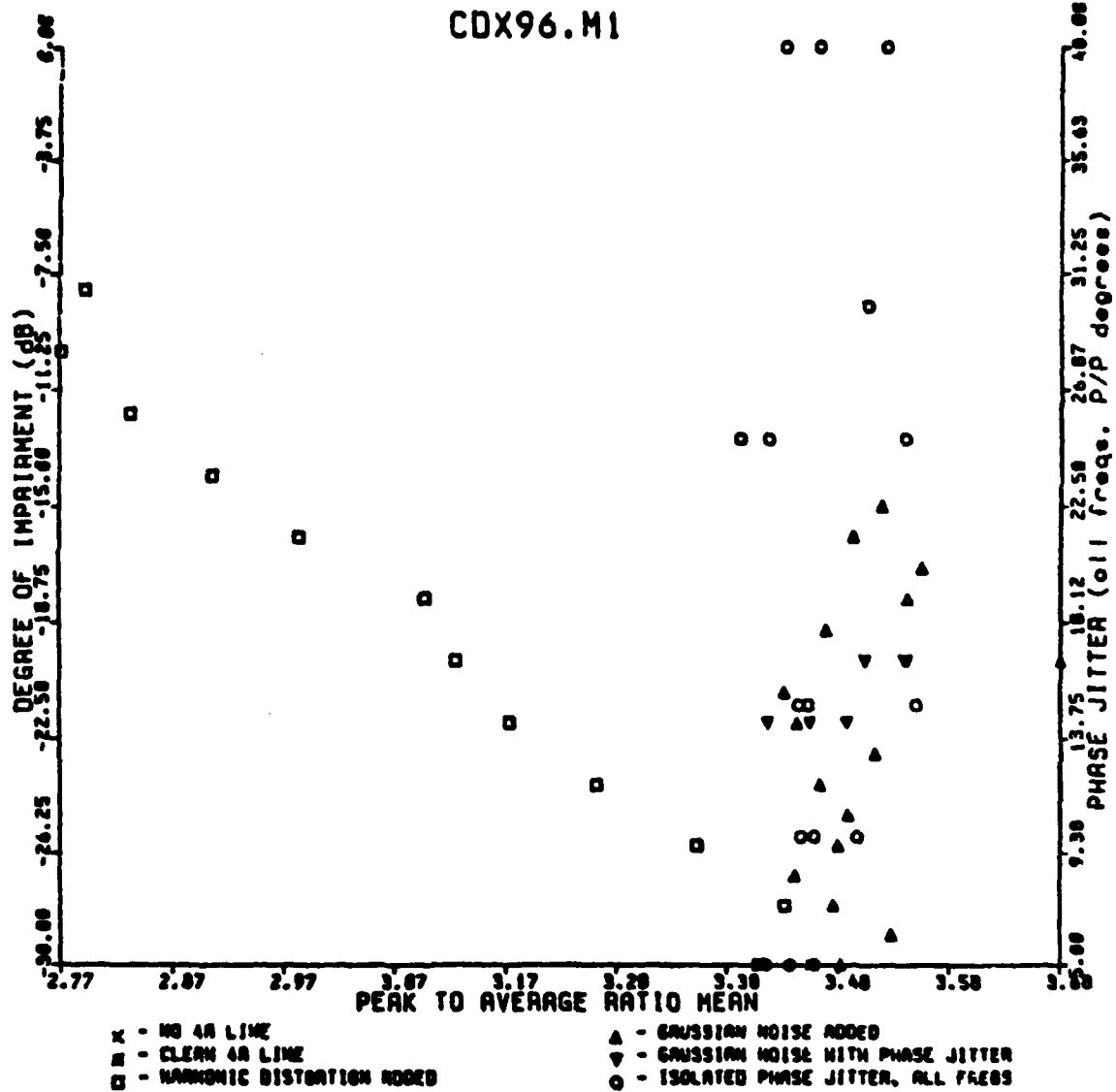
Figure 5-92: Peak to Average Ratio of the Rectified Signal
Waveform for the CODEX LSI-96 Modem

CDX96.M3
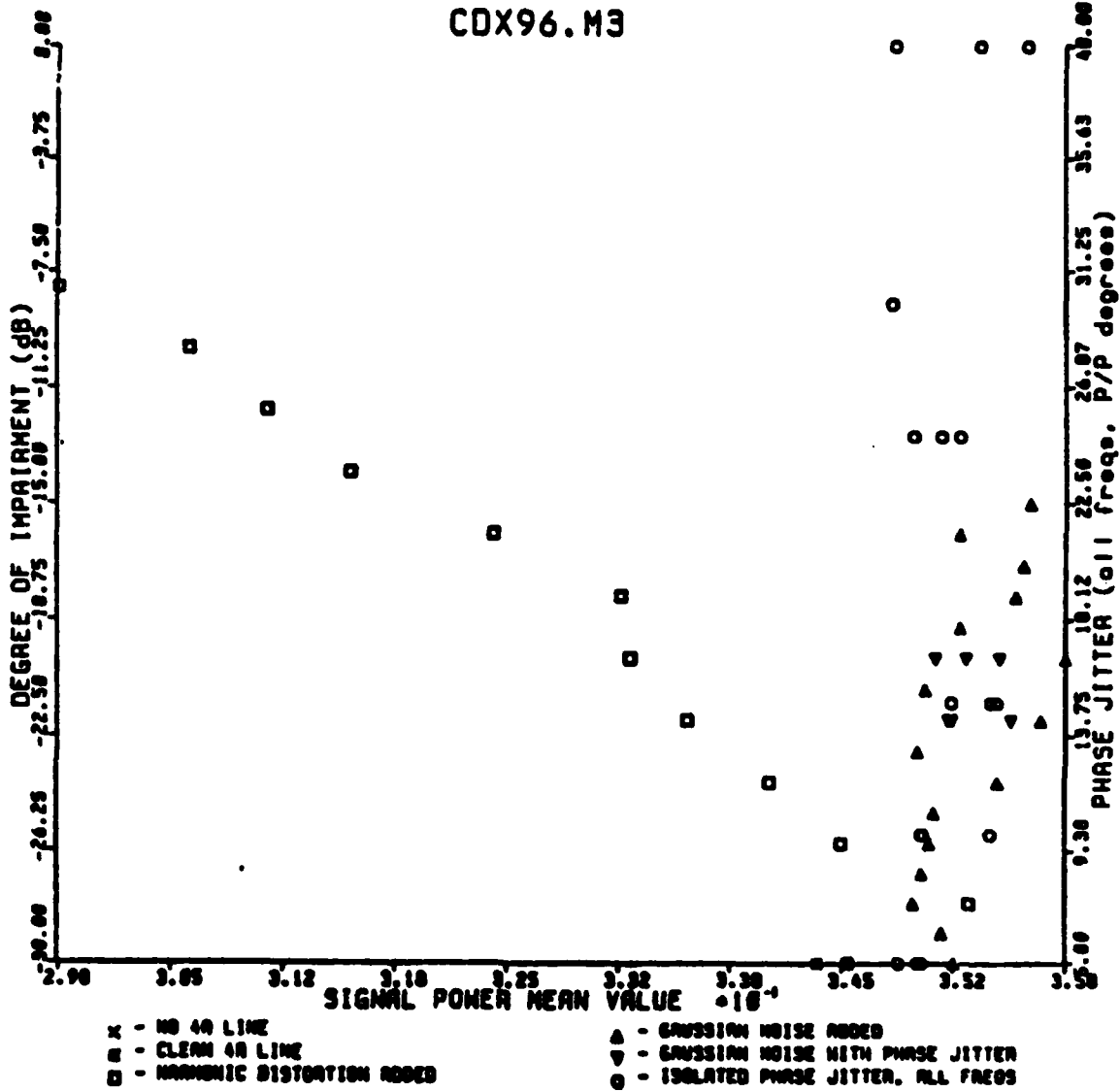
Figure 5-93: Peak to Average Ratio Variance of the Rectified
Signal Waveform for the CODEX LSI-96 Modem
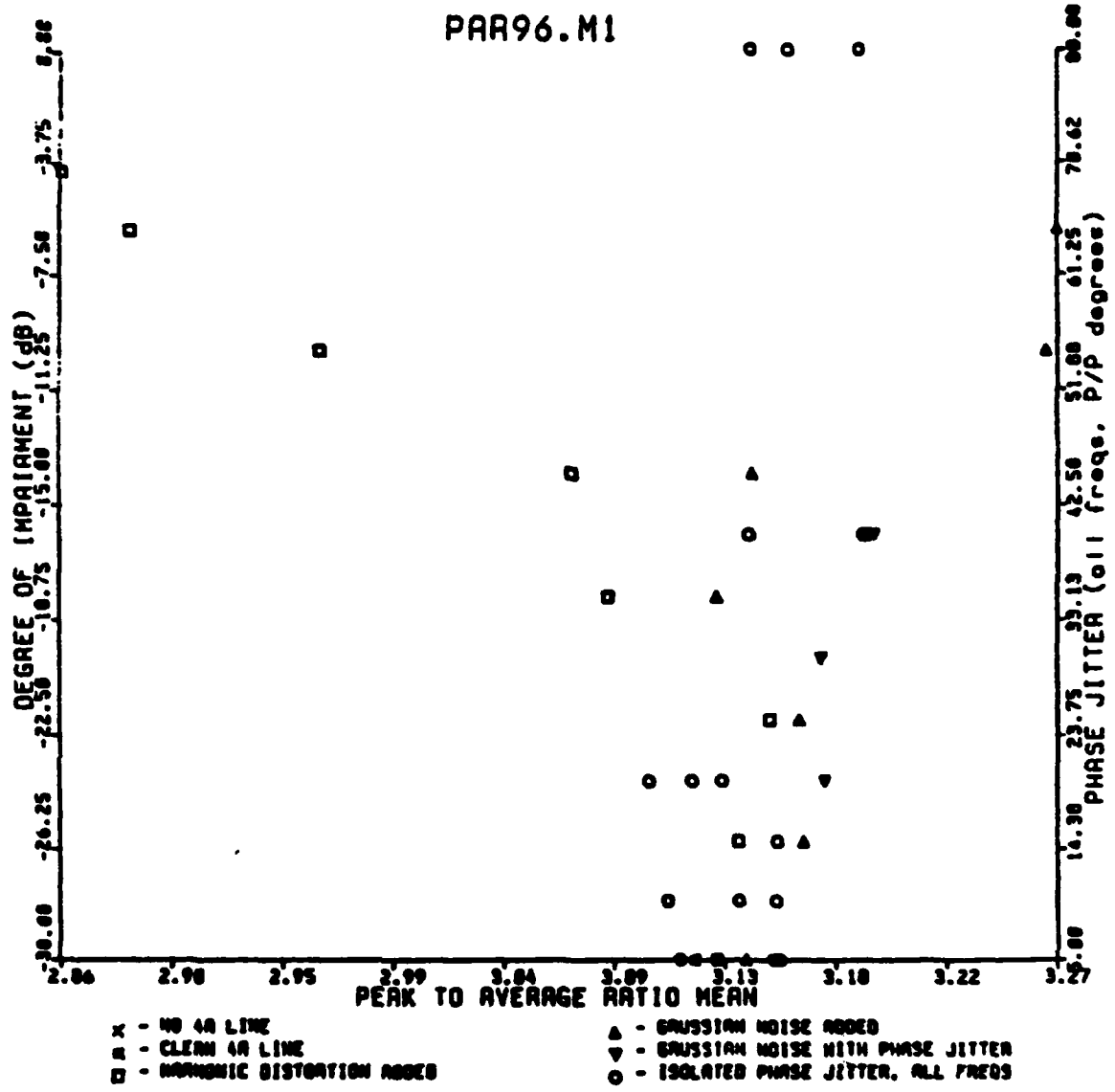
Figure 5-94: Peak to Average Ratio of the Rectified Signal Waveform for the PARADYNE LSI-96 Modem
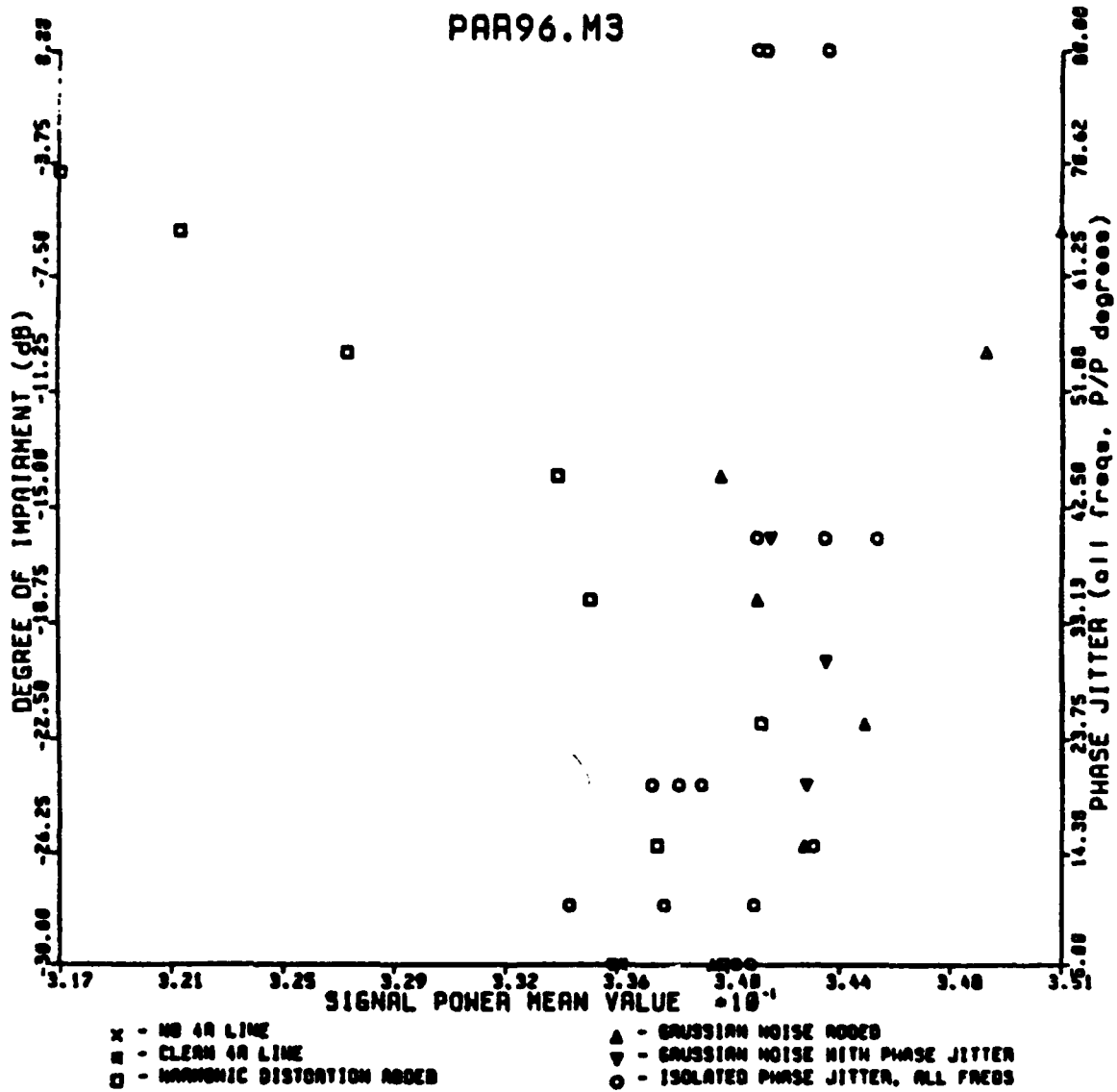
Figure 5-95: Peak to Average Ratio Variance of the Rectified Signal
Waveform for the PARADYNE LSI-96 Modem
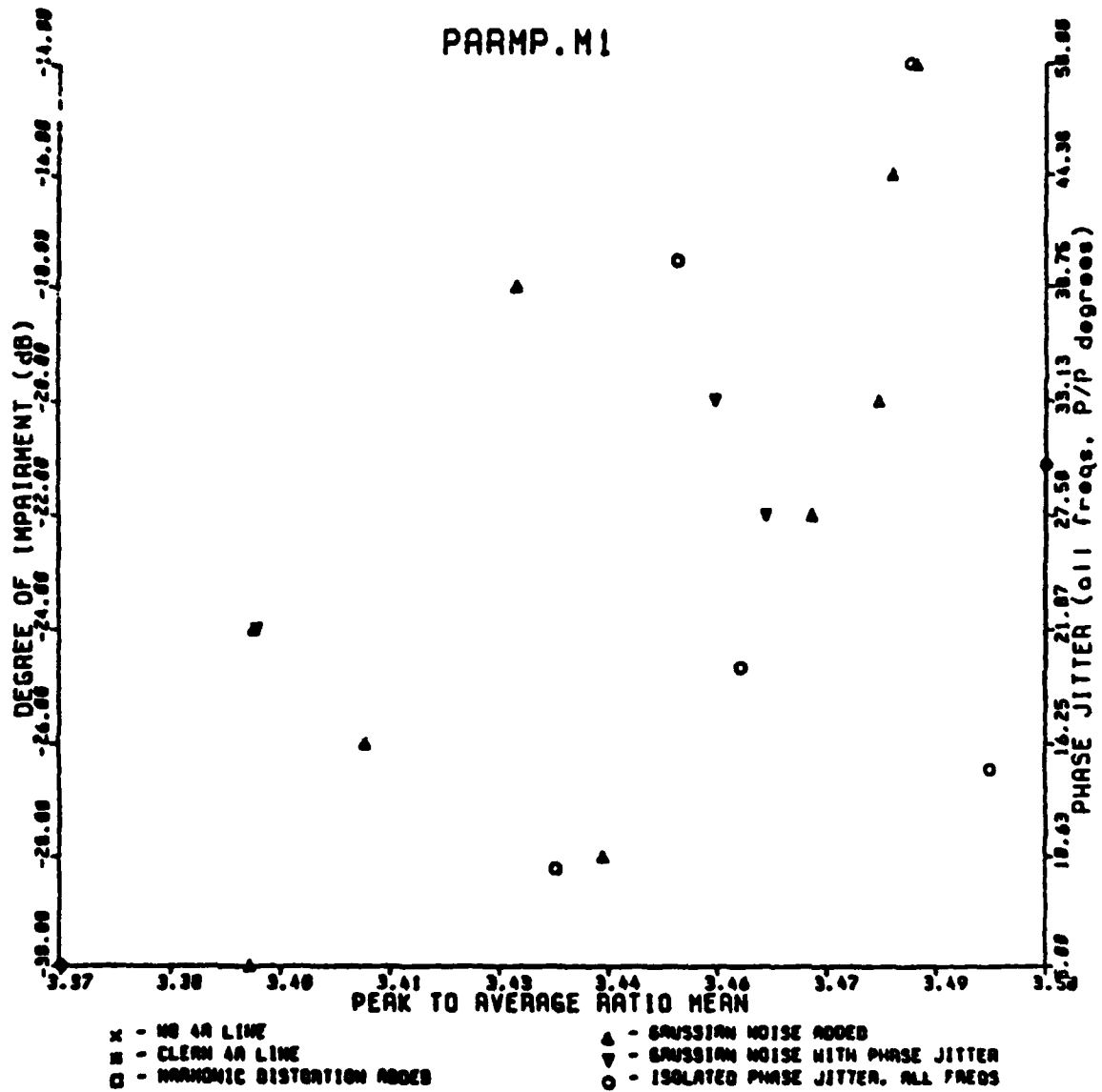
Figure 5-96: Peak to Average Ratio of the Rectified Signal
Waveform for the PARADYNE MP-96 Modem
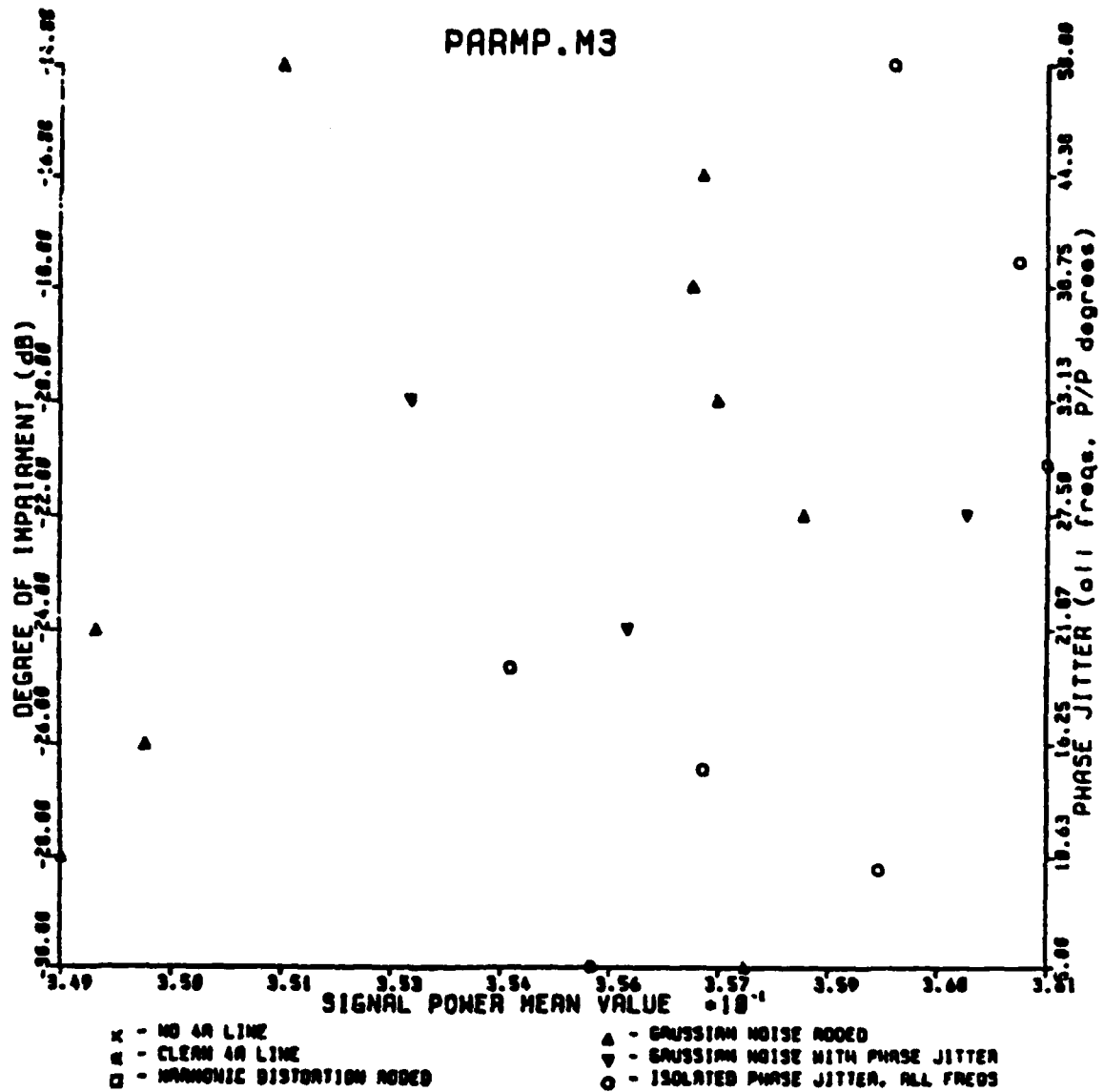
Figure 5-97: Peak to Average Ratio Variance of the Rectified
Signal Waveform for the PARADYNE MP-96 Modem
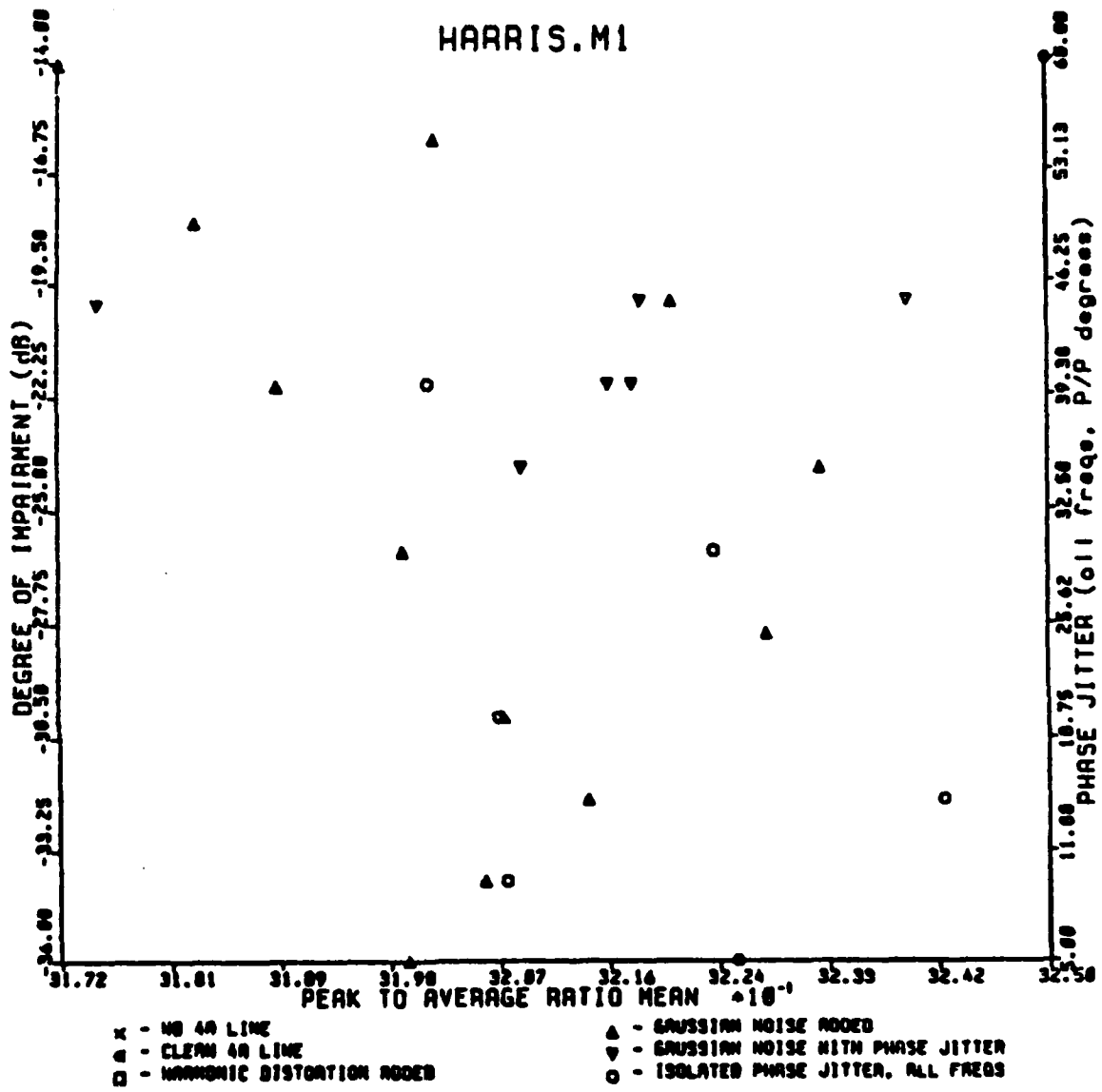
Figure 5-98: Peak to Average Ratio of the Rectified Signal Waveform for the HARRIS 5238 Modem
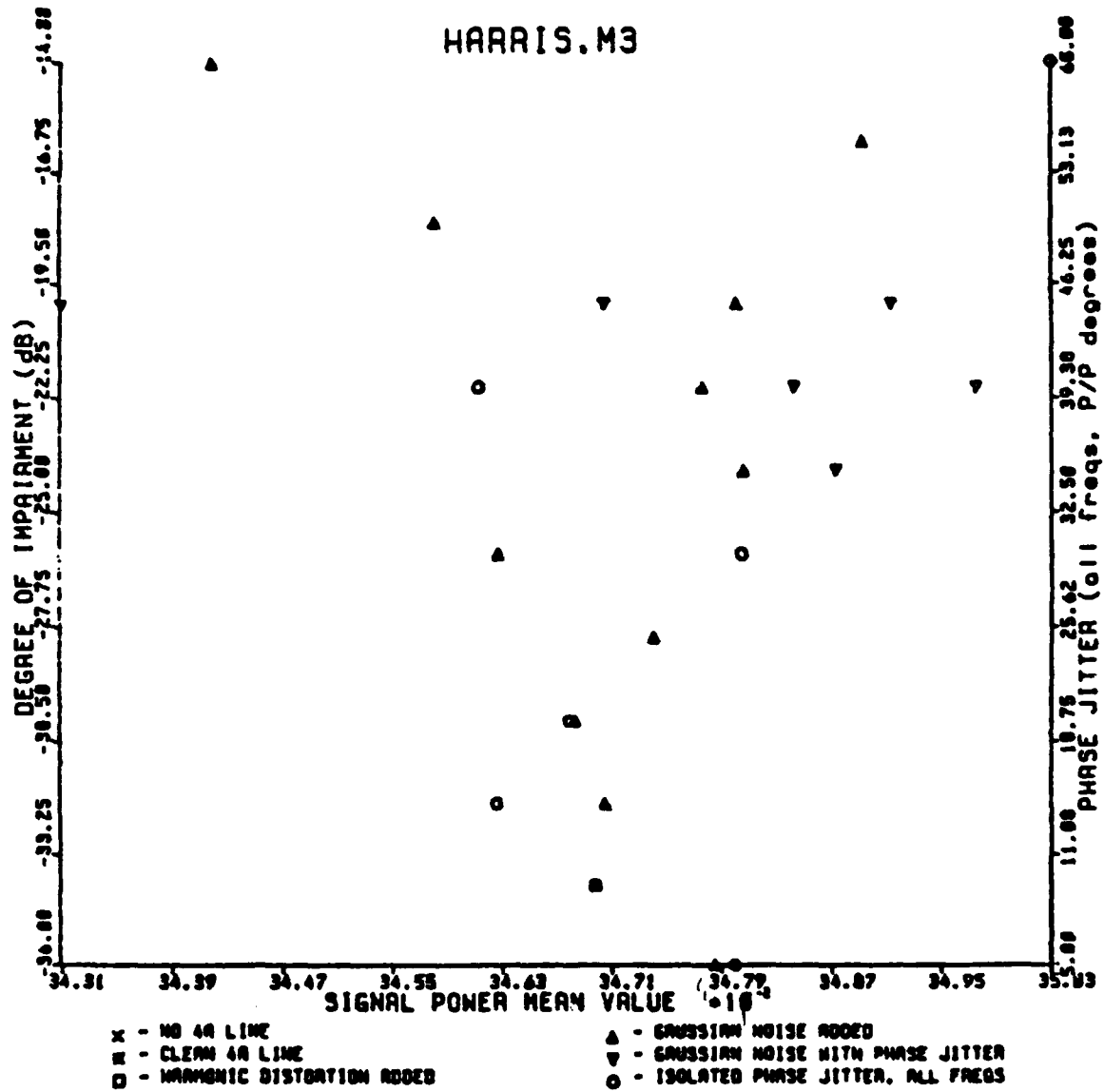
HARRIS.M3

Figure 5-99: Peak to Average Ratio Variance of the Rectified
Signal Waveform for the HARRIS 5238 Modem

REFERENCES

[1] RADC-TR-69-107, "Wireline Simulator, " ADCOM, 1970 (866966).

[2] "Technical Manual For Wireline Simulator Modification," Dynatron Corporation, 1976.

[3] RADC-TR-79-55 "Modem Identification Experiments, 1979.

[4] "Interactive Digital Receiver Simulator (IDRS), System Users Manual and Program Documentation," 1979, Contract #F30602-78-C-0174.

[5] Interpolation and Decimation of Digital Signals - A Tutorial Review," Ronald E. Crochiere and Lawrence R. Rabiner, Proceedings of the IEEE, Vol. 69, No. 3, March 1981.

[6] "Interactive Pattern Analysis and Classification," J. W. Sammon, Jr., IEEE Transactions on Computers, Vol. C-19, No. 7, July 1970.

[7] "Considerations of Sample and Feature Size," Donald H. Foley, IEEE Transactions on Information Theory, Vol. IT-18, No. 5, September 1972.

6. ALGORITHM IMPLEMENTATION

Based on the investigations described previously, several algorithms have been found which appear valuable in support of the hierarchical approach to channel quality monitoring. In this section we describe the implementation of selected algorithms into a demonstration system capable of performing gross channel characterization, generic modem traffic classification, and determination of the type and degree of degradation present on the channel.

The system is implemented in a modular fashion, a single task performing a specified operation. The sequence of tasks is directed by the Indirect Command File Processor capability under the RSX11M operating system.

Figure 6-1 shows the block diagram of Phase 1, the gross channel characterization. Phase 1 is broken up into two distinct operations. Phase 1A is the peak/average (μ_{PA}) and peak/average variance (σ_{PA}) estimator of the rectified input signal. For all the modems in the MSA data base, these two measures fall within a given range. This range information is stored on the disk in a user-adjustable file. When an input is processed, the parameters μ_{PA} and σ_{PA} are estimated for a 256-sample window and compared against the stored range information. If both measures fall within the given range, the channel is declared "acceptable"; otherwise it is rejected. It is interesting to note that test tones, voice, and most noise will not pass because of the excessively low and high parameter values.

Phase 1B is not used in the go/no go channel decision; rather, it represents a collection of signal processing algorithms which have been shown to be generally effective in enhancing generic parameter information (baud rate and/or carrier frequency) in the input signal. They are implemented in an optional execution mode so the user can elect to receive this output in graphic form for his analysis purposes. The phase 1B output includes the raw and rectified signal power spectrum, lattice filter 2-stage rectified and not
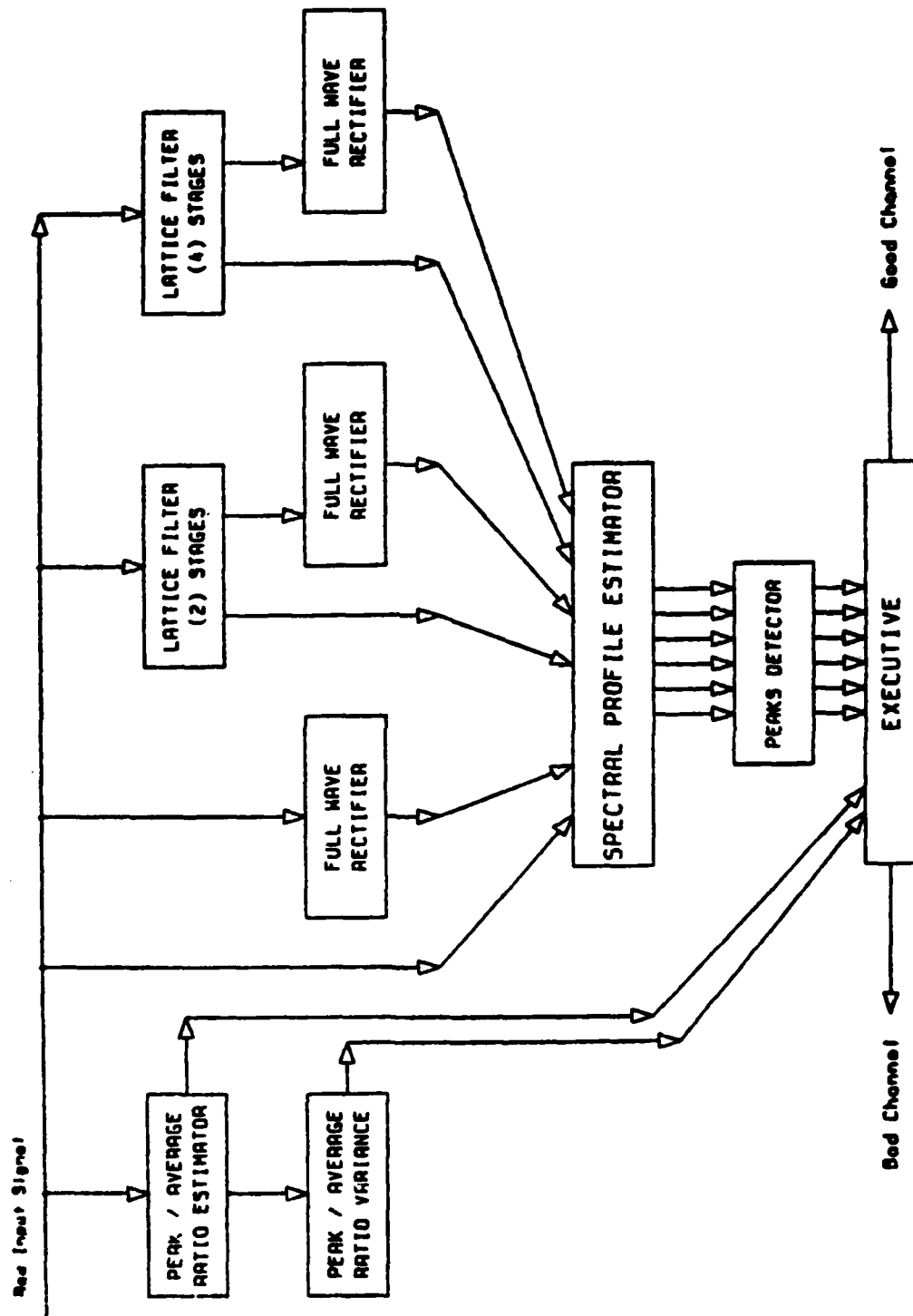
PHASE 1 GO / NO-GO DECISION BLOCK DIAGRAM

Figure 6-1

rectified power spectrum and lattice filter 4-stage rectified and not rectified power spectrum. These six spectrums are summarized in a peaks analysis report.

Given the "acceptable" channel decision, Phase 2 is executed to classify the generic modem type. In Phase 2 (Figure 6-2) the lags 1, 2, 3, 4, and 6 are generated for the autocorrelation of the 1-bit quantized input signal. An 8000 or 3000 sample correlation window is used. For each window available from the input signal, a feature vector of the 5 lags is generated and stored in a disk file. The vector file is then processed by a Fisher discriminant pair logic classifier against 3 logics, the outcome of which are the BAUD, MODULATION, and combined MODULATION/BAUD class indicators. For each logic, the majority class is declared the result. Given that either of the first two classifiers agrees with the combined modulation/baud logic result, the signal parameters are confirmed. If disagreement in the logics results, the decision is that the signal represents either a bad channel or an unknown modem. In this case, no further analysis can be done on this signal. In an operational system, another input sample could be requested before making a final determination.

Given a decisive output, the modulation type, baud rate, and carrier frequency (via table look-up) are available for further signal processing. The classifiers used are those developed previously with OLPARS support. The average overall percentage correct is approximately 97+%. Multiple vectors and multiple classifiers with a degree of certainty weighting in the review of the three logic results provide an overall generic identification of high reliability.

Phase 3 of the system actually performs the channel quality assessment (Figure 6-3). Given the generic ID information, the signal is FM demodulated and applied to a data transition threshold device appropriate for that modem type. The residue is 200 Hz low-pass filtered and a high resolution power spectrum is generated. A specialized peaks search routine detects phase

6-3
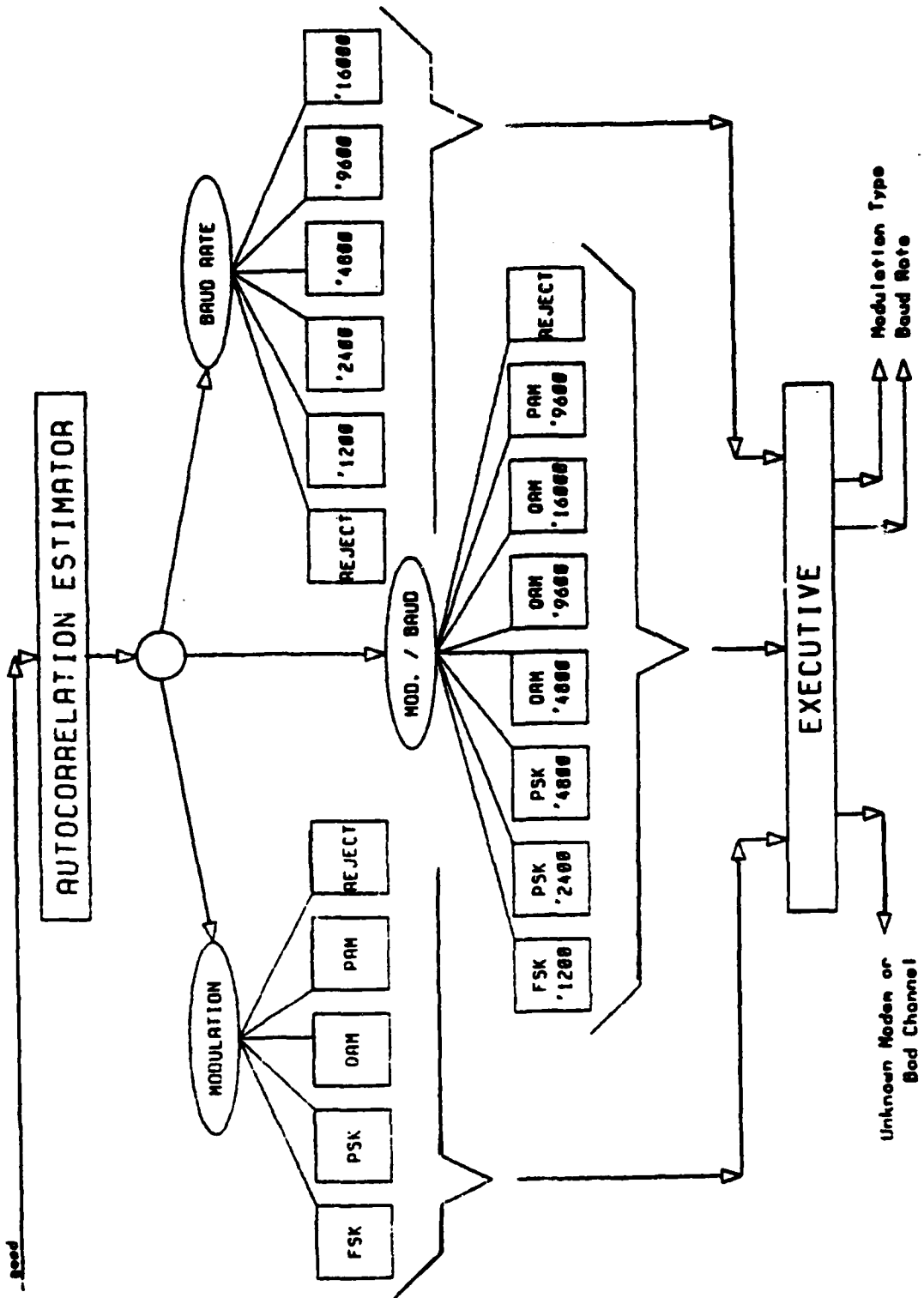
PHASE 2 GENERIC CLASSIFIER BLOCK DIAGRAM

Figure 6-2
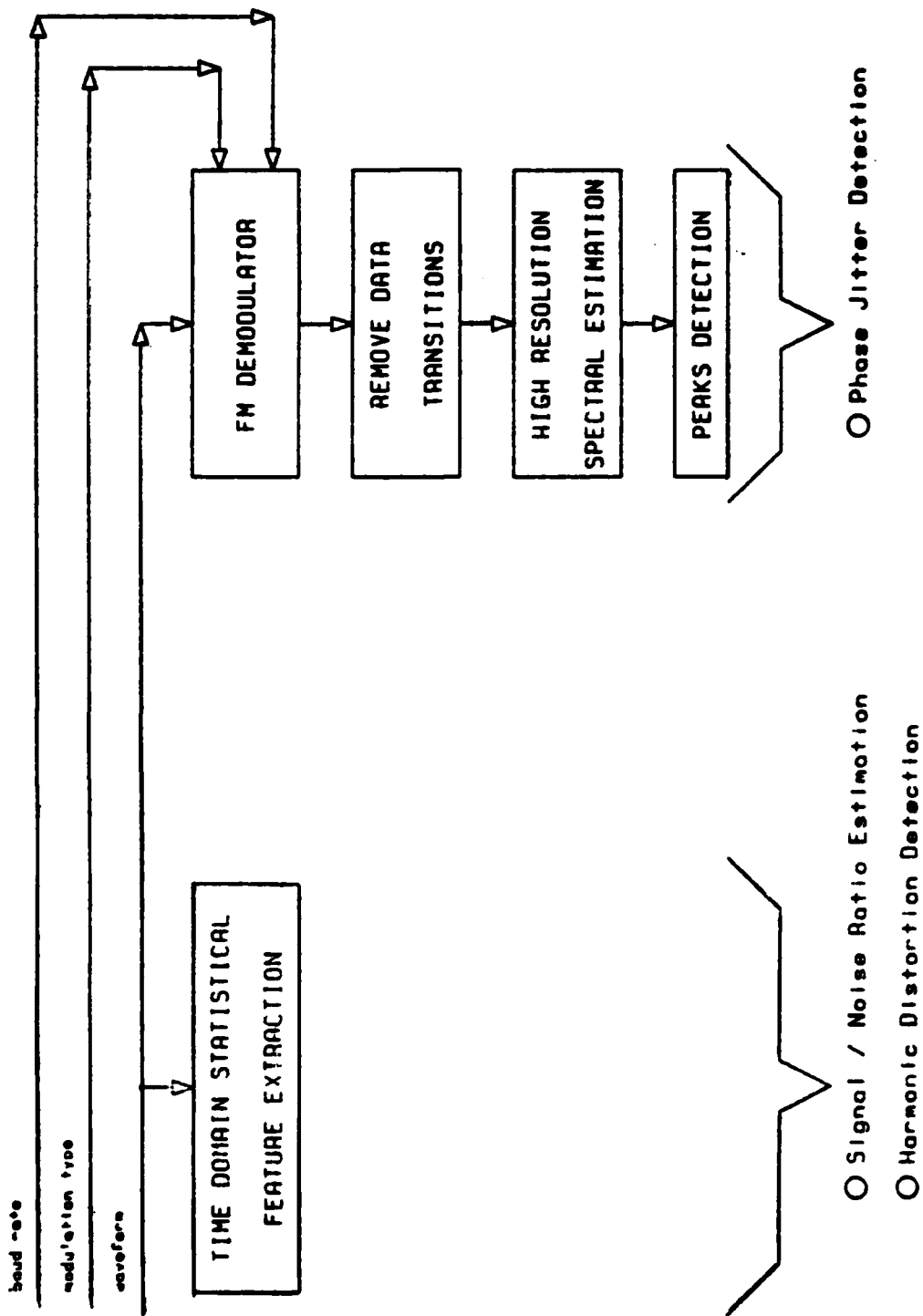
PHASE 3 CHANNEL CHARACTERIZATION BLOCK DIAGRAM

Figure 6-3

jitter components and reports them to the user.

In addition, the signal parameters μ_{PA} and σ_{PA} are used in a look-up fashion into a file containing a template of those parameters for this modem. The template look-up returns the type of impairment, if any, (from Gaussian noise or harmonic distortion) and the estimated degree of the impairment. Figure 6-4 shows the format of a template file, either for μ_{PA} or σ_{PA}. For any calculated measure of μ_{PA} or σ_{PA}, there is only one corresponding value in the template file which directly indicates the impairment (HD, GOOD DATA, or AGN) and the amount present. The results of the demonstration system implementation are discussed in the next section.
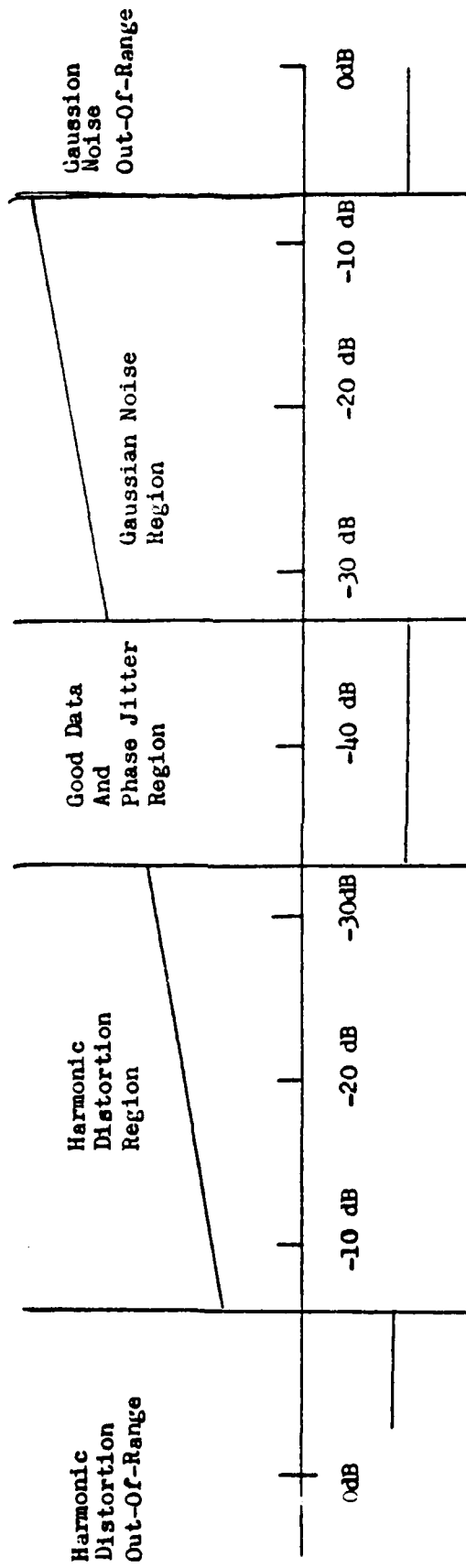
Figure 6-4

Impairment Classification Template
File Format

7. RESULTS OF THE DEMONSTRATION SYSTEM

The demonstration system described in the previous section was implemented under the MSA effort. The results of the system should be considered separately for each of the three phases of the system operation.

Phase 1 of the system performed a gross channel-quality analysis on the unknown modem signal. The peak-to-average value of the rectified signal and the variance of that measurement over approximately two seconds of input data were sufficient to make the decision. The range of these parameters was calculated for the entire database and was used as an acceptable range for the channel. Although the "classifier" would (by design) declare all of the MSA modems as "acceptable," it does reject test tones, voice, and most noise.

Phase 2 of the system performed the modem generic type ID by applying three Fisher classifiers to sample vectors consisting of lags 1,2,3,4 and 6 of the signal auto-correlation function calculated over either a 3000 or 8000 sample window on the 1-bit quantized input signal. The individual accuracy of these classifiers was described in Section 5.2. The three classifiers, together with the degree of certainty logic built into the system. form an exceptionally accurate ID capability for the signal modulation strategy and baud rate independent of the type and degree of impairment affecting the signal.

The most difficult aspect of the channel monitoring problem, however, is the third phase of the hierarchy; the determination of the type and degree of impairment degrading the line. The peak to average ratio of the rectified signal and the variance of that measurement serve as a basis for the determination of AGN or HD on the line. Although this technique was developed to identify impairment at the generic modem level, it was found that the variations in collection parameters and the post-collection processing required for some modems introduced sufficient coloration into the database to

mask out the "fine-grain" measurements required in the impairment characterization. It was shown that generically identical modems possess the same behavior pattern with regard to the measurements extracted but that they are slightly inconsistent in range. For this reason, a fourth classifier was added to Phase 2 to provide the actual ID of the modem. The ID is used in selection of a template for that modem, which is then used in the determination of the impairments present.

To evaluate the effectiveness of the AGN and HD impairment classifier, the assumption as made that -25dB and less AGN present or -25dB HD present still represented a "good" quality line. The decisions of the two classifiers were treated separately when counting incorrect decisions. Table 7-1 shows the ability of the demonstration system to detect AGN or HD on the in-service data channel to the accuracy specified. For the 1200/2400 bit/second modems the overall ability to detect AGN or HD to within 3dB was 95.3%. For the 9600 bit/second CODEX LSI-96 modem, AGN and HD were identified within 4dB of the actual value 84.0% of the time. For the PARADYNE LSI-96, PARADYNE MP-96 and HARRIS 5238 modems, the demonstration system was not able to accurately declare the impairments present.

The system was successful in demonstrating the potential usefulness of the phase jitter detection algorithm. The detection of phase jitter was accomplished by demodulating for the FM component, threshold detecting for data transitions and removing them by subtracting out the expected transition value, smoothing the residue and generating a high-resolution power spectrum. The phase jitter component is increased up to 15dB. Although contract time did not allow the mechanism to translate the spectral result to actual degrees of jitter developed, a high resolution peaks analysis routine does locate the peaks and provide all necessary amplitude and spectral noise measurements.

Table 7-2 shows the detectable levels of phase jitter for the demonstration system even in the presence of noise. For the amount specified, approximately a 3dB increase over the noise floor for the tone or its

Table 7-1 (a) Combined AGN/HD Classifiers Overall Percent Correct
by Range for 1200 and 2400 Bit/Second Modems

MODEM	+ 1dB	+ 2dB	+ 3dB	Total Decisions
Lenkurt 26- C	84.4%	84.4%	90.6%	64
MD-674	87.0%	92.6%	98.2%	54
Hughes HC-276	96.6%	96.6%	98.3%	58
Code LSI-48 Mode B	71.9%	78.1%	90.6%	32
Weco 207-A2	85.4%	91.7%	97.9%	48
Overall	86.3%	89.5%	95.3%	256

Table 7-1 (b) Combined AGN/HD Classifiers Overall Percent Correct
by Range for 4800 Bit/Second and up Modems

MODEM	+ 2dB	+ 3dB	+ 4dB	Total Decisions
Codes LSI-48 Mode A	67.9%	75.0%	89.3%	28
Codex LSI-48 Mode C	46.4%	50.0%	50.0%	28
Codex LSI-96	73.0%	81.0%	84.0%	100
Paradyne LSI-96	*	*	*	
Paradyne MP-96	*	*	*	
Harris 5238	*	*	*	
*below 50%				

Generic Modem Type	Detectable Jitter Level
FSK 1200 bits/sec.	10°
DPSK 2400 bits/sec.	30°
DPSK 4800 bits/sec.	30°
QAM 4800 bits/sec.	50°
QAM 9600 bits/sec.	40°
PAM 9600 bits/sec.	80°
QAM 16000 bits/sec.	60°

Table 7-2   Detectable level of phase jitter for a 3dB component above
the background noise of the FM residual spectrum.

harmonics was generally evident. The exception was 10Hz jitter which was nearly undetectable by this scheme.
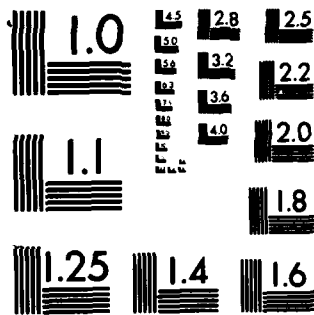
MICROCOPY RESOLUTION TEST CHART
NATIONAL BUREAU OF STANDARDS-1963-A

8. CONCLUSIONS AND RECOMMENDATIONS

Throughout the course of this effort, PAR Technology Corporation has developed and demonstrated algorithms effective in the monitoring of in-service VF data lines. A hierarchical approach to performance monitoring was presented and implemented in the form of a demonstration software system. Through demonstration, it was shown that reliable performance monitoring can be achieved for 1200 and 2400 bits/second modems. Not only could the type of impairment be recognized from among Gaussian noise, odd harmonic distortion, and phase jitter, but the degree of the impairment was also indicated. Some success was also shown for the higher speed modems although the accuracy decreased.

The results of this effort form the basis for further investigation and show the practicality of an eventual hardware implementation. It must be realized, however, that the results shown under this effort are based on a limited database. First, there were several problems with the database collection. The early collection effort suffered from poor dynamic range and misadjusted A/D converter. The overall length of samples was not consistent, nor was the impairments available per modem sampled. Finally, two different sample rates were used: 12.8 KHz and 17.2 KHz. Although the latter was much more desirable for the "fine-grain" information being sought, it was necessary to down-sample that data to facilitate using the entire database at a single sample rate.

The next step toward an operational performance monitoring capability is the evaluation and expansion of the current algorithms on a more complete database. The collection must be performed under controlled conditions, greatly expanding the depth currently available to include duplicates when possible. In addition, when a sample modem is collected, perhaps the signal could be put over an actual telephone loop back circuit and then collected. This would illustrate immediately the effectiveness of algorithms under test

on actual data.

In review of the algorithms developed, let us consider each phase briefly. The go/no go channel decision performed in Phase 1 is quite accurate and easily computed. The generic type classifier of Phase 2 is based on the 1-bit quantized signal autocorrelation function. This is simply a 1-bit A/D converter in a hardware implementation. The classifiers are computationally efficient as well as accurate. The Phase 3 AGN and HD detection as demonstrated here is computationally simple; in fact, it is the same computation performed in Phase 1. The accuracy can probably be improved upon simply by increasing the sample rate of the collection. The phase jitter detection as presented here is rather complex and computationally difficult. A more suitable approach is carrier phase tracking. The error signal from the tracking device (which could be a phase-locked-loop or PPL) will show the phase jitter component. Although more difficult to implement, the impairment in accuracy should well be worth the effort. Further, in a hardware implementation, the utilization of a PPL is fairly standard. The PPL is equally sensitive to low frequency jitter (10hz) as well as higher frequency jitter. It is not difficult to see how this technology could readily be implemented to service a network whose population was 4800 bit/second and slower modems. We have demonstrated the first step. The expansion and validation of the current algorithm foundation on an extensive and reliable database is the bridge toward an operational capability.

Appendix A

Modeling of Voice Frequency Digital
Communication Facilities for Performance Monitoring Purposes

J. W. Modestino
Electrical, Computer and Systems Engineering Department
Rensselaer Polytechnic Institute
Troy, New York 12181

I. Introduction:

There are several techniques available for performance monitoring of voice frequency (VF) digital communications channels as discussed in [1]. One such technique is the use of adaptive channel modeling techniques as described, for example, in [2]-[3] for use on the microwave line-of-sight (LOS) channel. Specifically, a finite-parameter model of the physical transmission facility is constructed. The free parameters of this model are then adjusted by an appropriate adaptive algorithm to provide a close fit to a given channel chosen for performance evaluation. In the present note we will attempt to develop an appropriate finite-parameter model for the digital VF channel where the use of the word channel in this context is intended to include both the modem transmitter as well as actual transmission facilities. That is, we are interested in degradations introduced by the modem itself as well as the physical propagation channel. The issue of how the free parameters are to be adapted to a particular channel are described only briefly here.

II. Preliminaries:

In what follows we make extensive use of complex narrowband representations of all signal and noise processes. Specifically, the received signal to be used for adaptive channel estimation is given by

$$r(t) = \sqrt{2}\ \text{Re}\{\tilde{r}(t)e^{j2\pi f_c t}\}\ ,\tag{1}$$

where f_c is an _assumed known_ carrier frequency in Hz, and

$$\tilde{r}(t) = r_c(t) - j r_s(t) \quad , \tag{2}$$

is the _complex envelope_ expressed in terms of lowpass waveforms $r_c(t)$ and $r_s(t)$ representing the _inphase_ and _quadrature_ (I/Q) components, respectively. The complex envelope $\tilde{r}(t)$ is furthermore assumed of the form

$$\tilde{r}(t) = \tilde{s}_0(t) + \tilde{n}(t) \quad , \tag{3}$$

where $\tilde{s}_0(t)$ is the complex envelope of the _received signal_ component and $\tilde{n}(t)$ is a complex noise process representing additive channel noise as well as possible adjacent channel interference effects. The _received signal_ component $\tilde{s}_0(t)$ is assumed modeled as the complex response of the channel to the _transmitted signal_ $\tilde{s}(t)$ at its input. For purposes of the present discussion, the channel is modeled as a linear time-invariant narrowband filter with complex impulse response function $\tilde{h}_c(t)$ as indicated in Fig. 1. In reality, the channel might well be nonlinear and/or time varying. Nevertheless, the channel can at least be expected to be time-invariant over intervals that are long relative to typical measurement intervals. The question of channel nonlinearities is somewhat more difficult to address. However, since most of the modulation strategies of interest possess constant envelopes the presence of narrowband nonlinearities is not expected to have a large influence on the performance of the digital data link. At any rate the question of channel nonlinearities remains to be more fully explored in ongoing work.

We assume that the transmitted signal $\tilde{s}(t)$ is normalized so that

$$E_s = \int_0^{T_s} |\tilde{s}(t)|^2 dt, \tag{4}$$

represents the signal energy where T_s is the baud interval. Furthermore, we restrict attention to digital signaling formats such that $\tilde{s}(t)$ has the

representation

$$s(t) = \sqrt{\frac{E_s}{T_s}} \sum_i \varepsilon_i \bar{h}_m(t - iT_s - \tau) e^{j\theta} . \qquad (5)$$

Here, $\bar{h}_m(t)$ is a complex waveform vanishing outside the interval $[0, T_s]$ and $\{\varepsilon_i\}$ is a complex sequence which depends upon the data to be communicated in a manner specific to the modulation strategy employed. For example, the case $\varepsilon_i = \pm 1$ and $\bar{h}_m(t) = u_0(t)$ with $u_0(t)$ the real baseband pulse waveform

$$u_0(t) = \begin{cases} 1 & ; & 0 \leq t \leq T_s \\ 0 & ; & \text{elsewhere} , \end{cases} \qquad (6)$$

corresponds to conventional coherent BPSK modulation. Similarly, arbitrary MPSK can be handled by appropriate choice of $\{\varepsilon_i\}$. The quantities τ and θ in (5) are random timing epoch and phase offset, respectively. Generally these will be functions of time. For the time being we will assume that both τ and θ are known at the receiver to arbitrary accuracy. Without loss of generality then we assume both τ and θ are zero in (5).

The received signal component can then be represented over the measurement interval $[-NT_s, NT_s]$ as

$$s_0(t) = \sqrt{\frac{E_s}{T_s}} \sum_{i=-N}^{N} \varepsilon_i \bar{h}(t - iT_s) \qquad (7)$$

where $\bar{h}(t) \triangleq \bar{h}_m * \bar{h}_c(t)$ is the convolution of the complex modulator waveform $\bar{h}_m(t)$ and the complex impulse response $\bar{h}_c(t)$ of the channel. The overall impulse response $\bar{h}(t)$ is, of course, not known since the channel response $\bar{h}_c(t)$ is in general unknown. Nevertheless, it may be possible to adaptively estimate this quantity which should provide useful information on the present state of the channel. A scheme for accomplishing this is illustrated in Fig. 2. Here the complex envelope $\bar{r}(t)$ is passed through a filter with a complex impulse response

$\bar{h}_r(t)$ and then sampled at the output in synchronism with the baud rate. The timing information will presumably come from a bit synchronizer which must be replicated as part of the modem. The sampled output $\{\bar{r}_i\}$ is then compared to an estimated sequence $\{\hat{r}_i\}$ obtained by applying the estimated data sequence $\{\hat{c}_i\}$ to a finite parameter model of the channel. The estimated data sequence $\{\hat{c}_i\}$ will be assumed to come from the modem output which is replicated as part of the performance monitoring unit. It is shown in Fig. 2 as being obtained at the output of an appropriately defined decision device. We assume that the error rate is reasonably small so that the occasional errors do not have a profound effect on overall system performance. Assuming that an appropriate finite-parameter model of the channel is available, the expected output sequence $\{\hat{r}_i\}$ is compared to the actual sequence $\{\bar{r}_i\}$ to generate the error sequence $\{\varepsilon_i\}$. An appropriate adaptive algorithm is then employed to estimate and track changes in the channel parameters. Clearly, the reason for including the receiving filter in Fig. 2 is to obtain a SNR advantage in the comparison of expected and actual channel outputs.

In order to determine an appropriate finite-parameter model for the channel, note that the sampled output sequence is given by

$$\bar{r}_i = \int_{-\infty}^{\infty} \bar{r}(\tau)\bar{h}_r(t-\tau)d\tau \Big|_{t=iT_s} \quad ; \quad i=0,\pm 1,\pm 2,\ldots, \qquad (8)$$

or in normalized form

$$\bar{r}_i = \sqrt{\frac{2E_s}{N_0 BT_s}} \sum_{k=-N}^{N} \bar{c}_k \bar{h}_{i-k} + \bar{n}_i \quad , \qquad (9)$$

where $\{\bar{n}_i\}$ is a complex zero-mean Gaussian sequence whose I/Q components are each of unit variance,

$$B \triangleq \frac{1}{2\pi} \int_{-\infty}^{\infty} |\tilde{H}_r(j\omega)|^2 d\omega \quad, \tag{10}$$

is the equivalent rectangular bandwidth of the receiving filter[†] in Hz, and finally

$$\tilde{h}_{i-j} \triangleq \int_{-\infty}^{\infty} \tilde{h}(t-iT_s)\tilde{h}_r(jT_s-t)dt, \quad i,j=0,\pm1,\ldots \tag{11}$$

The sampled output sequence can be rewritten in the form

$$\tilde{z}_i = \sqrt{\frac{2E_s}{N_0 BT_s}}\, c_i + \sqrt{\frac{2E_s}{N_0 BT_s}} \sum_{\substack{k=-N \\ k\neq i}}^{N} c_k \tilde{h}_{i-k} + \tilde{n}_i \quad, \tag{12}$$

where we assume $\tilde{h}_0=1$ which is merely a conservation of energy constraint. The second term in (12) is a distortion term resulting from ISI produced by co-channel distortions on the channel.

From the preceding it is clear that a reasonable model for the channel is the tapped delay line (TDL) illustrated in Fig. 3. Specifically, we assume the channel can be modeled as a TDL with a total of 2L+1 taps and corresponding tap weights $\tilde{g}_i$, $i=0,\pm1,\pm2,\ldots,\pm L$. In the next section we describe how the tap weights may be adjusted to estimate and track the instantaneous state of the channel.

III. Adaptive Adjustment Procedure:

Define the performance criterion as

$$J(\underline{g}) = E\{|\tilde{z}_i-\hat{z}_i|^2\} \tag{13}$$

where $\underline{g}^T=(\tilde{g}_{-L}, \tilde{g}_{-L+1},\ldots,\tilde{g}_0,\ldots,\tilde{g}_L)$ represents the tap gain vector of dimension (2L+1) and $\hat{z}_i$ represents the TDL filter output according to

$$\hat{z}_i = \sum_{j=-L}^{L} \tilde{g}_j c_{i-j} \quad, \tag{14}$$

[†] Here $\tilde{H}_r(j\omega)$ is the system transfer function of the receiving filter with impulse response $\tilde{h}_r(t)$.

where for simplicity we assume that $\hat{c}_i = \tilde{c}_i$, i.e., no decision errors made. The performance criterion, which is to be minimized through choice of $\underline{g}$, can be expressed as

$$J(\underline{g}) = E\{|\hat{z}_i - \sum_{j=-L}^{L} \underline{g}_j \tilde{c}_{i-j}|^2\}$$

$$= E\{|\hat{z}_i|^2\} - 2Re\{\sum_{j=-L}^{L} \underline{g}_j E\{\hat{z}_i^* \tilde{c}_{i-j}\}\}$$

$$+ \sum_{j=-L}^{L} \sum_{k=-L}^{L} \underline{g}_j \underline{g}_k^* E\{\tilde{c}_{i-j} \tilde{c}_{i-k}^*\} . \tag{15}$$

This last result can be rewritten in vector matrix form according to

$$J(\underline{g}) = E\{|\hat{z}_i|^2\} - \underline{\psi}^\dagger \bar{Q}^{-1} \underline{\psi} + [\underline{g} - \bar{Q}^{-1} \underline{\psi}]^\dagger \bar{Q}[\underline{g} - \bar{Q}^{-1} \underline{\psi}] , \tag{16}$$

where $\bar{Q}$ is a $(2L+1) \times (2L+1)$ matrix with (k, ℓ) component

$$\bar{q}_{k,\ell} = E\{\tilde{c}_{i-k}^* \tilde{c}_{i-\ell}\} = \bar{q}_{\ell,k}^* , \tag{17}$$

and $\underline{\psi}$ is a $(2L+1)$ vector with k'th component

$$\psi_k = E\{\hat{z}_i \tilde{c}_{i-k}^*\} \quad ; \quad k=0,\pm 1,\ldots,\pm L \tag{18}$$

The "$\dagger$" in (16) indicates complex conjugate transpose. It is easily seen that the optimum tap connection vector is that which minimizes the quadratic form in (16) with the result

$$\underline{g}_{opt} = \bar{Q}^{-1} \underline{\psi} . \tag{19}$$

This solution can be determined by an iterative gradient procedure provided the gradient of the functional $J(\underline{g})$ can be determined. Specifically, we propose use of the $\underline{steepest\ descent}$ procedure where $\underline{g}_0$ is an initial guess and the successive estimates are determined according to

$$\underline{g}_{i+1} = \underline{g}_i - h \underline{\nabla}(\underline{g}_i) \quad ; \quad i=0,1,\ldots, \tag{20}$$

with h the step size at each iteration and the gradient $\underline{\nabla}(\underline{g})$ is determined according to

$$\underline{V}(\underline{g}) \triangleq \frac{\partial J(\underline{g})}{\partial \underline{g}} = 2\tilde{Q}[\underline{g} - \tilde{Q}^{-1}\underline{\psi}] \quad , \tag{21}$$

or equivalently,

$$\underline{V}(\underline{g}) = 2[\tilde{Q}\underline{g} - \underline{\psi}] = -2E\{\hat{e}_i \underline{c}_i\} \quad , \tag{22}$$

where $\hat{e}_i = r_i - \hat{r}_i$ is the error signal and $\underline{c}_i^T = (c_{i+L}, c_{i+L-1} \cdots, c_i, \ldots, c_{i-L})$ is the transmitted data sequence.

The difficulties with implementing the steepest descent algorithm as described by (20) is that the gradient in (22) requires an ensemble average. As an alternate we propose use of the "noisy" gradient estimate

$$\underline{V}(\underline{g}_i) = -2[\hat{e}_i \underline{c}_i] \quad , \tag{23}$$

which is the typical approach used in practice.

IV. Summary and Conclusions:

We have described one approach to modeling and adaptive estimation of the characteristics of VF communication lines. Several things are required to complete this work. First, techniques should be developed for estimating performance analytically in terms of the estimated parameter vector $\underline{g}$. Also pattern recognition techniques should be explored for classifying the degradation using the vector $\underline{g}$ as a pattern vector. Some experimental results should be obtained using this approach. Finally, we should investigate more accurate modeling approaches to include nonlinear effects in a finite-parameter channel model.

References

1. J. W. Modestino, "A Hierarchical Approach to Performance Monitoring of Voice Frequency Lines", unpublished PAR report, Jan. 1981.

2. P. A. Bello, et al., "Adaptive Channel Measurement Study", RADC-TR-75-243, Sept. 1975.

3. L. E. Jankauskas, et al., "Technical Control of the Digital Transmission Facilities of the Defense Communication System", IEEE Trans. on Commun., vol. COM-28, pp. 1516-1523, Sept. 1980.

$$\tilde{s}(t) \longrightarrow \boxed{\begin{array}{c}\text{Linear Time-Invariant} \\ \text{Filter} \\ \tilde{h}_c(t)\end{array}} \longrightarrow \tilde{s}_0(t)$$

Received
Signal
Component
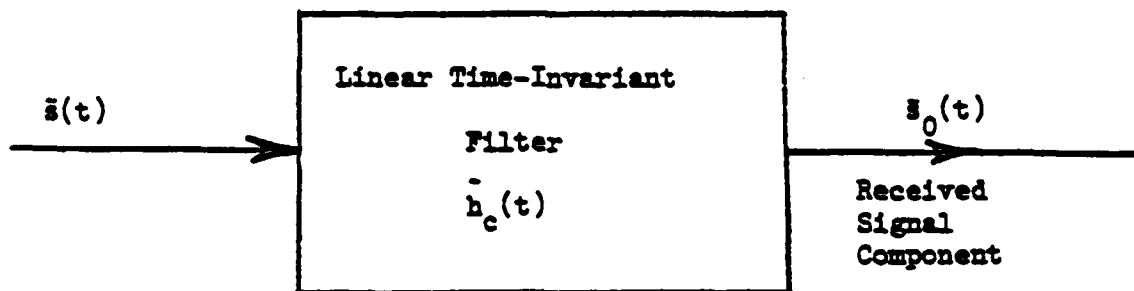
Figure 1

Generation of Received Signal Component

$\tilde{r}(t)$

$\tilde{h}_r(t)$

$\{\tilde{f}_i\}$

Decision
Device

$\{\tilde{c}_i\}$

Finite-Parameter
Channel
Model

$\{\hat{\tilde{f}}_i\}$

$-$
$+$
$\sum$

$\{\tilde{e}_i\}$

update

Adaptive
Algorithm
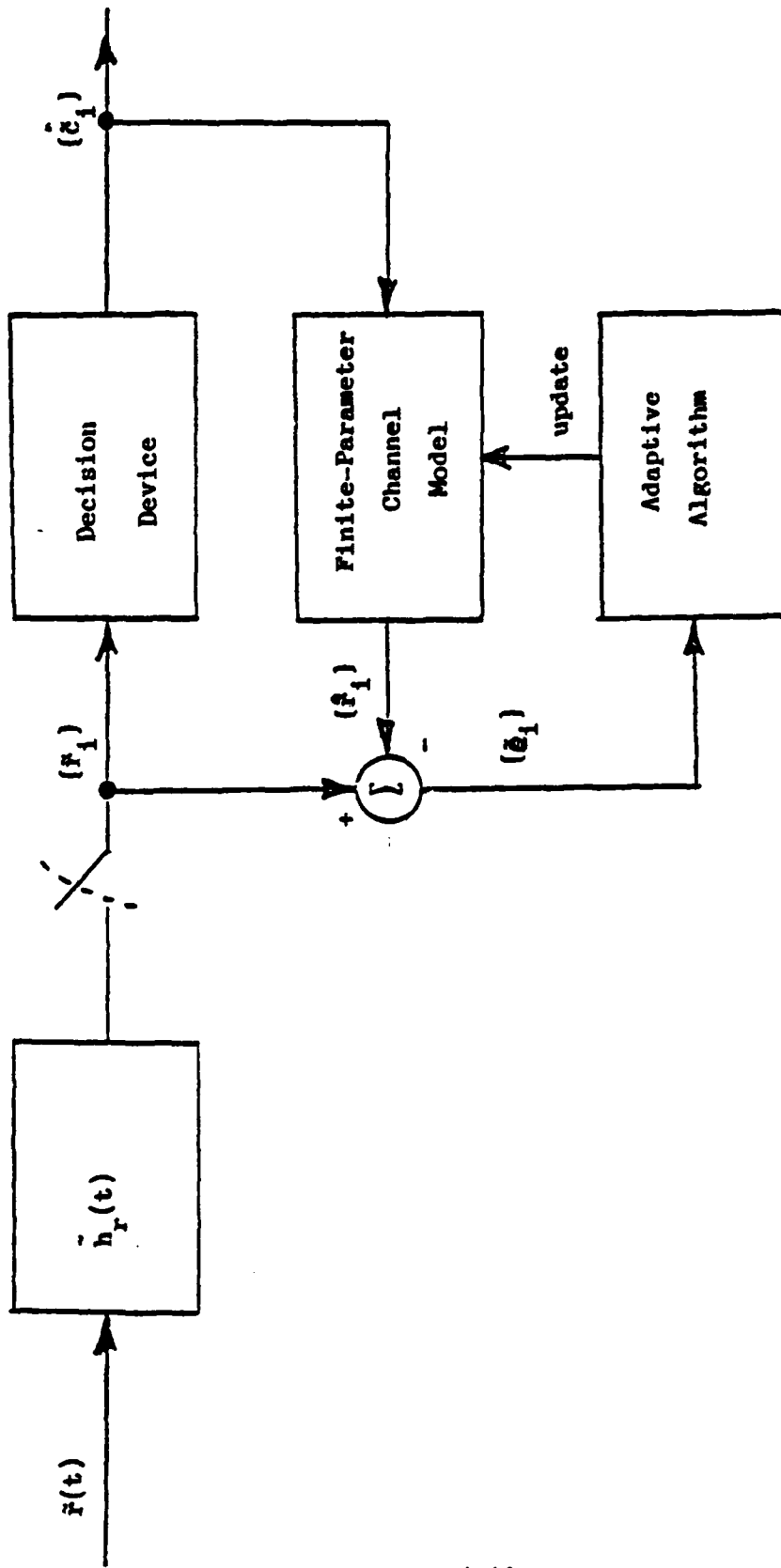
Figure 2

Decision-Directed Adaptive Channel Estimation Procedure.
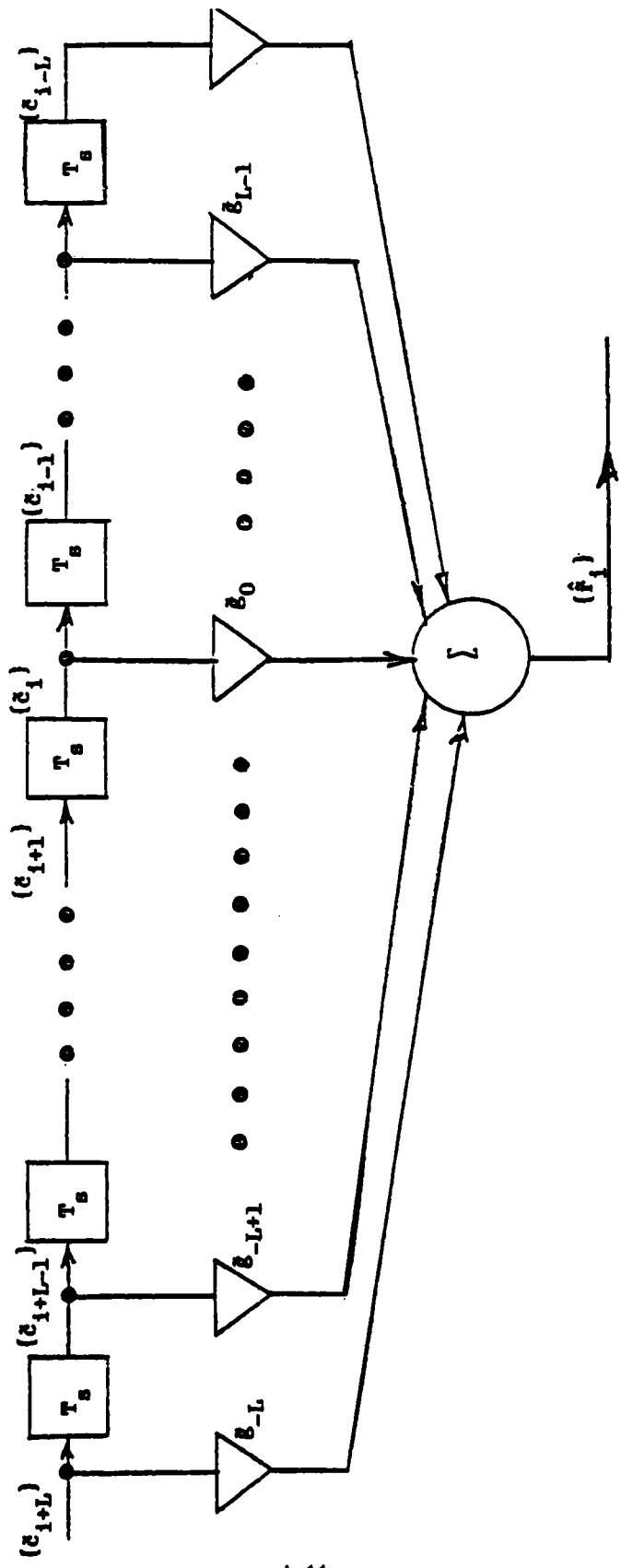
Figure 3

Tapped Delay Line (TDL) Channel Model

Appendix B

Further Results on Modeling of Voice Frequency
Digital Communication Links for Performance Monitoring Purposes

J. W. Modestino
Electrical, Computer and Systems Engineering Department
Rensselaer Polytechnic Institute
Troy, New York 12181

I. Introduction:

In previous work [1], an adaptive approach to performance monitoring
of digital communication systems operating on voice frequency (VF) lines
was described. This approach, which was an initial attempt at formulating
and solving the problem, is limited in a number of ways. Most important
among these limitations are the fact that the modulation format must be
known a priori and a replica of the actual receiver modem be constructed,
and the fact that only linear channel distortions can be treated in this
way. It is of some interest to devise alternative techniques, adaptive or
otherwise, which remove either or both of these limitations. In the pre-
sent note we describe one such technique which at least allows modeling of
nonlinear distortion effects.

II. Preliminaries:

The Volterra series expansion can be used to represent the output of a
nonlinear system with memory in powers of the input. This fact has been very
useful in the analysis of the input/output behavior of nonlinear baseband
systems as described, for example, in [2]-[5]. The extension to narrowband
signals described in terms of inphase and quadrature (I/Q) components is
relatively straightforward. In particular, suppose that $x(t)$ and $y(t)$ are
narrowband signals representing the input and output respectively of a

narrowband, although possibly nonlinear, system as illustrated in Fig. 1. Here we assume that $x(t)$ and $y(t)$ can be represented in the form

$$x(t) = \sqrt{2}\ \text{Re}\{\tilde{x}(t)e^{j\omega_c t}\}\ ,\tag{1a}$$

and

$$y(t) = \sqrt{2}\ \text{Re}\{\tilde{y}(t)e^{j\omega_c t}\}\ ,\tag{1b}$$

with ω_c the carrier frequency in radians/second and $\tilde{x}(t)$, $\tilde{y}(t)$ the corresponding complex envelopes. The input/output behavior of this system is assumed described by the complex Volterra series

$$\tilde{y}(t) = \sum_{n=1}^{\infty} \int_{-\infty}^{\infty} d\tau_1 \int_{-\infty}^{\infty} d\tau_2 \cdots \int_{-\infty}^{\infty} d\tau_n \tilde{h}_n(t-\tau_1,t-\tau_2,\ldots,t-\tau_n)\prod_{i=1}^{n}\tilde{x}(\tau_i),\tag{2}$$

where the $h_n(t_1,t_2,\ldots,t_n)$ are called Volterra kernels. For a <u>linear</u> system all terms except the first vanish and we have

$$\tilde{y}(t) = \int_{-\infty}^{\infty} \tilde{h}_1(t-\tau)\tilde{x}(\tau)d\tau\ ,\tag{3}$$

in which case $\tilde{h}_1(t)=\tilde{h}(t)$ is simply the complex envelope of the impulse response $h(t)$ of the linear narrowband filter. The impulse response $h(t)$ then has the representation

$$h(t) = 2\ \text{Re}\{\tilde{h}(t)e^{j\omega_c t}\}\ .\tag{4}$$

Another special case occurs when the system is nonlinear but memoryless. It follows that the Volterra kernels are described by

$$\tilde{h}_n(t-\tau_1,t-\tau_2,\ldots,t-\tau_n) = a_n \prod_{i=1}^{n}\delta(t-\tau_i)\tag{5}$$

where $\delta(\cdot)$ is the delta function. From (2) then we have

$$\tilde{y}(t) = \sum_{n=1}^{\infty} a_n\tilde{x}^n(t)\ ,\tag{6}$$

which is merely a representation of the output as a power series expansion

of the input complex envelope. One can conceive other instantaneous or zero-memory nonlinearities which distort the amplitude and phase in decidedly different ways. These important special cases will be treated in later work.

Finally, consider the n-fold Fourier transform

$$\bar{H}_n(\omega_1,\omega_2,\ldots,\omega_n) = \int_{-\infty}^{\infty} dt_1 \int_{-\infty}^{\infty} dt_2 \cdots \int_{-\infty}^{\infty} dt_n \bar{h}_n(t_1,t_2,\ldots,t_n) \exp\{-j(\omega_1 t_1 + \omega_2 t_2 + \ldots \omega_n t_n)\} . \quad (7)$$

Clearly $\bar{H}_1(\omega)$ is the familiar complex transfer function of a narrowband linear system given by

$$\bar{H}_1(\omega) = \int_{-\infty}^{\infty} \bar{h}_1(t) e^{-j\omega t} dt . \quad (8)$$

By analogy, the quantity $\bar{H}_n(\omega_1,\omega_2,\ldots,\omega_n)$ will be called the n'th-order complex Volterra transfer function.

III. Application to Adaptive Performance Monitoring:

As in [1] we shall assume the received signal to be of the form

$$r(t) = \sqrt{2} \operatorname{Re}\{\hat{r}(t)e^{j\omega_c t}\} , \quad (9)$$

with

$$\hat{r}(t) = \hat{s}_0(t) + \hat{n}(t) , \quad (10)$$

where $\hat{s}_0(t)$ is the complex envelope of the _received signal_ component and $\hat{n}(t)$ is a complex noise process representing additive channel noise as well as possible adjacent channel interference effects. The _received signal_ component $\hat{s}_0(t)$ is assumed modeled as the complex response of the channel to the _transmitted signal_ $\hat{s}(t)$ at its input. We assume the _transmitted signal_ is of the form

$$\hat{s}(t) = \sqrt{\frac{E_s}{T_s}} \sum_i \hat{c}_i \bar{h}_m(t - iT_s - \tau) e^{j\theta} , \quad (11)$$

with $\bar{h}_m(t)$ a complex waveform vanishing outside the interval $[0, T_s]$, and $\{c_i\}$ a complex sequence which depends upon the data to be communicated in a manner specific to the modulation strategy employed. The quantities τ and θ in (11) are random timing epoch and phase offset, respectively. As in [1], we will assume for the time being that both τ and θ are known to arbitrary accuracy at the receiver. Without loss of generality then we assume that both τ and θ in (11) are zero.

The channel behavior will be modeled in terms of a truncated complex Volterra series. Specifically, we assume that

$$s_0(t) = \sum_{n=1}^{K} \int_{-\infty}^{\infty} d\tau_1 \int_{-\infty}^{\infty} d\tau_2 \cdots \int_{-\infty}^{\infty} d\tau_n \, \bar{h}_{c,n}(t-\tau_1, t-\tau_2, \ldots, t-\tau_n) \prod_{i=1}^{n} \bar{s}(\tau_i), \quad (12)$$

for some choice of $\bar{h}_{c,n}(t)$, $n=1,2,\ldots,K$. For ease of exposition we take the case $K=2$ in what follows. The case of finite K follows in similar fashion except the algebra is a bit tedious. Thus

$$s_0(t) = \int_{-\infty}^{\infty} \bar{h}_c(t-\tau)\bar{s}(\tau) d\tau + \int_{-\infty}^{\infty}\int_{-\infty}^{\infty} \bar{h}_c(t-\tau, t-\nu)\bar{s}(\tau)\bar{s}(\nu) d\tau d\nu , \quad (13)$$

where we have suppressed the dependence upon[†] n in writing $h_c(\cdot)$ and $h_c(\cdot,\cdot)$ for $h_{c,1}(\cdot)$ and $h_{c,2}(\cdot,\cdot)$, respectively. The overall VF channel model is then as illustrated in Fig. 2.

The received signal component can then be represented over the measurement interval $[-NT_s, (N+1)T_s]$ as

$$s_0(t) = \sqrt{\frac{E_s}{T_s}} \sum_{i=-N}^{N} \bar{c}_i \bar{h}(t-iT_s) + \frac{E_s}{T_s} \sum_{i=-N}^{N} \sum_{j=-N}^{N} \bar{c}_i \bar{c}_j \bar{h}(t-iT_s, t-jT_s) , \quad (14)$$

[†] This should cause no confusion since the linear and quadratic filtering functions are readily identified by whether it is a function of one or two arguments.

where $\bar{h}(t) \overset{\Delta}{=} \bar{h}_m * \bar{h}_c(t)$ is the convolution of the complex modulator waveform $\bar{h}_m(t)$ and the complex impulse response $\bar{h}_c(t)$ of the channel. Similarly, the quantity $\bar{h}(t,s)$ is the two-dimensional (2-D) convolution $\bar{h}(t,s) \overset{\Delta}{=} \bar{h}_m ** \bar{h}_c(t,s)$ defined by

$$\bar{h}(t,s) = \int_{-\infty}^{\infty} \int_{-\infty}^{\infty} \bar{h}_m(t-\tau)\bar{h}_c(\tau,\nu)\bar{h}_m(s-\nu)d\tau d\nu . \qquad (15)$$

It should be obvious how additional high-order convolution products arise if the Volterra series of (12) is truncated for some value $K>2$. In the case under consideration neither $\bar{h}(\cdot)$ or $\bar{h}(\cdot,\cdot)$ is known and must be adaptively estimated from the output of the VF channel.

As in [1], we assume that the channel output $\bar{r}(t)$ is passed through a narrowband filter with complex impulse response $\bar{h}_r(t)$ and sampled in synchronism with the baud rate to generate the sequence

$$\bar{r}_i = \int_{-\infty}^{\infty} \bar{r}(\tau)\bar{h}_r(t-\tau)d\tau \Big|_{t=iT_s} \quad ; \quad i=0,\pm 1,\pm 2,\ldots, \qquad (16)$$

or in normalized form

$$\bar{r}_i = \sqrt{\frac{2E_s}{N_0 BT_s}} \sum_{k=-N}^{N} \bar{c}_k \bar{h}_{i-k} + \sqrt{\frac{2E_s}{N_0 BT_s}} \sum_{k=-N}^{N} \sum_{\ell=-N}^{N} \bar{c}_k \bar{h}_{i-k,i-\ell}\bar{c}_\ell + \bar{n}_i , \qquad (17)$$

Here, $\{\bar{n}_i\}$ is a complex zero-mean Gaussian sequence whose I/Q components are each of unit variance,

$$B \overset{\Delta}{=} \frac{1}{2\pi} \int_{-\infty}^{\infty} |H_r(j\omega)|^2 d\omega , \qquad (18)$$

is the equivalent rectangular bandwidth of the receiving filter in Hz,

$$\bar{h}_{i-j} \overset{\Delta}{=} \int_{-\infty}^{\infty} \bar{h}(t-jT_s)\bar{h}_r(iT_s-t)dt, \quad i,j=0,\pm 1,\pm 2,\ldots, \qquad (19)$$

and finally,

$$\bar{h}_{i-k,i-\ell} \triangleq \sqrt{\frac{T_s}{T_s}} \int_{-\infty}^{\infty} \bar{h}(t-kT_s, t-\ell T_s) \bar{h}_r(iT_s-t)dt \quad ; \quad i,k,\ell=0,\pm1,\pm2,\ldots, \quad (20)$$

It should be noted at this point that we have written these last two express-
ions only in terms of $i-j$ in the case of (19) and the double index $i-k$, $i-\ell$
in the case of (20). Justification for this, which is not immediately appar-
ent, is relatively straightforward.

From the preceding, it is clear that a reasonable finite-parameter model
of the channel is of the form

$$\hat{r}_i = \sum_{j=-L}^{L} \bar{g}_j c_{i-j} + \sum_{k=-L}^{L} \sum_{\ell=-L}^{L} c_{i-k} \bar{p}_{k,\ell} c_{i-\ell} \quad . \quad (21)$$

The first term has an interpretation as a conventional tapped delay line (TDL)
as in [1], while the second term on the right-hand side of (21) represents a
quadratic operation on the data sequence which is a bit more difficult to
interpret.

One interpretation to be given to the quadratic operation in (21) is to
express it in terms of vector matrix notation according to

$$\sum_{k=-L}^{L} \sum_{\ell=-L}^{L} c_{i-k} \bar{p}_{k,\ell} c_{i-\ell} = \langle \underline{c}_i , \bar{\underline{P}} \underline{c}_i \rangle \quad , \quad (22)$$

where $\underline{c}_i^T = (c_{i+L}, c_{i+L-1}, \ldots, c_i, \ldots, c_{i-L+1}, c_{i-L})$, while $\bar{\underline{P}}$ is a $(2L+1)\times(2L+1)$
matrix with (k,ℓ) component $\bar{p}_{k,\ell}$, $k,\ell=0,\pm1,\pm2,\ldots,$ L. We will assume that $\bar{\underline{P}}$
is positive definite and symmetric in which case it can be factored in the
form $\bar{\underline{P}} = \bar{\underline{B}}^T \bar{\underline{B}}$ where $\underline{B}$ is an upper triangular matrix. It follows that

$$\sum_{k=-L}^{L} \sum_{\ell=-L}^{L} c_{i-k} \bar{p}_{k,\ell} c_{i-\ell} = \langle \underline{c}_i' , \underline{c}_i' \rangle = \sum_{j=-L}^{L} c_{i-j}'^2 \quad , \quad (23)$$

where $\underline{c}_i' = \bar{\underline{B}} \underline{c}_i$. In fact, under the preceding assumptions we have

$$c_{i-k}' = \sum_{\ell=k}^{L} \bar{b}_{k,\ell} c_{i-\ell} \quad , \quad (24)$$

which is in general a time-varying filtering operation. For example, with $k=0$ we have

$$\bar{c}_i' = \sum_{\ell=0}^{L} \bar{b}_{0,\ell} \bar{c}_{i-\ell} \tag{25}$$

$$= \sum_{\ell=0}^{L} \bar{a}_\ell \bar{c}_{i-\ell} \quad ,$$

where $\bar{a}_\ell \triangleq \bar{b}_{0,\ell}$. We will assume that the filtering operation represented by the matrix $\underline{B}$ can be approximated by the input/output relationship in (25). This will be the case, of course, if $\bar{b}_{k,\ell} = \bar{b}_{0,\ell-k}$ which we assume to be approximately true. The sequence $\{\bar{a}_\ell\}$ then has an interpretation as the impulse response sequence associated with a linear, causal and time-invariant finite-impulse response (FIR) digital filter, which can again be realized as a TDL. Indeed, the overall channel model can be realized as a parallel combination of two TDL's with a squaring device and an accumulator associated with the quadratic branch. A possible realization of this structure is illustrated in Fig. 3. As indicated, there are a total of $(3L+2)$ coefficients to be specified, $(2L+1)$ coefficients $\{\bar{a}_k\}_{k=-L}^{L}$ and $(L+1)$ coefficients $\{\bar{a}_k\}_{k=0}^{L}$. In the next section we propose an adaptive procedure for estimating these coefficients on the basis of past transmissions.

IV. Adaptive Adjustment Procedure:

As indicated in the preceding section, the output of the nonlinear channel model can be expressed in the form[†]

$$\hat{z}_i = \sum_{j=-L}^{L} \bar{a}_j \bar{c}_{i-j} + \sum_{j=-L}^{L} \left[\sum_{k=0}^{L} \bar{a}_k \bar{c}_{i-j-k} \right]^2 = \hat{z}_i' + \hat{z}_i'' \quad . \tag{26}$$

[†] We are implicitly assuming a decision directed scheme $\hat{c}_i = \bar{c}_i$ as discussed previously in [1]. Also $\{\hat{z}_i'\}$ represents the output of the linear branch while $\{\hat{z}_i''\}$ represents the output of the quadratic branch as illustrated in Fig. 3.

Now define the performance measure

$$J(\underline{z},\underline{a}) = E\{|z_i - \hat{z}_i|^2\} , \tag{27}$$

where $\underline{z}^T = (\tilde{z}_{-L}, \tilde{z}_{-L+1}, \ldots, \tilde{z}_0, \ldots, \tilde{z}_L)$ and $\underline{a}^T = (\tilde{a}_0, \tilde{a}_1, \ldots, \tilde{a}_L)$ represent the tap gain vectors in Fig. 3 of dimension $(2L+1)$ and $(L+1)$, respectively. This performance measure is to be minimized by simultaneous choice of $\underline{z}$ and $\underline{a}$, and can be rewritten as

$$J(\underline{z},\underline{a}) = E\{|z_i|^2\} - 2\text{Re}\{\sum_{j=-L}^{L} \tilde{z}_j E\{z_i^* \tilde{c}_{i-j}\}\}$$

$$+ 2\text{Re}\left\{\sum_{j=-L}^{L} \tilde{z}_j \sum_{m=0}^{L} \sum_{n=0}^{L} \tilde{a}_m^* \tilde{a}_n^* \sum_{k=-L}^{L} E\{\tilde{c}_{i-j} \tilde{c}_{i-k-m}^* \tilde{c}_{i-k-n}^*\}\right\}$$

$$+ \sum_{j=-L}^{L} \sum_{k=-L}^{L} \tilde{z}_j \tilde{z}_k^* E\{\tilde{c}_{i-j} \tilde{c}_{i-k}^*\}$$

$$- 2\text{Re}\left\{\sum_{m=0}^{L} \sum_{n=0}^{L} \tilde{a}_m \tilde{a}_n \sum_{j=-L}^{L} E\{z_i^* \tilde{c}_{i-j-m} \tilde{c}_{i-j-n}\}\right\} \tag{28}$$

$$+ \sum_{m=0}^{L} \sum_{n=0}^{L} \tilde{a}_m \tilde{a}_n^* \sum_{u=0}^{L} \sum_{v=0}^{L} \tilde{a}_u \tilde{a}_v^* \sum_{j=-L}^{L} \sum_{k=-L}^{L} E\{\tilde{c}_{i-j-m} \tilde{c}_{i-j-u} \tilde{c}_{i-k-n}^* \tilde{c}_{i-k-v}^*\} .$$

While this expression looks quite complicated, it is shown in Appendix A that it can be simplified somewhat and rewritten in vector matrix notation according to [†]

$$J(\underline{z},\underline{a}) = E\{|z_i|^2\} - [\bar{\psi} - \bar{\lambda}(\underline{a})]^\dagger \bar{Q}^{-1} [\bar{\psi} - \bar{\lambda}(\underline{a})]$$

$$+ [\underline{z} - \bar{Q}^{-1}(\bar{\psi} - \bar{\lambda}(\underline{a}))]^\dagger \bar{Q} [\underline{z} - \bar{Q}^{-1}(\bar{\psi} - \bar{\lambda}(\underline{a}))]$$

$$- 2\text{RE}\{\text{tr}[\bar{\Psi} \underline{a} \underline{a}^T]\} + \text{tr}\{\underline{a} \underline{a}^\dagger \bar{\Lambda}(\underline{a})\} \tag{29}$$

Each of the terms in this last expression are defined explicitly in Appendix B, to which the reader is referred to for details. Furthermore, it follows easily

---

[†] Here the dagger "†" indicates complex conjugate transpose.

that the optimum choice for $\underline{z}$ and $\underline{a}$ are found as solutions to the simultaneous equations

$$\nabla_{\underline{z}} J(\underline{z},\underline{a}) \triangleq \frac{\partial J(\underline{z},\underline{a})}{\partial \underline{z}} = \mathrm{Re}\{\bar{\underline{Q}}[\underline{z} - \bar{\underline{Q}}^{-1}(\bar{\underline{\psi}} - \bar{\underline{\lambda}}(\underline{a}))]\} = 0 \quad , \tag{30a}$$

and

$$\nabla_{\underline{a}} J(\underline{z},\underline{a}) \triangleq \frac{\partial J(\underline{z},\underline{a})}{\partial \underline{a}}$$

$$= 4\mathrm{Re}\{\bar{\underline{\phi}}(\underline{z})\underline{a}\} - 4\mathrm{Re}\{\bar{\underline{\gamma}}\underline{a}\}$$

$$+ 4\mathrm{Re}\{\bar{\underline{\Lambda}}(\underline{a})\underline{a}\} = 0 \quad . \tag{30b}$$

In general, these simultaneous nonlinear equations are difficult to solve. Nevertheless, the solution can be determined by an iterative gradient procedure. Specifically, we propose use of a <u>steepest descent</u> procedure where $\underline{z}_0$ and $\underline{a}_0$ are initial guesses and the successive estimates are determined according to

$$\underline{z}_{i+1} = \underline{z}_i - h\nabla_{\underline{z}} J(\underline{z}_i,\underline{a}_i) \; ; \quad i=0,1,\dots , \tag{31a}$$

and

$$\underline{a}_{i+1} = \underline{a}_i - h\nabla_{\underline{a}} J(\underline{z}_i,\underline{a}_i) \; ; \quad i=0,1,\dots , \tag{31b}$$

where h is the step size at each iteration and the gradients are determined from (30).

To provide some physical interpretation to this procedure, consider the gradient $\nabla_{\underline{z}} J(\underline{z},\underline{a})$ of (30a), i.e.,

$$\nabla_{\underline{z}} J(\underline{z},\underline{a}) = 2\mathrm{Re}\{\bar{\underline{Q}}\underline{z} - (\bar{\underline{\psi}} - \bar{\underline{\lambda}}(\underline{a}))\} = -2\mathrm{Re}\{E\{\delta_i \underline{c}_i^*\}\} \tag{32}$$

where $\delta_i = \hat{z}_i - \hat{a}_i$ is the error signal and, as previously, $\underline{c}_i^T = (\delta_{i+L}, \delta_{i+L-1}, \dots, \delta_i, \dots, \delta_{i-L+1}, \delta_{i-L})$ is the transmitted data sequence. Similarly, we have

$$\nabla_{\underline{a}} J(\underline{z},\underline{a}) = -4RE\{E\{\delta_i \underline{b}_i^*\}\} \quad , \tag{33}$$

where now $\underline{b}_i$ is an (L+1)-vector with k'th element

$$b_k = \sum_{j=-L}^{L} \tilde{c}'_{i-j}\tilde{c}_{i-j-k} \quad ; \quad k=0,1,\ldots,L \quad , \tag{34}$$

with $\{\tilde{c}'_{i-j}\}$ the sequence of outputs of the upper tapped delay line in Fig. 3 with components generated according to (25), i.e.,

$$\tilde{c}'_{i-j} = \sum_{n=0}^{L} \tilde{a}_n \tilde{c}_{i-j-n} \quad ; \quad j=0,\pm 1,\pm 2, \ldots,\pm L \quad . \tag{35}$$

The difficulties with implementing the steepest descent algorithm as described above is that the gradients in (32) and (33) require ensemble averages. As an alternate we propose use of the "noisy" gradient estimates

$$\nabla_{\underline{g}} J(\underline{g},\underline{a}) \simeq -2\mathrm{Re}\{\tilde{e}_i\tilde{c}_i^*\} \quad , \tag{36a}$$

and

$$\nabla_{\underline{a}} J(\underline{g},\underline{a}) \simeq -4\mathrm{Re}\{\tilde{e}_i\tilde{b}_i^*\} \quad , \tag{36b}$$

which is the approach usually adopted in practice.

V. Summary and Conclusions:

We have described an approach to modeling and adaptive estimation of the characteristics of VF communication lines subject to nonlinear distortion effects. As noted previously in [1], it remains to develop analytical techniques for estimating error rate performance in terms of the estimated parameter vectors $\underline{g}$ and $\underline{a}$. Also to be investigated are pattern recognition techniques for classifying the degradation using the vectors $\underline{g}$ and $\underline{a}$ as parameter vectors. Finally, we note that the approach described here is limited to linear modulation strategies. It remains to determine how adaptive estimation techniques can be used with nonlinear modulation formats.

Appendix A

Vector-Matrix Formulation of Performance Criterion

Consider the performance criterion $J(\underline{\tilde{g}}, \underline{\tilde{a}})$ as given by (28) of the text. This can be written as

$$J(\underline{\tilde{g}}, \underline{\tilde{a}}) = J_1(\underline{\tilde{g}}, \underline{\tilde{a}}) + J_2(\underline{\tilde{a}}), \tag{A-1}$$

where $J_1(\underline{\tilde{g}}, \underline{\tilde{a}})$ depends upon both $\underline{\tilde{g}}$ and $\underline{\tilde{a}}$ and is obtained as the sum of the first four terms in (28), i.e.,

$$J_1(\underline{\tilde{g}}, \underline{\tilde{a}}) \overset{\Delta}{=} E\{|\tilde{r}_i|^2\} - 2\mathrm{Re}\left\{ \sum_{j=-L}^{L} \tilde{g}_j E\{\tilde{r}_i^* \tilde{c}_{i-j}\} \right\}$$

$$+ 2\mathrm{Re}\left\{ \sum_{j=-L}^{L} \tilde{g}_j \sum_{m=0}^{L} \sum_{n=0}^{L} \tilde{a}_m^* \tilde{a}_n^* \sum_{k=-L}^{L} E\{\tilde{c}_{i-j}\tilde{c}_{i-k-m}^* \tilde{c}_{i-k-n}^*\} \right\}$$

$$+ \sum_{j=-L}^{L} \sum_{k=-L}^{L} \tilde{g}_j \tilde{g}_k^* E\{\tilde{c}_{i-j}\tilde{c}_{i-k}^*\} \quad . \tag{A-2}$$

Similarly, the term $J_2(\underline{\tilde{a}})$ depends only upon $\underline{\tilde{a}}$ and consists of the last two terms of (28), i.e.,

$$J_2(\underline{\tilde{a}}) = -2\mathrm{Re}\left\{ \sum_{m=0}^{L} \sum_{n=0}^{L} \tilde{a}_m \tilde{a}_n \sum_{j=-L}^{L} E\{\tilde{r}_i^* \tilde{c}_{i-j-m}\tilde{c}_{i-j-n}\} \right\}$$

$$+ \sum_{m=0}^{L} \sum_{n=0}^{L} \tilde{a}_m \tilde{a}_n^* \sum_{u=0}^{L} \sum_{v=0}^{L} \tilde{a}_u \tilde{a}_v^* \sum_{j=-L}^{L} \sum_{k=-L}^{L} E\{\tilde{c}_{i-j-m}\tilde{c}_{i-j-u}\tilde{c}_{i-k-n}^* \tilde{c}_{i-k-v}^*\}. \tag{A-3}$$

We concentrate upon each of these terms separately.

After some algebra it is easily shown that

$$J_1(\underline{\tilde{g}}, \underline{\tilde{a}}) = E\{|\tilde{r}_i|^2\} - [\underline{\tilde{\psi}} - \underline{\tilde{\lambda}}(\underline{\tilde{a}})]^\dagger \underline{\tilde{Q}}^{-1}[\underline{\tilde{\psi}} - \underline{\tilde{\lambda}}(\underline{\tilde{a}})] + [\underline{\tilde{g}} - \underline{\tilde{Q}}^{-1}(\underline{\tilde{\psi}} - \underline{\tilde{\lambda}}(\underline{\tilde{a}}))]^\dagger \underline{\tilde{Q}}[\underline{\tilde{g}} - \underline{\tilde{Q}}^{-1}(\underline{\tilde{\psi}} - \underline{\tilde{\lambda}}(\underline{\tilde{a}}))]. \tag{A-4}$$

Here, $\underline{\tilde{\psi}}^T \overset{\Delta}{=} (\tilde{\psi}_{-L}, \tilde{\psi}_{-L+1}, \ldots, \tilde{\psi}_0, \ldots, \tilde{\psi}_L)$ is a $(2L+1)$-vector with k'th component

$$\bar{\psi}_k = E\{\hat{r}_i \hat{c}^*_{i-k}\} \; ; \quad k=0,\pm 1, \ldots, \pm L. \tag{A-5}$$

Similarly, $\bar{\underline{Q}}$ is a $(2L+1)\times(2L+1)$ matrix with (k,ℓ) component

$$\bar{q}_{k,\ell} = E\{\hat{c}^*_{i-k}\hat{c}_{i-\ell}\} = \bar{q}^*_{\ell,k} \; ; \quad k,\ell=0,\pm 1, \ldots, \pm L. \tag{A-6}$$

Finally, $\bar{\underline{\lambda}}^T(\underline{\hat{a}}) = (\bar{\lambda}_{-L}, \bar{\lambda}_{-L+1}, \ldots, \bar{\lambda}_0, \ldots, \bar{\lambda}_L)$ is a $(2L+1)$-vector with k'th component

$$\bar{\lambda}_k = \sum_{m=0}^{L} \sum_{n=0}^{L} \hat{a}_m \hat{a}_n \sum_{\ell=-L}^{L} E\{\hat{c}^*_{i-k}\hat{c}_{i-\ell-m}\hat{c}_{i-\ell-n}\} \; ; \quad k=0,\pm 1,\ldots,\pm L, \tag{A-7}$$

and we have written $\bar{\underline{\lambda}}(\underline{\hat{a}})$ as an explicit function of $\underline{\hat{a}}$ to emphasize this dependence as indicated by (A-7). It should be noted in particular that the gradient with respect to $\underline{\hat{g}}$ is given by

$$\nabla_{\underline{\hat{g}}} J_1(\underline{\hat{g}},\underline{\hat{a}}) \triangleq \frac{\partial J_1(\underline{\hat{g}},\underline{\hat{a}})}{\partial \underline{\hat{g}}} = 2\text{Re}\{\bar{\underline{Q}}[\underline{\hat{g}} - \bar{\underline{Q}}^{-1}(\bar{\underline{\psi}} - \bar{\underline{\lambda}}(\underline{\hat{a}}))]\} \tag{A-8}$$

Similarly,[†]

$$\nabla_{\underline{\hat{a}}} J_1(\underline{\hat{g}},\underline{\hat{a}}) \triangleq \frac{\partial J_1(\underline{\hat{g}},\underline{\hat{a}})}{\partial \underline{\hat{a}}} \tag{A-9}$$

$$= 4\text{Re}\{\bar{\underline{\phi}}(\underline{\hat{g}})\underline{\hat{a}}\} \;, \tag{A-9}$$

with $\bar{\underline{\phi}}(\underline{\hat{g}})$ an $(L+1)\times(L+1)$ matrix depending upon $\underline{\hat{g}}$ with (m,n) element

$$\bar{\phi}_{m,n}(\underline{\hat{g}}) = \sum_{j=-L}^{L} \hat{g}_j \sum_{k=-L}^{L} E\{\hat{c}_{i-j}\hat{c}^*_{i-k-n}\hat{c}^*_{i-k-n}\} = \bar{\phi}^*_{n,m}(\underline{\hat{g}}) \;. \tag{A-10}$$

Now from the definition of $J_2(\underline{\hat{a}})$ in (A-3) we can rewrite this in the form

$$J_2(\underline{\hat{a}}) = -2\text{Re}\{\text{tr}[\bar{\underline{\Psi}}\underline{\hat{a}}\underline{\hat{a}}^T]\} + \text{tr}[\underline{\hat{a}}\underline{\hat{a}}^\dagger \bar{\underline{\Lambda}}(\underline{\hat{a}})] \;. \tag{A-11}$$

Here $\bar{\underline{\Psi}}$ is a $(L+1)\times(L+1)$ matrix with (m,n) element

$$\bar{\psi}_{m,n} = \sum_{j=-L}^{L} E\{\hat{r}^*_i\hat{c}_{i-j-m}\hat{c}_{i-j-n}\} = \bar{\psi}_{n,m} \; ; \quad m,n=0,\pm 1,\ldots,\pm L \;. \tag{A-12}$$

[†] Here it is easier to go back to the definition of $J_1(\underline{\hat{g}},\underline{\hat{a}})$ given in (A-2).

Finally, the matrix $\bar{\underline{\Lambda}}(\underline{a})$ is an $(L+1)\times(L+1)$ matrix depending explicitly upon $\underline{a}$ with (m,n) element

$$\bar{\lambda}_{m,n} = \sum_{u=0}^{L} \sum_{v=0}^{L} a_u a_v^* \sum_{j=-L}^{L} \sum_{k=-L}^{L} E\{\tilde{c}_{i-j-m}\tilde{c}_{i-j-u}\tilde{c}_{i-k-n}^*\tilde{c}_{i-k-v}^*\} = \bar{\lambda}_{n,m}^* \quad . \tag{A-13}$$

It follows after some elementary algebra that

$$\nabla_{\underline{a}} J_2(\underline{a}) = \frac{\partial J_2(\underline{a})}{\partial \underline{a}} = -4\mathrm{Re}\{\bar{\underline{v}}\underline{a}\} + 4\mathrm{Re}\{\bar{\underline{\Lambda}}(\underline{a})\underline{a}\} \quad . \tag{A-14}$$

B-13

References

1. J. W. Modestino, "Modeling of Voice Frequency Digital Communication Facilities for Performance Monitoring Purposes", unpublished PAR report.

2. E. Bedrosian and S. O. Rice, "The Output Properties of Volterra Systems (Nonlinear Systems with Memory) Driven by Harmonic and Gaussian Inputs", Proc. of IEEE, vol. 59, pp. 1688-1707, Dec. 1971.

3. J. J. Bussgang, L. Ehrman, and J. W. Graham, "Analysis of Nonlinear Systems with Multiple Inputs", Proc. of IEEE, vol. 62, pp. 1088-1119, Aug. 1974.

4. W. J. Lawless and M. Schwartz, "Binary Signaling over Channels Containing Quadratic Nonlinearities", IEEE Trans. on Commun., vol. 22, pp. 288-297, March 1974.

5. D. D. Weiner and J. F. Spina, Sinusoidal Analysis and Modeling of Weakly Nonlinear Circuits, Van Nostrand Reinhold, Co., New York, NY. 1980.

$$x(t) = \sqrt{2} \, \text{Re}\{x(t)e^{j\omega_c t}\}$$

Narrowband System

$$y(t) = \sqrt{2} \, \text{Re}\{y(t)e^{j\omega_c t}\}$$
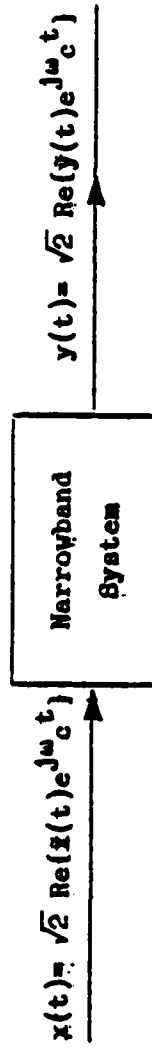
Figure 1

Typical Narrowband Nonlinear Systems

B-15
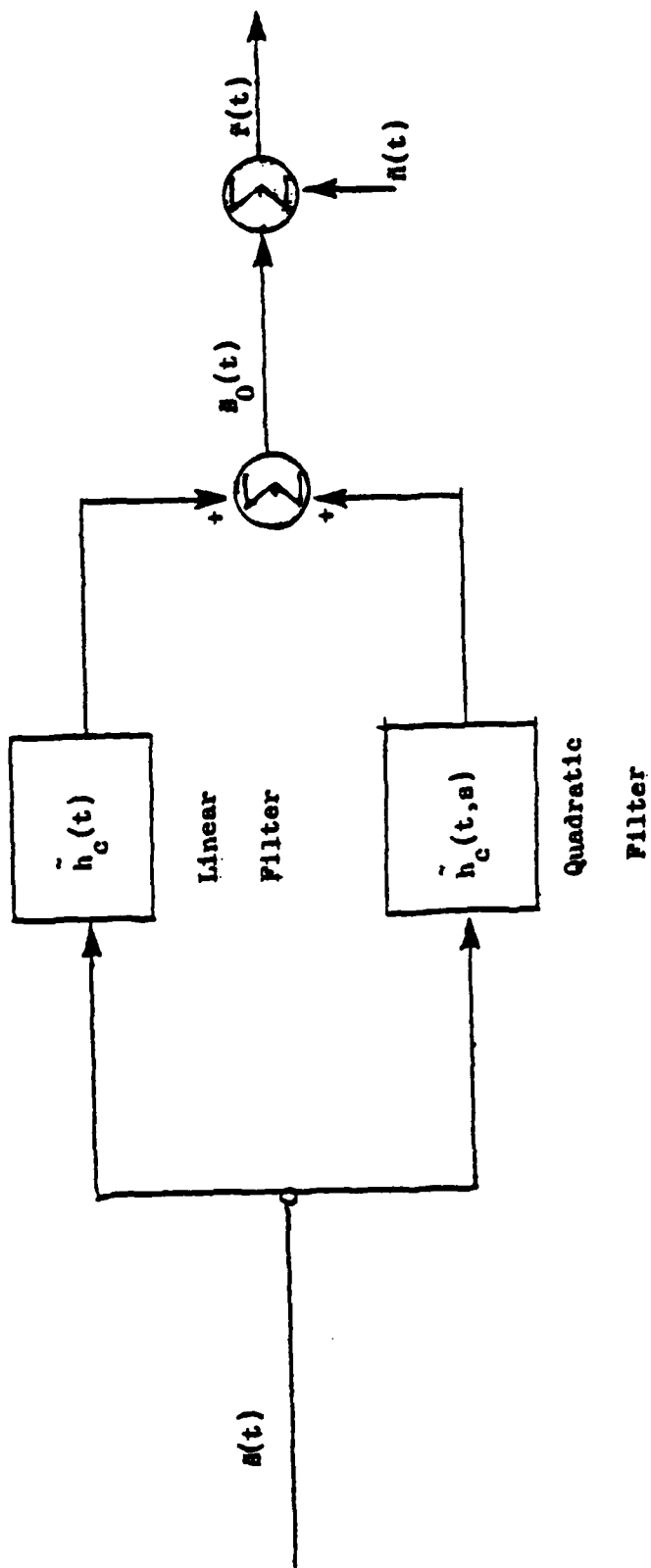
Figure 2

Truncated Complex Volterra Series
Representation of Channel
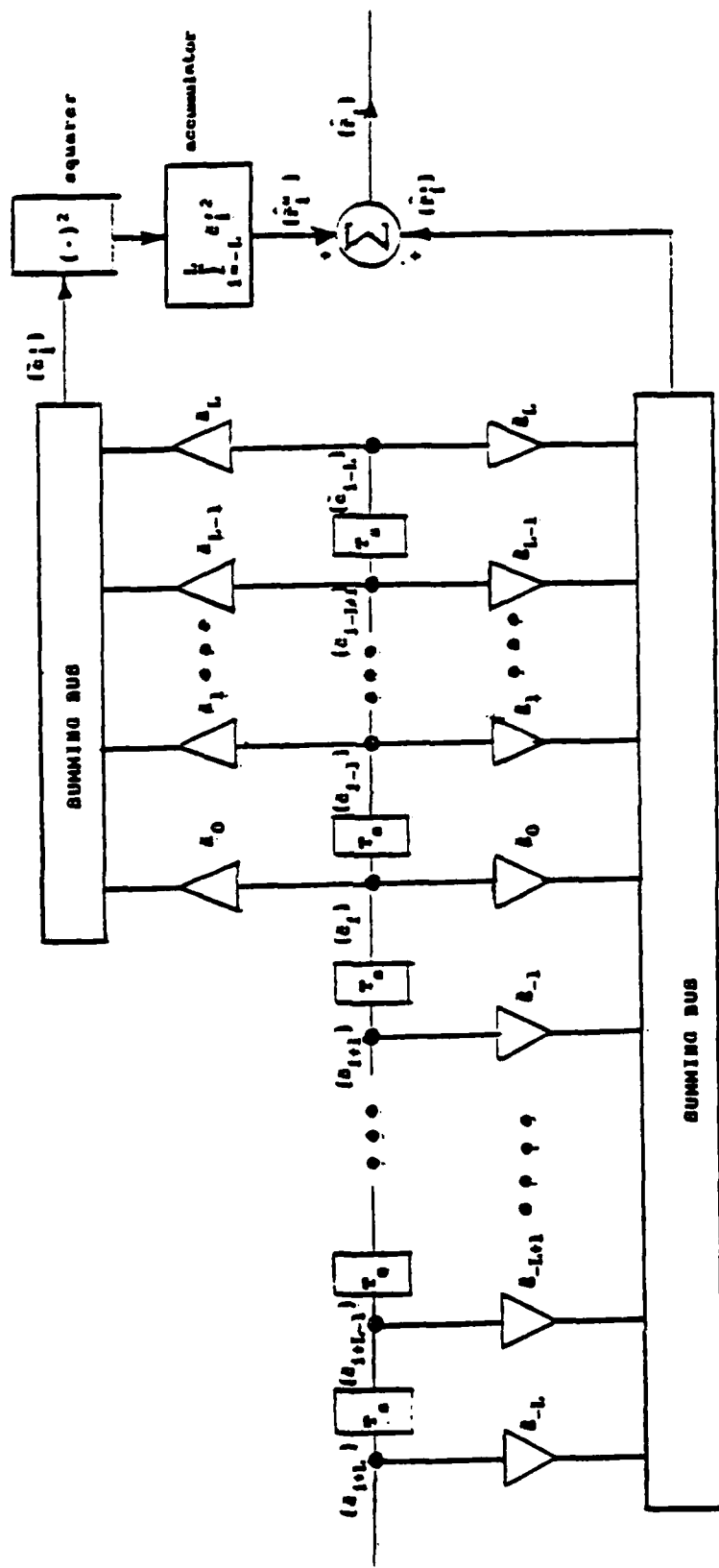
FIGURE 3

Block Diagram of Nonlinear Channel Model
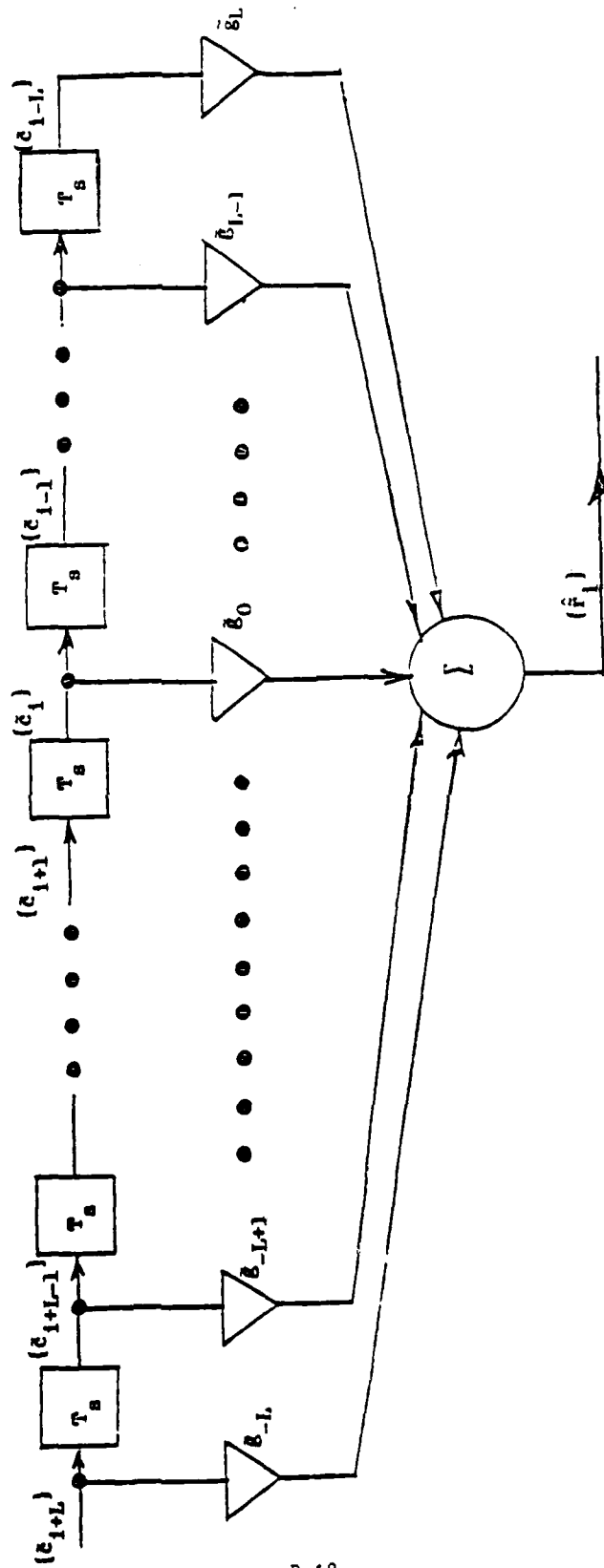
Figure 3-α

Tapped Delay Line (TDL) Channel Model

Appendix C

Appendix C

Modem Signature Analysis Demonstration System Users Guide

C.1 Overview

The MSA demonstration system is implemented as modular tasks linked together with the RSX11M Indirect Command File processor. This facilitates the removal of certain modules for other applications without code modification.

On the DICEF PDP 11/40 system, the MSA directory is [3,3]. Command files exist together with the sources in that directory so that a complete rebuild of the software system can be effected with the command;

@ MSABLD

The rebuild would only be necessary in cases of operating system modification.

In order to operate the MSA demonstration system, the user must be in the MSA directory and have the desired input waveform files in the same directory. The waveform is expected to be in a fixed (IDRS) format file which has the following attributes:

- unformatted

- direct access organization

- 512 bytes per record

Record 1 of the file is a header containing the information shown in Table C-1. This data format is harmonious with most A/D collection systems. Data is

stored from record 2 on, 1 sample per two-byte integer word. Also it is assumed that the waveform is sampled at 12.8 Kc.

C.2 Operation of the MSA Demonstration System

With the 12.8Hz sampled waveform in the MSA directory, [3,3], the MSA command file is invoked with the command

@ MODEM.

The interaction is now explained.

*DO YOU WISH TO SKIP PHASE 1B? [Y/N]:

Optionally the generation of the raw and rectified signal spectra and the power spectra for the 2- and 4-stage lattice filtered signals, both rectified and not, can be omitted from the experiment. Since none of this output is used in the phase 1 go/no go decision these calculations are not required.

*AUTOCORRELATION BUFFER LENGTH (3K OR 8K):

Here the user specifies the correlation length as "3K" or "8K" points. Note that more vectors result for the "3K" decision.

*AUTOMATED [Y/N]:

The system can process in batch mode if the data is located on magtape "mounted" on the tape drive and a list of the desired magtape files is contained in "WAVENAME.LST" in the format illustrated by the command file prompt.

*WAVEFORM FILE TO BE PROCESSED?

This requests the name of the input signal to process, assuming that automated mode was not selected. This is the end of the user interaction.

Output from a sample run is shown in Figures C-1 through C-11 for the CODEX LSI-48 Mode B modem with 60 Hz phase jitter at 64° P/P added. The output is self-documenting with the possible exception of the peaks detector summaries which are described in the next section.

C.3 MSA Demonstration System Program Reference Manual

The Command File Structure

The 'MSA Command File' is divided into 3 main phases:

1. Gross Channel Quality Analysis

2. Modem Generic Type ID

3. Channel Impairment Characterization

Each of these phases is further subdivided into smaller tasks, all linked by the RSX11M Indirect Command File Processor. The structure is detailed in the following section.

C.3.1 Phase 1: Go/No Go Decision

C.3.1.1 Phase 1A: Gross Channel Quality Estimation

The Go/No Go decision of the channel is performed using time domain statistics:

- Rectified Peak/Average Signal Ratio

- Rectified Signal Peak/Average Ratio Variance

Programs:

NORMALIZE -   normalize inputs the specified raw IDRS formatted waveform,
converts to R#4 data as required, removes any residual bias
caused by the A/D Converter, and normalizes the waveform to
unity power. The output waveform has the extension ".NRM".

EVLSTS -   accepts the (".NRM") normalized waveform and computes the rec-
tified signal peak to average ratio and rectified signal peak
to average ratio variance.

A reference file "EVLSTS.DAT" contains the user-settable
acceptable limits for each of these (2) tests. The output from
the program is the PHASE IA summary and a flag passed back to
the Indirect Command File Processor signaling either 'CHANNEL
ACCEPTED' or 'CHANNEL REJECTED'.

C.3.1.2   Phase 1B: Signal Spectral Enhancement

Phase 1B is a collection of signal processing algorithms deemed promising
in enhancing certain spectral components, such as baud or carrier, to a point
where they are suitable for classification features for generic typing or
impairment characterization. This phase consists of (3) major algorithms
linked as shown in Figure C-1.

Programs:

RECT -   accepts an input waveform and creates a full wave rectified
output waveform. Input and output filenames are specified.

MSLFLT -   is the multi-stage lattice filter. Input and output waveforms
            are specified with the desired number of filter stages.

PWRSPT -   is the spectral estimator. The input waveform is specified and
            successive 1024-point real-to-complex FFT's are performed and
            averaged to a maximum of 10. The output is in waveform format,
            512 points (bins) long.

PEAKDT -   is the peaks detector which operates on the spectrum created by
            PWRSPT. Only specified frequency ranges of the spectrum are
            considered as noted on the output listing. Each of the 6 spec-
            trums generated in Phase 1B are processed concurrently, and the
            results are consolidated onto a single output summary page.

            A sample cell from the peaks detector has the following format
            and fields:

                        M 2170. Hz
                        C   0. Hz
                        @5.db,. Hz

                where:

                "M" = maximum frequency in band
                "C" = center of valid spectral spike
                "@" = minimum clear pulse height above noise in order
                      that a spike be declared valid
                "," = BW of the valid component "@"dB down.

                NOTE: If no acceptable spike was found,
                       "C" and "," values will be zero.

C.3.2 Phase 2: Modem Generic Type Classifier

Five lags of the autocorrelation (1,2,3,4 and 6) of the 1-bit quantized signal are generated for the user-specified window of 3K or 8K samples. All of the normalized signal is processed and the output vector file (.VEC) contains one vector of 5 lag measurements each for each non-overlapping window available in the input waveform.

The vectors are run through four Fisher classifiers:

- Modulation Type
- Baud Rate
- Combined Modulation Type - Baud Rate
- Modem ID

Programs:

ACORR -   generates specified lags of the autocorrelation of the normalized input waveform. Lag 0 is used for normalizing the vector (other lags). The program creates a ".VEC" file suitable for input directly into the Fisher classifier (or OLPARS). The length of each correlation window is user-specified at 3000 or 8000 samples.

FHREXE -   is the Fisher Discriminate pair classifier. Input files are ".VEC" vector files and a summary is produced together with flags signaling the .AT processor as to the outcome. The logic library is user specified.

PHASE2 -   Phase2 is the executive program which compiles summary and effects final Phase 2 logic decision of modulation and baud.

            If the baud rate or modulation type classifier rejects the input, the EXEC will recover provided that the combination classifier and

the remaining baud or type classifier agree.

The Modem ID classifier is not used in this decision, rather it is required in Phase 3 in lieu of consistent database collection parameters.

C.3.3 Phase 3 – Channel Impairment Characterization

Phase 3 consists of two sub-phases; the statistical channel characterizer for the estimation of channel S/N and harmonic distortion, and the phase jitter detector.

Programs:

EVLIMP   the peak-to-average ratio and the peak/average ratio variance of the rectified signal are calculated and used to index into a template file identified by the modem ID classifier of Phase 2. The requirement for the fingerprint level ID of modem is imposed by the unexplained discrepancies in the signal formats due most likely to the inconsistent collection parameters, sample rate, etc.

The result of the template search is the classification result for the presence and degree of HD or AGN on the line in the form of the Phase 3A executive summary.

DEMODI   is the IIR filter demodulator. The generic identification indicates a disk file (for example, DPSK1200.PRM) which contains the mix frequency and proper filters for the demodulation of this generic type.

For the three cases of bits/symbol 1, 2, and 3, the FM transition removal tasks are:

> REMBIT1
> REMBIT2
> REMBIT3

The actual ID of the modem is used here to indicate the proper thresholds for the operation. The thresholds are stored on disk under the name S".PRM" where 'S' is the symbol of the modem signal. The input extension ".FM" is assumed and ".NFM" (No FM) file is produced for specified input waveform file.

RESAMP   Applies a 200Hz low-pass Butterworth 2-pole filter to smooth the ".NFM" input file. The signal is resampled by 4 and stored back on disk.

PWRSPT   As described earlier, the power spectrum generator operates on the specified input, the resampled no-FM signal in this case, and produces a single line power spectrum. This is plotted for the user.

MODPEAKDT   is the modified peaks detector which operates on the FM spectrum. The output is as shown below:

line

(1)   M   25Hz

(2)   7.22dB

(3)   C   0Hz

(4)   @2dB,   0Hz

(5)   MP

(6)   M   19Hz

(7)   6.14dB

where

line (1) is the maximum frequency component in the specified band

line (2) is the power of the line (1) component

line (3) is the center frequency of the component or is 0 if no
          unique spike is found

line (4) is the component bandwidth at 2dB below the peak, or is
          0 if no component is found

line (5) is the cause for rejection of the spike (if it is
          rejected):
          MP = multiple peaks

          PO = peaks overlapping band edge

line (6)   is the maximum frequency of the second highest spectral component in the specified band

line (7)   is the maximum power level of the second highest spectral component in the specified band.

In addition, an estimate of the noise floor for the 0–200Hz band is given in the leftmost column. This serves as a reference when examining spectral power levels of the peaks detector output.

WORD	DESCRIPTION
1	No. of Channels
2,3	Sample Rate (I*4)
4	Start Time (Hours)
5	Start Time (Minutes)
6	Start Time (Seconds)
7	End Time (Hours)
8	End Time (Minutes)
9	End Time (Seconds)
13	Run Number
14	Data Type (0; Integer 9 32-bit Floating Point)
17,18	Number of Data Records (I*4)

All Words are I*2 unless otherwise specified. Only
the sample rate and data type are used by the MSA
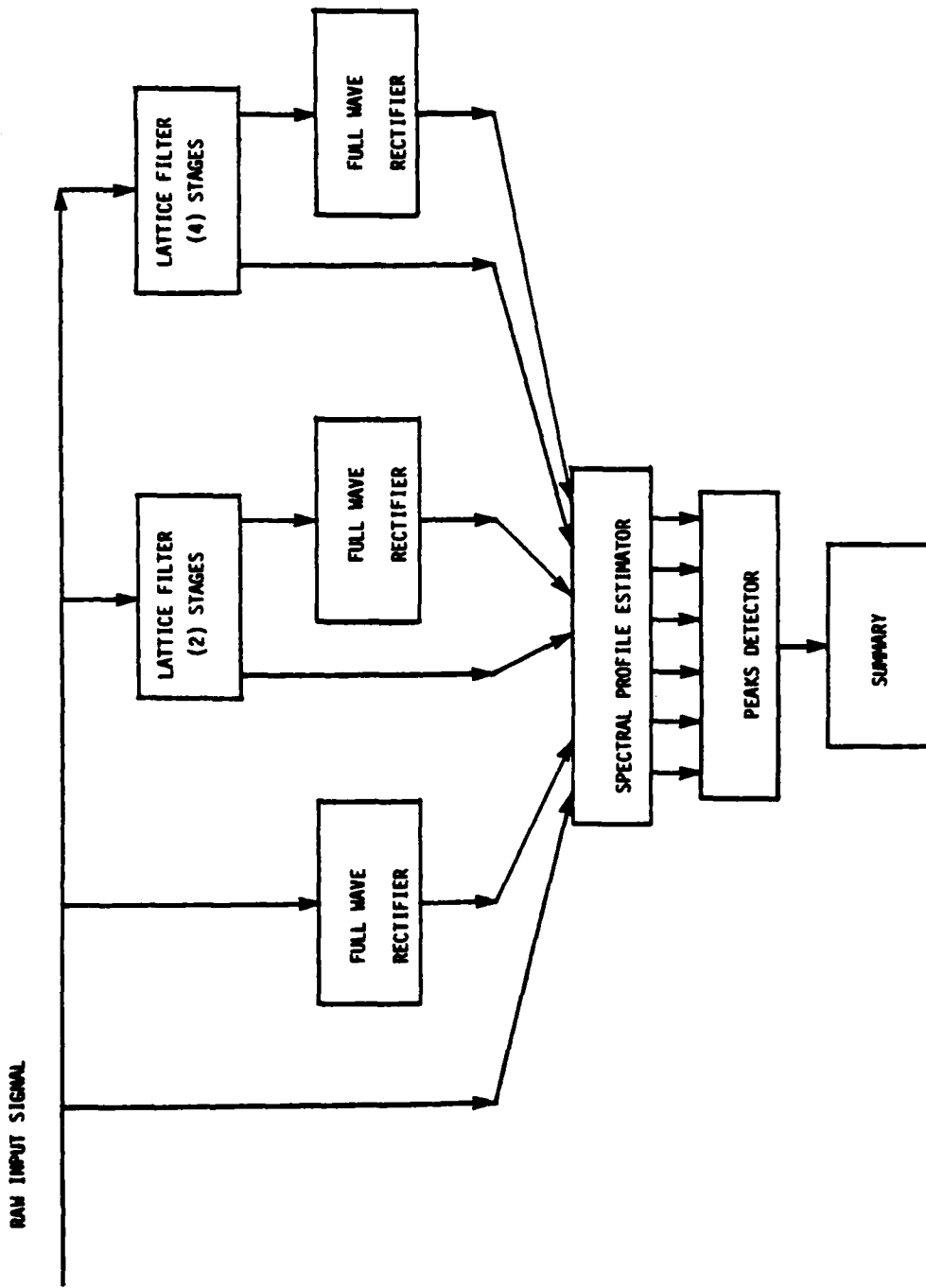software.

Table C-1   IDRS Waveform Header

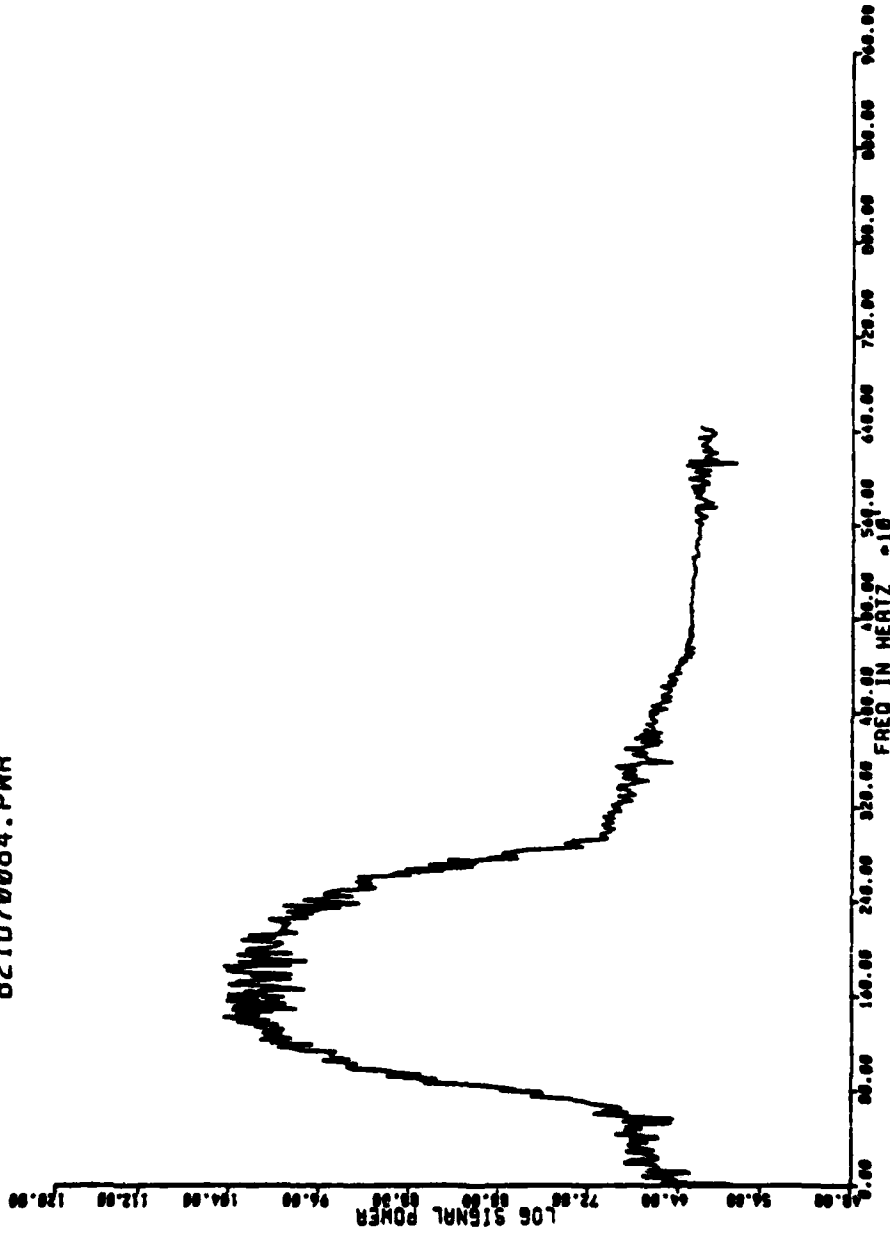Figure C-1
Flow Diagram for Phase 1A Spectral Enhancement

Figure C-2

Signal Power Spectrum

C-13

B21D70064.PR
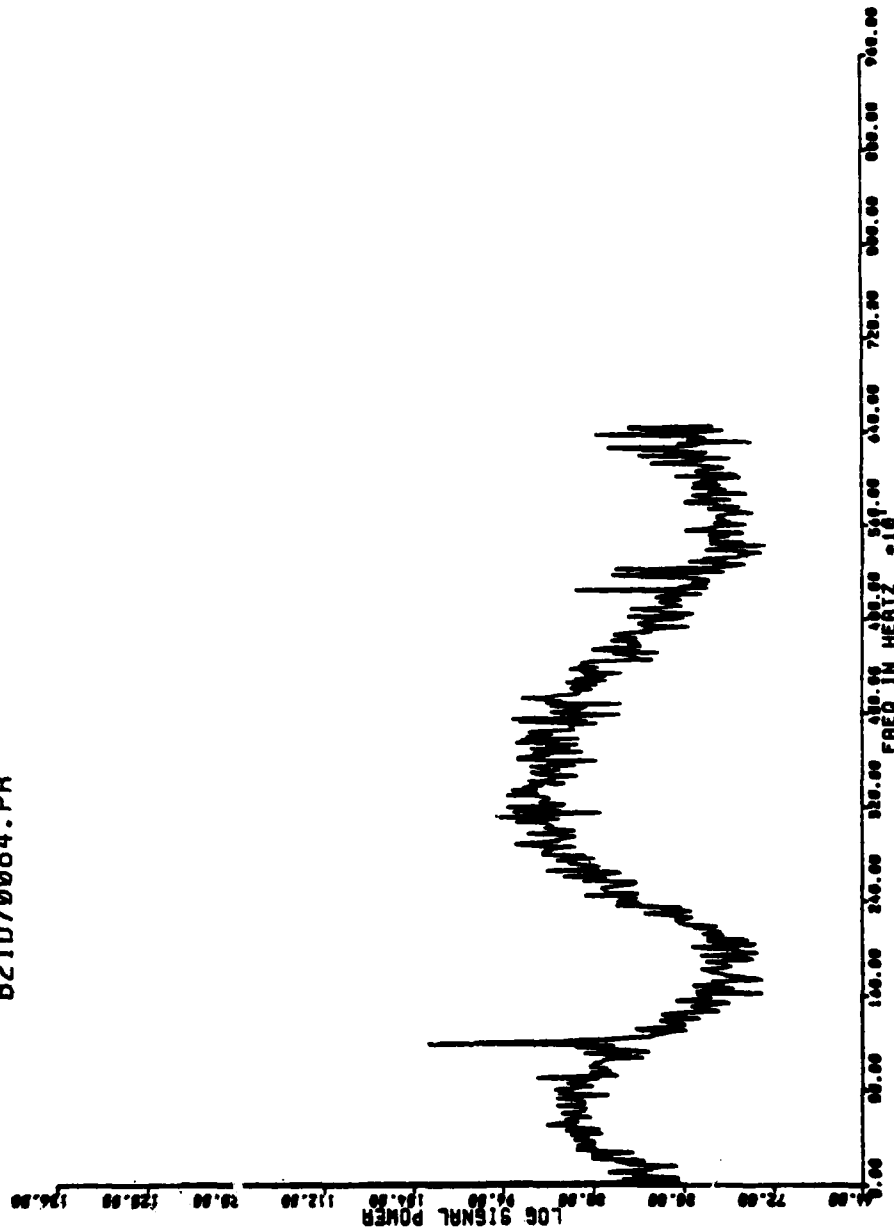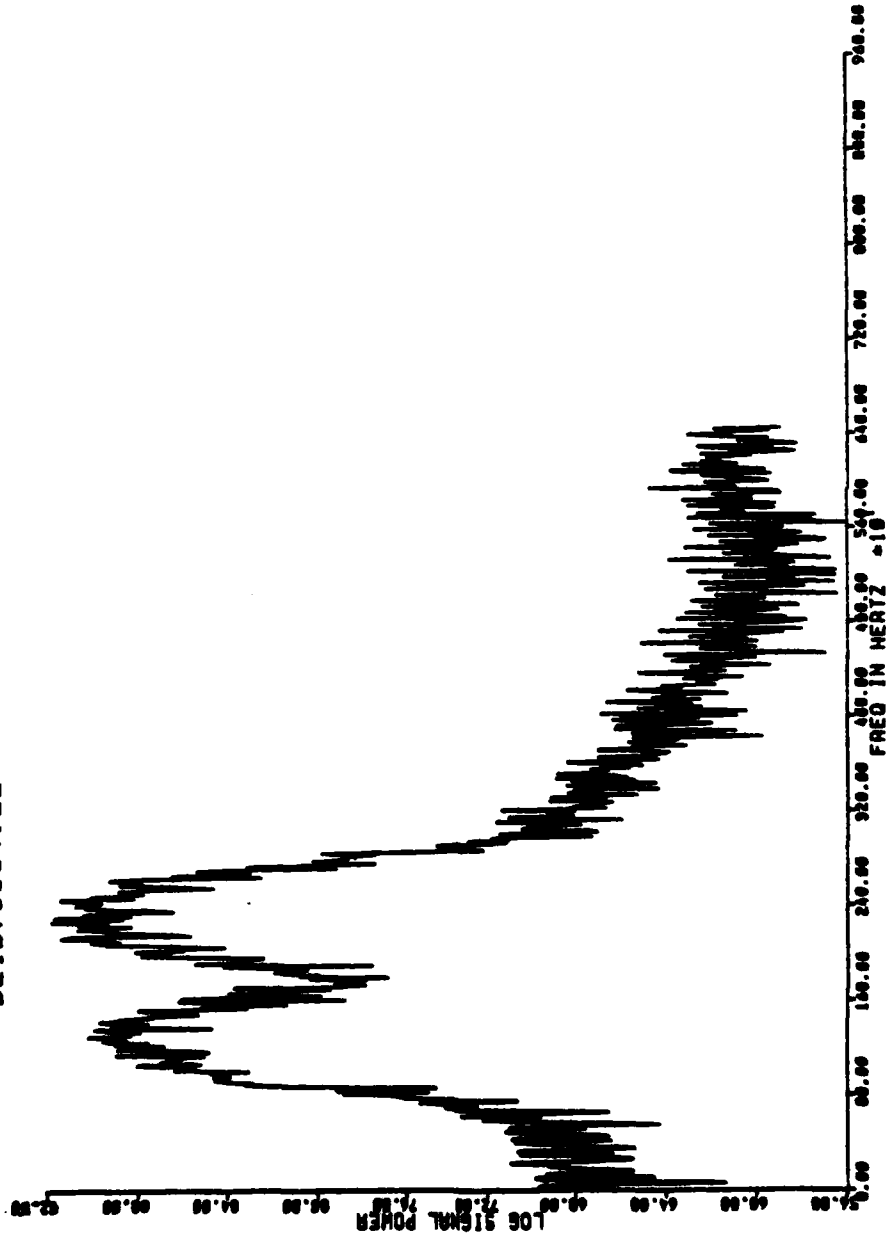
Figure C-3

Rectified Signal Power Spectrum

Figure C-4

Power Spectrum of 2-stage Lattice Filter Residue

B21070064.L2R
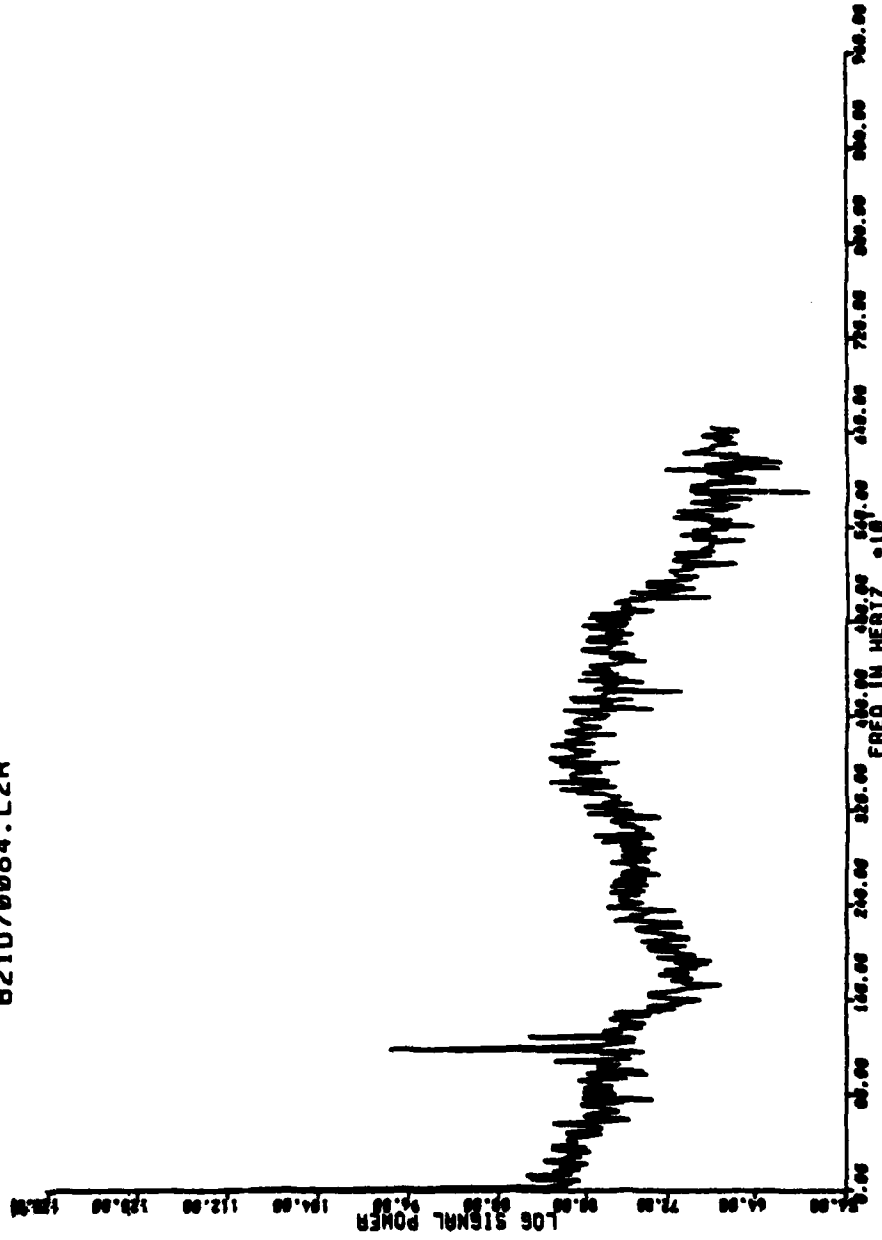

Figure C-5

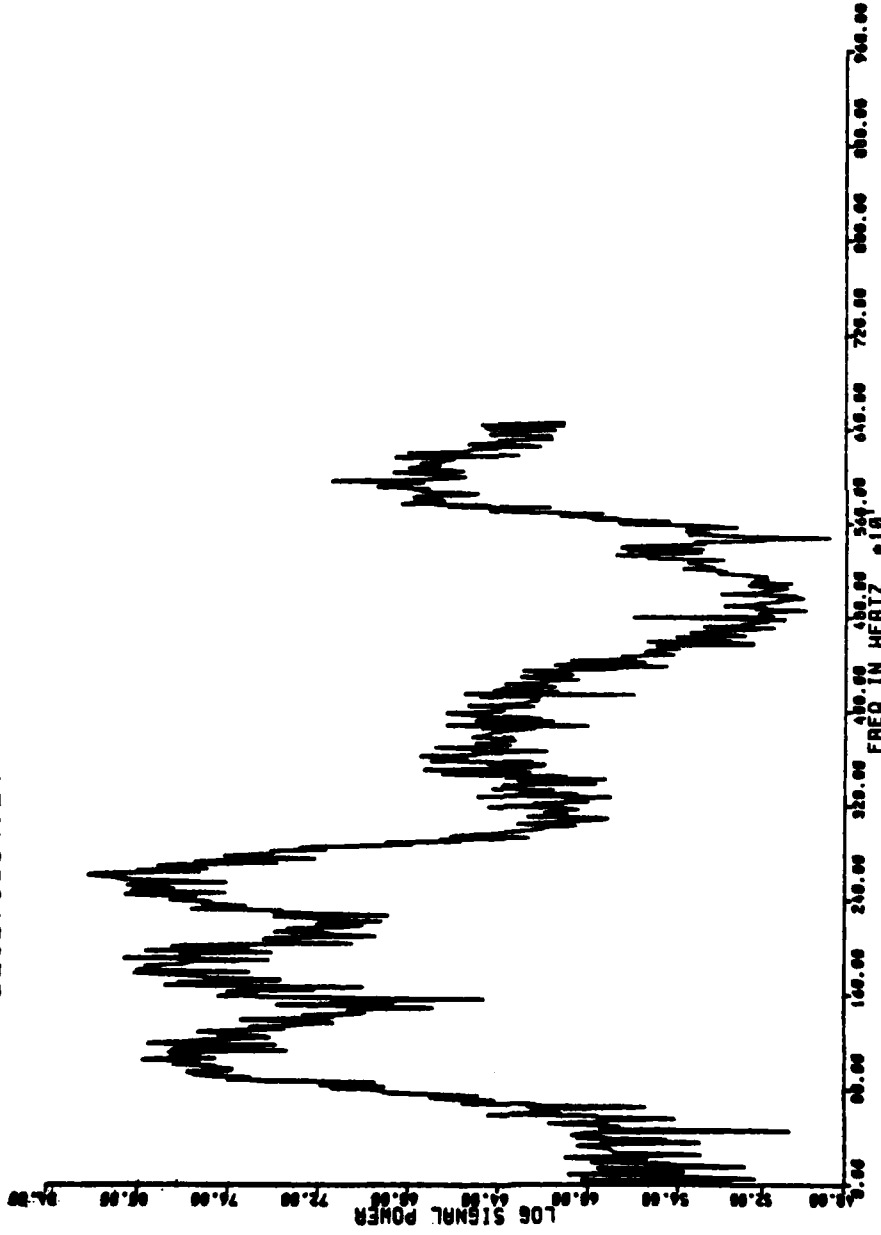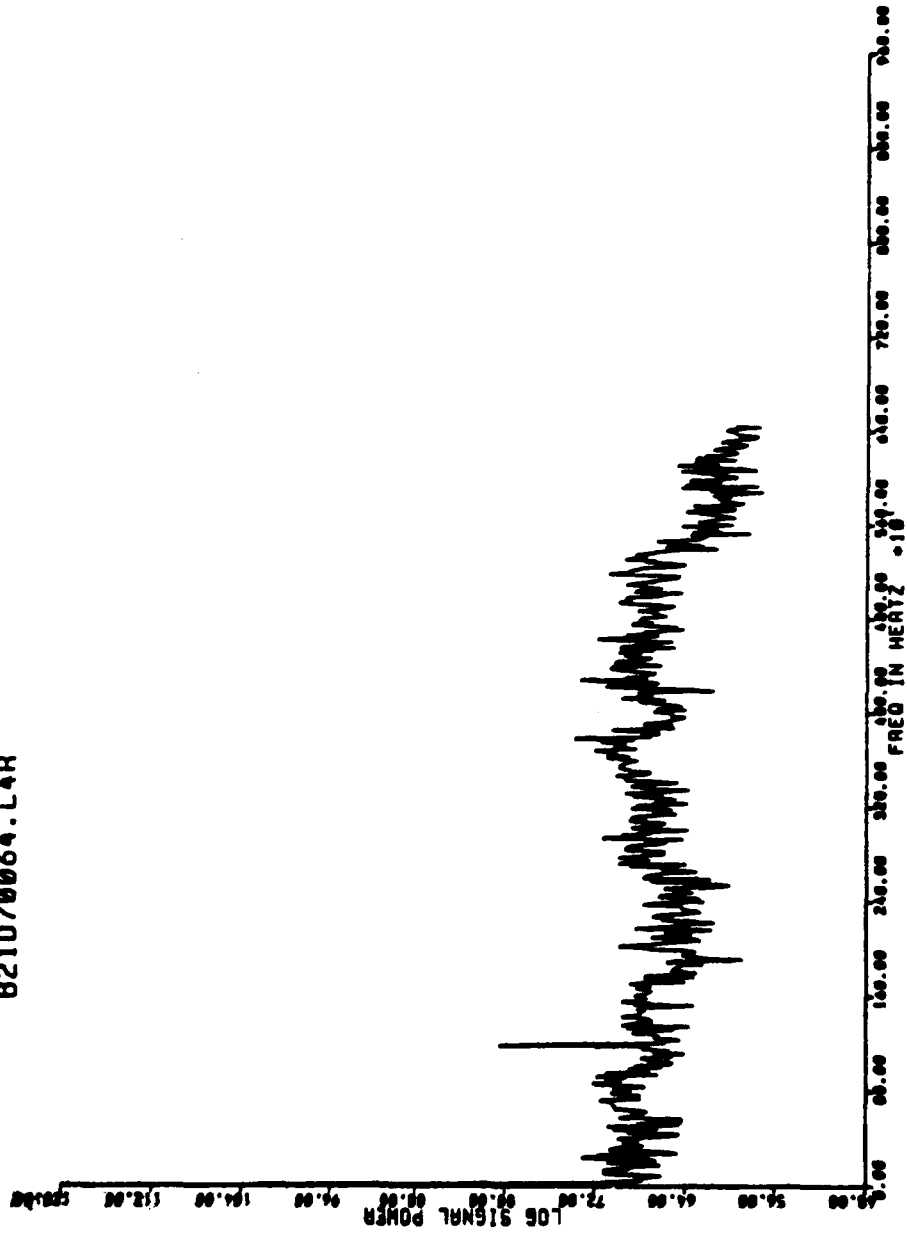Power Spectrum of 2-stage Lattice Filter Residue Rectified

Figure C-6

Power Spectrum of 4-stage Lattice Filter Residue

B21D78064.L4R

Figure C-7

Power Spectrum of 4-stage Lattice Filter Residue Rectified

OPER PWR	BAUD RATES				CARRIER FREQUENCIES			
	1200. hz	1600. hz	2400. hz	2667. hz	4800. hz	1700. hz	1800. hz	2853. hz
PR	M 1383. hz C 0. hz e S.db, 0.hz	M 1584. hz C 0. hz e S.db, 0.hz	M 2414. hz C 0. hz e S.db, 0.hz	M 2716. hz C 0. hz e S.db, 0.hz	M 5054. hz C 0. hz e S.db, 0.hz	M 1848. hz C 0. hz e S.db, 0.hz	M 1848. hz C 0. hz e S.db, 0.hz	M 2892. hz C 0. hz e S.db, 0.hz
L2	M 1507. hz C 1194. hz e S.db, 25.hz	M 1685. hz C 0. hz e S.db, 0.hz	M 2615. hz C 0. hz e S.db, 0.hz	M 2892. hz C 0. hz e S.db, 0.hz	M 5042. hz C 5029. hz e S.db, 25.hz	M 1685. hz C 0. hz e S.db, 0.hz	M 2012. hz C 0. hz e S.db, 0.hz	M 3118. hz C 0. hz e S.db, 0.hz
L2R	M 1295. hz C 0. hz e S.db, 0.hz	M 1507. hz C 0. hz e S.db, 0.hz	M 2452. hz C 0. hz e S.db, 0.hz	M 2691. hz C 0. hz e S.db, 0.hz	M 4966. hz C 0. hz e S.db, 0.hz	M 1886. hz C 0. hz e S.db, 0.hz	M 2012. hz C 0. hz e S.db, 0.hz	M 2904. hz C 0. hz e S.db, 0.hz
L4	M 1194. hz C 1182. hz e S.db, 25.hz	M 1635. hz C 0. hz e S.db, 0.hz	M 2515. hz C 0. hz e S.db, 0.hz	M 2766. hz C 0. hz e S.db, 0.hz	M 4934. hz C 0. hz e S.db, 0.hz	M 1823. hz C 0. hz e S.db, 0.hz	M 1961. hz C 0. hz e S.db, 0.hz	M 2992. hz C 0. hz e S.db, 0.hz
L4R	M 1194. hz C 0. hz e S.db, 0.hz	M 1785. hz C 0. hz e S.db, 0.hz	M 2615. hz C 0. hz e S.db, 0.hz	M 2691. hz C 0. hz e S.db, 0.hz	M 4992. hz C 0. hz e S.db, 0.hz	M 1785. hz C 0. hz e S.db, 0.hz	M 1911. hz C 0. hz e S.db, 0.hz	M 2892. hz C 0. hz e S.db, 0.hz
	M 1194. hz C 1182. hz e S.db, 25.hz	M 1710. hz C 0. hz e S.db, 0.hz	M 2603. hz C 0. hz e S.db, 0.hz	M 2779. hz C 0. hz e S.db, 0.hz	M 4941. hz C 0. hz e S.db, 0.hz	M 1710. hz C 0. hz e S.db, 0.hz	M 2012. hz C 0. hz e S.db, 0.hz	M 2942. hz C 0. hz e S.db, 0.hz

Figure C-8

Phase 1 Executive Summary

```
•••••••••  PHASE 2: EXECUTIVE SUMMARY •••••••••

DATA FILE: B21D70064.VEC
NUMBER OF DATA VECTORS:    8


LOGIC FILE: MODTYP.F3K
     F    P    D    Q    •
     0    0    8    0    0

   MODULATION: PSK/DPSK


LOGIC FILE: BAUDRT.F3K
     1    2    3    4    5    •
     8    0    0    0    0    0

   BAUD RATE: 1200


LOGIC FILE: MODBRT.F3K
     F    D    d    Q    q    A    P    •
     0    8    0    0    0    0    0    0

   MODULATION, BAUD RATE: PSK/DPSK,1200


LOGIC FILE: MODEMID.F3K
     a    b    c    d    h    l    m    p    r    w    x    •
     0    7    0    0    0    0    0    0    0    1    0    0

   MODEM TYPE: CODEX LSI-48, MODE B

FINAL DECISION:

   MODULATION, BAUD RATE: PSK/DPSK,1200
```

Figure C-9

Phase 2   Executive Summary

********** PHASE 3A   EXECUTIVE SUMMARY **********

REFERENCE LIBRARY: b

••
PROCESSING B21D70064.NRM·

••--- RESULTS OF THE PEAK/AVERAGE RATIO CLASSIFIER ---••

•• NO SIGNIFICANT HARMONIC DISTORTION OR GAUSSIAN NOISE DETECTED ••

••--- RESULTS OF THE PEAK/AVERAGE RATIO VARIANCE CLASSIFIER ---••

•• NO SIGNIFICANT HARMONIC DISTORTION OR GAUSSIAN NOISE DETECTED ••
        ••••••••••• PHASE 3B: EXECUTIVE SUMMARY ••••••••••

FILE: B21D70064

		18. hz	60. hz	120. hz	180. hz
NOISE 4.05 db	M	25. hz 7.22 db	63. hz 13.33 db	135. hz 5.04 db	185. hz 5.38 db
	C @ 2.db,	0. hz 0.hz	60. hz 6.hz	0. hz 0.hz	0. hz 0.hz
	MP M	19. hz 6.14 db	0. hz 0.00 db	123. hz 5.04 db	195. hz 3.95 db

Figure C-10

Phase 3 Executive Summary
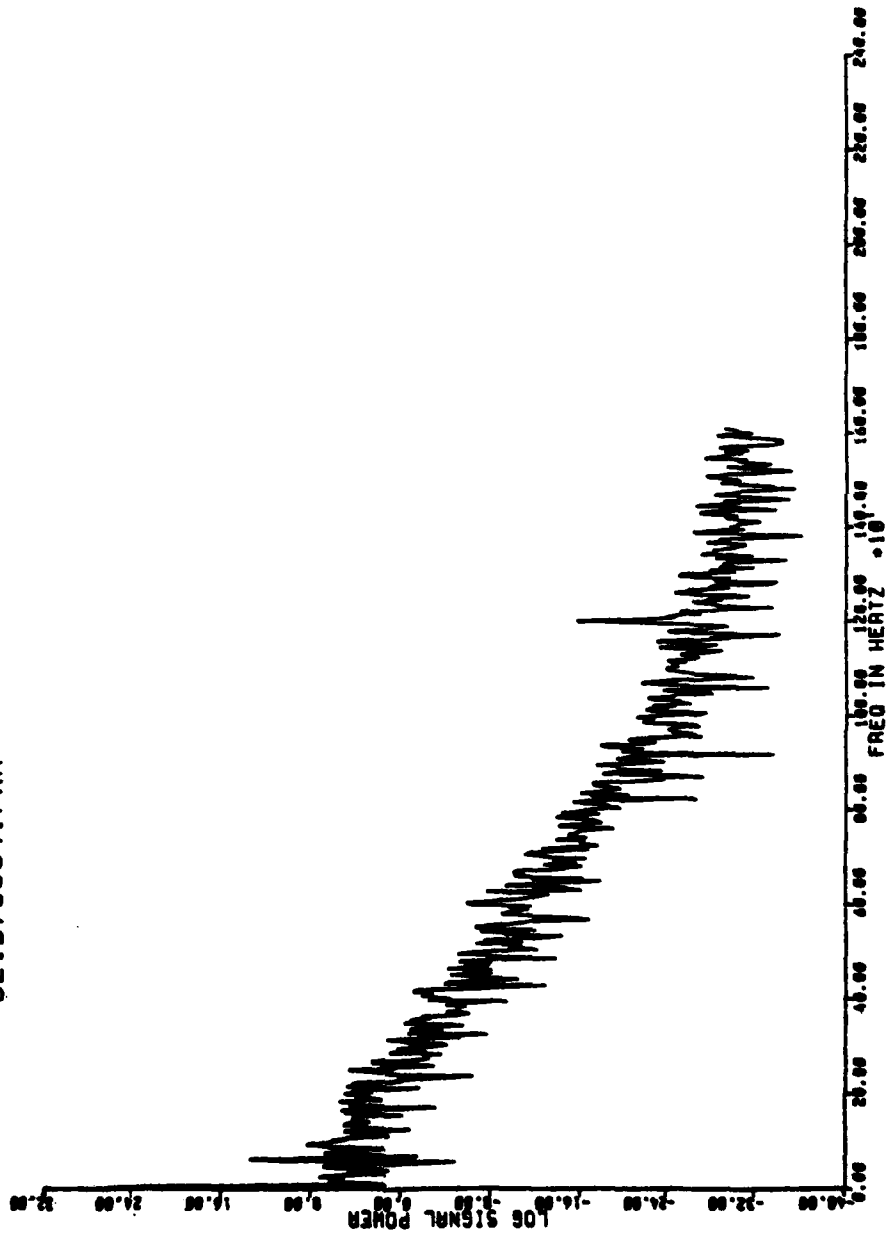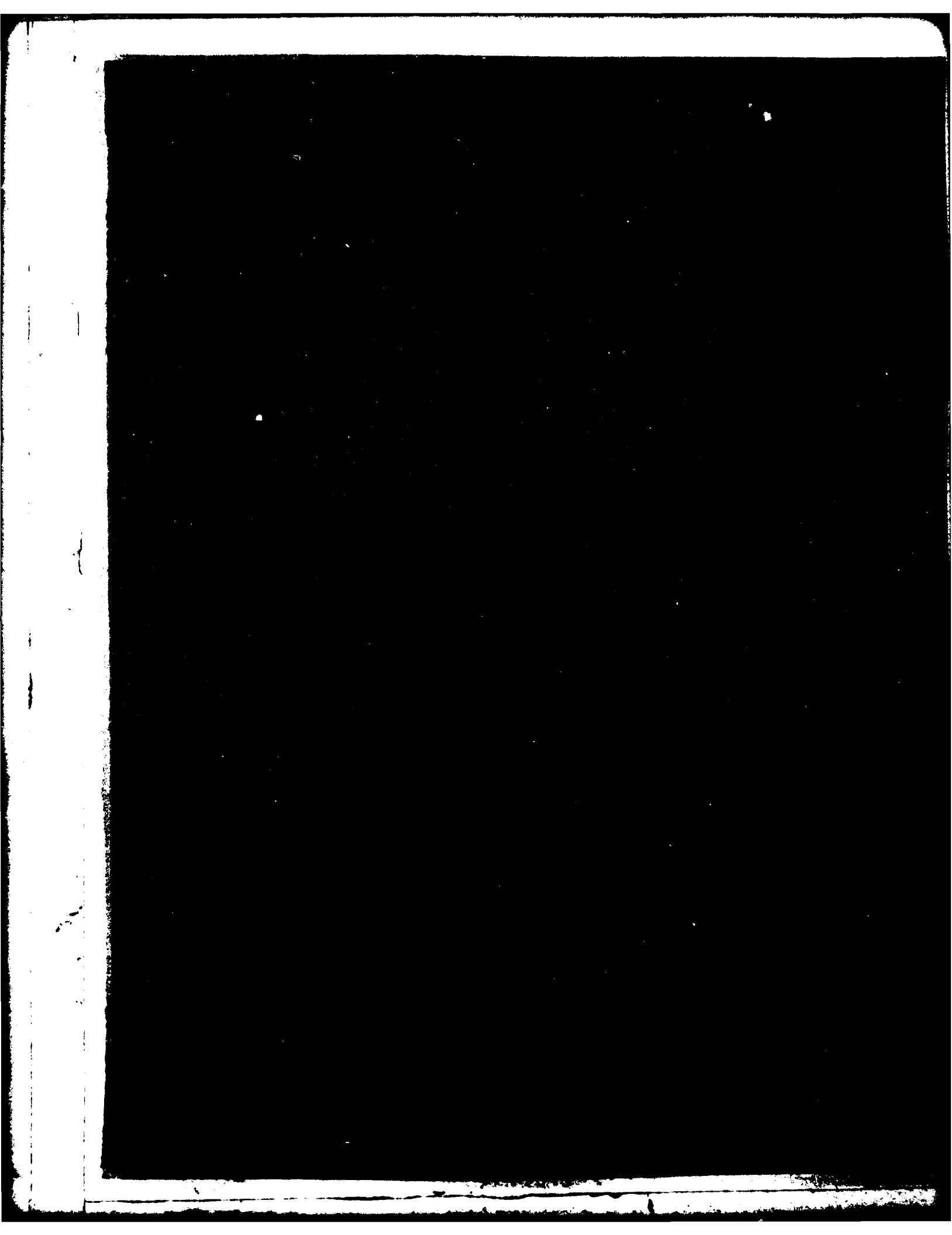
Figure C-11

FM Spectrum After Enhancement Showing 60 Hz Phase
Jitter at 64% P/P Enhanced 8dB Above the Noise Floor

END

DATE
FILMED

6 – 83

DTIC